Oligonucléotides à Porphyrines Pendantes : vers des Nano-Matériaux Multi-Porphyriniques Auto-Assemblés

Sonja Merkaš

Université Paul Sabatier-Toulouse III et Université de Zagreb

THESE

présentée en vue de l'obtention du grade de

DOCTEUR DE L'UNIVERSITE PAUL SABATIER-TOULOUSE III
ET L'UNIVERSITE DE ZAGREB

Spécialité : Chimie Macromoléculaire et Supramoléculaire

SONJA MERKAŠ

OLIGONUCLEOTIDES A PORPHYRINES PENDANTES : VERS DES NANO-MATERIAUX MULTI-PORPHYRINIQUES AUTO-ASSEMBLES

Directeurs de thèse : Dr. Nathalie SOLLADIE
Prof. Mladen ŽINIĆ

Soutenue au mois de Novembre 2006 devant la commission d'examen :

D. BASSANI, Directeur de recherche CNRS, Université Bordeaux	Rapporteur
M. MALET-MARTINO, Professeur à l'Université Paul Sabatier	Examinatrice
J. L. PIERRE, Professeur à l'Université Joseph Fourier	Examinateur
N. SOLLADIE, Chargée de recherche, Laboratoire de Chimie de Coordination	Directrice
I. PIANTANIDA, Chargée de recherche, Ruđer Bošković Institut	Examinateur
H. VANČIK, Professeur à l'Université de Zagreb	Rapporteur
M. ŽINIĆ, Professeur, Ruđer Bošković Institut	Directeur

This dissertation was carried out as part of the bilateral scientific collaboration, in the Group for Synthesis of Porphyrinic Systems, Laboratoire de Chimie de Coordination of CNRS Toulouse, under supervision of Dr. Nathalie Solladié and in the Laboratory for Supramolecular and Nucleoside Chemistry of Institute Ruđer Bošković Zagreb, under supervision of Prof. Mladen Žinić.

I give a great gratitude to my thesis supervisor and director of Institute Ruđer Bošković for employing me into his Laboratory, for lot of trust, unquestionable support and understanding during these years, and for his intellectual support.

I would like to thank Prof. Jean-Jacques Bonnet, director of Laboratoire de Chimie de Coordination.

A big thank you goes to Dr. Nathalie Solladié for receiving me into her group as her student and as a true friend and colleague, for enormous trust, confidence and patience invested in me, countless advices and support which guided me throughout this work. I thank her for all her professional and personal qualities.

I would like to thank Dr. Dario Bassani and Prof. Hrvoj Vančik, for kindly accepting to grade this work. Also many thanks to Prof. Myriam Malet-Martino, Dr. Ivo Piantanida and Prof. Jean-Louis Pierre for accepting to examine this work.

I am very grateful to Dr. Yannick Coppel in NMR Service of Laboratoire de Chimie de Coordination on his inestimable contribution in NMR analysis, constant willingness to explain the beauty of NMR spectroscopy, big understanding.

For huge and timely help with calculations of complexation constants, advices and availability I thank Dr. Ivo Piantanida in Laboratory for Supramolecular and Nucleoside Chemistry of Institute Ruđer Bošković.

Thank you, Haiko Herschbach and Prof. Alan Van Dorsselaer in Laboratoire de spectrométrie de masse des macromolécules biologiques et des édifices supramoléculaires in Strasbourg, for mass analysis. Also, I thank Dr. Catherine Claparols and Ms Nathalie Martins in Service commun de Spectrometrie de masse at the University Paul Sabatier for contribution in mass analysis.

I thank Dr. Régis Laurent in Molecular, Macromolecular and Supramolecular main group Chemistry in Laboratoire de Chimie de Coordination for huge help with analytical SEC and nice, clean, neat spectra.

Many thanks to Dr. Mladen Litvić and Dr. Ivica Cepanec for their suggestions and discussions on advantages and drawbacks of various synthetic methods.

I thank to Jean-François Nierengarten for all support.

Thanks to Marijana Radić-Stojković for support and help in the Laboratory for Supramolecular and Nucleoside Chemistry, especially during those initial "get to know the world of complexations" days. Also thanks to Lidija-Marija Tumir for every help with measurements and calculations.

Thanks to Phillipe Eyraud for "as soon as possible" publications, most of all for moral support when I was needed, bright thoughts, and availability.

I am especially grateful to all my colleagues and friends in Labs in France and in Croatia.
Nicolas Aubert, petite Souhaila Bouatra, Juan-Luise Delgrado de la Cruz, Majdi Lahd Geagea, Aline Gegout, Uwe Hahn, Adrian Kaeser, Jerome Roeser, Vincent Troiani, Maxence Urbani, Mathieu Walter. Many thanks to Dr. Régis Rein.
Thank you all for your friendship and unmeasurable help.

I would like to thank Dr. Biserka Žinić for her trust and moral support. Many thanks to Dr. Janja Makarević and Dr. Milan Jokić for their enthusiasm, encouragement, advices. I would like to thank to Dr. Vesna Čaplar, Mrs. Elizabeta Furić, Zoran Džolić, Nataša Šijaković-Vujičić, Dr. Leo Frkanec, Dr. Tomislav Portada.
Thanks to Mrs. Barica Baborsky for her help with administrative issues.

A Huge Love to my petite Teresa, for her especial role in many situations during these years of our friendship, for enormous moral support, patience and understanding, for all those tasty dinners, lunches....for all our pleasant and unforgettable moments. Thanks for being in my life !

Finally, without financial support this work would not have been done. For it I would like to thank the Ministry of Science, Technology and Sports of the Government of Croatia, the Embassy of France in Croatia and the Government of France.

Many, many thanks to all who have helped me in any way in this three years work which is outlined in the following pages.

Merci beaucoup a tous les gens que j'avais plaisir a recontre pendant ma vie etudiante en France.

Once again, Many Thanks to all my friends !

PUSE MAMI, TATI !

VELIKE PUSE ANČICI !

NAJVEĆE PUSE POGORELIĆU !

TABLE OF CONTENTS

TITLE OF THE DISERTATION:

Oligonucleotides with Pendant Porphyrins: towards Self-Assembled Multi-Porphyrinic Nano-Materials.

SUMMARY OF THE DISERTATION:

The light-harvesting antennae in the photosynthetic system consist of a large number of pigments, which are responsible for absorption of photons. The extraordinary efficiency of the excited state migration among the pigments is ascribed to their parallel orientation and favoured spacing within the light-harvesting complexes. This arrangement, controlled by weak interactions between pigments and polypeptides, assumes three ring-shaped light-harvesting antennae.

Aiming to organize porphyrins in accordance with the natural system, we have chosen oligonucleotidic backbone for the elaboration of multi-porphyrinic nanosystems. In this respect, the synthesis of oligonucleotides functionalized with porphyrins was realized. The preparation of these systems was based on oligomerization at O-3' and O-5' positions of the 2'-deoxyuridine derivative functionalized with a porphyrin. Architecture of our system has been designed on the basis of rigid and flexible linkers. The porphyrins were appended to C-5 position of the uracile by a rigid linker and the uridines were mutually linked by a flexible linker, with the goal to work out parallel orientation of porphyrins *via* anticipated conformation of the oligonucleotidic chain. In this context, we have synthesized the mono-, di-, tetra- and octa-deoxynucleosides with pendant porphyrins.

An appropriate arrangement of free-base and zinc(II) porphyrins within the oligonucleotidic molecular wire allowed us to highlight an energy transfer. The contribution of the zinc(II)-porphyrin to the emission of the free-base pophyrins was evidenced.

The range of oligonucleotides have been metallated with zinc(II) targeting to examine effectiveness of the oligomerization degree of these molecular architectures on their ability to complex a bidentate base such as DABCO. We have observed that the coordination of DABCO is favoured as one goes toward higher degree of oligomerization due to imposed conformational pre-organization within the oligonucleotidic backbone.

At last, we were interested in self-assembly by means of hydrogen bonding, which could be established between the uracil nucleobase and a complementary synton such as triazine functionalized with porphyrins. The quantitative studies of stability of those supramolecular architectures have evidenced an influence of secondary intermolecular π-π interactions between the porphyrins within the supramolecular complex.

KEY WORDS:

Porphyrins, Uridines, Oligonucleotides, Hydrogen bond, Self-assembly, Supramolecular complexes, Energy transfer, Fluorescence.

TITRE DE LA THESE :

Oligonucléotides à Porphyrines Pendantes: vers des Nano-Matériaux Multi-Porphyriniques Auto-Assemblés.

RESUME DE LA THESE:

Les antennes collectrices d'énergie lumineuse du système photosynthétique sont constituées d'un grand nombre de pigments collecteurs de photons. L'extraordinaire efficacité de migration d'un état excité le long de ces pigments est attribuée à leur orientation parallèle et à leur positionnement favorable au sein des complexes collecteurs. Cet arrangement, contrôlé par des interactions faibles entre pigments et polypeptides, prend la forme de 3 anneaux qui constituent les antennes collectrices d'énergie lumineuse.

Dans le but d'organiser des porphyrines dans l'espace de façon similaire au système naturel, un squelette oligonucléotidique a été choisi pour l'élaboration de nanosystèmes multi-porphyriniques. C'est dans cette optique que nous avons réalisé la synthèse d'oligodeoxynucléotides fonctionnalisés par des porphyrines. La préparation de ces systèmes est fondée sur l'oligomérisation en O-3'et O-5' d'un dérivé de la 2'-deoxyuridine fonctionnalisé par une porphyrine. L'architecture de ces systèmes a été dessinée sur la base de liaisons rigides et souples. Dans le but d'imposer par la conformation de la chaîne oligonucléotidique une organisation parallèle aux porphyrines, ces dernières sont greffées en C-5 de l'uracile par un espaceur rigide et les uridines reliées entre elles par une liaison souple. Un mono-, un di-, un tetra- et un octa-deoxynucléotides à porphyrines pendantes ont notamment été synthétisés.

Un agencement approprié des porphyrines base-libre et métallées au Zn(II) au sein du fil moléculaire oligonucléotidique a permis de mettre en évidence un transfert d'énergie de l'état excité de la porphyrine de Zn(II) vers les porphyrines base-libre. On observe une nette contribution de la porphyrine de Zn(II) à l'émission des porphyrines base-libre.

La série des oligonucléotides a été métallée au Zn(II) dans le but d'examiner l'effet du degré d'oligomérisation de ces architectures moléculaires sur leur capacité de complexation de bases bidendates telle que le DABCO. Nous avons pu montrer que la coordination de DABCO est favorisée au fur et à mesure de l'élévation du degré d'oligomérisation grâce à la pré-organisation conformationnelle qui s'instaure au sein du squelette oligonucléotidique.

Enfin, nous nous sommes intéressés à l'auto-assemblage par liaisons hydrogène que peut établir la base nucléique uracile avec un synton complémentaire telle que la triazine fonctionnalisée par des porphyrines. Des études quantitatives de stabilisation des architectures supramoléculaires ont mis en évidence des interactions intermoléculaires secondaires de type π-π entre les porphyrines au sein du complexe supramoléculaire formé.

MOTS CLES:

Porphyrines, Uridines, Oligonucléotides, Liaison hydrogène, Auto-assemblage, Complexes supramoléculaire, Transfert d'énergie, Fluorescence.

NASLOV DISERTACIJE:

Oligonukleotidi sa vezanim porfirinima: prema samo-organizirajućim multi-pofirinskim nano-materijalima.

SAŽETAK DISERTACIJE:

Antene skupljačice svjetlosne energije u fotosintetskim sistemima sadrže veliki broj pigmenata koji su odgovorni za apsorpciju fotona za fotosintezu. Izvanredna efikasnost prijenosa energije pobuđenog stanja među pigmentima pripisuje se njihovoj paralelnoj orijentaciji i pogodnom razmaku unutar kompleksa skupljači-svjetla. Takav raspored, kontroliran slabim interakcijama između pigmenata i polipeptida, poprima oblik tri prstena koji tvore antene skupljačice-svjetla.

Ciljajući da organizacija porfirina u prostoru bude slična prirodnom sistemu, za razradu multi-porfirinskih nanosistema odabran je oligonukleotidni skelet. U tom smislu realizirana je sinteza oligonukleotida funkcionaliziranih porfirinima. Priprava tog sistema temeljena je na procesu oligomerizacije na O-3' i O-5' pozicijama 2'-deoksiuridinskog derivata funkcionaliziranog porfirinom. Arhitektura tog sistema dizajnirana je na bazi krutih i fleksibilnih poveznica. S ciljem da bi konformacija oligonukleotidnog lanca nalagala paralelnu organizaciju porfirina, zadnje spomenuti su na C-5 uracila vezani preko krute veze, a uridini su međusobno povezani flaksibilnom vezom. U tom kontekstu sintetizirani su mono-, di-, tetra-, i okta-deoksinukleozidi sa prikvačenim porfirinima.

Odgovarajući raspored slobodno-baznog i cink(II) porfirina unutar oligonukleotidne molekulske niti omogućio je istaknuti transfer energije pobuđenog stanja cink(II)-porfirina prema slobodno-baznom porfirinu. Uočen je doprinos cink(II)-porfirina emisiji slobodno-baznog porfirina.

U porfirinske jezgre u seriji oligonukleotida uveden je cink(II) kako bi se ispitao utjecaj stupnja oligomerizacije tih molekulskih arhitektura na njihovu sposobnost kompleksacije bidentatnih baza, kao što je DABCO. Mogli smo pokazati da koordinaciji DABCO-a pogoduju viši stupnjevi oligomerizacije zahvaljujući konformacijskoj pre-organizaciji koja se postiže duž oligonukleotidnog skeleta.

Krajnji interes za samo-združivanje putem vodikovih veza moguć je između uracilne nukleobaze i komplementarnog sintona, kao što je triazin funkcionaliziran porfirinima. Kvantitativna ispitivanja stabilnosti tih supramolekulskih arhitektura istaknula su utjecaj sekundarnih intermolekulskih π-π interakcija među porfirinima unutar supramolekulskog kompleksa.

KLJUČNE RIJEČI:

Porfirini, Uridini, Oligonukleotidi, Vodikova veza, Samo-združivanje, Supramolekulski kompleksi, Transfer energije, Fluorescencija.

I - INTRODUCTION

Dans la nature, de nombreux organismes différents, allant du domaine des plantes aux bactéries, utilisent la photosynthèse. La forme la plus connue de photosynthèse est celle qui est effectuée par les plantes ou les algues, de même que par les bactéries, qui sont responsables d'une majeure partie de ce processus dans les océans. Le plus utilisé de tous les systèmes photosynthétiques est sans conteste celui de la *bactérie pourpre*. Dans ces bactéries, la photosynthèse fonctionne grâce à des photosystèmes qui utilisent l'énergie de la lumière pour induire des photoréactions vers des potentiels électrochimiquement stables et qui est stockée sous forme d'énergie chimique. L'énergie induite par la lumière est absorbée par un réseau de pigments, des *bactériochlorophylles* ou des *caroténoïdes*. Les pigments qui absorbent l'énergie dans la bactérie photosynthétique sont liés de façon non covalente à deux types de protéines membranaires, l'une formant un centre réactionnel (CR), et l'autre formant des complexes à effet d'antenne. Soulignons que seulement quelques pigments dans le CR prennent part directement aux réactions photochimiques, tandis qu'un réseau de pigments est nécessaire pour l'effet d'antenne en capturant la lumière du soleil et en convoyant l'état excité vers le CR. Les membranes photosynthétiques de la bactérie pourpre contiennent deux types de complexes qui collectent la lumière : le LH2 est l'antenne extérieure puisque l'énergie collectée va vers le CR à travers une autre antenne qui est l'antenne intérieure LH1, cette dernière entourant alors immédiatement le CR. Le premier processus de la photosynthèse chez la bactérie consiste en l'absorption d'un photon par l'antenne LH2. Le rôle de l'assemblage sous forme de cercle de BChl et caroténoïdes dans la matrice protéinique est celui d'une antenne, absorbant les photons qui arrivent sur la surface relativement large qu'ils couvrent. Tout le système collecteur de lumière de la bactérie photosynthétique met en jeu une hiérarchie énergétique prononcée. Cette dernière induit un système de type « cascade » des états excités qui canalisent la migration de l'état excité de l'antenne extérieure LH2 à travers LH1 vers le CR. Les transfert l'état excité qui partent en cascade vers le CR impliquent de rapides processus au sein des complexes et de plus lents processus entre les complexes, définis comme des transferts complexes pigment-protéine (LH2→LH2, LH2→LH1, LH1→CR), respectivement. L'efficacité de ces transferts d'énergie est due aux caractéristiques structurales originales des complexes LH de la bactérie, à savoir une organisation circulaire des agrégats BChl. En principe, un transfert d'un état excité dans les systèmes photosynthétiques à effet d'antenne est décrit par un mécanisme de type Förster, qui est la conséquence de la distance relativement large entre les pigments.

Les pigments dans le système photosynthétique naturel sont structuralement voisins des porphyrines. Par conséquent, des porphyrines chimiquement stables ont été largement utilisées pour mimer le système à effet d'antenne naturel puisqu'elles possèdent une large bande d'absorption qui couvre entièrement le spectre visible. De plus, les porphyrines sont des briques de base assez populaires puisqu'elles peuvent être facilement synthétisées et fonctionnalisées, elles sont larges et rigides, elles sont riches spectroscopiquement et elles possèdent de remarquables propriétés photochimiques. Ces avantages ont motivé de nombreux chimistes pour la création d'antennes collectrices de lumière à base d'unités porphyriniques et pour l'exploration de leurs propriétés photochimiques. Dans le but de mimer la grande efficacité des systèmes photosynthétiques naturels, qui est basée sur une bonne organisation des molécules pigments, le squelette portant les chromophores porphyriniques devra posséder des capacités structurales auxquelles il sera possible de se fier.

1. PHOTOSYNTHESIS.

It has been estimated that the average yearly incidence of solar radiation at the earth's surface amounts to several orders of magnitude more energy than is consumed by its population.[1] Clearly, harnessing this energy is an important endeavor that will reduce our dependence on fossil fuels. With limited supplies of fossil fuels and increasing concern about CO_2 emissions, further development of photosynthesis-based technologies for energy collection is certainly warranted. Indeed, our own existence depends on light-harvesting by the plethora of photosynthetic organisms in the biosphere. These organisms have evolved intricate and extremely efficient mechanisms for the transduction of light into chemical energy in the form of ATP.[1] If we are to utilize sunlight in a similar fashion, it is not unreasonable to borrow some design concept from structures who have evolved over billions of years. However, photosynthesis and related processes can be applied to many more areas than just solar energy conversion. For example, many synthetic pigments have found biomedical uses in tumor detection due to their fluorescent features; in biotechnology field, photosynthetic organisms play an increasing role for the production of enzymes. Research in photosynthesis in all facets has proven to have opened many doors in a variety of disciplines. Hence, it is likely that photosynthesis and its applications will help to shape an increasingly broad area of exciting discoveries and innovative ideas.

In the nature, photosynthesis is carried out by many different organisms, ranging from plants to bacteria, Figure 1. The best known form of photosynthesis is the one carried out by higher plants and algae, as well as by cyanobacteria and their relatives, which are responsible for a major part of photosynthesis in oceans.

Figure 1. *Examples of photosynthetic organisms: leaves from higher plants flanked by colonies of photosynthetic purple bacteria (left) and cyanobacteria (right).*

To date, the most studied of all photosynthetic systems is probably that of purple bacteria.[2-8] Purple photosynthetic bacteria are a group of anaerobic prokaryotes that are commonly found in the anaerobic layers in aquatic environments. Their typical habitat places them in the water column below oxygenic photosynthetic organisms such as aquatic plants, algae and cyanobacteria. Photosynthesis in these organisms is driven by photosystems that use energy of light for light driven reactions toward stable electrochemical potential which is stored as chemical energy by series of dark reactions. The energy provided by light is absorbed by a network of antenna pigments, primarily chlorophylls or bacteriochlorophylls and carotenoids. Chlorophylls absorb light in the red and blue parts of spectra, while carotenoids absorb blue-green light (hence plants are green). As a consequence, light of these wavelengths is not available for the purple bacteria which are present deeper in the lake. The purple bacteria, therefore, have evolved a form of photosynthesis using bacteriochlorophylls (Bchl) and carotenoids. These pigments can harvest the light energy in the near infrared (NIR) and green regions of the spectrum.

1.1. The purple bacterial photosynthetic unit.

All photosynthetic organisms have developed from a few common components a rather divergent set of antenna complexes. Anoxygenic photosynthetic (purple and green) bacteria employ a single reaction center (RC). Oxygen-evolving photosynthetic organisms, e.g., cyanobacteria and plants, posses in their photosynthetic units (PSU) two RCs of different types, namely PS-I and PS-II, and additional light-harvesting (LH) complexes that display significant structural variability among species.[8-11] A valuable model for understanding the multiprotein photosynthetic apparatus is extensively studied in anoxygenic photosynthetic organism of purple bacteria.[2-8]

The light-absorbing pigments in bacterial photosynthesis are non-covalently bound to two types of integral membrane proteins, one forming RC and the other forming light-harvesting or antenna complexes, Figure 2. It is worth to mention that only few pigments in the RC directly take part in photochemical reactions, while an array of pigments serve as light-harvesting antennae by capturing the sunlight and funnelling electronic excitation toward the RC.[12] The combination of RC with aggregates of chlorophylls and associated carotenoids, namely LH complexes is called the PSU, and it is universal in both photosynthetic bacteria, and higher plants.[9,11,13,14]

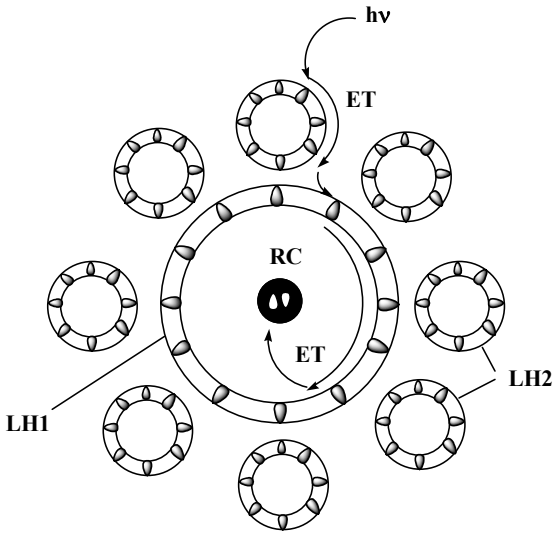

Figure 2. *Schematic representation of bacterial light-harvesting complexes (LH1 and LH2), showing the different protein-embedded light-absorbing porphyrins arranged in circles around the reaction center (RC). The path of energy transfer (ET) is indicated by arrows.*

In most purple bacteria, the photosynthetic membranes contain two types of LH complexes with distinct biochemical and spectroscopic properties. The LH2 is the outer antenna, because the energy it collects flows to its final destination through another[3,4] LH1 or inner antenna complex[6,15,16] which immediately surrounds the RC[17,18] to which the light energy is transferred. For some bacteria, such as *Rhodopsedomonas (Rps.) acidophila* and *Rhodopsirillum (Rs.) molischianum* strain DSM 120,[3,4,19] exists a third type of light-harvesting complex, LH3. A 1/1 stoichiometry exists between the RC and LH1;[20] the number of LH2 and LH3 varies according to growth conditions such as light intensity and temperature.[21] The photosynthetic apparatus can contain up to about 10 LH2 around each LH1; LH2 of *Rps. acidophila* contain nine αβ-heterodimers. The atomic structure of LH2 assembly has nine identical units, each consisting of two fairly short α-helical polypeptides, nine α-apoproteins and nine helical β-apoproteins, and associated pigment molecules between these protein walls. Within one unit, each αβ-heterodimers coordinates three BChls and one carotenoid, and therefore they absorb at different wavelengths. The pronounced energetic hierarchy in the light-harvesting systems is based on the following spectral features: LH2 absorbs maximally at 800 and 850 nm, and LH1 absorbs at lower energy (875 nm). The energy cascade imposes directionality on the energy transfer reactions and ensures that the light energy absorbed by LH2 is funnelled 'downhill' to LH1 and onto the RC. Analysis of the LH1 and LH2 structures indicates that each BChl of the B850 ring of LH2 and of the B875 ring of LH1 in noncovalently bound to three side-chain atoms of the α- or β-apoprotein such that the BChls are held in a rigid orientation. The planar organization of the BChls in the PSU is optimal for the transfer of electronic excitation to the RC.

Today, structures of the major components of the bacterial photosynthetic apparatus are available at atomic resolution. The RC from *Rps. viridis* was the first membrane protein to have its 3D structure solved to high resolution by J. Deisenhofer, R. Huber and H. Michel. For this groundbreaking work these authors were awarded the Nobel Prize for Chemistry in 1988.[17,18] The high resolution crystal structures of LH2 have been determined from *Rps. acidophila* by G. McDermott *et al.* in 1995.[3,4] The structure of LH1 was investigated by electron crystallography of two-dimensional crystals from *Rhodospirillum rubrum*.[6] Based on high degree of homology of the αβ-heterodimer of LH1 from *Rb. sphaeroides* to that of LH2 of *Rs. molischianum*, an atomic structure for LH1 of *Rb. sphaeroides* has been modelled.[19,22]

1.2. Structural features of light-harvesting antennae.

The primary process in bacterial photosynthesis is the absorption of a photon by the LH antenna system. The role of ring-shaped assembly of BChl and carotenoid moieties embedded in a protein matrix is that of antenna, absorbing photons that strike the relatively large surface area that they cover. The crystal structure of the LH2 complex from the purple photosynthetic bacterium *Rhodopseudomonas acidophila* strain 10050 has revealed a modular complex with pigment molecules enclosed by protein, Figure 3.[4]

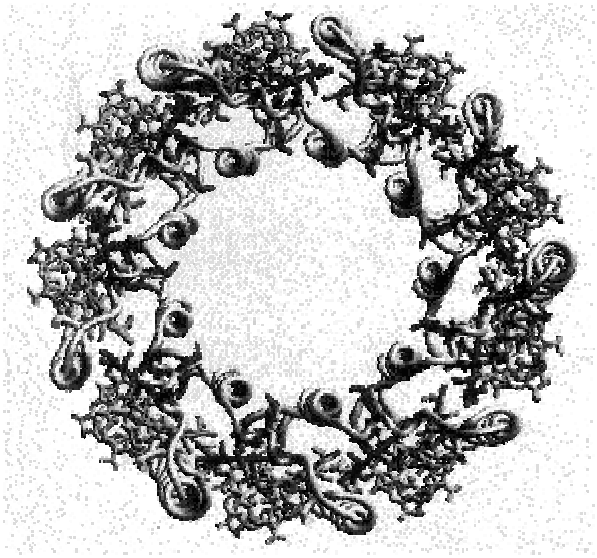

Figure 3. *The nonameric LH2 complex from Rhodopseudomonas acidophila; the α-helical segments are represented as ribbons with the α-apoproteins inside and the β-apoproteins outside. The two distinct groups of coordinated bacteriochloropyll molecules (for clarity reasons are shown only as porphyrin macrocycles).*

The LH2 complex is composed of light-absorbing pigments, bacteriochlorophyll *a* (BChl *a*) and carotenoids, which are non-covalently bound to low-molecular-weight hydrophobic α- and β-apoproteins. The α-apoprotein contains 53 amino acids, and the β-apoprotein 41. The full structure of the antenna complex is $\alpha_9\beta_9$ nonamer with αβ-heterodimer as the basic structural element. The transmembrane helices of nine α-apoproteins are packed side by side to form a hollow cylinder of radius 18 Å. The nine helical β-apoproteins are arranged radially with the α-apoproteins to form an outer cylinder of radius 34 Å. Between these two concentric rings of transmembrane α-helical proteins each α-β-polypeptide pair binds three BChls and one carotenoid. Hence, BChl *a*-binding histidines of the α (His 31) and β (His 30) apoproteins face outwards and inwards, respectively, forming a complete ring of 18

overlapping BChl *a* molecules situated near the periplasmic membrane surface. The nine remaining BChl *a* molecules are packed between the β-apoprotein helices. The group of nine Bchl *a* molecules absorb at 800 nm (B800) and eighteen tightly coupled ones absorb at 850 nm (B850). In this B800-850 complex carotenoid absorbs visible light at 500 nm. An estimation of the stoichiometric amount of carotenoid in the complex suggested a carotenoid/BChl ratio of 1/2, accordingly 13-14 molecules for this assembly. It was found that carotenoid is not associated with any single apoprotein, though it spans the depth of the membrane.

The LH1 complex has a very similar structure; it is the ring-shaped assembly built up from the same type of molecular units as LH2 embedded in a protein matrix that immediately surrounds the RC. It is a hexadecameric aggregate of αβ-heterodimers, namely $\alpha_{16}\beta_{16}$ oligomer that is considerably wider then LH2 to accommodate the RC. It contains a single ring of 32 tightly coupled Bchl molecules with the main absorption band at 875 nm (B875). It is remarkable that antenna complexes result from the self-aggregation of a large number of identical, noncovalently bonded trans-membrane helices, BChls, and carotenoids. Among this, the protein cage not only provides a 'scaffold' that correctly orientates the pigments for optimal rates of energy transfer, but also creates an environment that can control the wavelengths at which the different groups of Bchls absorb light, thereby creating the energy funnel described above.

The bacterial LH complexes bear no structural resemblance to the plant LH complex (LHC-II), even though some governing principles of construction, in particular the distance between chlorophylls and their close association with the photoprotective carotenoids, are similar in both cases.[7] LHC-II is the most abundant LH complex located in chloroplasts of green plants. Its structure features twelve or more chlorophylls and two carotenoids as light-absorbing agents per polypeptide, and lacks the repetitive simplicity of LH1 and LH2. The two complexes represent quite different answers to the same biological problem of efficient light absorption and energy transfer in a membrane.

1.3. Energy transfer within the photosynthetic unit.

Photosynthetic bacteria evolve a pronounced energetic hierarchy in the light-harvesting system. The hierarchy furnishes a cascade-like system of excited states that funnels electronic excitation from the outer LH2 through LH1 to the RC. The excitation transfer cascading into the RC involves faster intracomplex and slower intercomplex processes, defined as excitation transfer within each pigment-protein complex (LH2, LH1, RC) and between pigment-protein complexes (LH2→LH2, LH2→LH1, LH1→RC), respectively. The high efficiency of excitation energy transfer arises from the intriguing structural feature of the bacterial LH complexes notably their circular organization of BChl aggregates. It was found that entire excitation transfer in the PSU occurs in less then 100 ps and with about 95% efficiency.[5]

When an 800 nm photon is absorbed, excitation energy of the B800 is transferred within LH2. Excitation dynamics in LH2 can be described as a sequence of transfer steps between two spectral bands, from B800 to B850. It takes 0.7 ps for the energy to be transferred from B800 to the B850 ring of Bchl molecules.[5,23] It is known that the excitation energy absorbed by carotenoids at the wavelength of 500 nm is transferred to the same B850 ring within 0.2 ps.[5] Once the excited state reaches B850 ring it is delocalized between the B850 Bchls in a few tens of fs. The extremely rapid delocalization between the B850 BChls in LH2 can be reached on account of favourable orientation and close proximity, hence strong interactions, leading to coherent superpositions, termed excitons.[23,24] The ring of B850 BChl molecules acts rather like a 'storage ring' at which any part is available for energy transfer to any neighbouring LH1 complex. The B850 and B875 pigments are facing the same side of the membrane and therefore energy can easily jump the short distance between the adjacent complexes. This intercomplex energy transfer proceeds within 3~5 ps.[25] The LH1 absorbs at a longer wavelength providing an energy funnel for the RC, which acts as an energy sink. The final step corresponds to energy transfer from LH1 to the special BChl pair electron donor in the RC. The slow 35 ps transfer time shows that this is the slowest step in the overall trapping of light energy by the RC.[5,26] This slow rate is a direct consequence of the size of the RC protein, which prevents a shorter antenna-RC distance. In this way, the energy contained in any photon that strikes the pigments within the extensive LH system is conducted in a very short time, and with minimal loss of energy, from the point where it is absorbed to where it is needed.

In principle, an excitation transfer in photosynthetic antenna systems is in most cases described as incoherent Förster hopping.[2,5] Due their relatively large distance an energy

transfer from B800 to B850 and between the B800 molecules was characterized by incoherent Förster mechanism. Further, even the larger distance of ~30 Å found between LH2 and LH1 indicates as well Förster energy transfer. Among these, the exciton concept has sometimes been applied for photosynthetic antenna systems. Depending on the strength of exciton coupling between the chromophores, the energy transfer can lay in the strong coupling limit (coherent) and weak coupling limit (hopping), or intermediate regime.[27]

2. PORPHYRIN-BASED LIGHT-HARVESTING ANTENNAE.

The word *porphyrin* is derived from the Greek *purphura* meaning purple, and all porphyrins are intensely coloured.[28] Porphyrins belong to macrocyclic compounds which commonly occur in nature, both as metal free species or as metalloporhyrins. They play very important roles in various biological processes, among which photosynthesis is the most essential representative. Their structurally related pre-eminent representatives in nature are: heme, chlorophylls, bacteriochlorophylls, and vitamin B_{12}.

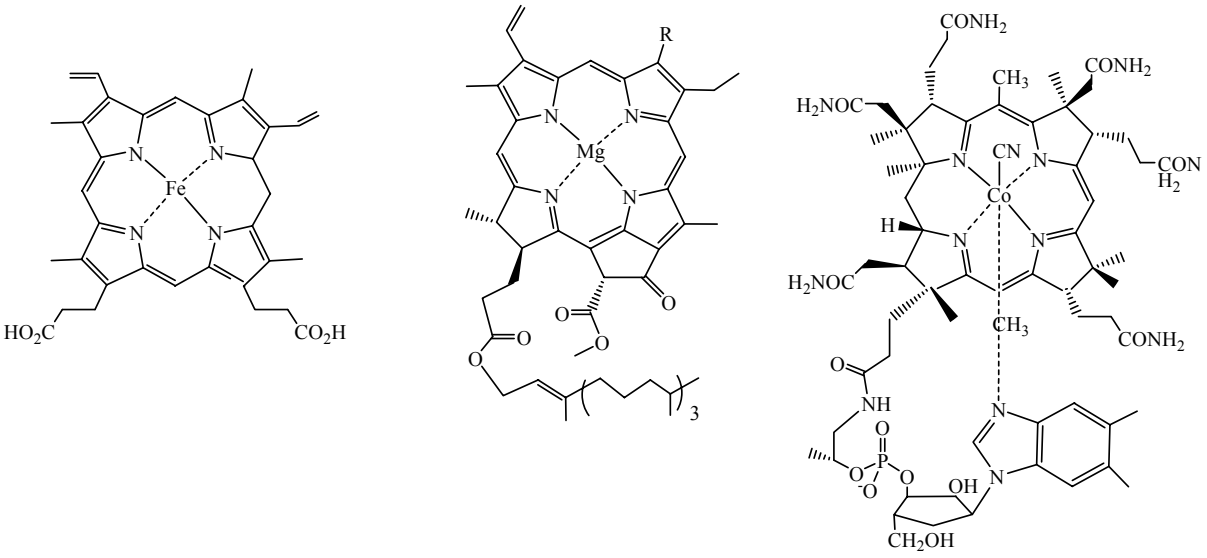

Heme

R= CH_3 Chlorophyll a
R= CHO Chlorophyll b

Vitamin B_{12}

Figure 4. *Pre-eminent representatives of porphyrins in nature.*

In all natural photosynthetic systems, the chlorophylls and bacteriochlorophylls play a major role in the light-harvesting cycle. Using bacteriochlorophylls in artificial antenna systems is difficult since they are not chemically stable. Therefore, chemically stable porphyrins have been used extensively in mimicry of the natural antenna systems due to their broad range of optical absorption covering the entire visible spectra. Moreover, porphyrins are popular building blocks because they are easily sythesized and functionalized, they are large and rigid, they are spectroscopically rich, and they have remarkable photochemical properties.[29-32] Behind the efficiency of photosynthetic organisms, pigment molecules are non-covalently bound to polypeptides in a specific and highly ordered manner. The antenna polypeptides determine the type, number, position, orientation, distance and environment of the pigments.[7,8] Their structural features have motivated chemists to design artificial light-harvesting antennae consisting of multiple porphyrin units and to explore their photochemical properties. Further on, we represent some molecular architectures of light-harvesting multi-porphyrinic arrays developed in the field of better understanding of geometry-dependent photochemical events involved in biological photosynthesis in accordance with the disposition proposed by T. Aida and co-workers.[33]

2.1. Ring-shaped light-harvesting antennae.

Ring-shaped multiporphyrinic arrays[34-39] are interesting candidates for artificial light-harvesting antennae which are intended to mimic structural aspects of the ring-like chromophore arrays in photosynthetic purple bacteria. Cyclic hexamer I consists of an alternating arrangement of zinc and free-base porphyrins joined by diphenylacethyne linker.[40] It has been synthetized by a palladium-mediated coupling of a zinc complex of bis(4-acethynylphenyl)porphyrin and a free-base bis(3-iodo-phenyl)porphyrin in the presence of a template molecule.

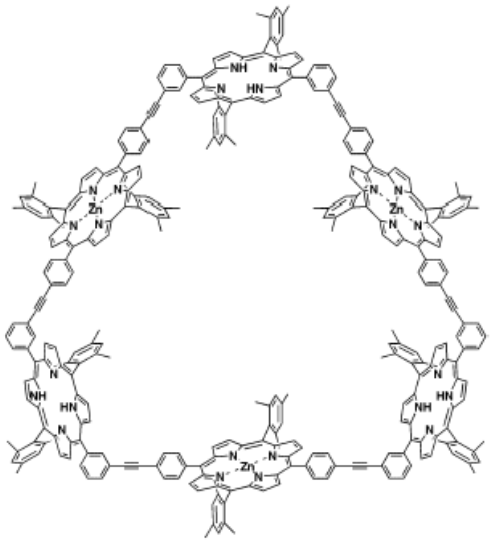

Figure 5. *Cyclic hexamer I synthesized by Lindsey and coll.*[40]

The distance from the center of the zinc porphyrin plane to the center of the cavity has been found to be 15.2 Å, and from the zinc to the free-base porphyrin 17.6 Å. Time-resolved spectroscopy has shown that the photoexcited singlet state of the zinc porphyrin units has a lifetime (τ) of 17 ps, from which the zinc porphyrin-to-free-base porphyrin energy transfer rate constant (k_{ENT}) and the quantum efficiency (Φ_{ENT}) have been evaluated to be 2.9 x 10^{10} s^{-1} and 99%, respectively.

In contrast, cyclic hexamer II, which consist of five zinc porphyrin units and a single free-base porphyrin unit, shows a Φ_{ENT} value of only 40%.[41]

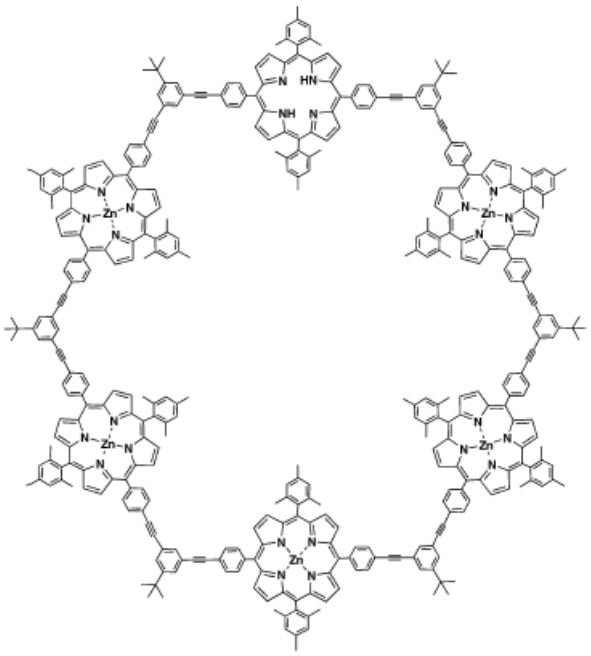

Figure 6. *Cyclic hexamer II synthesized by Gossauer and coll.*[41]

Although the advantages of such ring-shaped chromophore arrays over linear analogues in intramolecular energy transfer have been discussed in the literature,[42] the realization of energy transfer along the ring system still remains a challenge.

2.2. Star-shaped light-harvesting antennae.

Star-shaped porphyrin pentamers consisting of a focal free-base porphyrin unit attached to four peripheral zinc porphyrin units have been extensively studied as simple models of biological light-harvesting antennae. Compound III is an early example of a multiporphyrin array that makes use of dipenylethyne spacers. The synthesis of ethyne-linked porphyrin units was examined in order to establish coupling conditions suitable for the synthesis of the arrays. The pentamer III has been synthesized by homogeneous palladium-mediated coupling of a tetraiodo free-base porphyrin as a core unit and monoacethynyl zinc porphyrin units as a peripheral units.[43]

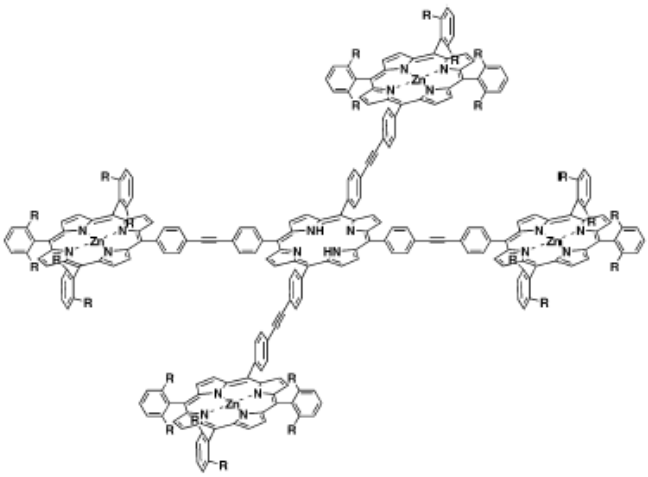

Figure 7. *Star-like pentamer III synthesized by Lindsey and coll.*[43]

The center-to-center distance of the core free-base porphyrin unit to the peripheral zinc porphyrin units has been found to be 20 Å. The electronic donor-acceptor interaction has been shown weak, the absorption spectrum of the compound III is thus a superposition of the spectra of the component parts. The zinc porphyrin-free-base porphyrin energy transfer efficiency (Φ_{ENT}) has been estimated to be ~90%, based on the fluorescence quenching of the zinc porphyrins and on the near-matching of the excitation and absorption spectra.[44]

The tetranucleosidic pentamer IV has been prepared by construction of the central free-base porphyrin unit from uridine-zinc porphyrin conjugate functionalized with benzaldehyde at C-5 position of the uridine under conditions developed by Lindsey. This compound contains flexible linkers, thus allowing the zinc porphyrin units to wrap around and electronically shield the free-base porphyrin unit.[45]

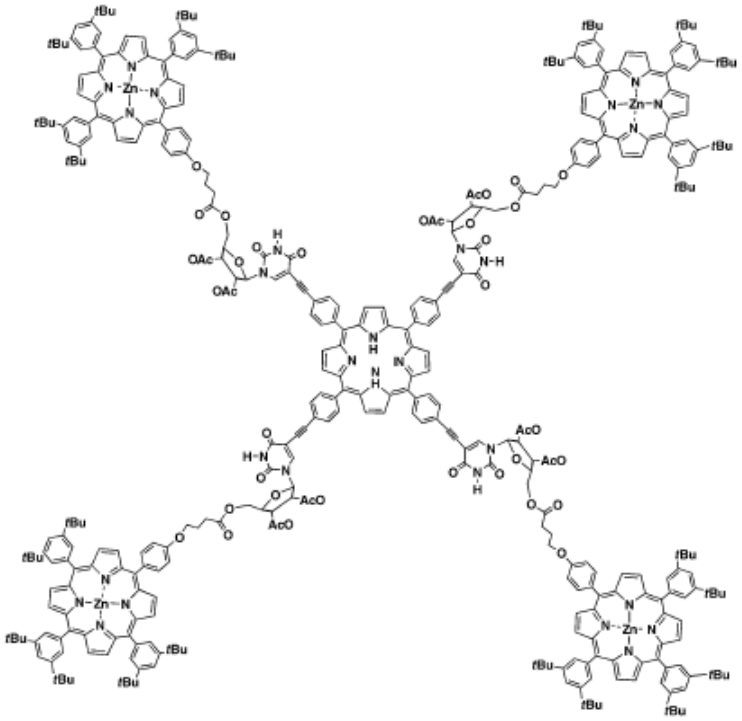

Figure 8. *Star-like pentamer IV synthesized by Solladié and coll.*[45]

Nevertheless, steady-state fluorescence spectroscopy studies have shown that compound IV displays essentially identical zinc porphyrin-to-free-base porphyrin energy transfer characteristics as compound III.

2.3. Windmill-shaped light-harvesting antennae.

The synthesis and photochemical properties of windmill-shaped multiporphyrin arrays have been investigated; their molecular structures allow incorporation of a larger number of chromophore units in three-dimensionally orthogonal geometry, thereby increasing the absorption cross-section. Windmill-like multiple zinc-porphyrin arrays with a *meso-meso*-coupled zinc porphyrin dimer (V, n= 1,2) as its center have been synthesized as well as polymeric homologues.[46,47]

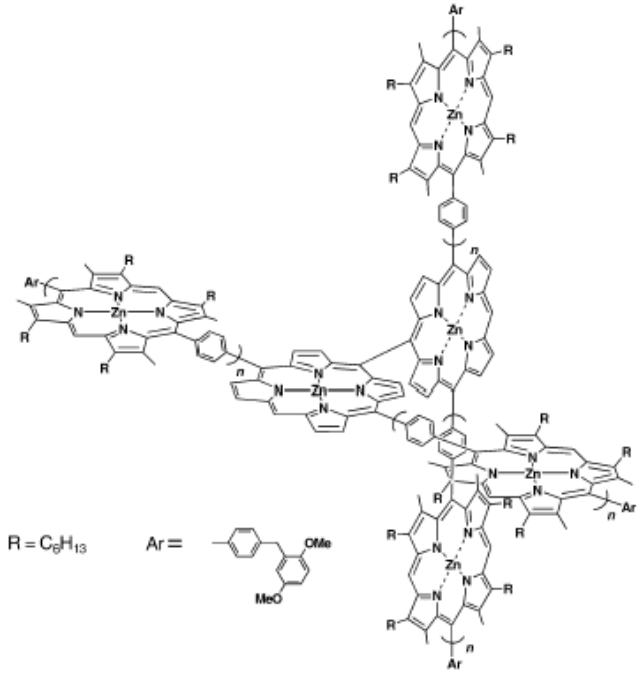

Figure 9. *Windmill-like zinc-porphyrin array V (n= 1,2) synthesized by Osuka and coll.*[46,47]

An advantageous feature of compound V as a light-harvesting functional unit has been revealed in energy gradient from the peripheral zinc porphyrin units to the *meso-meso*-coupled zinc porphyrin dimer in the singlet state. Namely, the singlet state of the focal zinc porphyrin dimer in V has slightly lower energy (2.08 eV) then those at the periphery (2.15 eV). The energy difference (0.07 eV) has enabled the excitation energy flow from the periphery to the central core. In fact, photoexcitation of V at 540 nm results in an enhanced emission from the *meso-meso*-linked zinc porphyrin units (651 nm) at the expense of the fluorescence from the peripheral zinc porphyrin units (580 and 629 nm). Time-resolved spectroscopy has revealed that the emission from the peripheral porphyrin units that predominated at an early stage decay more rapidly than that from the diporphyrin core. It thus has been shown that V has dual fluorescence decay behaviour, which is composed of two exponential components with lifetimes of 27 ps (72%) and 1.6 ns (28%) which are assignable to the decays of the peripheral and core zinc porphyrin units, respectively. It was interpreted that the short-lived component mainly reflects the decay of the singlet state of the peripheral porphyrin units and that the longer lived component mainly reflects the decay of the singlet state of the focal zinc porphyrin dimer.

2.4. Dendritic light-harvesting antennae.

Example of dendritic multiporphyrin arrays includes a nonameric zinc porphyrin array constructed with a combination of rigid and flexible linkers, ethynylene and ester, respectively. Compound VI, which consists of an energy-accepting free-base porphyrin core decorated with eight energy-donating zinc porphyrin units, was synthesized for photochemical studies.[48]

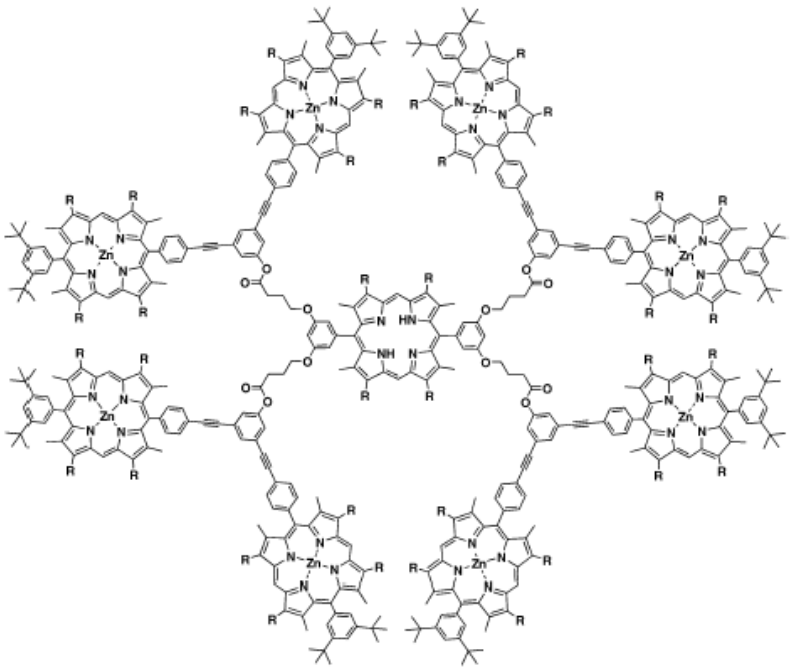

Figure 10. *Dendrimer-like nonamer VI synthesized by Sanders and coll.*[48]

The absorption spectrum of VI has been shown to be a superposition of the spectra of the constituent monomeric porphyrins, suggesting a relatively weak electronic interaction between the porphyrins. Excitation of the zinc porphyrin units results in fluorescence emission of the free-base porphyrin focal core as a result of a zinc porphyrin-to-free-base porphyrin energy transfer. Evaluation of the fluorescence decay profile of the zinc porphyrin units shows that the energy transfer takes place rather slowly (k_{ENT}= 9 x 10^8 s^{-1}) with a quantum efficiency (Φ_{ENT}) of 60%. The fluorescence quantum yield of the free-base porphyrin core is virtually identical to that of the model porphyrin monomer.

3. AIMS OF THE THESIS.

In the photosynthetic systems, the extraordinary efficiency of the energy migration over long distances with minimal loss of energy is ascribed to the favored spacing and orientation of the chromophores which are held in an appropriate parallel orientation. The symmetrical arrangement of the chromophores is based on α-helical polypeptides which bind these molecules in a specific and highly ordered manner. Beyond the control of the structure of multi-chromophoric arrays, monitoring the spatial orientation of the chromophores in artificial light-harvesting devices is a challenge of growing interest.

With the aim of mimicking such systems, the scaffold for the porphyrin chromophores should be based on molecular components with reliable structural abilities. In terms of their structural features, oligonucleotides are favorable candidates for this purpose. Therefore, chemically modified oligodeoxynucleotides with pendant porphyrins were envisaged. The synthetic strategy has involved oligomerization of the relevant uridine-porphyrin conjugate in 3'-5' stepwise manner by using ether-ester type of spacer of suitable length. The elaborated covalent bonding between uridine-porphyrin units has featured flexible linker to work out anticipated helicoidal organization of the modified oligonucleotidic backbone and parallel orientation of appended porphyrin units. To this end, a series of uridine-porphyrin conjugates of different range, i.e. up to octamer, were synthesized.

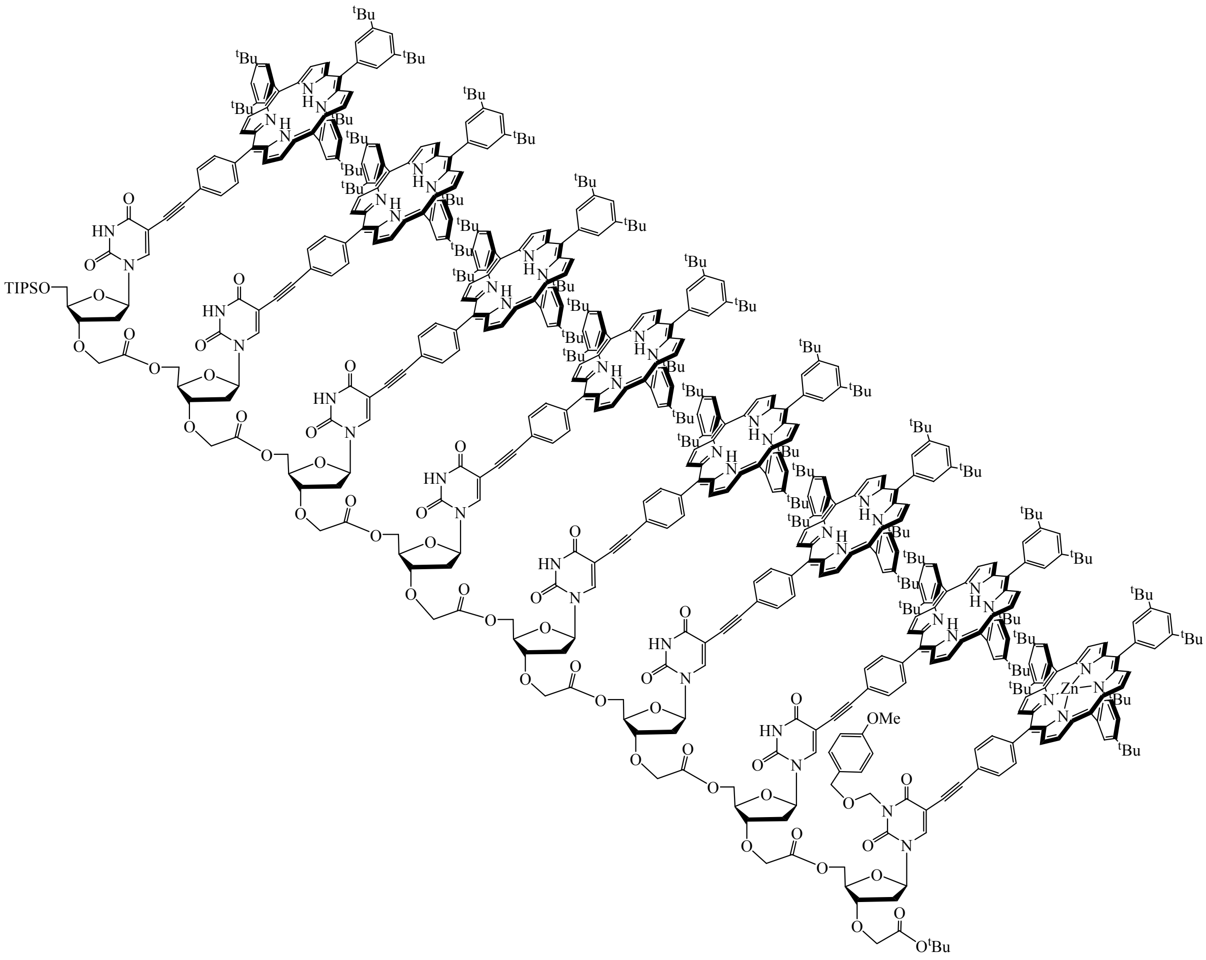

The envisaged spatial organization is related to the conformation that was found by CD analysis of the nona-porphyrin with nucleosidic linker, which was synthesized in our laboratory.[49] The optical activity displayed by the compound was attributed to a porphyrin helicity induced by the enantio-purity of the nucleosidic linkers.

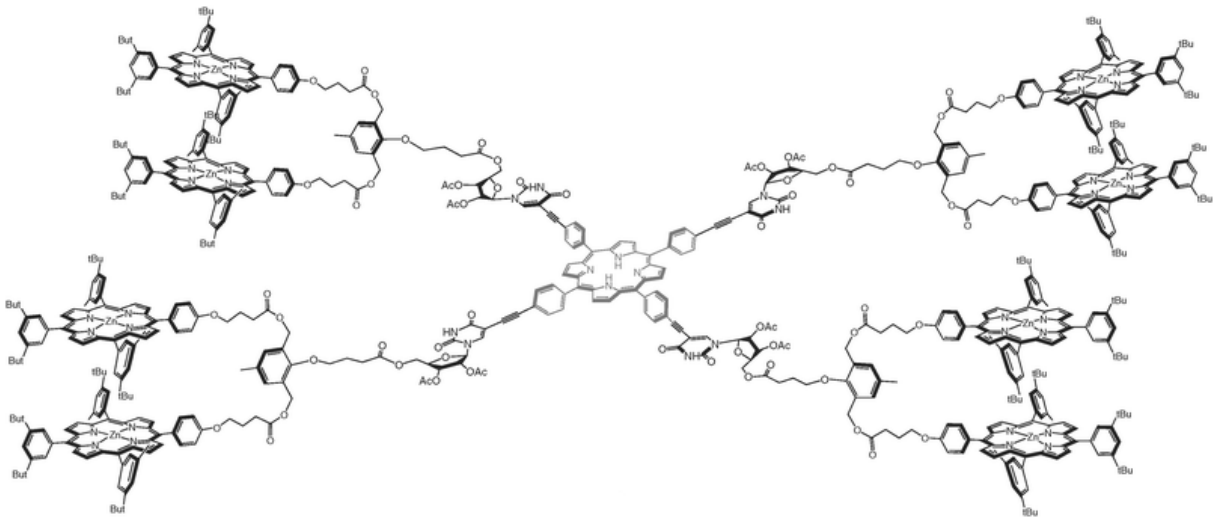

It is also related to the polypeptidic backbone with pendant porphyrinic array, which was synthesized in our laboratory.[50] The VCD analysis of that octamer has shown that it is in the form a right-handed 3_{10} helix.[51]

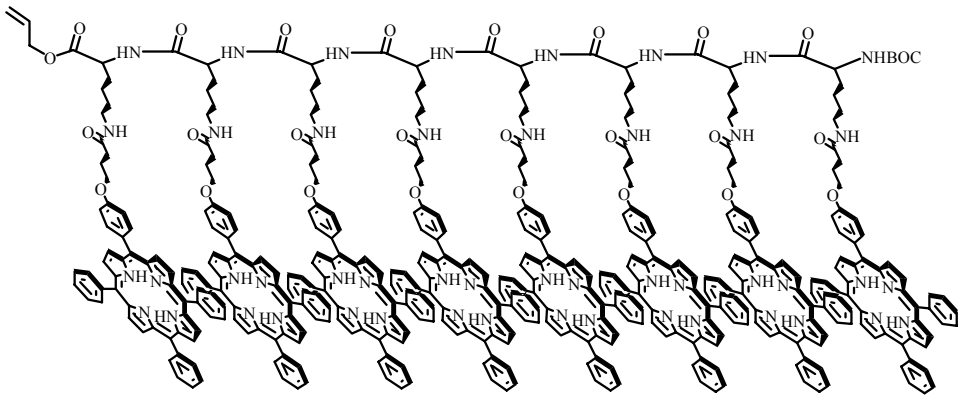

Mimicry of the natural light-harvesting complexes has led us to construct supramolecular assemblies with the porphyrin array. Therefore, after complete metallation with zinc(II), obtained porphyrin arrays were subjected to formation of organized assemblies through axial coordination of the small, rigid, bidentate ligand such as 1,4-diazabicyclo[2.2.2]octane (DABCO).

In addition, our efforts have been focused on construction of supramolecular assemblies through simultaneous recognition by hydrogen-bonding and π-π interactions between uridine-porphyrin conjugate and a rationally designed porphyrin-based triazine receptors. By varying

the sequence of metallated and free-base porphyrins, this study has served to provide the noncovalently bounded photosynthetic system through which photoinduced energy transfer might be facilitated.

II – RESULTS AND DISCUSSION

Notre intérêt s'est focalisé sur la synthèse de complexes artificiels collecteurs de lumière comprenant des porphyrines attachées de façon covalente à des oligonucléotides modifiés tels que des squelettes biopolymères. L'utilisation d'oligonucléotides modifiés en tant que squelette nous a été dictée par notre volonté de former des réseaux de porphyrines organisés. Les modifications des nucléosides et des substituants sur la porphyrine ont été choisies de manière à obtenir l'orientation parallèle désirée des porphyrines le long du fil oligonucléosidique. La stratégie de synthèse est basée sur l'oligomérisation des unités uridines avec des porphyrines variées, métallées ou non, suivant les propriétés physico-chimiques que nous désirerons obtenir. Les unités uridines-porphyrines élaborées ont été couplées en 3'-5', comme les nucléotides dans l'ADN ou l'ARN naturels, en utilisant des espaceurs de type éther-ester pour obtenir la longueur appropriée. L'oligomérisation, par réaction d'estérification entre l'acide en position 3' et l'alcool en position 5', est fondée sur un choix approprié de déprotection sélective des deux groupes protecteurs, *tert*-butyle pour l'ester et triisopropylsilyle pour l'alcool. De cette façon, une stratégie de synthèse itérative de type divergente-convergente peut être appliquée pour l'oligomérisation. Le lien internucléosidique éther-ester est stable, neutre et induit un squelette flexible. L'architecture de notre système est basée sur une combinaison de liens flexibles et rigides de telle sorte que les porphyrines sont accrochées à la position appropriée de l'uracile par l'intermédiaire du lien rigide acétylénique, et la connexion covalente entre les unités uridine-porphyrine est un lien flexible. Ces liens covalents ont été employés afin d'obtenir une structure hélicoïdale et par la même, une orientation parallèle des porphyrines à travers la conformation en hélice du squelette oligonucléotidique. De manière analogue aux brins simples hautement organisés et aux structures double hélices des oligonucléotides dans les systèmes biologiques, nous espérons obtenir un espacement ainsi qu'une orientation préférentiels des macrocycles porphyriniques. Dans cette optique, nous avons réalisé la synthèse de systèmes uridine-porphyrine de type dimère, tétramère et octamère.

Les systèmes uridine-porphyrine ont été soumis à une analyse conformationnelle en utilisant la spectroscopie RMN et des études préliminaires de photochimie ont été réalisées en utilisant les spectroscopies d'absorption et de fluorescence. La spectroscopie RMN s'est révélée être un bon point de départ pour la détermination de la conformation de la molécule. Les spectres RMN des systèmes moléculaires synthétisés ont été initialement enregistrés dans le chloroforme deutéré. Comme on l'attendait, les spectres n'étaient pas suffisamment exploitables pour l'assignement des protons et pour l'analyse conformationnelle subséquente. Afin de remédier à ce problème, un effet de solvant a été examiné. Sur la base d'interactions

présumées par liaisons hydrogènes entre les unités uracile, nous avons utilisé de l'acétone deutéré comme solvant polaire puisque nos composés ne sont pas solubles dans le DMSO deutéré. D'un autre côté, en considérant l'interaction entre les systèmes π, la faible séparation des pics pourrait être évitée avec un solvant anisotrope magnétique tel que le benzène deutéré. Après comparaison entre le benzène deutéré pur, l'acétone deutérée pure de même que des mélanges variés d'acétone deutérée, de benzène deutéré et de chloroforme deutéré en proportions différentes, l'acétone deutéré fournit la meilleure résolution des signaux. Les interactions électroniques entre deux ou plusieurs unités porphyriniques identiques ou presque similaires ont été étudiées au sein de tous les systèmes dimère, tétramère et octamère. Ces derniers sont constitués d'une porphyrine de zinc sur l'uridine terminale du squelette nucléosidique et de porphyrines base-libre sur toutes les autres uridines dans le squelette. Une telle constitution permet d'étudier la migration des états excités. Ainsi, nous nous attendons à ce que l'énergie photonique absorbée par la porphyrine de zinc terminale soit transférée vers les porphyrines base-libre le long du réseau. L'existence d'un transfert d'énergie dans nos systèmes porphyriniques a été examinée par spectroscopie de fluorescence.

Ces dernières années, les chercheurs se sont investis dans le développement de différentes méthodes visant à mimer les complexes naturels collecteurs de lumière, en utilisant une approche non covalente pour l'assemblage des unités porphyrines dans l'optique d'obtenir un espacement et une orientation favorable entre les chromophores. La construction d'assemblages multi-chromophoriques a conduit à réveiller l'intérêt de la chimie de coordination en vue de former des réseaux ordonnés pour effectuer de la reconnaissance moléculaire. Dans ce contexte, différents systèmes substituées par des porphyrines de zinc(II), de type dimère et tétramère, ont été préparés par réaction de métallation. Ces réseaux porphyriniques, ainsi que la simple porphyrine de zinc en tant que référence, ont été utilisés pour la formation d'assemblages moléculaires par coordination axiale du petit ligand bidentate, le DABCO. Nous avons étudie la coordination de ce ligand bifonctionnel rigide aux porphyrines quant à la pré-organisation du squelette oligonucléotidique, et l'orientation parallèle des porphyrines que cette coordination peut induire. Ces systèmes moléculaires synthétisés sont capables de s'organiser puisque leur architecture est fondée sur une combinaison de liens rigides et flexibles. La stabilité et les différents types de complexes obtenues ont été analysés par titrations UV-visible.

L'autre processus d'auto-assemblage auquel nous nous sommes intéressés est basé sur un concept de complémentarité des liaisons hydrogène : un récepteur à base d'uracile possédant des capacités de reconnaissance spécifique a été envisagé. Du chlorure cyanurique

a été employé dans la construction du récepteur artificiel, afin d'inclure une séquence de liaisons hydrogène à trois points, capable de l'associera de la base uracile dans le processus de reconnaissance. La substitution du chlorure cyanurique en utilisant différentes amines, y compris la porphyrine-amine, permis l'obtention de systèmes triazines porphyriniques simple et double, comprenant divers sites de liaisons hydrogène. D'un autre côté, la base uracile employée dans la formation des espèces supramoléculaires est une forme modifiée de l'uridine avec des porphyrines pendantes. A travers la structure subtile de l'ADN, qui est stabilisée par liaisons hydrogène et interactions « π-stacking », les opérations simultanées de ces deux interactions ont été envisagées dans les processus de formation de nos complexes entre les dérivés triazine-porphyrine et les systèmes uridine-porphyrine en raison de leurs caractéristiques structurales spécifiques.

SYNTHESIS OF CHEMICALLY MODIFIED OLIGONUCLEOTIDIC BACKBONE WITH PENDANT PORPHYRINS

Synthetic nucleotides with modified heterocycle, sugar, and phosphodiester backbone moieties, as well as those labeled with fluorescent dyes have numerous and diverse applications. It is well known that numerous nucleoside analogues are biologically active. In this line, synthetic oligonucleotides with modified internucleosidic phosphodiester linkage have emerged as potential therapeutics in antisense technology.[52-58] Interest in antisense oligonucleotides is beyond their ability to bind with messenger RNA encoding a disease-related protein and then specifically inhibiting the synthesis of that protein. Linking porphyrins and related fluorescent tags to nucleosides by means of covalent bonds have resulted in promising class of systems with an application in areas such as energy- and electron transfer processes,[45,59-67] molecular recognition and transport,[68-73] antiviral and anticancer therapies,[74] as well as inhibition of gene expression.[75-77]

Our interest was focused on artificial light harvesting complexes and in this respect porphyrins covalently attached to modified oligonucleotides as biopolymer scaffolds. The synthesis of light-harvesting material was inspired by natural photosynthetic system and guided by the desire to exert control over spacing and orientation between the porphyrins. Porphyrins, similar in structure to the naturally occurring pigments, chlorophylls, but more amenable to synthetic manipulations, have been used in the preparation of a potential photonic nanodevice. The modified oligonucleotides were employed as scaffold aiming to formation of an organized porphyrin arrays. The modifications of the nucleosides and the selection of the substituents at the porphyrins were performed to provide desired parallel orientation of the porphyrins.

1.1. STRATEGY OF THE SYNTHESIS.

For the desired arrangement of the porphyrin chromophores, molecular backbone with characteristic structural abilities is required. In terms of its structural features, oligonucleotide is a good candidate for this purpose, Figure 1.1. The oligonucleotidic backbone was modified and the porphyrins appended to an appropriate position along the backbone aiming to obtain parallel orientation of the porphyrins. Such interporphyrinic organization was anticipated due to possible helix formation along the oligonucleotidic backbone.

Figure 1.1 *Double helical oligonucleotide.*

The chemically modified deoxyribonucleotides were employed in construction of one-dimensional and multidimensional nanostructures. The synthetic strategy was based on oligomerization of the uridine units functionalized with various porphyrins that are metallated or not, depending on the photochemical properties we were interested to prompt. The elaborated uridin-porphyrin units were coupled in 3'-5' stepwise fashion, like nucleotides in natural DNA and RNA, using ether-ester type of spacer of suitable length. The ether-ester internucleosidic linkage is stable, neutral and achiral group that provide a flexible backbone. Taken together, architecture of our system is based on combination of rigid and flexible linkers in such a way that porphyrins were appended to an appropriate position of the uracils by the rigid acetylenic linker, and the covalent connectivity between the uridin-porphyrin units feature flexible linker. These covalent linkers were employed to work out anticipated helicoidal structure of oligonucleotidic backbone, and thereby parallel orientation of the porphyrins. According to highly organized single strands, as well as double-helical structures

of oligonucleotides, we expected to obtain preferential spacing and orientation of the porphyrin macrocycles. In this respect we synthesized the range of uridine-porphyrin conjugates, monomer (**1**), dimer (**2**), tetramer (**3**), and octamer (**4**) which is shown in Figure 1.2.

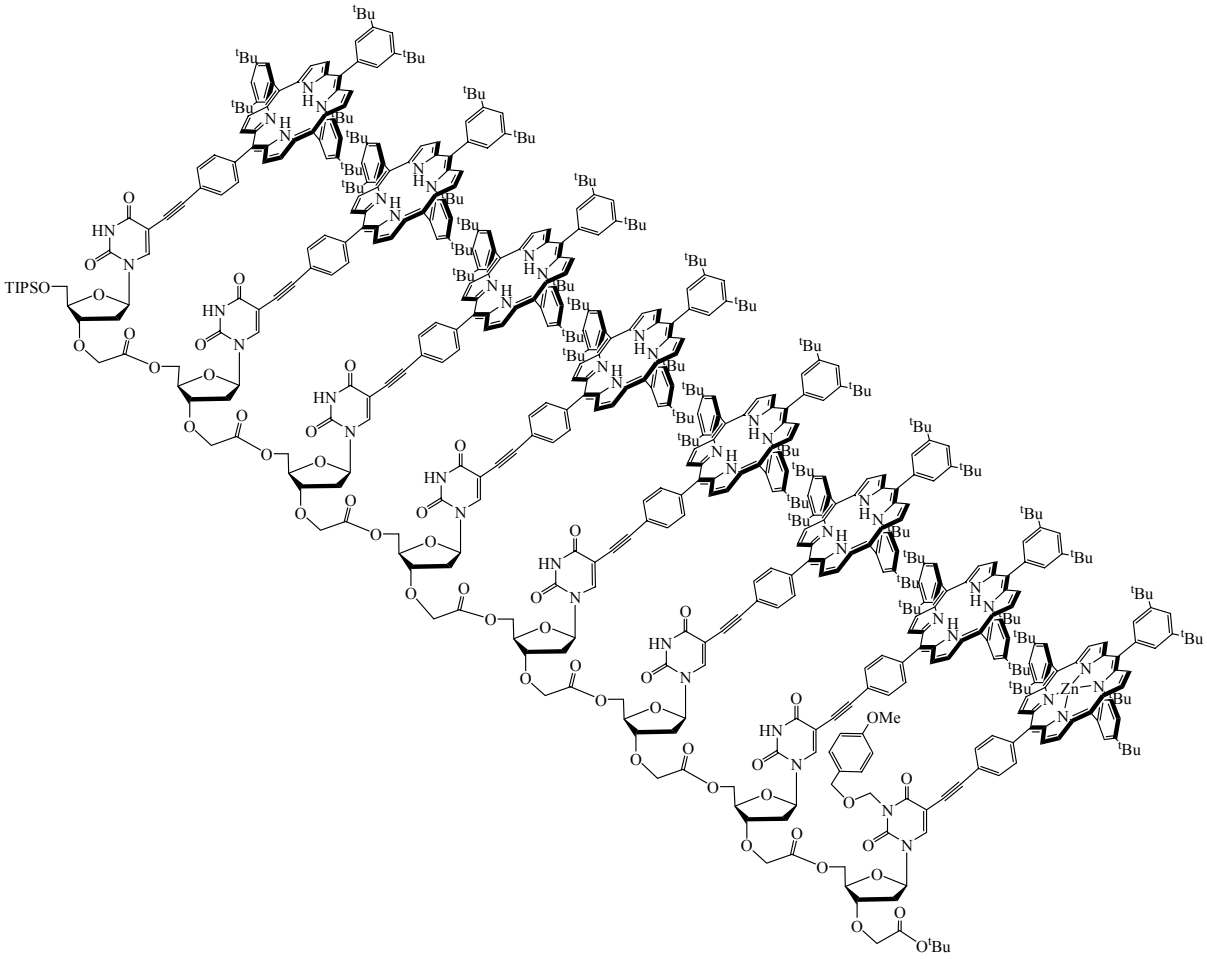

Figure 1.2 *Octamer (4), characterized by eight covalently connected uridinic units bearing various porphyrins, one terminal Zn(II) and seven free-bases.*

Figures 1.3 represent the retrosynthetic path elaborated in the construction of the modified oligodeoxyribonucleotidic array with pendant porphyrins. The selective multistep protection and deprotection strategies have been required to furnish oligomerization derivatives, Figure 1.3 a.

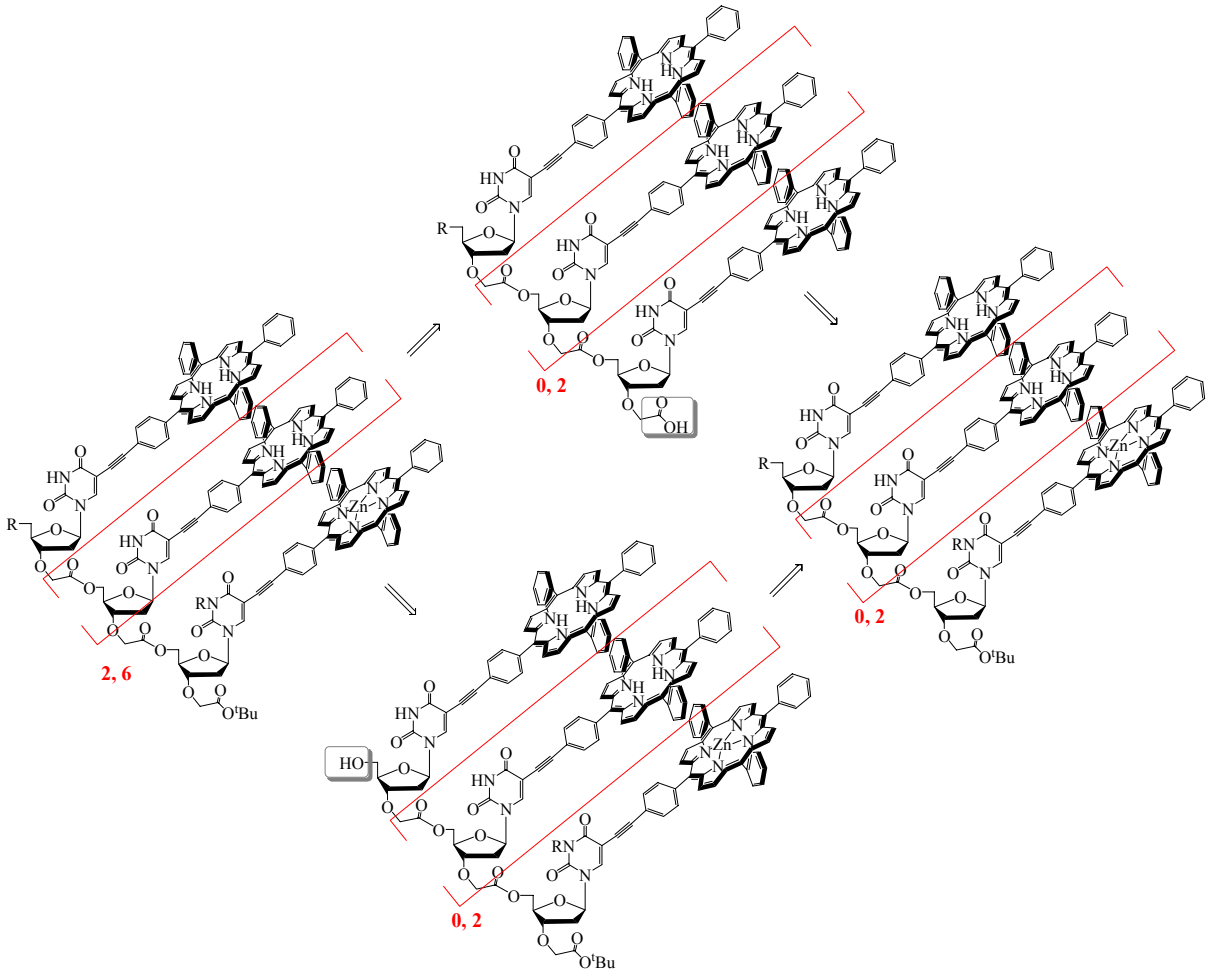

Figure 1.3 a *Oligomerization process. For clarity reasons tert-butyl groups at meso-phenyls are omitted.*

The oligomerization by esterification of the carboxylic acid at C-3' of one uridine-porphyrin unit with the alcohol at C-5' of the other unit was based on the selective cleavage of both *tert*-butyl group from the ester at the 3'-position and triisopropylsilyl group from the hydroxyl at the 5'-position. In this manner an iterative divergent-convergent synthetic strategy of the oligomerization was performed. The synthetic path toward monomer **1** involved protection of N-3 at the uracil with the group which is resistant to nucleophiles and stable to basic conditions. The linkage between corresponding uridine and porphyrin was attained by the coupling reaction of the iodo derivative of 2'-deoxyuridine (**6**) and terminal acetylene of the zinc porphyrin (**14**), Figure 1.3 b.

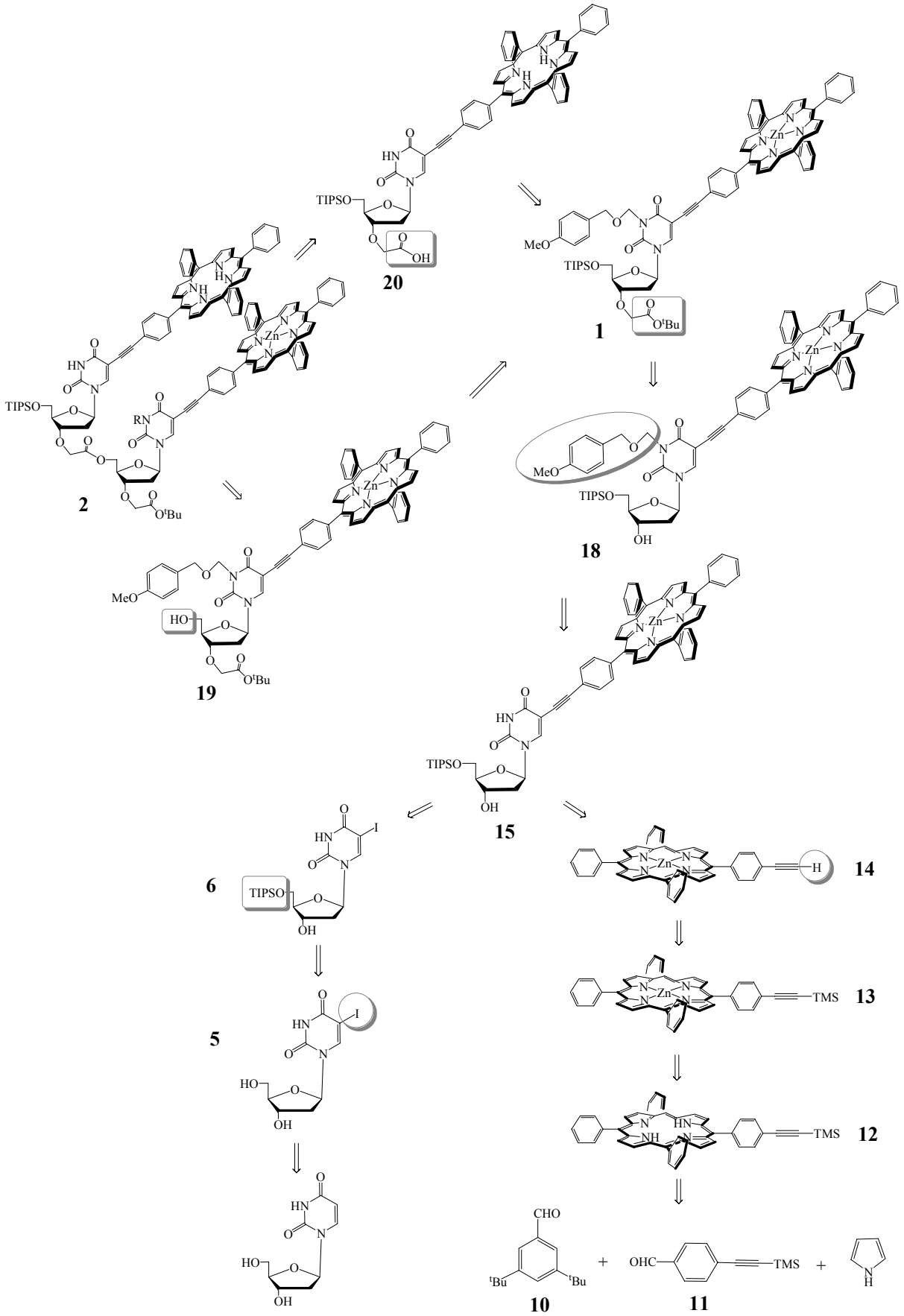

Figure 1.3 b *Retrosynthetic path to dimer* ***2****. For clarity reasons tert-butyl groups at meso-phenyls are omitted.*

1.2. FUNCTIONALIZATION OF THE 2'-DEOXYURIDINE.

The first part of the synthesis comprised the stepwise functionalization of commercially available 2'-deoxyuridine at both C-5 of the uracil nucleobase and C-5' of the ribose, Figure 1.4. Hence, iodination followed by protection of primary hydroxyl group of the ribose enabled the carbon-carbon Sonogashira coupling between uridine and porphyrin.

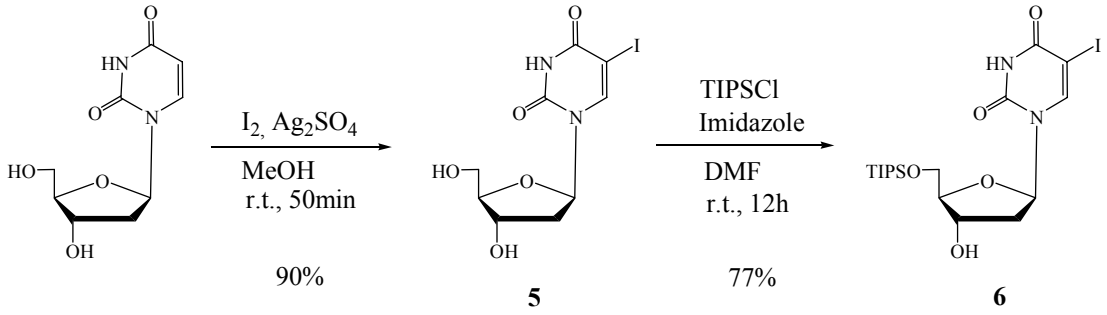

Figure 1.4 *Functionalization of the 2'-deoxyuridine at both C-5 of the uracil and C-5' of the ribose.*

1.2.1. Preparation of 5-iodo-2'-deoxyuridine (5).

Halogenated pyrimidine and purine nucleosides have been prepared by direct reaction with halogens. Iodination of pyrimidine bases takes place under vigorous conditions. The first 5-iodination of uridine and 2'-deoxyuridine using an iodine-nitric acid system was described by Prusoff and co-workers.[78] Dale et al. have affected iodination of ill-defined 5-mercuriuridine derivative mixtures in aqueous alcohol.[79] *N*-Iodosuccinimide has been utilized for iodination of pyrimidine nucleosides.[80] Iodine monochloride has been found to yield 5-iodouracil, but it can also lead to base cleavage.[81,82]

The method that we used for conversion of 2'-deoxyuridine to its 5-iodo derivative **5** is based on elemental iodine and silver sulfate as an agent for generation of electrophilic iodo specie.[83] Metal-halogen exchange between equimolar quantities (1.2 equivalent) of iodine and silver sulfate in methanol occurs instantaneously. The presence of electrophilic iodo species could be visualized by change of colour of silver sulfate in the brown solution (from white to yellow). Once 2'-deoxyuridine was added, the reaction progress could be visualized by decoloration of the reaction solution. The reaction came to completion in 50 minutes. The

product **5** was isolated by filtration and purified by crystallization from methanol; other methods of purification had to be abandoned due to its poor solubility in organic solvents and good solubility in water. Therefore, 5-iodo-2'-deoxyuridine (**5**) was obtained with an overall yield of 90%.

1.2.2. Preparation of 5'-*O*-triisopropylsilyl-5-iodo-2'-deoxyuridine (6).

The regioselectivity is the main issue in the chemistry of polyfunctional nucleosides.[84] There is a vast range of reagents for protection of ribose hydroxyl groups, and considerable part belongs to silyl based protecting groups. Silyl ethers have been widely used to protect hydroxyl groups since they can be prepared easily under mild conditions.[85,86] In addition, selective silylation of primary hydroxyl groups can be performed in the presence of secondary and/or tertiary alcoholic functions.

We employed triisopropylsilyl (TIPS) protecting group due to its stability under various reaction conditions and ease of cleavage in the presence of fluoride-ion source. The selectivity of protection was enabled due to sufficient difference in reactivity among primary and secondary alcoholic functions. The reaction was performed in dimethylformamid (DMF), which was previously dried over molecular sieves, at room temperature in the presence of 1.1 equivalent of triisopropylchloride and 2 equivalents of imidazole. After stirring the reaction mixture for 12 hours, the product was isolated by dichloromethane/water extraction. The crude product was purified by column chromatography on silica. We obtained 5'-*O*-triisopropylsilyl-5-iodo-2'-deoxyuridine (**6**) in 77% yield. The moderate yield could be addressed to some unreacted residues of **5**, and to some extent non-selectively protected ribose i.e. protected at both C-5' and C-3'. The unreacted **5** remained in aqueous phase and "double" protected **5** was isolated by column chromatography.

The functionalization of hydroxyl group at the 5'-position of the uridine provided enhanced solubility of 5-iodo-2'-deoxyuridine (**5**) in widely used organic solvents, in particular triethylamine, which was employed as solvent in the Sonogashira carbon-carbon coupling between uridine and porphyrin.

1.3. SYNHESIS OF PORPHYRINS.

There are two general approaches to obtain desired porphyrin: modification of a naturally occurring porphyrin (e.g. heme) or total synthesis. Although convenient, modification of naturally occurring porphyrins poses great limitations on the choice of peripheral substituents because certain substituents can not be modified easily. Nevertheless, such limitations can be overcome by total synthesis, which involves preparation of pyrrole and aldehyde subunits with desired subsituents. Most existing model systems are based on two families of porphyrins: the *β*-substituted porphyrins (analogs of naturally occurring hemes, chlorophylls) and the *meso*-substituted porphyrins. *Meso*-substituted porphyrins bearing specific pattern of functional groups are valuable components in the synthesis of porphyrin-based biomimetic systems. *Meso*-tetraphenylporphyrins offer attractive features in this context and have been used in a wide variety of studies. The first tetraphenylporphyrin was synthesized 71 years ago by Rothemund, who caused benzaldehyde and pyrrole in pyridine to react in a sealed bomb at 150 °C for 24 h.[87] Subsequently the two methods relating to condensation of pyrroles and aldehydes were developed.

- The older method was developed in 1967 by A. D. Alder and F. R. Longo.[88]
- The more recent one was developed by J. S. Lindsey in 1986.[89-95]

1.3.1. Synthesis of tetraphenylporphyrins developed by A. D. Alder and F. R. Longo.

Alder and Longo modified the Rothemund reaction for *meso*-tetraphenylporphyrins by allowing benzaldehyde and pyrrole to react for 30 min in refluxing propionic acid (141 °C) open to the air, Figure 1.5.[88,89] They were assuming that both yield and rate of the condensation of pyrrole and benzaldehyde depend on acidity, solvent, temperature, availability of atmospheric oxygen, and initial concentration of the reagents.

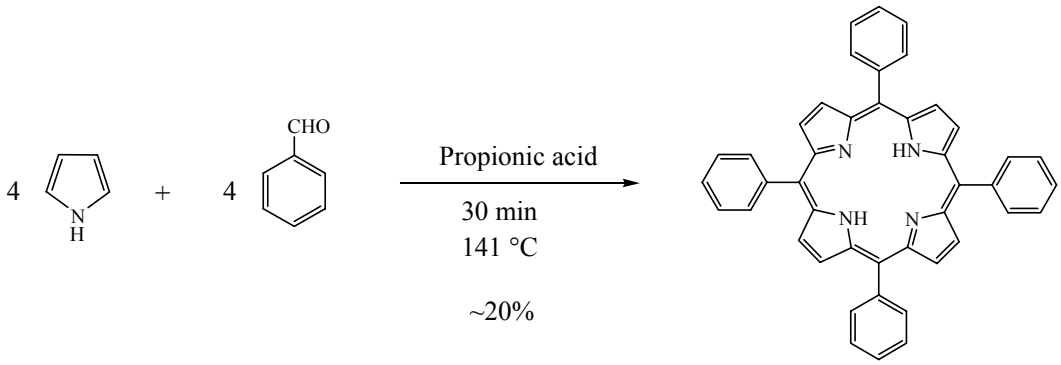

Figure 1.5 *Synthesis of meso-tetraphenylporphyrin developed by A. D. Alder and F. R. Longo.*

These comparatively milder reaction conditions have allowed a wider selection of substituted benzaldehydes to be converted to the corresponding porphyrins in yields of up to 20%. The reaction is also amenable to large-scale synthesis and multigram quantities of many porphyrins have been prepared. Nevertheless, this methodology suffers from several limitations. First, the harsh reaction conditions result in complete failure with benzaldehydes bearing sensitive functional groups. Second, the high level of tar produced presents purification problems, especially with those porphyrins that do not crystallize or precipitate at the end of the reaction. Third, the batch-to-batch reproducibility of the reaction is often rather poor.

The synthetic needs of porphyrin chemistry were not completely satisfied by this methodology. At the very least necessity arose for preparation of small quantities of porphyrins from sensitive aldehydes in high yields without encountering difficult purification problems.

1.3.2. Synthesis of tetraphenylporphyrins developed by J. S. Lindsey.

J. S. Lindsey developed mild and clean procedure for preparation of sophisticated tetraphenylporphyrin systems in small quantities and in yields of around 50%.[89-95] The design of synthetic strategy developed by J. S. Lindsey was based on studies of equilibrium cyclizations and biomimetic studies of porphyrin biosynthesis. The concept of this procedure began from the thermodynamic stability of macrocyclic structures. Hence, the main feature of this method is that the cyclic tetraphenylporphyrinogen is thermodynamically favored over

the linear polypyrrylmethanes when benzaldehyde and pyrrole are condensed. This equilibrium in condensation of benzaldehydes and pyrroles is reached at room temperature due to their reactivity. The addition of an oxidant irreversibly converts porphyrinogen to the aromatic porphyrin.

The yield of porphyrin is dependent on a variety of factors, including nature of the oxidant and the acid catalyst, duration of condensation period, and concentration of acid, pyrrole, and benzaldehyde. The maximum yield of tetraphenylporphyrin is obtained when a solution of dry methylene chloride or chloroform under N_2 atmosphere is charged with reagents. The equilibrium in the porphyrinogen reaction is highly concentration dependent. The dilution of reaction mixture to 10^{-2} M favors cyclization in the porphyrinogen reaction, it also deters the polymerization process necessary to attain the tetrapyrromethane (containing 4 benzaldehyde and 4 pyrrole components) stage. Formation of the tetrapyrromethane is a prerequisite for cyclization to the porphyrinogen, as it is explained later. In the normal irreversible cyclization reactions high dilution increases the yield. However, when the cyclization step is preceded by a reversible association step, high dilution does not afford high yields.

The concentrations of benzaldehyde and pyrrole are critical determinants of the ultimate yield of porphyrin. The maximum yield of porphyrin is observed at equimolar benzaldehyde and pyrrole concentrations of 10^{-2} M. Both 10-fold higher and 10-fold lower concentrations decline yields markedly. The rate of porphyrinogen formation is proportional to the acid concentration. The two standard catalysts can be employed in about their standard concentrations, boron trifluoride etherate ($BF_3 \cdot OEt_2$) at the concentration of 3.3×10^{-3} M and trifluoroacetic acid (TFA) at around 10^{-2} M; higher or lower acid concentrations significantly change the point in the reaction of the maximum porphyrinogen yield. However, application of one or both of the standard catalysis conditions results in reasonable yields of porphyrin for most aldehydes.

The oxidation of porphyrinogen to porphyrin can be performed with either 2,3,5,6-tetrachlorobenzoquinone (*p*-chloranil) or 2,3-dichloro-5,6-dicyanobenzoquinone (DDQ). The addition of DDQ at room temperature gives a nearly instantaneous conversion of porphyrinogen to porphyrin and polypyrromethanes to polypyrromethenes. *p*-Chloranil is a much milder oxidant which gives better yields, and for this reason is used in preparative purposes. For complete reaction *p*-chloranil requires exposure time of 1 hour in refluxing chloroform. After termination of porphyrin-forming process, neutralization of the acid catalyst should be exerted by addition of triethylamine prior to evaporation of the solvent. The

product workup involves passage of the concentrated crude reaction mixture over a chromatography column. The polypyrromethene components usually bind near the top of the column, while porphyrins and residual unreacted benzaldehydes pass through the column.

In the respect of better understanding of the observed concentration dependence the overall porphyrin reaction is presented in Figure 1.6.[92]

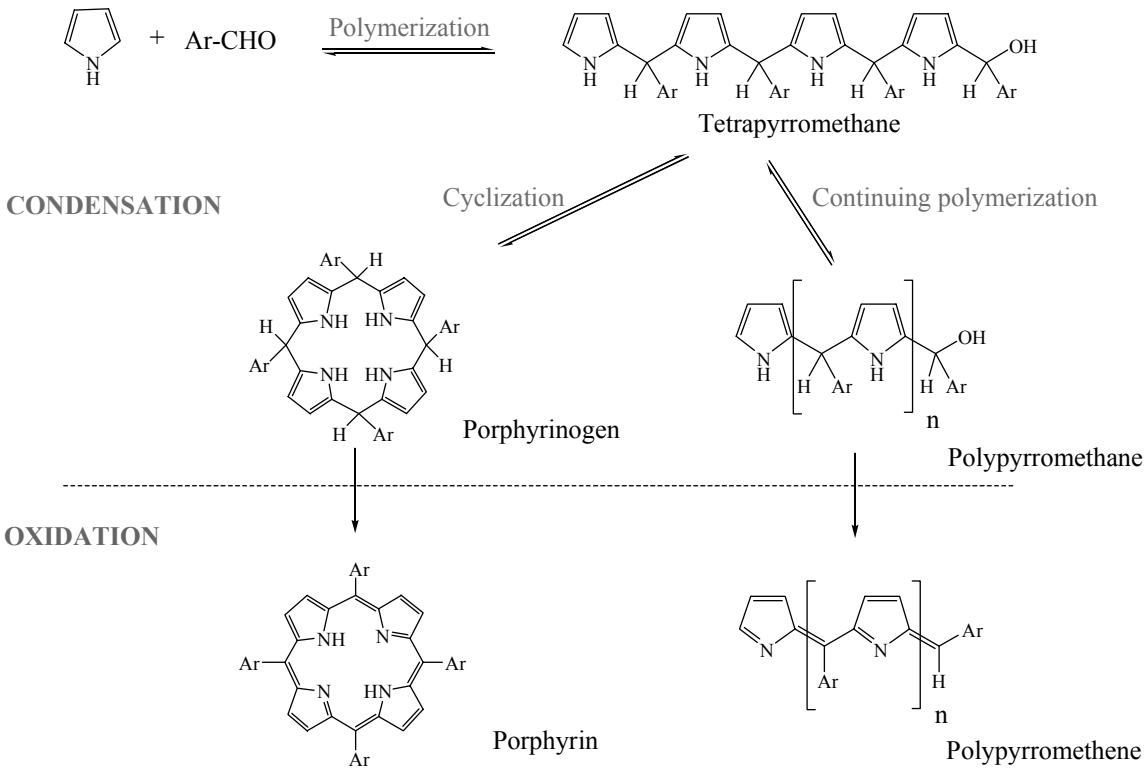

Figure 1.6 *Schematic outline of the porphyrin formation. Pyrrole and aldehyde reversible condensation to the tetrapyrromethane which can cyclize to the porphyrinogen or continue polymerization to the polypyrromethanes. The addition of an oxidant converts the porphyrinogen to the aromatic porphyrin and the polypyrromethane to the polypyrromethene.*

The predominant stage of the overall synthesis is the condensation process of benzaldehyde and pyrrole that provides polypyrromethane oligomers and the cyclic porphyrinogen, Figure 1.7.[92]

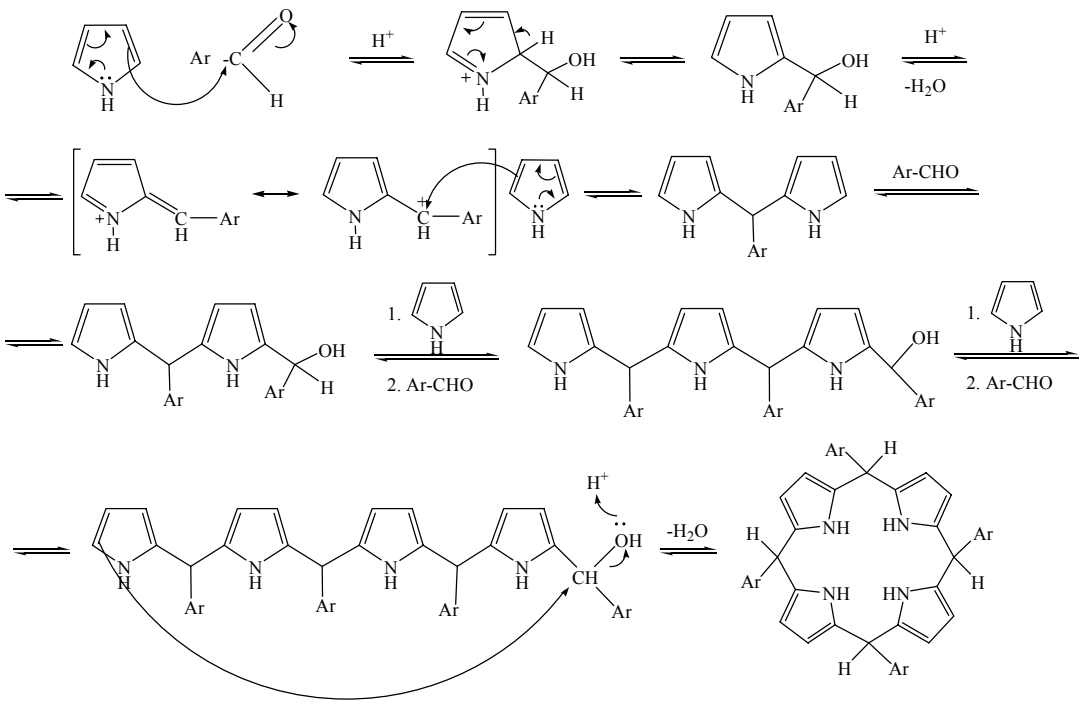

Figure 1.7 *The mechanism of the porphyrinogen reaction.*

All reactions are assumed to be reversible and concentrations of all components are thereby coupled *via* mass action at equilibrium. The degree of polymerization is proportional to the starting concentration of monomers. The tetrapyrromethane (containing 4 benzaldehyde and 4 pyrrole components) can cyclize to form the porphyrinogen, and the yield of porphyrinogen is therefore linked to the yield of tetrapyrromethane. A change in the starting monomer concentrations and initial acid addition changes the equilibrium distribution profile of the oligomers, and the yield of porphyrinogen is altered through its dependence on the equilibrium tetrapyrromethane concentration. The decline in porphyrinogen yield that occurs is accompanied by a shift of the oligomer composition to shorter species (oligomer truncation) or by continuation of polymerization process to higher molecular weight polypyrromethanes. Oligomer truncation can result from reactions giving reversible formation/disassembly of polypyrromethanes in conjunction with irreversible side reactions that cause fragmentation of polypyrromethanes.

The systematic examination of the yield-concentration dependence revealed that at pyrrole and aldehyde concentration of 10^{-2} M the competing cyclization and polymerization processes are in balance. At higher concentration (10^{-1} M) the oligomer equilibrium distribution is shifted predominantly to higher molecular weight components. At lower

concentrations (10^{-3} M) the distribution is shifted predominantly toward shorter oligomers. In each case the yield of the tetrapyrromethane is decreased relative to that at 10^{-2} M, resulting in a concomitant decrease in the yield of porphyrinogen.

This synthetic procedure developed by J. S. Lindsey enables to convert complex substituted benzaldehydes to porphyrins in good yield. By this method, quantities of porphyrins up to 1 g can be easily prepared from sensitive aldehydes without encountering difficult separation problems. In addition, the reaction conditions are compatible with a wide variety of functional groups and protecting groups. Therefore, due to the idiosyncrasies of porphyrin chemistry (difficulty with purification, low solubilities, susceptibility to oxidation and reduction, lability to base, demetalation with acid, photosensitivity, etc.), it is generally desirable to perform as many synthetic transformations as possible prior to forming the porphyrin.

1.3.3. Preparation of A_3B porphyrins.

The ability to prepare porphyrin macrocycle bearing specific pattern of functional groups requires architectural design. The strategy of the synthesis of *meso*-substituted porphyrins depends on the desired arrangement of different substituents.[94,95] Generally, the synthetic routes become more elaborate as the number of different substituents increases. For example, symmetric A_4 porphyrin bears four identical functional groups and could be readily synthesized under mild conditions in the one-flask reaction of pyrrole and the corresponding aldehyde. On the other hand, introduction of two different types of substituents around the porphyrin periphery can be achieved in an expedient manner, by the mixed aldehyde condensation. The condensation of pyrrole and two aldehydes, A and B, in two-step one-flask reaction affords a statistical mixture of six substituted porphyrins which can be separated by extensive chromatography, Figure 1.8.[93] The chromatographic separation of the mixture obtained by this two aldehydes synthesis provides the following types of *meso*-substituted porphyrins: A_4, A_3B, *trans*-A_2B_2, *cis*-A_2B_2, AB_3, B_4.

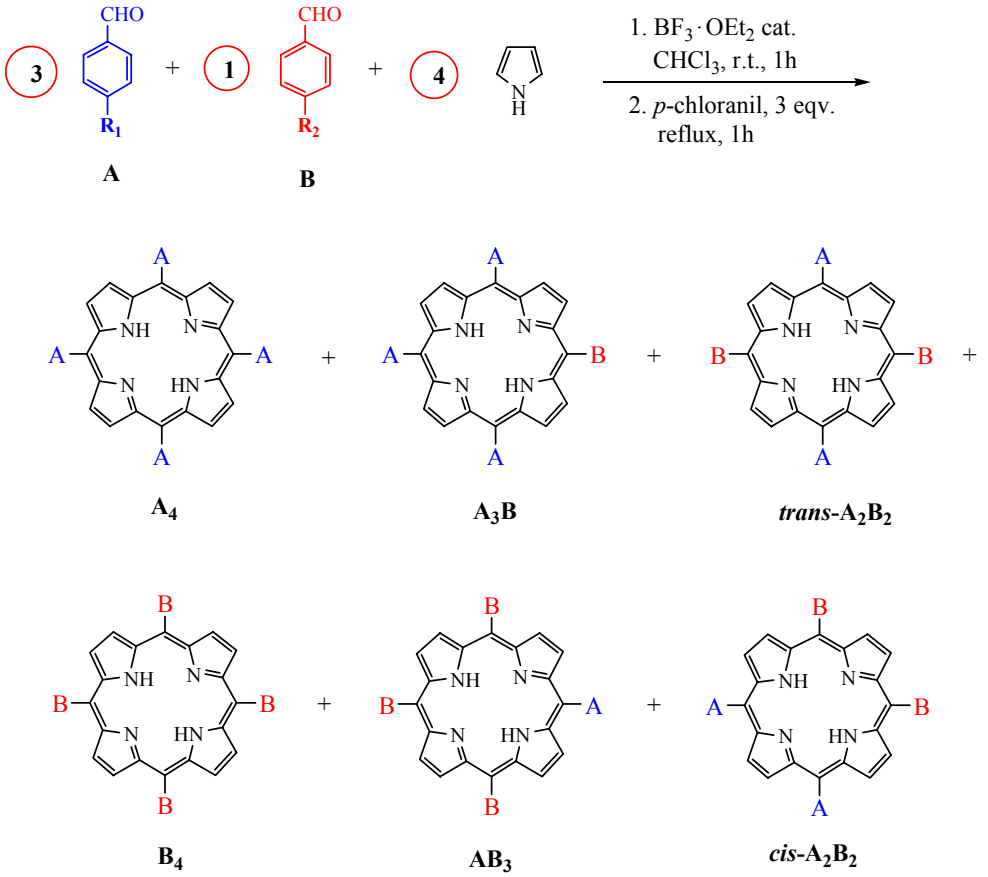

Figure 1.8 *Synthesis of A_3B porphyrin via mixed aldehyde condensation (aldehydes **A** and **B**) and pyrrole.*

The represented conditions relate to successful formation of the desired A_3B-porphyrin in optimal yield. Two different substituents of the A_3B-porphyrin should impart chromatographic separability, porphyrin solubility, and provide other aspects particular to the target model system. In general, a substituent A affords solubility while substituent B features reactive peripheral functional group.[93] In this case it can be assumed that a relative polarity and a size difference between the substituents facilitate separation of A_3B-porphyrin. Hence, separability of the A_3B-porphyrin from the other porphyrin components in mixed aldehyde condensation depends on both polarity and size difference between the aldehydes. The overall yield of A_3B-porphyrin in these reactions varies between 5 and 25%, depending on the reactivity of the aldehydes.

1.4. SYNTHESIS OF THE A_3B ZINC(II) PORPHYRIN (14).

The second part of the synthesis consists of A_3B porphyrin preparation according to envisaged functionalization. Desired porphyrin was prepared by synthesis developed and optimized by J. S. Lindsey.[89-95] Two specific aldehydes were selected to be used in direct coupling reaction with pyrrole leading to corresponding target system. In terms of enhanced solubility of the corresponding porphyrin, benzaldehyde functionalized with 3,5-di-*tert*-butyl groups was the best choice. These groups provide facial-encumbrance of porphyrins as a mean of face-to-face aggregation, thereby achieving enhanced solubility. Solubility is essential for carrying out synthetic transformations, purification procedures, and diverse studies. The solubility problem is significant with planar porphyrins, especially in arrays composed of multiple porphyrins in defined architecture that we aiming at. On the other hand, benzaldehyde B (**11**) provides reactive acetylene group at the *p*-position of the aryl ring. Both functional groups are readily soluble in organic solvents and are compatible with the mild reaction conditions in porphyrin synthesis. In numerous porphyrin arrays acetylene and phenylacetylene groups have been used as linkers between porphyrins, because of their substantial contribution to coupling efficiency.[44,96-101] In our case phenylacetylene group at the *meso*-position of the porphyrin enabled formation of the porphyrin-uridine conjugate. Prior to the coupling of the porphyrin and the uridine, free-base porphyrin **12** was metallated with zinc(II), and then the terminal acetylene was deprotected. The retrosynthetic path elaborated in preparation of targeted A_3B zinc(II) porphyrin (**14**) bearing 3,5-di-*tert*-butylphenyl groups and terminal acetylene is presented in Figure 1.9.

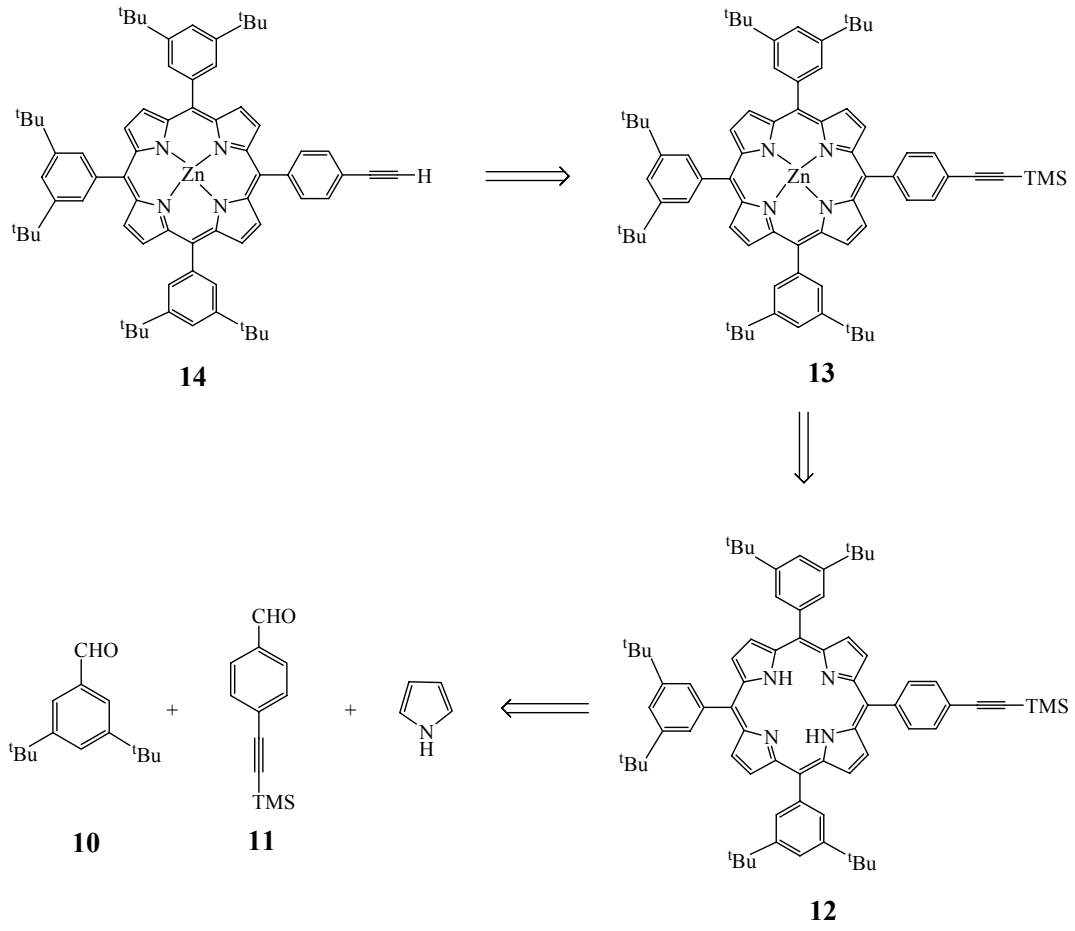

Figure 1.9 *Retrosynthetic path explored in the preparation of A_3B zinc(II) porphyrin* ***14****.*

As presented, realization of the designed synthesis of the porphyrin is related to prefunctionalization of the benzaldehydes. In this context, the syntheses of benzaldeydes **10** and **11** were imposed.

1.4.1. Preparation of 3,5-di-*tert*-butylbenzaldehyde (10).

The corresponding benzaldehyde **10** bearing di-*tert*-butyl group was prepared in three steps synthesis from commercially available toluene, Figure 1.10.[102-104]

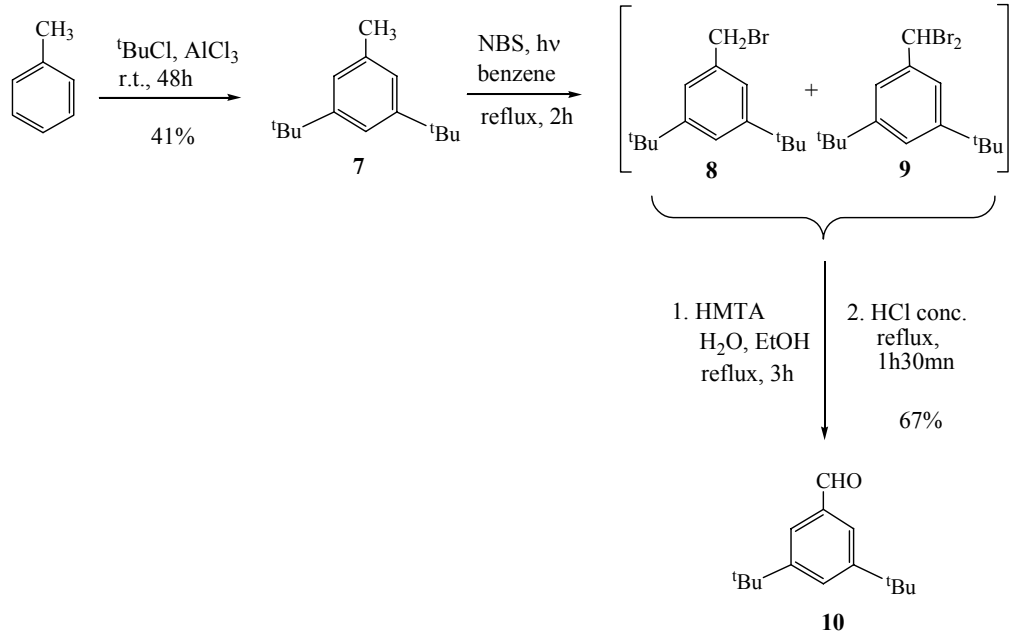

Figure 1.10 *The synthetic route toward 3,5-di-tert-butyl-benzaldehyde A* ***(10)****.*

In the first step aromatic ring of the toluene was alkylated by using Fridel-Crafts alkylation procedure.[105] In this aromatic electrophilic substitution toluene was used also as a solvent. The reaction was performed in presence of 4 mol% of aluminium chloride as a Lewis acid catalyst and 1.9 equivalents of *tert*-butyl chloride as an alkylating agent. Addition of aluminium chloride is exothermic and should be performed in small portions. Since we used tertiary reagent in the presence of powerful catalyst, most probably is that alkylation was proceeding through free *tert*-butyl cation. Once formed, free *tert*-butyl cation rapidly attacks the ring. After 48 hours of stirring at room temperature reaction products were separated by fractional distillation under vacuum. The methyl group is an activating and the electrophile may be directed to the *ortho* or *para* position. In the case of the *tert*-butyl cation as an electrophile, due to steric hindrance considerations, the main product of the reaction is the *meta* di-substituted toluene **7**, obtained in 41% yield. The poor yield is addressed to the mono-alkylated toluene at the *meta* and *para* positions.

The second step included bromination of the methyl group of 3,5-di-*tert*-butyltoluene (**7**) by the free-radical substitution with *N*-bromosuccinimide (NBS).[106] As a chain reaction-initiator a visible light was applied through the projector of 150 W. This photolytic reaction was performed in refluxing benzene with 1.5 equivalents of NBS; usually besides NBS as a brominating agent, nonpolar solvents are used. The successful initiation of the reaction can be testified by the colour change of the solution, from the uncoloured to the dark orange, due to bromine liberation. Once the free radical Br· was formed the propagation step was triggered. The reaction progressed *via* free-radical chain mechanism represented in Figure 1.11.

Initiation catalysed by visible light:

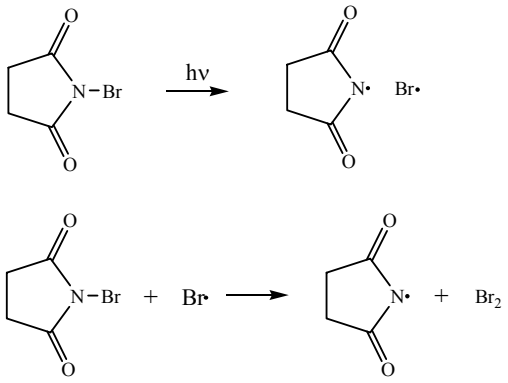

Propagation and Termination:

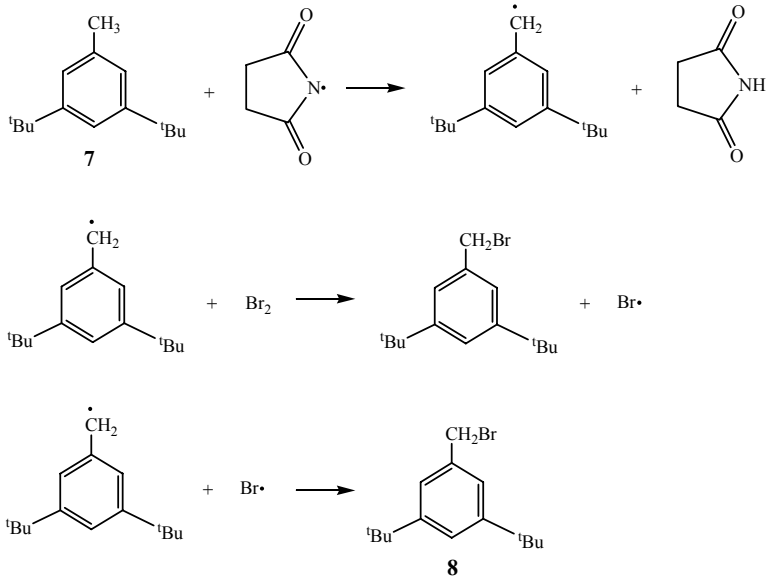

Figure 1.11 *The mechanism of the free-radical bromination of 3,5-di-tert-butyltoluene 7 performed by substitution with N-bromosuccinimide (NBS).*

Although the bromination substitution was continuing to the higher alkyl bromide, i.e. $ArCHBr_2$ **9**, in Figure 1.11 are presented first two propagation steps and the termination step that was leading to $ArCH_2Br$ **8**. Hence, the free-radical chain bromination afforded monosubstituted **8** and disubstituted **9** derivative with no trace of substitution at other positions.

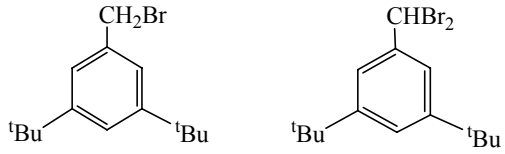

8 **9**

Since the three bromo derivatives could be formed in the presence of a larger molar ratio of NBS, only 1.5 equivalents of NBS were applied. Completion of the termination process was visualized by decoloration of the solution caused by consumption of the bromine. The isolation of monobromo (**8**) and dibromo (**9**) derivatives entailed removal of the white precipitate of NHS by filtration and evaporation of benzene. Characterization of the isolated mixture by ^1H NMR spectroscopy elucidated presence of monobromo derivative **8** in 38% and dibromo derivative **9** in 62%. The obtained mixture of derivatives was applied to the synthesis of benzaldehyde **10** without further purification.

The third step provided desired 3,5-di-*tert*-butyl-benzaldehyde A (**10**). In this respect two different approaches, according to two bromo derivatives, were employed in one-pot synthesis. Conversion of monobromo derivative **8** and dibromo derivative **9** to benzaldehyde **10** was implying oxidation and hydrolysis, respectively.[103] Oxidation of the compound **8** was performed by the Sommelet reaction,[104,105] whereby aldehydes are produced from benzylic halides by the action of hexamethylenetetramine (HMTA). This reaction formally proceeds in three stages: formation of hexaminium salt, its conversion to an amine and formation of an aldehyde. Although only the last stage is actual Sommelet reaction, the entire process was conducted without isolation of intermediates. To the solution of two bromo derivatives in a mixed solvent system water/ethanol, 2.8 equivalents of HMTA were added. Cleavage of the resulting salt provided corresponding amine, which converted to the imine ($ArCH_2N{=}CH_2$) with formaldehyde liberated from the reagent. The key step then followed: transfer of hydrogen from the second mole of the arylamine to the imine:

$$ArCH_2N{=}CH_2 + ArCH_2NH_2 \rightarrow ArCH_2NHCH_3 + ArCH{=}NH.$$

The imine was then hydrolyzed by water to yield the aldehyde. Hereafter, concentrated hydrochloric acid was added to the reaction mixture in a dropwise manner to hydrolyze dibromo derivative **9**. The majority of 3,5-di-*tert*-butyl-benzaldehyde A (**10**) was isolated by crystallization, while residues were purified by column chromatography on silica. Therefore, 3,5-di-*tert*-butyl-benzaldehyde **10** was obtained in overall 67% yield.

1.4.2. Preparation of 4-trimethylsilylethynyl-benzaldehyde (11).

The synthetic route to the targeted porphyrin-uridine system relied on the porphyrin bearing terminal acetylene. The introduction of this functional group in the porphyrin required preparation of 4-ethynylbenzaldehyde B (**11**). As presented in Figure 1.12 synthesis of the benzaldehyde **11** was performed by using Sonogashira coupling of commercially available 4-bromobenzaldehyde and trimethylsilylacetylene.

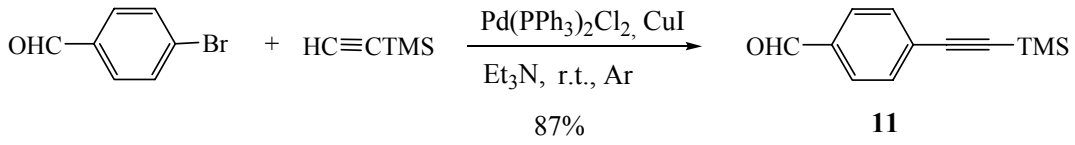

Figure 1.12 *Synthesis of 4-trimethylsilylethynyl-benzaldehyde B (**11**).*

This Pd-mediated cross-coupling reaction of acetylene with aryl halide in the presence of the palladium complex is extensively used in organic chemistry and materials science for the preparation of terminal and internal alkynes.[107-115] The Sonogashira cross-coupling reaction is well-known as being one of the most important and widely used reactions for construction of carbon-carbon bond. The reaction conditions are mild, and many reactions can be performed at room temperature. The catalytic systems that we employed include $PdCl_2(PPh_3)_2$ together with CuI as the cocatalyst and triethylamine as a solvent, Figure 1.12. The presence of CuI results in formation of some Cu(I) acetylides that can undergo oxidative homocoupling reaction of acetylenes, when exposed to air. The first observation of homocoupling of terminal acetylenes was made by Glaser in early 1869.[116,117] Since then

many groups have modified the reaction to obtain symmetrical and unsymmetrical butadiynes.[107]

Although acetylene homocoupling reactions can be useful from the synthetic and application point of view, formation of the homocoupling product in our case was undesirable. Hence, we carried out Sonogashira reaction under argon atmosphere targeting crosscoupling product, and indeed, we obtained bicoupling product in 87% yield. Triethylamine, employed as a solvent, was extensively bubbled with argon prior utilization, thus minimizing the presence of oxygen in the reaction mixture. The Pd(II) soluble yellow complex, $PdCl_2(PPh_3)_2$, was applied as a precursor of palladium(0). The Pd(0) is the active catalyst formed *in situ*. A molar ratio that we used was 2:1 copper to palladium, since it has been shown to be the best for coupling with acetylenes. CuI (5 mol %) was employed as a cocatalyst because it activates acetylenes by forming a copper acetylide. An appropriate justification of the Sonogashira reaction protocol leading to crosscoupling and homocoupling products is given by the mechanism presented in Figure 1.13.[108]

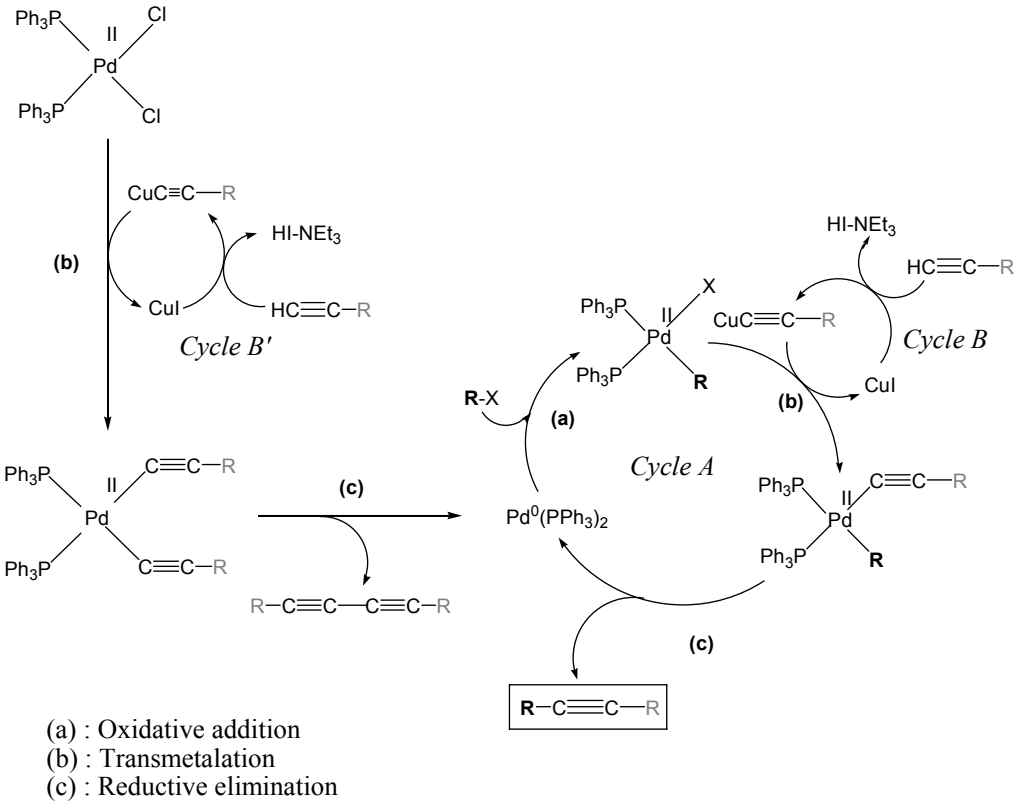

Figure 1.13 *Proposed mechanism for an overall Sonogashira coupling reaction.*

As presented in Figure 1.13 the protocol of Sonogashira reaction is constructed from combination of two catalytic cycles *A* and *B*. Prior to the proper catalytic cycle, the active Pd(0) catalyst has to be generated. Copper acetylide is formed from acetylene and CuI cocatalyst. Copper acetylides then undergo transmetallation with Pd(II). The active catalyst Pd(0) is then generated by reductive elimination of butadiyne. At this stage, reaction proceeds with oxidative addition of aryl halide to the active Pd(0) complex. Once the terminal acetylene is deprotonated by the amine it forms copper acetylide; liberated HI is trapped by an amine. Copper acetylide is more active then acetylene and undergoes transmetalation with Pd(0) to form the acetynyl-Pd-R specie. Reductive elimination is the final step that implies elimination of the desired crosscoupling product. In this way, active catalyst, $Pd(PPh_3)_2$, is being regenerated *in situ*.

Isolation of 4-trimethylsilylethynyl-benzaldehyde **11** required consecutive washings of its dichlomethane solution with: 2% solution of ethylenediaminetetra-acetic acid (EDTA) disodium salt, 0.35 M solution of sodium thiosulfate ($Na_2S_2O_3$), saturated solution of ammonium chloride (NH_4Cl), and water. EDTA disodium salt eliminates possible Cu(II) cations which can be formed by disproportion of the Cu(I) in aqueous solution. Eventual bluish color of aqueous phase indicates elimination of Cu(II) complexes. Solution of sodium thiosulfate affects reduction of possibly formed iodine. At the final stage purification by silica-gel chromatography afforded benzaldehyde **11** in 87% yield, with the rest comprising bis(trimethylsilylbutadiyne) as anticipated per reported procedure.

1.4.3. Synthesis of the A_3B porphyrin (12).

Porphyrin bearing three di-*tert*-butylphenyl groups and one phenylacetylene group at the *meso* positions was prepared following the procedure for the synthesis of porphyrins developed by J. S. Lindsey.[89-95] This one-flask synthesis in two stages involves condensation of aldehyde and pyrrole (polymerization and cyclization) followed in time sequence by oxidation. In terms of porphyrin **12** a mixed aldehyde condensation was prompted harnessing 3,5-di-*tert*-butyl-benzaldehyde A (**10**) and 4-trimethylsilylethynyl-benzaldehyde B (**11**). The reaction conditions were modified in accordance with desired A_3B porphyrin: 3 equivalents of benzaldehyde **10**, 1 equivalent of benzaldehyde **11** and 4 equivalents of pyrrole, Figure 1.14.

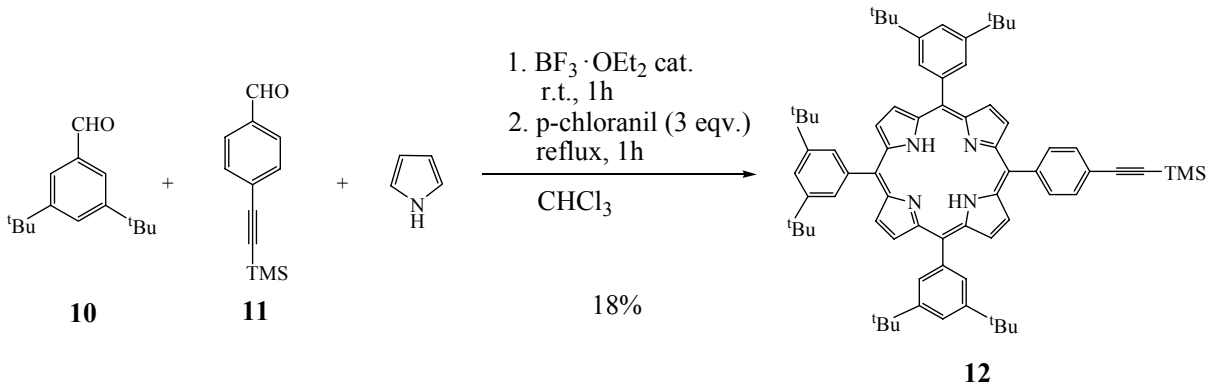

Figure 1.14 *Synthesis of A_3B porphyrin **12** by mixed aldehyde condensation developed and optimized by J. S. Lindsey.*

The reaction was performed in chloroform dried over molecular sieves. Chloroform was charged with benzaldehydes, pyrrole and boron trifluoride etherate under argon atmosphere. The concentrations of the benzaldehydes and pyrrole were equimolar (10^{-2} M). The acid catalyst, boron trifluoride etherate ($BF_3 \cdot OEt_2$) was applied in concentration of 3.3 x 10^{-3} M. The reaction was allowed to proceed at room temperature until the porphyrinogen was reached. The course of the condensation was examined by TLC analysis of aliquots oxidized by DDQ, following the formation of the porphyrin. After one hour at room temperature the reaction mixture was charged with an oxidant 2,3,5,6-tetrachlorobenzoquinone (*p*-chloranil) and allowed to stir at reflux for one hour. Neutralization of the acid catalyst with triethylamine was performed prior to evaporation of the solvent. The product isolation comprised a passage of the concentrated crude reaction mixture over chromatography columns. Polypyrromethene components usually bind near the top of the column, while a mixture of porphyrins freed from reagents and byproducts pass through the column. The repetitive column chromatography on silica-gel afforded A_3B porphyrin **12** in 18% yield. The distribution of other porphyrin products isolated by columns was: 10% of the homosubstituted A_4 porphyrin, 3% of the *trans*-A_2B_2, 8% of the *cis*-A_2B_2 and 2% of the AB_3. Among these, the content of the B_4 porphyrin was approximated to be less then 1%, as it was not isolated. Obtained porphyrin **12** was characterized by ^{1}H NMR and UV-visible spectroscopy. Its characterization and comparison with zinc counterpart is provided further on.

1.4.4. Insertion of the zinc(II) in the cavity of free-base porphyrin 12.

Insertion of the zinc to free-base porphyrin **12** was preferable prior to Sonogashira reaction to obviate possible metallation of the porphyrin in the presence of copper and palladium. Moreover, the use of zinc porphyrin template was indispensable for the designed synthetic path toward monomer **1** since free-base porphyrins are not stable in the presence of strong bases. Besides the other metals, initially we decided to concentrate on zinc porphyrins for the following reasons: they are diamagnetic so are readily studied by NMR; they are easy to prepare from free base porphyrins and are readily demetallated with dilute acid, but they are stable to moisture, air and silica; they have favorable photochemical properties; they form five-coordinate complexes with amines easily measured by UV-visible spectroscopy.[97,100,118] The employed metallation process implied exposure of the free-base porphyrin solution to 2 equivalents of zinc acetate dihydrate ($Zn(OAc)_2 \cdot 2H_2O$) at reflux of chloroform, Figure 1.15.

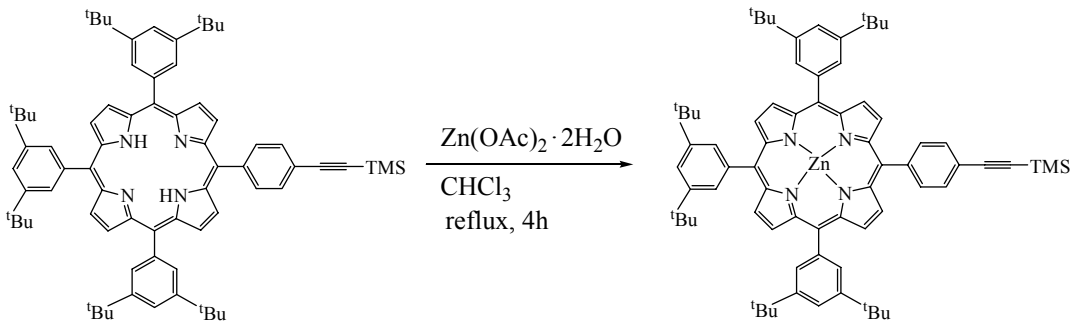

Figure 1.15 *Insertion of the zinc(II) ion in the porphyrin cavity of* ***12****.*

The reaction course was followed by thin layer chromatography (TLC) and UV-visible absorption spectroscopy. Since on TLC plates free base and zinc porphyrin **12** and **13** were characterized with the similar retention factor, an appropriate justification for the reaction completion was coming from two Q-bands in the visible region of the absorption spectra. However, by TLC an evolution of byproducts could have been visualized. To reach a complete conversion to the corresponding zinc derivative, the reaction mixture was refluxed during 4 hours. The presence of zinc porphyrin **13** was corroborated by absorption spectra. After washing with water and evaporation of solvent, purification by flash silica column afforded zinc(II) porphyrin **13** in 95% yield.

1.4.5. Deprotection of the terminal acetylene of zinc(II) porhyrin 13.

The last stage in envisaged functionalization of the porphyrin, prior to Sonogashira coupling with the uridine, was cleavage of trimethylsilyl protection from the acetylene. The terminal acetylene **14** was obtained in 97% yield by treatment of **13** with potassium carbonate (K_2CO_3) in mixed solvent system tetrahydrofuran/methanol (1:1), Figure 1.16. Isolation of the product imposed neutralization with saturated solution of ammonium chloride (NH_4Cl) prior to washing with water. The purification of the resulted porphyrin **14** was performed by filtration through the silica column.

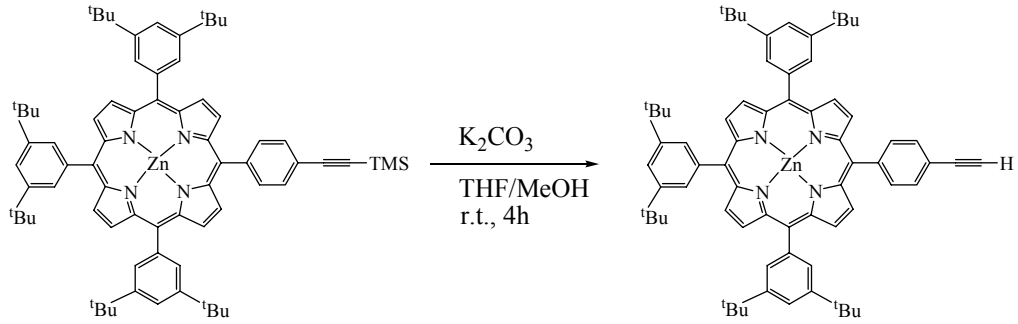

13 **14**

Figure 1.16 *Cleavage of TMS-group from the terminal acetylene.*

At this stage we approached to the synthesis of the targeted porphyrin-uridine conjugate, putative monomer (**1**) from which a construction of the modified oligonucleotidic backbone with pendant porphyrins started.

1.5. CHARACTERIZATION OF THE FREE-BASE (12) AND THE ZINC(II) (13) PORPHYRINS.

The free-base (**12**) and the zinc (**13**) porphyrins bearing three di-*tert*-butylphenyl groups and one phenylacetylene group at *meso* positions were readily characterized by ^{1}H NMR and UV-visible absorption spectroscopy. Both, NMR chemical shifts and electronic spectra are striking properties of the porphyrin ring due to the delocalized π system and its associated ring currents.[119-130]

The basic structure of porphyrin macrocyclic ring consists of four pyrrolic subunits linked by four methine bridges as shown in the following Figure 1.17.[119]

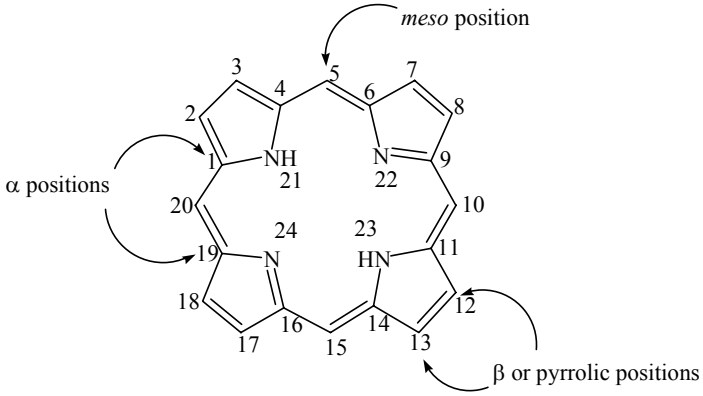

Figure 1.17 *Nomenclature of the porphyrin core proposed by the International Union of Pure and Applied Chemistry (IUPAC).*

The porphyrin ring is an aromatic system containing 26 π-electrons, eight of which are localized on the central nitrogens and others 18 of them are in the 20-membered periphery. It obeys Hückel's rule of aromaticity in that it posses 4n+2 π electrons which are delocalized over the macrocycle. An additional significant feature of aromaticity is planarity, revealed by X-ray crystallography. The most of X-ray crystal structures of porphyrin molecules exhibit planar or near-planar conformation of the macrocycles. The aromatic character of a porphyrin has been established by NMR and UV-visible spectroscopy.

The porphyrin ring is very stable to concentrated acids (e.g. sulfuric acid), and it itself can act as both acid and base. Strong bases such as alkoxides can remove two protons

(pKa~16) from the inner nitrogen atoms to form dianion. On the other hand, two free pyrrolic nitrogen atoms (pKb~9) can be protonated easily with acids such as triflouroacetic acid.

1.5.1. Characterization by ^{1}H NMR spectroscopy.[119-123]

The chemical shifts of porphyrinic protons are dependent on their distance and orientation with respect to the delocalization pathway of the π-electrons of the ring. A notable feature of the ^{1}H NMR spectra arises from anisotropic diamagnetic susceptibility of the ring. This susceptibility was rationalized in terms of an induced circulation of the delocalized π-electrons in an applied magnetic field. An induced magnetic field generated by the ring current effect being dependent upon the orientation of the aromatic system with respect to the applied magnetic field. Due to this anisotropic effect from the porphyrin ring current, NMR signals for the deshielded *meso* and β or pyrrolic protons at the porphyrin periphery show up at low field (8 to 10 ppm), whereas the signals for the shielded protons on the inner nitrogen atoms show up at very high field (-2 to -4 ppm). The porphyrin ring is dominated by a global diamagnetic circulation of π electrons that extends over all twenty-six unsaturated atoms; the σ electrons make only a small contribution at this high above molecular plane.

The ^{1}H NMR spectra of the A_3B porphyrin show typical chemical shifts with multiple resonances consistent with an expected pattern of substituents at the porphyrin macrocycle. Substituted *meso*-phenyls indicate a small impact to the π-electron ring current of the porphyrin ring, presumably because of generally minimal π-overlap between the phenyl and the porphyrin rings. This hindrance arises from the large phenyl-porphyrin dihedral angles, which result from steric interactions with the β-hydrogens. The chemical shifts of the pyrrolic protons in the spectrum of the free-base porphyrin (**12**) showed up at higher field than in the spectrum of the zinc porphyrin (**13**), Figure 1.18 and 1.19, respectively. Beyond diamagnetic current of the zinc porphyrin π-electrons, deshielding effect resulted in shift of the pyrrolic protons of zinc porphyrin **13** for about 0.1 ppm. The proton chemical shifts of the *meso*-phenyls and their substituents were not affected with ring current change since they are situated either above or below the plane of the porphyrin ring. The NH protons inside the core of free-base porphyrin appeared at very high field, since they experience the largest ring current shifts. Hence, the principal changes in the ^{1}H NMR spectrum of the zinc porphyrin (**13**) were reduced to the loss of high field signal for NH protons, Figure 1.19.

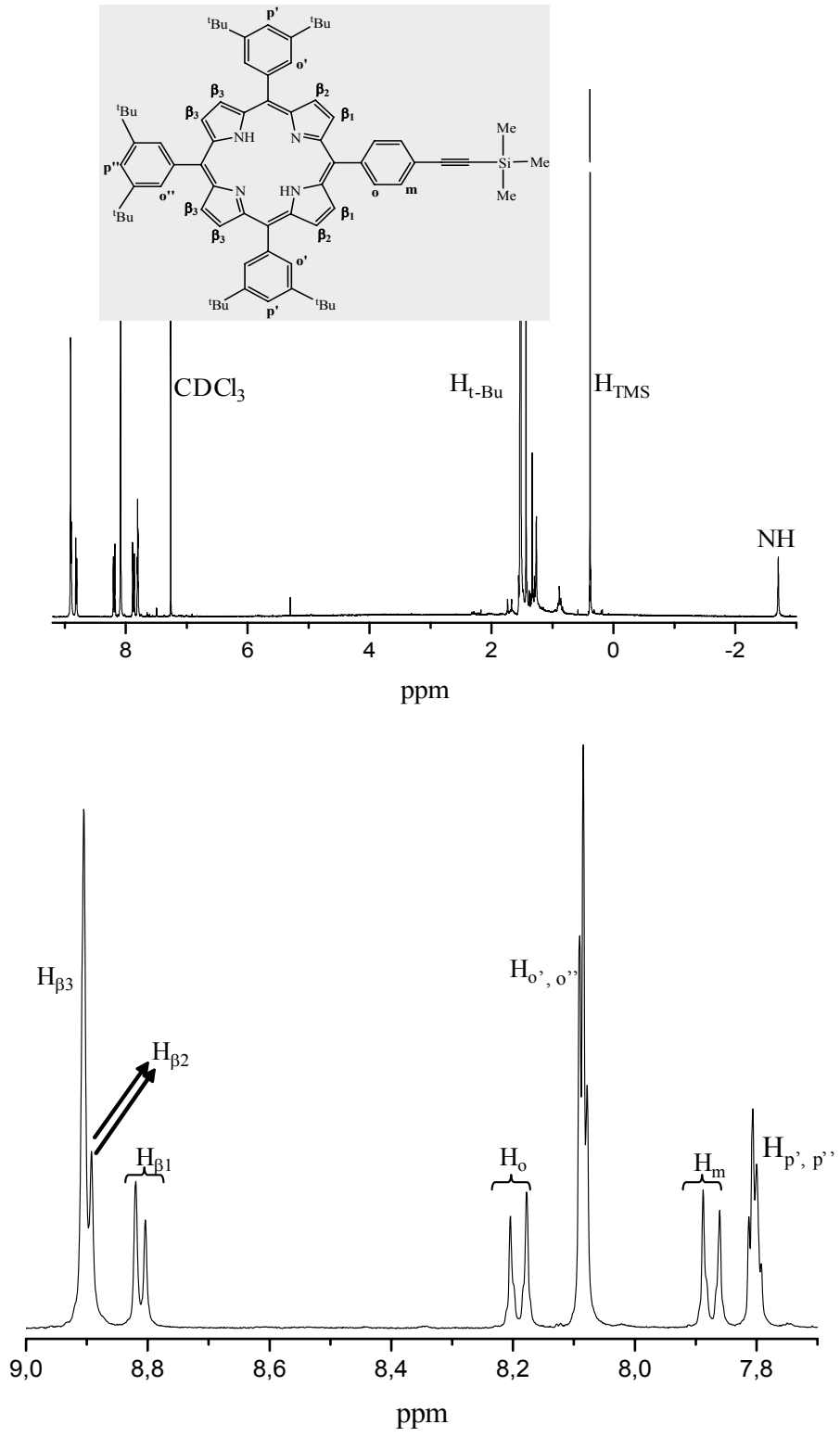

Figure 1.18 *^{1}H NMR spectrum of free-base porphyrin* ***12*** *in $CDCl_3$ at 297 K.*

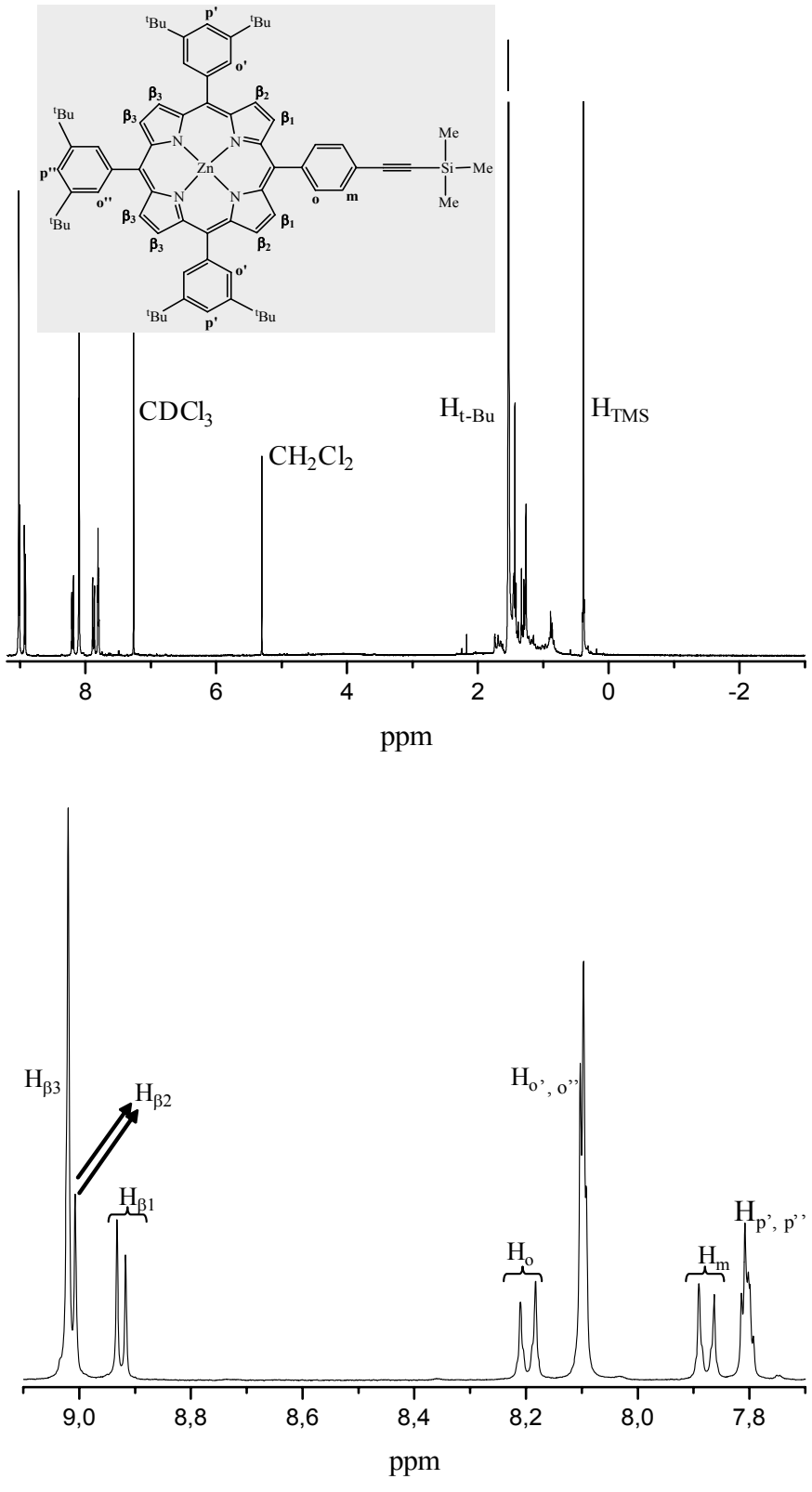

Figure 1.19 *^{1}H NMR spectrum of zinc porphyrin* ***13*** *in $CDCl_3$ at 297 K.*

1.5.2. Characterization by UV-visible absorption spectroscopy.[124-130]

In the electronic absorption spectra, the highly conjugated porphyrin macrocycle shows strong transition to the second excited state ($S_0 \rightarrow S_2$) in near-UV region (about 400 nm), which is referred to the Soret or B band, followed by several weaker absorption maxima (Q bands) at higher wavelengths (500 to 700 nm), which correspond to weak transitions to the first excited state ($S_0 \rightarrow S_1$). Both, Soret or B band and Q bands originate from $\pi \rightarrow \pi^*$ electronic transitions of conjugated double bonds of the porphyrin macrocycle. The qualitative interpretation of the absorption spectra of porphyrins relies on simple molecular orbital theory and the Gouterman's "four-orbital model",[125] with the transition dipole moment treated as a set of transition monopoles distributed across the π-system. As a result of its local D_{2h} symmetry, the free-base porphyrin has four dipole transitions: $Q_x(0\text{-}0)$ and $Q_y(0\text{-}0)$, and their harmonic transitions $Q_x(0\text{-}1)$ and $Q_y(0\text{-}1)$. On the other hand, for the zinc porphyrin with its D_{4h} symmetry, the x and y directions are identical, so that the two dipole transitions are degenerated. Whereas Q_x and Q_y transitions behave identically, the two different absorption bands can be observed due to harmonic vibrations Q(0-0) and Q(0-1). The explanation of spectra in terms of $\pi \rightarrow \pi^*$ transitions in the Gouterman's "four-orbital model" involves combination of electron transitions from two highest occupied molecular orbitals (HOMO and HOMO-1) to a degenerate pair of lowest unoccupied molecular orbitals (LUMO). The highest occupied orbitals have symmetry a_{2u} and a_{1u} and the lowest empty orbitals have symmetry e_g. The two highest occupied π orbitals (a_{2u} and a_{1u}) have about the same energy. Although it can be assumed that this would lead to two almost coincident absorption bands due to $a_{2u} \rightarrow e_g$ and $a_{1u} \rightarrow e_g$ transitions, in fact these two transitions mix together by a process known as configurational interactions result in two bands with very different intensities and wavelengths. Hence, a constructive interference leads to the intense short-wavelength B band, while the weak long-wavelength Q band results from destructive combinations. The two types of positions on the porphyrin periphery are referred to as *meso* and β. The a_{1u} orbital has nodes at all four *meso* positions whereas the a_{2u} orbital has high coefficients at these sites, Figure 1.20.[129]

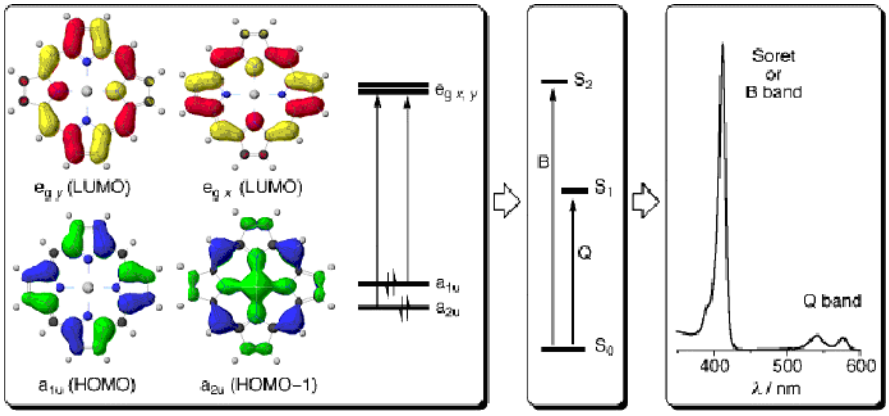

Figure 1.20 *The four Gouterman molecular orbitals explain the absorption spectra of simple zinc porphyrins.*

In accordance with the nodal pattern of a_{1u} and a_{2u} orbitals of electronic structures at the ground state of the porphyrins, the first orbital has major contributions on α and β carbons and the second one has a large contribution on nitrogens and *meso*-carbons. Variations of the peripheral substituents on the porphyrin ring often cause only a slight perturbation of the electronic structure, and by that, minor changes in the intensity and wavelength of absorption maxima. The small impact of *meso*-phenyl substituents is result of minimal π-overlap between the phenyl and the porphyrin rings, due to the large phenyl-porphyrin dihedral angles, which result from steric interactions with the β-hydrogens.

The UV-visible spectra of the free-base (**12**) and the zinc (**13**) porphyrins were recorded in dichloromethane at room temperature. The adherence to Lambert-Beer's law was verified by quantitative analysis, which implied an absorbance recording of the porphyrin solution after successive addition of small aliquots from its stock solution of well-defined concentration. If probed solutions adhere to the law, the molar absorption coefficient can be calculated from the slope of a linear dependence of the absorption on concentrations of the porphyrin solution at each wavelength. In this manner, the molar absorption coefficient can be calculated for the Soret band and for each absorption maxima in the Q-bands region, by changing a concentration of the stock solution. The examined concentrations of the porphyrin solution were adjusted according to absorbance, which recommendatory should cover the range between 0.5 and 1.2. This absorbance interval corresponds to concentration of around 10^{-6} M for the Soret band, and around 10^{-5} M if the absorption of the Q-bands is measured.

The obtained molar extinction coefficients are presented in Table 1.1, while in Figure 1.21 one spectrum for each porphyrin, **12** and **13**, is extracted from the entire measurements.

	λ_{max} (nm)	ε (M^{-1} cm^{-1})
Free-base porphyrin **12**	422	506 800
	517	18 600
	553	10 900
	592	5 600
	647	5 600
Zinc(II) porphyrin **13**	422	558 100
	549	21 500
	588	6 200

Table 1.1 *Electronic absorption maxima and corresponding molar extinction coefficients calculated from the slope of linear dependence of absorption on concentration.*

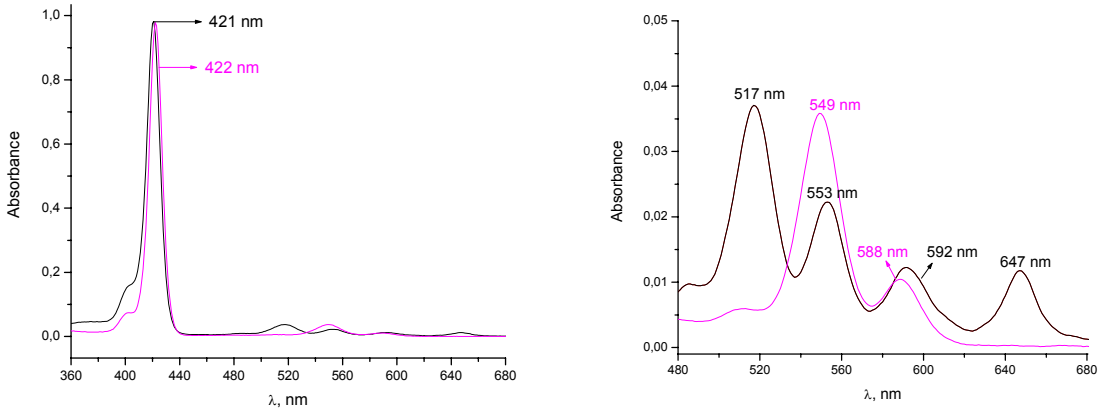

Figure 1.21 *UV-visible absorption spectra of free-base porphyrin* ***12*** *(black line) at concentration of 1.94 x* 10^{-6} *M and zinc porphyrin* ***13*** *(purple line) at concentration of 1.75 x* 10^{-6} *M, in dichloromethane at 297 K.*

1.6. SYNTHESIS AND CHARACTERIZATION OF MONOMER 1.

Design of nucleosides covalently modified with fluorescent tags such as porphyrins is a challenge of growing interest.[59-77] In respect to desired features, various linkers have been employed in attaching porphyrins to nucleosides.[59-61,64,71,72] Here, porphyrins were anchored to the appropriate position of the uridine by means of robust carbon-carbon bond.[62-64,70] The typical position for substitution at pyrimidines is position-5, because, although modified, nucleosides retain their ability to selectively recognize complementary molecules.[59-64,70,131-138]

1.6.1. Preparation of uridine-porphyrin conjugate 15 by Sonogashira reaction.

Straightforward method for the synthesis of porphyrin-uridine conjugate is palladium(0)-copper(I) catalyzed cross-coupling reaction of the 5-iodo uridine and the porphyrin functionalized with the terminal alkyne.[70,132-138] Hence, the Sonogashira coupling reaction was performed between iodo derivative **6** and terminal acetylene **14** in triethylamine using palladium(II)-copper(I) catalytic system, Figure 1.22. In order to render the starting materials soluble in triethylamine, 5-iodo-2'-deoxyuridine **5** was protected at C-5' with triisopropylsilyl group and porphyrin was functionalized with *tert*-butyl groups at *meso*-phenyls. The zinc porphyrin was employed due to possible metallation of the free-base porphyrin in the presence of copper and palladium.

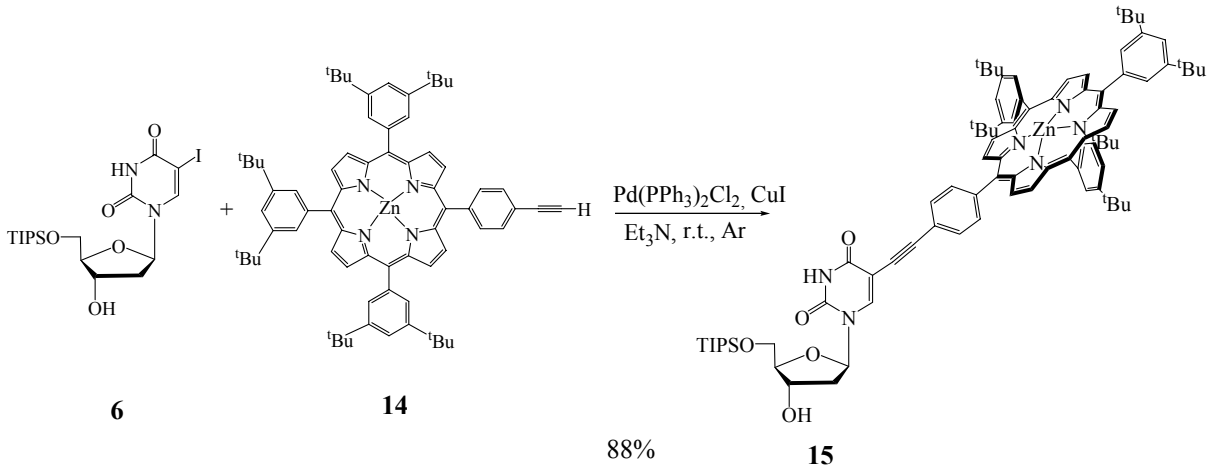

6 **14** **15**

Figure 1.22 *Sonogashira coupling between uridine* ***6*** *and zinc porphyrin* ***14****.*

This homogeneous palladium-mediated coupling reaction was performed under mild reaction conditions, at room temperature and under argon atmosphere to avoid the formation of undesired homocoupling product. In addition, triethylamine was extensively bubbled with argon prior utilization to minimize the presence of oxygen in the reaction mixture. The catalytic system that we employed for this reaction included $PdCl_2(PPh_3)_2$ and CuI, in a 1:2 mole ratio. Accordingly, 2.5 mol% of Pd(II) and 5.0 mol% of copper(I) iodide effected coupling. To increase the yield of the cross-coupling product over the homocoupling product the 1.1 equivalent of porphyrin **14** was employed. In these reaction conditions the reaction reached completion within ca. 40 hours. Isolation of the cross-coupling product **15** required consecutive washing of a dichloromethane solution of the crude reaction mixture with: 2% solution of ethylenediaminetetra-acetic acid (EDTA) disodium salt, 0.35 M solution of sodium thiosulfate ($Na_2S_2O_3$), saturated solution of ammonium chloride (NH_4Cl), and water. The final purification by column chromatography over silica provided uridine-porphyrin conjugate **15** in 88% yield.

The product was characterized by ^1H NMR and UV-visible spectroscopy. The ^1H NMR spectrum of **15** reflects the coupling product of uridine **6** and porphyrin **14** with multiple resonances consistent with two constituent parts, minus the acetylenic hydrogen from the porphyrinic contribution. Although the spectrum of the product consists of the sum of the corresponding spectra, resonances of the sugar and the porphyrin moieties are slightly shifted. The NMR signals of the porphyrin moiety are shielded and show up at higher field. The β pyrrolic protons are shifted for about 0.016 ppm, e.g. doublet of $H_{\beta 1}$ in **15** shows up at 8.904 ppm and in **14** at 8.921 ppm, whereas *meso*-phenyl protons are shifted for about 0.008 ppm, Figure 1.23. On the contrary, chemical shifts of the sugar moiety are slightly shifted downfield, presumably due to the porphyrin ring current. The low value of the observed shifts evidenced that porphyrin and uridine in **15** are spatially afar. Comparing the electronic spectra of uridine-porphyrin conjugate **15** and zinc porphyrin **14** in CH_2Cl_2, both show the same profile, with no considerable difference in absorption maxima and extinction coefficients. The obtained values which correspond to **15**: at 422 nm (ε= 569 100 M^{-1} cm^{-1}), at 549 nm (ε= 21 800 M^{-1} cm^{-1}) and at 589 nm (ε= 6 200 M^{-1} cm^{-1}).

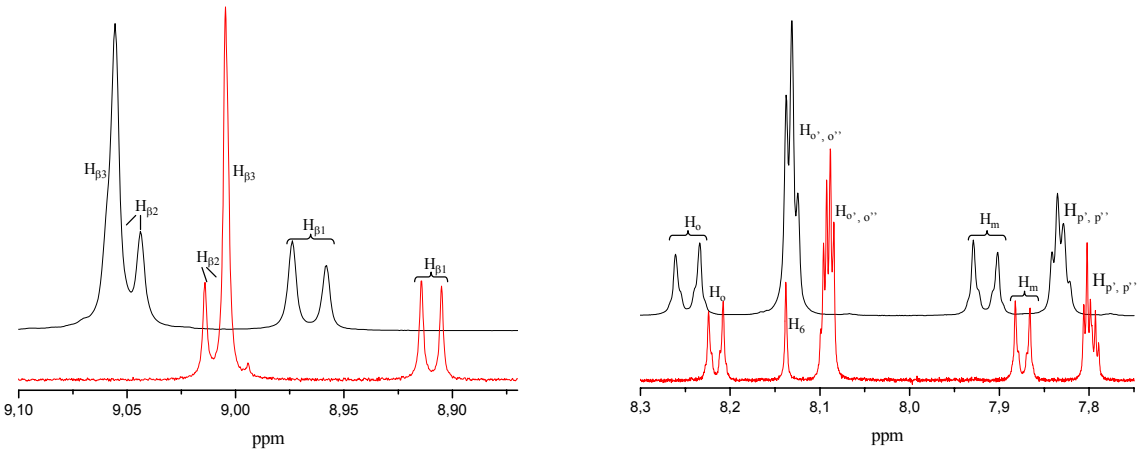

Figure 1.23 *Comparison of NMR spectra ($CDCl_3$, 300 MHz) of uridine-porphyrin conjugate* ***15*** *(bottom) and zinc porphyrin* ***14*** *(top) along with the low field region chemical shift assignments.*

1.6.2. Protection at N-3 of 15 with chloromethyl *p*-metoxybenzyl ether (17).

Prior to the nucleophilic substitution at C-3' of the ribose, N-3 position of the uracil had to be protected. The *p*-metoxybenzyloxymethyl group, which is stable to conditions required for the substitution, was prepared in two steps from *p*-metoxybenzylalcohol according to Figure 1.24.[139,140]

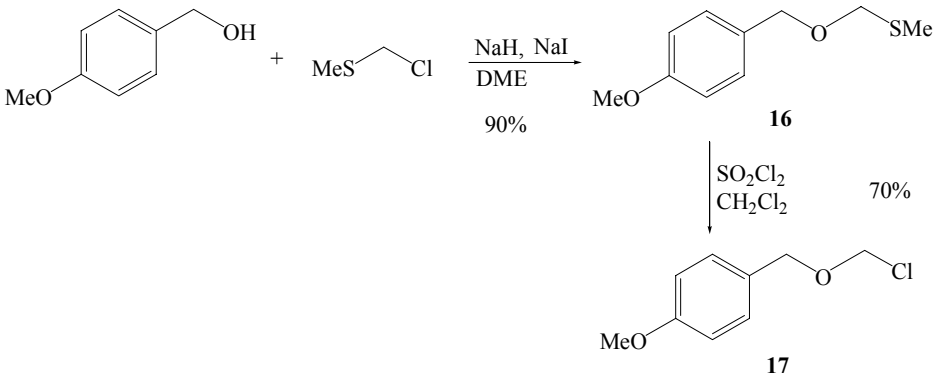

Figure 1.24 *Synthesis of chloromethyl p-metoxybenzyl ether (17).*

The first step in the synthesis of this appropriate protecting group included conversion of primary alcohol to ether. The reaction of the sodium salt of *p*-metoxybenzylalcohol in dimetoxyethane with iodomethyl methyl sulfide, formed in situ from chloromethyl methyl sulfide and sodium iodide, provided *O,S*-acetal **16**. After stirring for 1 h at 0 °C and another 5

h at room temperature the reaction mixture was poured into water and extracted with ether. Filtration of the crude product through a short column of silica-gel afforded the product as yellow oil in 90% yield. The product was evidenced by ^{1}H NMR spectroscopy.

Treatment of *O*,*S*-acetal **16** with 1.5 equivalents of sulfuryl chloride in dichloromethane at the temperature of -78 °C led to selective cleavage of the carbon-sulfur bond to give chloromethylbenzyl ether **17** and methanesufenyl chloride. The latter is volatile and was conveniently removed together with the solvent on evaporation at reduced pressure. The reaction was conducted at low temperature in order to prevent formation of *p*-metoxybenzylchloride. Obtained chloromethyl *p*-metoxybenzyl ether **17** is unstable and decomposes on heating and during storage.[139] Hence, the crude product had to be used in the successive reaction without any purification. According to the literature, the yield of product **17** was considered to be 70%.[139]

Finally, uracil base of **15** was selectively protected at N-3 with freshly prepared chloromethyl *p*-metoxybenzyl ether **17**, Figure 1.25.[53,62]

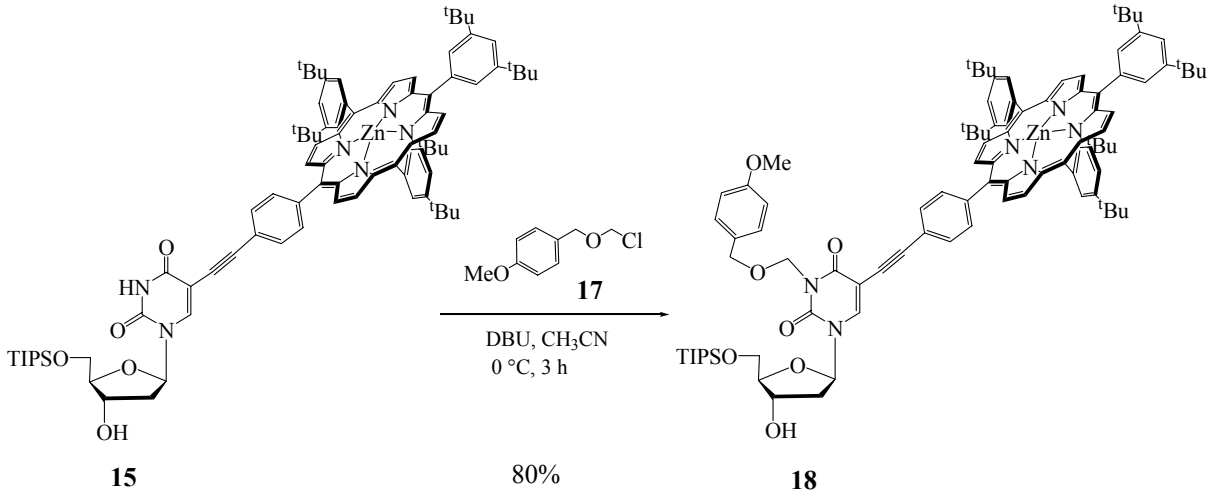

Figure 1.25 *Selective protection of uracil base **15** at N-3.*

To the solution of porphyrin-uridine conjugate **15** in acetonitrile cooled to 0 °C, 2.2 equivalents of 1.8-diazabicyclo[5.4.0]undec-7-ene (DBU) and 2 equivalents of **17** were added. The equivalents of **17** used in the reaction were calculated according to 70% purity and 1.2 stoichiometric equivalents. The reaction was carried out at low temperature in order to

prevent loss on yield which could have been caused by the reverse reaction. Thin layer chromatography visualisation of the reaction progress showed that maximum formation of the product **18** was reached within 3 hours. With longer reaction times the yield of the desired product decreased while the amount of the less polar material increased. However, purification of the crude product with silica-gel chromatography provided ca. 10% of uncharacterized less polar material, 80% of the protected porphyrin-uridine conjugate **18** and 10% of the unprotected starting material **15** (arranged by polarity). We assumed that the less polar material corresponds to alkylation of the 3'-hydroxyl group. The location of *p*-metoxybenzyloxymethyl group at N-3 was confirmed by ^{1}H NMR analysis of **18**, Figure 1.26.

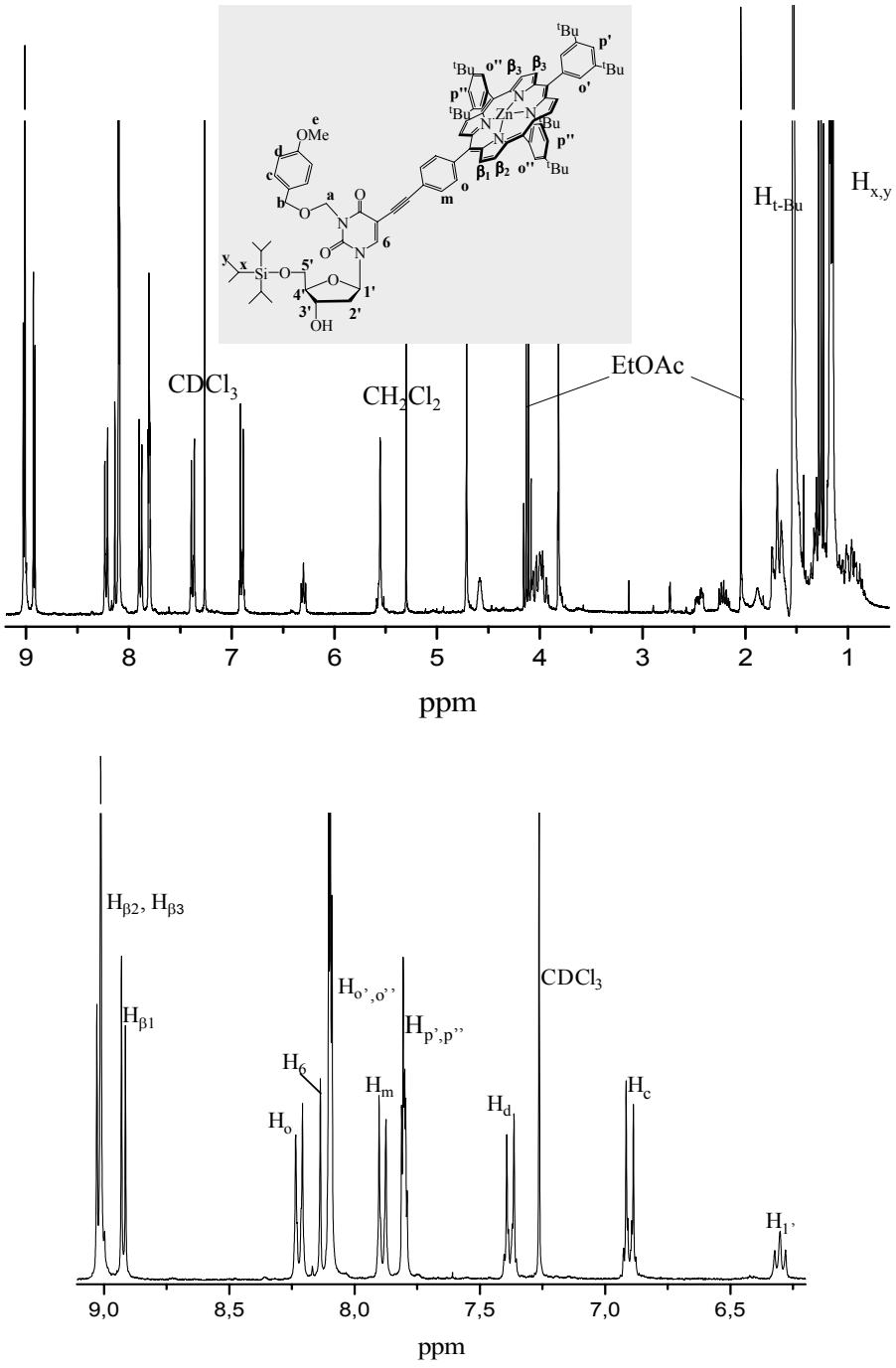

Figure 1.26 *^{1}H NMR spectrum ($CDCl_3$, 300 MHz) of* ***18****.*

The fact that chemical shifts of the sugar protons were largely independent on the protection indicates that the conformation of the conjugate is maintained. On the other hand, resonances of the porphyrinic protons were slightly deshilded. The β-pyrrolic protons and *meso*-aryl protons were shifted for 0.013 and 0.007 ppm, respectively.

After protection at N-3 of **15** we approached to the selective insertion of ether-ester functionality at C-3' of the ribose.

1.6.3. Etherification at C-3' of 18.

The monomer (**1**) was prepared by etherification of the selectively protected porphyrin-uridine conjugate **18**. The direct alkylation at C-3' of the ribose was realized by modified Williamson synthesis.[53] The porphyrin-uridine conjugate **18** was allowed to react with sodium hydride (NaH) in dry THF at 0 °C to room temperature. The obtained alkoxyde was substituted with *tert*-butyl 2-bromoacetate in the presence of tetrabutylammonium iodide (TBAI) as catalyst. In order to fine-tune the reaction conditions, the equivalents of sodium hydride, TBAI and the alkylating agent were systematically varied in dry THF under argon atmosphere, Table 1.2.

Entry:	***1***[a,b]	***2***[a,b]	***3***[a,b]	***4***[a,b]	***5***[b,c]
NaH, equiv.	1.7	1.9	2.2	2.8	1.9
TBAI, equiv.	0.3	0.3	0.5	0.5	0.3
t-Butylbromo acetate, equiv.	1.1	1.3	1.1	1.1	1.3
Desired product **1**	49%	62%	40%	20%	37%
Medium polar byproduct	/	/	8%	11%	5%
Starting **18**	36%	29%	27%	9%	21%
Other byproducts	7%	4%	20%	46%	30%

[a] These reactions were performed with 0.1 g of **18**.
[b] Concentration of reaction mixtures: 3.0×10^{-2} M. Yields after purification by column chromatography on silica-gel.
[c] The reaction performed with 0.6 g of **18**.

Table 1.2 *Optimisation of the etherification reaction with* ***18****.*

As noted in entries 1 to 4, the yield of the desired ether decreased and of byproducts increased when the number of equivalents for NaH was increased. Further variations of equivalents of TBAI and the alkylating agent were performed in the presence of 1.9 equivalents of NaH. These results suggested that 1.9 equivalents of NaH, 0.3 equivalents of TBAI and 1.3 equivalents of the alkylating agent are providing **1** in the best yield. The reaction conditions were explored further by performing the reaction on a larger scale, with 0.6 g of **18**. In these conditions, the desired product was obtained in the moderate yield with the rest being byproducts, as noted in entry 5 in Table 1.2. Finally, the reaction was performed in the conditions noted in entry 2, Figure 1.27.

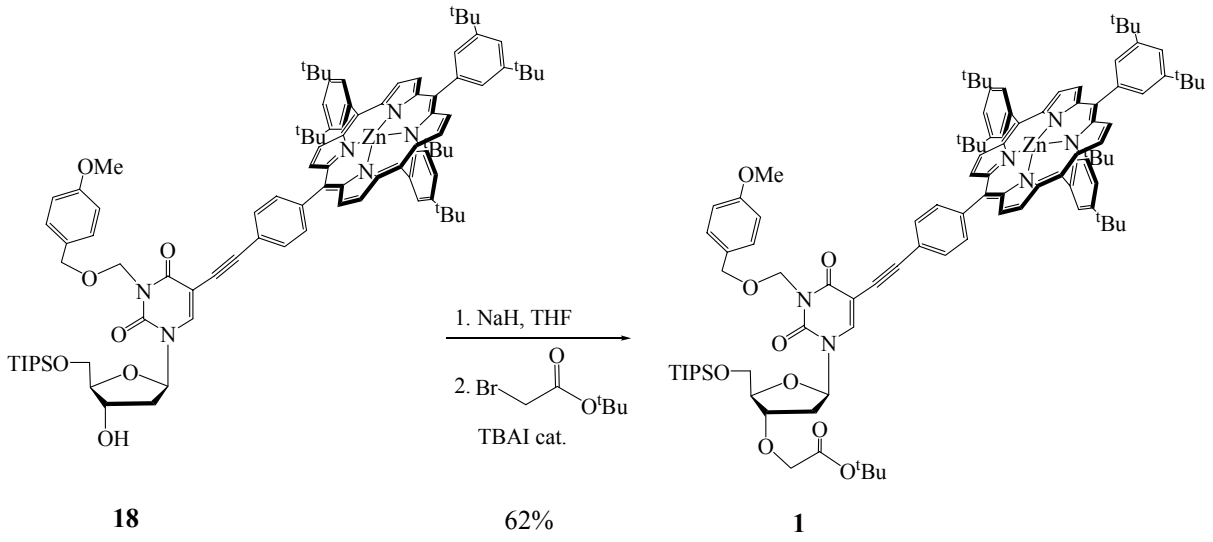

Figure 1.27 *Synthesis of monomer **1**.*

The reaction of deprotonation at C-3' was completed in 1 h at 0 °C and 4 h at room temperature. Then, the catalyst and the alkylating agent were added. The time course was monitored by thin layer chromatography following the formation of the target product **1** and disappearance of the starting compound **18**. Although extensive series of the experiments were carried out to improve the yield of the desired product, a certain amount of the starting material always remained unreacted or/and fell into byproducts. After stirring overnight at room temperature, the reaction mixture was quenched with water and concentrated. The residue was dissolved in dichloromethane and corresponding solution was washed with saturated solution of ammonium chloride and water. The monomer **1** was isolated by chromatography on silica-gel, together with uncharacterized more polar byproduct, residual

starting compound **18** and other byproducts. The isolated residual starting material was analyzed by ^{1}H NMR spectroscopy, and if any change in the structure was not evidenced it could be reused in the reaction.

Once monomer **1** was obtained we were able to apply an iterative divergent-convergent strategy of the oligomerization.

1.7. BUILDING OF THE OLIGONUCLEOTIDIC ARRAY WITH PENDANT PORPHYRINS.

The strategy of preparation of the porphyrin-uridine oligomers implies divergent approach to selective deprotection of the carboxylic acid at C-3'and the alcohol at C-5', which is followed by coupling of these two units. The *tert*-butyl as carboxylic blocking group and triisopropylsilyl group as 5'-*O*-blocking group were used in preference to other protecting groups due to their selective cleavage under mild conditions. The backbone growth is realized by the ester formation between C-3' of the upper unit and C-5' of the lower unit. Thereby coupling of such two monomeric units provided dimer, coupling of two dimeric units provided tetramer, and coupling of two tetrameric units provided octamer.

Hence, for monomer-acid **20** and monomer-alcohol **19** as targets, a divergent approach was pursued to cleave *tert*-butyl group at C-3' and triisopropylsilyl group at C-5' from monomer **1**. Then, monomer-acid **20** was esterified with **19** to provide dimer **2**. From dimer **2**, duplication of two deprotection steps afforded dimer-acid **22** and dimer-alcohol **21**, which were coupled to tetramer **3**. The same steps were repeated for the tetramer aiming to the final octamer **4**. This synthetic strategy afforded ability to control the sequence of metallated and free-base porphyrins in the array, and also the pattern of substituents of each uridine in the backbone. All oligomeric acids bear exclusively free-base porphyrins, while corresponding alcohols have zinc porphyrin at the terminal unit in the backbone. All the porphyrin-uridine oligomers were characterized by ^{1}H NMR spectroscopy, UV-visible and fluorescence spectroscopy, mass spectrometry, and examined for purity by elemental analysis or analytical size-exclusion chromatography.

It was assumed that this modified oligodeoxyuridines can provide very flexible backbone due to five atoms in the interuridinic linkage. In this context, each porphyrin would follow preorganization of the backbone, if considering that the bond between the porphyrin and the uridine is a straight line which drastically reduces rotational freedom. Also, it should be noted that in general oligonucleotides are molecular systems with well-organized structural features. Thus, it is logically to expect that the porphyrins along the array will be well-organized.

1.7.1. Selective deprotection of the alcohol at C-5' of the mono- and oligomers.

Among the others available, we have used triisopropylsilyl group as 5'-*O*-blocking group because it is stable to basic and acidic conditions. Although silyl ether linkage could be cleaved by using variety of reagents involving Lewis acids, we used fluoride ions due to mild reaction conditions.[52-54,86,141-144] Hence, triisopropylsilyl group was cleaved in the reaction with 2 equivalents of tetrabutylammonium fluoride (TBAF), as a source of the fluoride ion, in THF as a solvent at room temperature, Figure 1.28. The reaction mixture was concentrated, dichloromethane solution of the crude product was washed with water, and finally the product was purified by column chromatography on silica-gel. Desilylation of monomer **1** was clear and straightforward reaction which resulted with 96% yield.

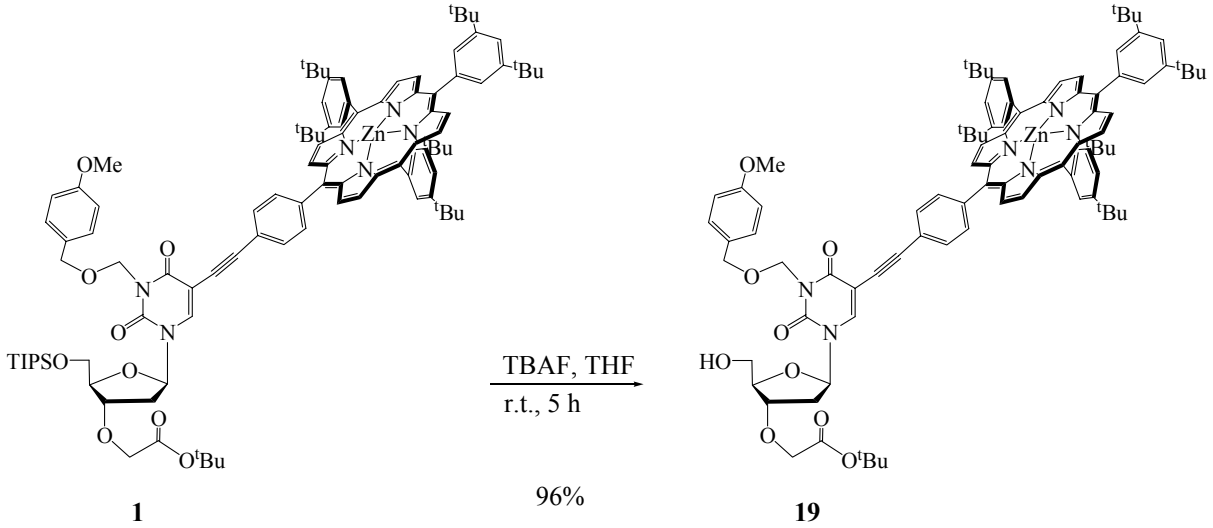

Figure 1.28 *Deprotection of the alcohol at C-5' of monomer **1**.*

Application of this procedure to dimer **2** provided dimer-alcohol **21** in 89% yield, while in the case of tetramer **3** the desired product **23** was obtained in 87% yield. The reaction course for the tetramer was difficult to follow by TLC due to close retention factors of the starting compound (**3**) and the product (**23**). In this respect, the reaction was stirred for 12 h at room temperature. All the products were corroborated by ^{1}H NMR spectroscopy, with disappearance of signals related to triisopropylsilyl group, namely at 1.26 ppm for CH and at 1.17 ppm for CH_3.

The proposed mechanisms establish that the cleavage of an *O*-silyl ether with fluoride ions proceeds through an initially formed pentacoordinate silicate which then provides corresponding alkoxyde and silyl fluoride.[86] Addition of two fluoride ions to form hexacoordinate silicate is also known and may facilitate the following collapse of the Si-O bond, setting free the alkoxyde. Nevertheless, generality of this migration is still under assumption.

1.7.2. Deprotection of the carboxylic acid at C-3' of the mono- and oligomers.

A part of the plan in the synthesis was dealkylation of *tert*-butyl ester under acidic conditions, i.e. the procedure using excess of trifluoroacetic acid (TFA) in dichloromethane.[145,146] Hence, the cleavage was attained upon treatment of monomer **1** or oligomers (**2** or **3**) with TFA/CH_2Cl_2 at 0 °C to room temperature. The reaction course was followed by monitoring the TLC spots that characterize disappearance of the starting compound (*n*-hexane/ethyl acetate as an eluent) and appearance of the product with the free carboxylic acid at C-3' (mixture of ethyl acetate, methanol and acetic acid as an eluent). On the basis of the results obtained by modifying the ratio of TFA/dichloromethane, it was found that 20% of TFA in dichloromethane (m/V (1:25) based on the starting mono- or oligomers) affords the highest yields of the target compounds. As purification procedure, the reaction mixture was diluted and neutralized by washing with water, and the crude product was subjected to purification by silica-gel column chromatography. The optimal conditions were applied to cleave *tert*-butyl group from monomer **1** affording product **20** in 75% yield, Figure 1.29.

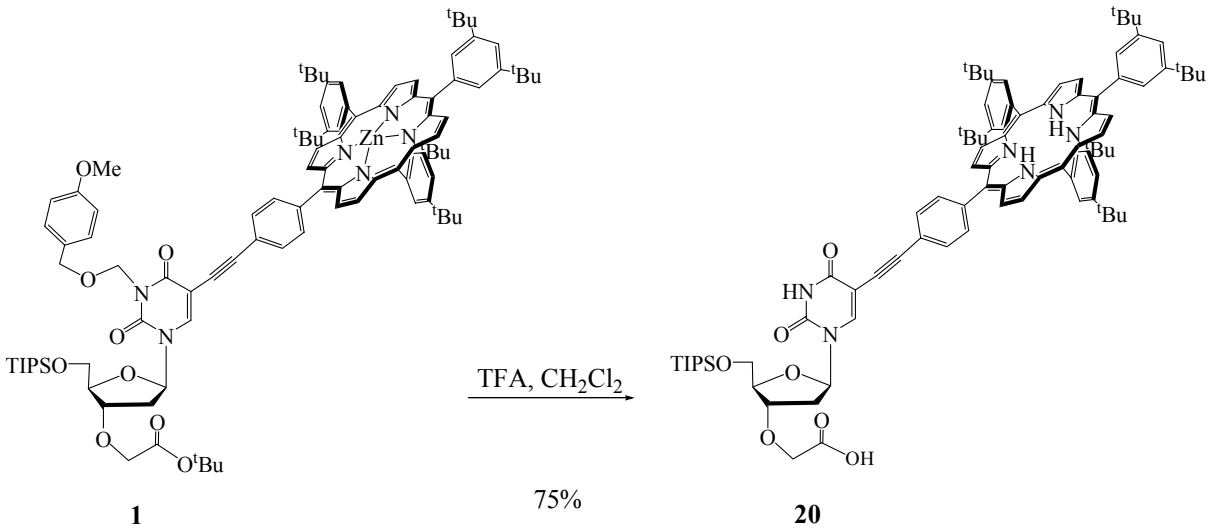

Figure 1.29 *Dealkylation of the carboxylic acid at C-3' of monomer **1**.*

In the same manner, from dimer **2** we obtained dimer-acid **22** in 73% yield, and from tetramer **3** desired product **24** in 78% yield. Besides the carboxylic acid at C-3', the structural characteristics of the products obtained in the reaction with TFA are: free-base porphyrins along the array and cleavage of the protection group at N-3 of the uracil, because *p*-metoxybenzyloxymethyl function is highly unstable in acidic conditions, Figure 1.30.[147-152] All the products were characterized by ^{1}H NMR spectroscopy.

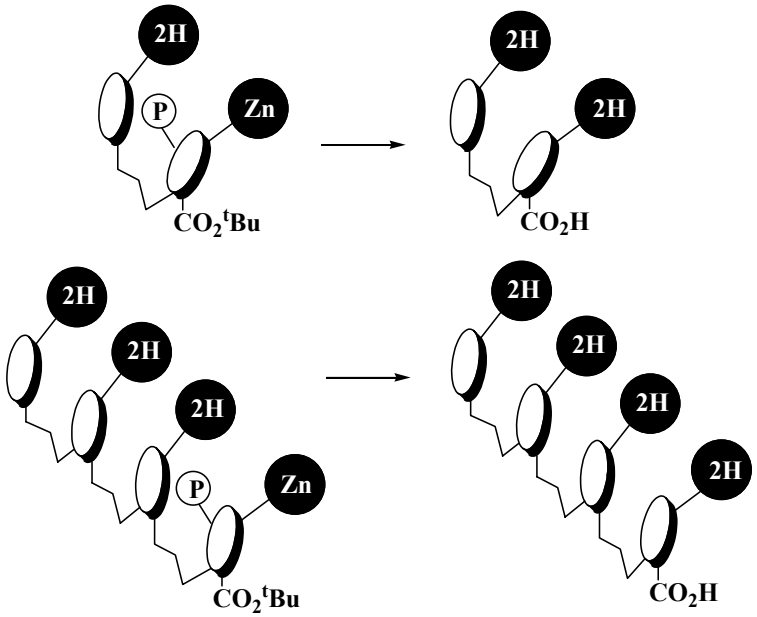

Figure 1.30 *The schematic presentation of the structural changes in the reaction of cleavage of tert-butyl group from the carboxylic acid of the dimer and the tetramer.*

1.7.3. Synthesis of dimer 2.

The straightforward coupling of monomer-acid **20** and monomer-alcohol **19** was performed according to Figure 1.31. The carboxylic acid **20** was esterified with alcohol **19** in the presence of the most commonly used dehydrating agent, dicyclohexylcarbodiimide (DCC).[153-156] The starting compounds in a 1:1 mole ratio were mixed with 1.4 equivalents of DCC and 2.1 equivalents of 4-dimethylaminopyridine (DMAP) in dichloromethane stabilized with amylene, to avoid unwanted side reactions.

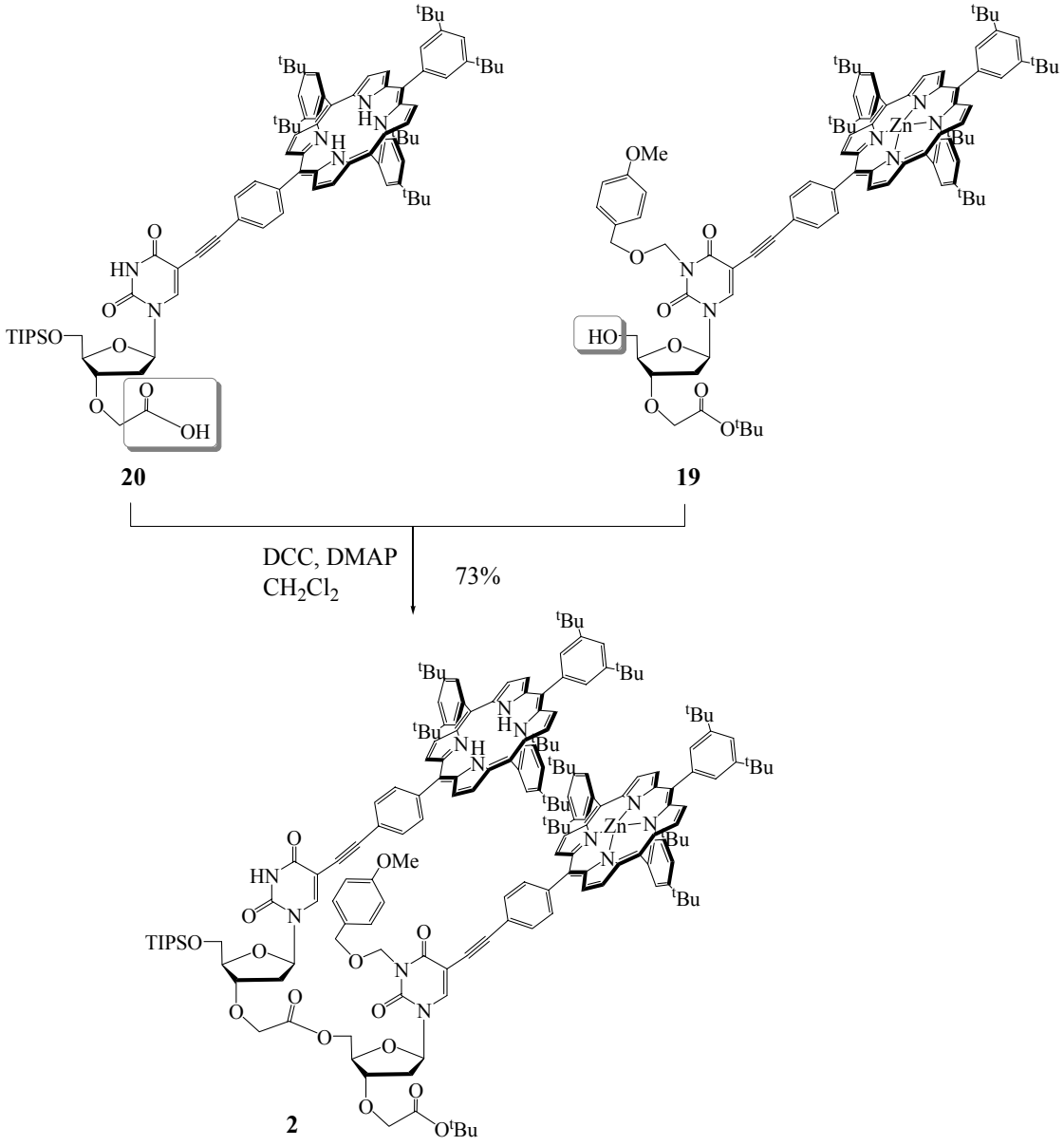

Figure 1.31 *Synthesis of dimer* ***2****.*

One of the limitations of the DCC method is the formation of *N*-acylurea. This problem was alleviated by addition of the base (DMAP), which serves to activate alcohol to nucleophilic attack by formation of the hydrogen bonded complex.[157] Besides, DMAP provided carboxylate **25** by deprotonation of the carboxylic acid. According to this, and the fact that an amine coordinates to zinc situated in the porphyrin core, a large excess of DMAP was employed in the reaction. The mechanism for the esterification which was enabled by double function of DMAP is presented in Figure 1.32.

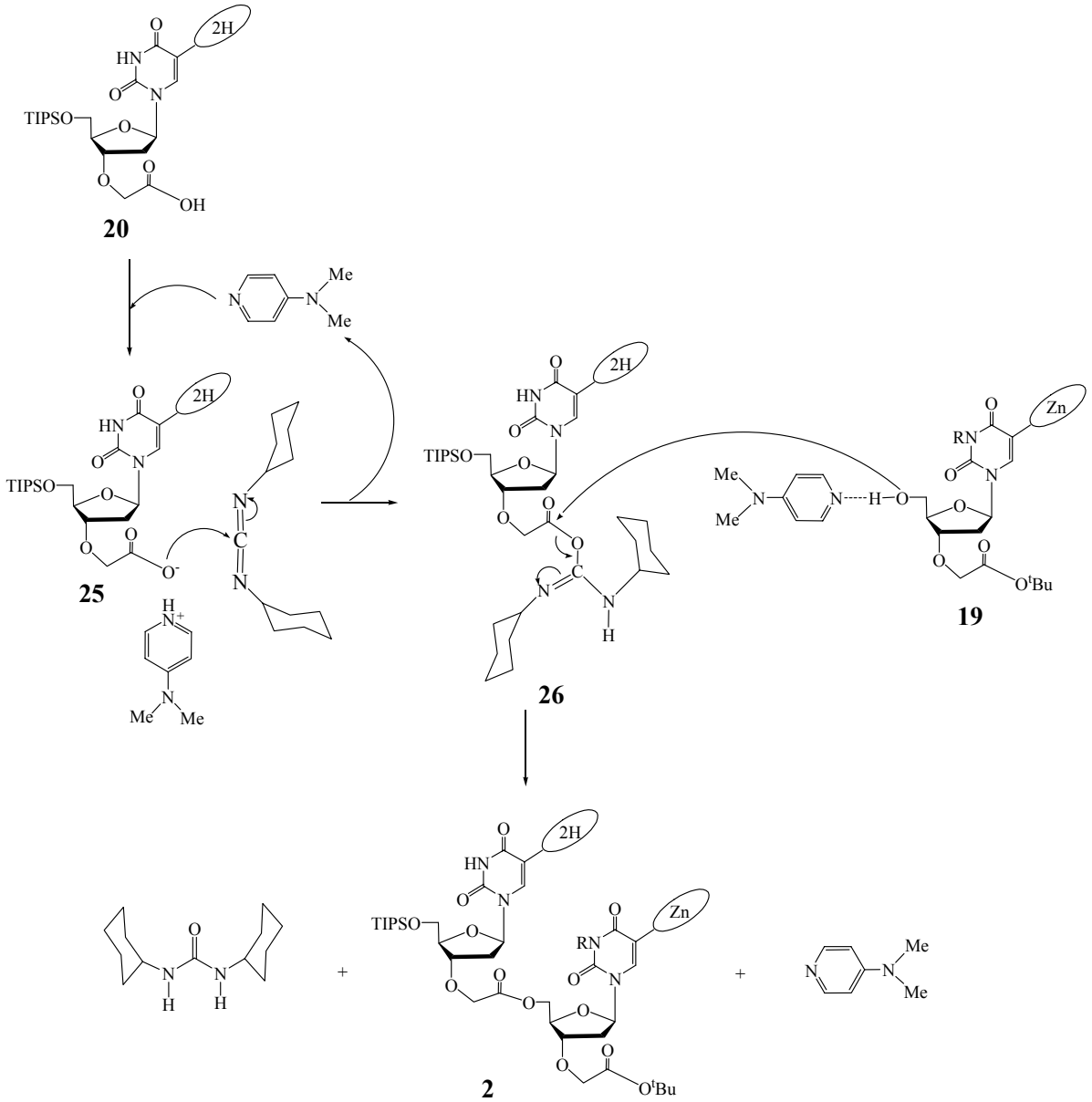

Figure 1.32 *Mechanism of esterification of monomer-acid* ***20*** *with monomer-alcohol* ***19*** *in the presence of DCC as a coupling reagent and DMAP as an activating agent.*

The reaction was initiated by addition of carboxylate **25** to DCC providing the active ester **26**, which was then attacked by nucleophilic alcohol **19** providing the desired ester. At this stage, the presence of an amine is crucial for weaker nucleophiles. If the nucleophile reacted too slowly, the diverse rearrangement of the active ester would provide corresponding *N*-acylurea **27** as the main product, Figure 1.33.

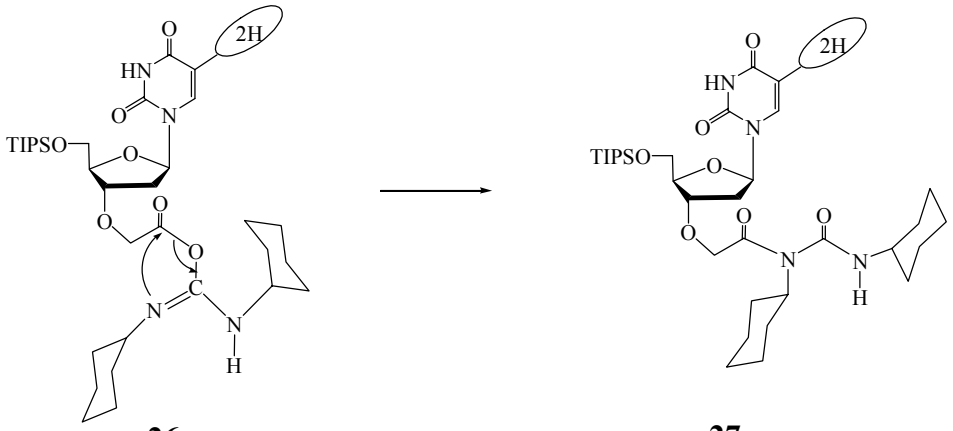

26 **27**

Figure 1.33 *Formation of N-acylurea derivative **27** as a possible side reaction.*

The reaction course toward dimer **2** was difficult to follow by TLC analysis (*n*-hexane/ethyl acetate (6.5:3.5)), because the spots of the starting alcohol **19** and the product were very close. However, the reaction was found to be complete after stirring overnight at room temperature, since the TLC of the reaction mixture was neat presenting only one spot. Within this favourable reaction path that provided desired dimer **2**, DCC was converted to its hydrated adduct, dicyclohexylurea (DCU). DCU was precipitated by addition of toluene to the crude product. The purification procedure involved the sequence of three chromatography columns on silica. Firstly, the crude reaction mixture was passed over flash silica column, then gel-permeation column (GPC) in toluene, and finally over silica-gel column. The targeted dimer **2** was obtained in 73% yield.

1.7.4. Synthesis of tetramer 3.

To prepare target compound **3**, dimer-alcohol **21** and dimer-acid **22** were coupled by the same esterification procedure that was used in the synthesis of dimer **2**, Figure 1.34. But, comparing to the synthesis of the dimer, the process towards pure tetramer was far more complicated.

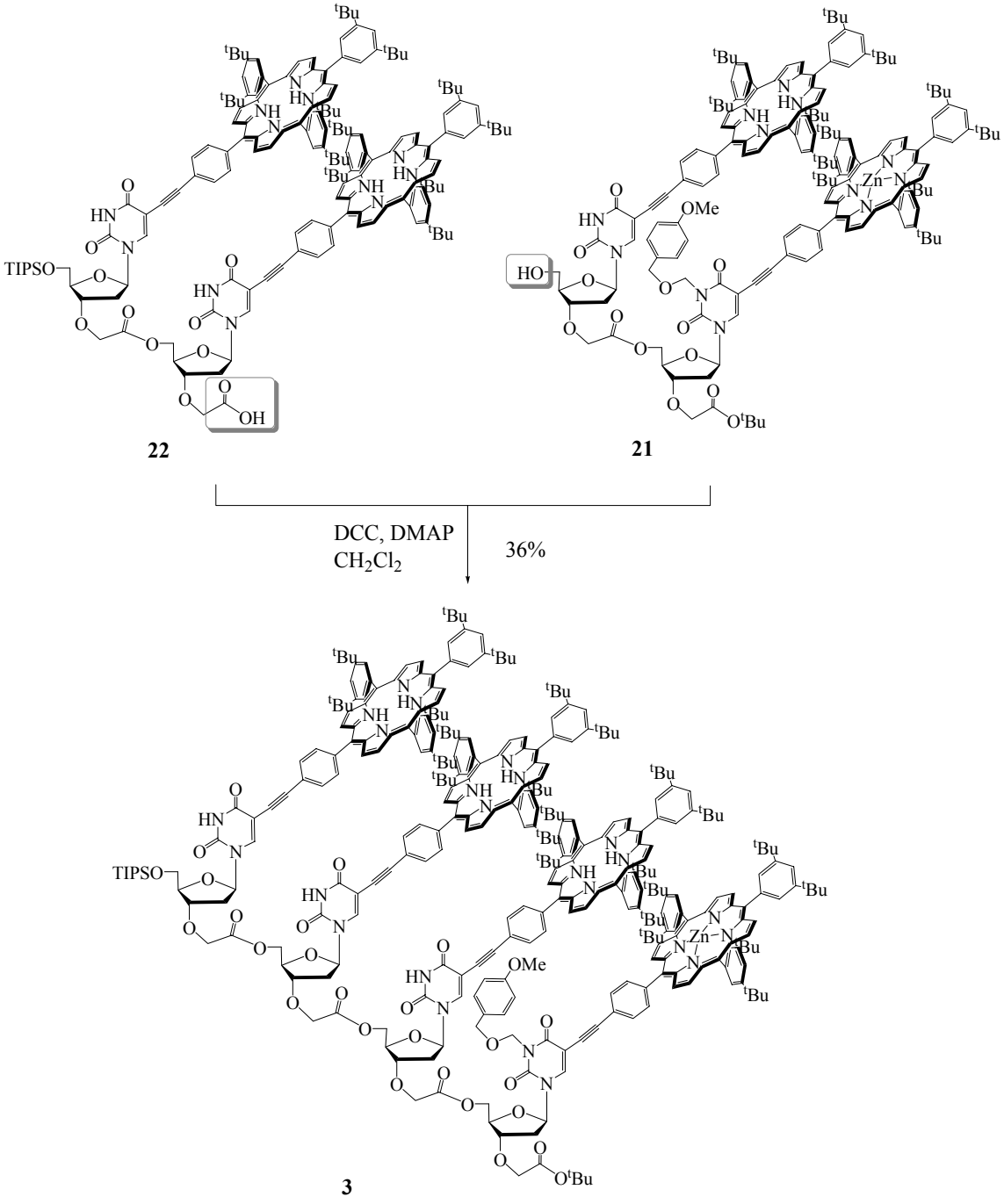

Figure 1.34 *Synthesis of tetramer **3**.*

In this reaction it was necessary to apply twice as much of the coupling agents (DCC and DMAP) than in the previous coupling reaction. Indeed, with the higher oligomerization level, reactions become more demanding and the reaction time significantly longer, presumably due to steric hindrance. In this respect, the formation of the tetramer was completed after 3 days of stirring at room temperature. The completion of the reaction was difficult to follow by TLC, because the few spots with similar retention factors were characterizing the crude reaction mixture. Along this line, purification of the product was tedious and time consuming, as involved four silica-gel columns and two GPC columns. The desired tetramer **3** was obtained in 36% yield, that is almost half of the yield obtained for dimer **2**.

1.7.5. Synthesis of octamer 4.

After the synthesis and the purification of tetramer **3**, application of the whole procedure towards octamer **4** was even more troublesome. The tetramer-acid **24** was esterified with tetramer-alcohol **23** in the presence of overall 3.5 equivalents of DCC, and 5.0 equivalents of DMAP and 0.6 equivalent of 1-hydroxybenzotriazole (HOBt),[158-159] which were added in three portions with one day interval, Figure 1.35.

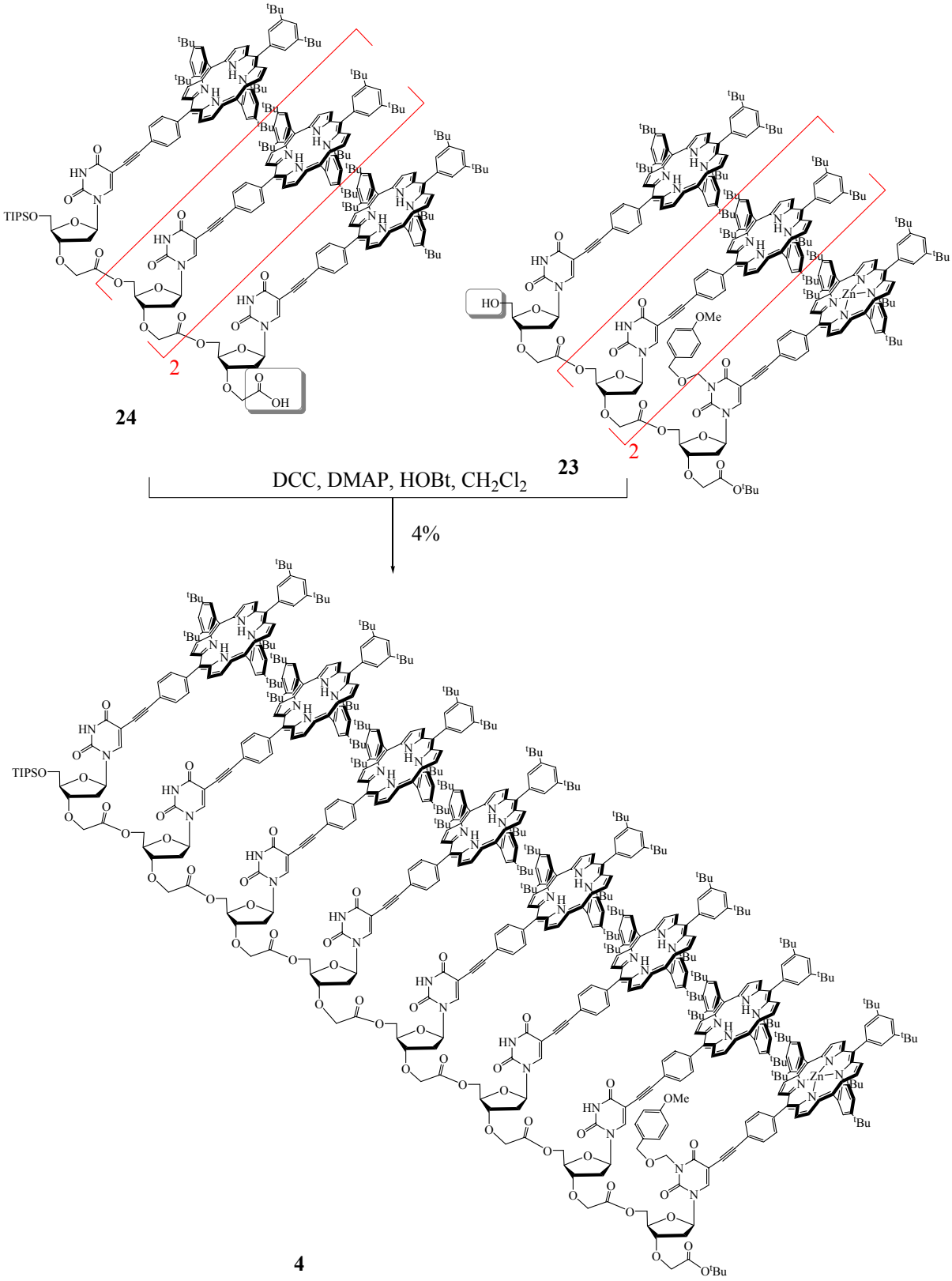

Figure 1.34 *Synthesis of octamer* ***4****.*

The HOBt was applied to the reaction mixture under, later justified, presumption that alcohol **23** is too sterically hindered compound to approach to ester **28** (analogue of the active ester **26** in the synthesis of dimer **2**). In other words, HOBt reacted with the carboxylic group activated by DCC providing the corresponding active ester **29**. Reaction of **29** with alcohol **23** activated by DMAP was facilitated with HOBt as a leaving group. The mechanism of this conversion is presented in Figure 1.36.

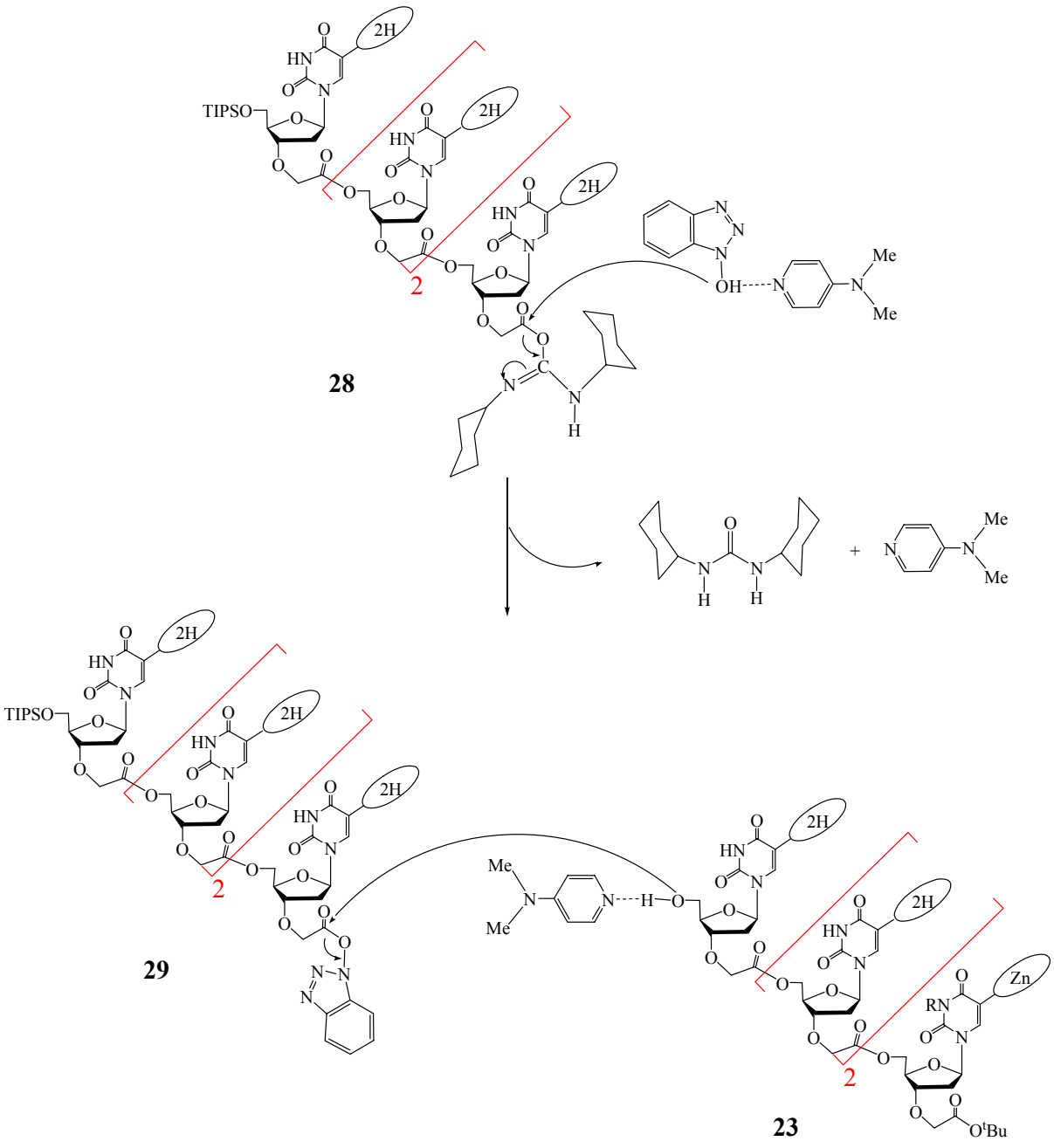

Figure 1.36 *Conversion of the carboxylic group activated by DCC (**28**) to active ester **29**, which facilitate the reaction with alcohol **23**.*

Thin layer chromatography of the reaction mixture was not too helpful in monitoring the reaction course. The TLC plates were presenting reaction mixture as one long trail. Moreover, ambiguity in the product characterization under that trail was even more troublesome because of accompanying impurities. An addition of a few drops of TEA to the eluting solvent didn't result with neater plates. Utilization of alumina as TLC adsorbent, instead silica-gel, was not useful as well. However, the reaction was stopped after four days of stirring at room temperature, since no trace of the starting materials was detected by TLC. The hydrated adduct of DCC, DCU was removed by the treatment of the crude product with toluene. The purification of the product is particular story of few months work. The difficulties were anticipated due to the molecular weight (MW= 10376.82 g mol^{-1}) and a number of functional groups disposed to weak secondary interactions. Several columns on silica-gel and even more gel-permeation chromatography columns were necessary before a small quantity of the octamer was isolated. For the purification of the product by chromatography columns we used silica-gel with bigger pores, 63 – 200 μm, instead of usually used 4 – 63 μm. The application of alumina, instead of silica-gel, for chromatography columns, resulted in worse separation. For gel-permeation chromatography Bio-Beads S-X1 were employed (molecular weight exclusion limit= 14000 g mol^{-1}) in toluene as a solvent. The purification process by GPC entailed separation of the target compound from lower molecular weight materials. Once one neat compound was isolated it was impossible to identify its structure by using NMR spectroscopy. The characterization by using NMR analysis in various solvents and at different temperatures was meaningless due to coalesced signals. Therefore, the identification of the target compound in isolated fractions was preformed by MALDI-TOF mass spectrometry. Finally, we obtained pure octamer **4** in a very small 4% yield, with around 10% of it in inseparable mixture with impurities. It is pointless to note that this yield is not significant, since inevitably a great quantity of the crude product was lost in manipulations (five silica-gel and eight gel-permeation chromatography columns).

The octamer **4** was examined for purity by analytical size-exclusion chromatography (SEC), and characterized by MALDI-TOF mass spectrometry, UV-visible and fluorescence spectroscopy, and as much as possible by ^{1}H NMR spectroscopy. The analytical SEC of the final product was performed in THF (2 mg in 1 mL) at room temperature with the flow rate of 1.0 mL/min. The obtained chromatogram corroborated the purity of the product with the single pick at the retention time of 7.8 min, Figure 1.37.

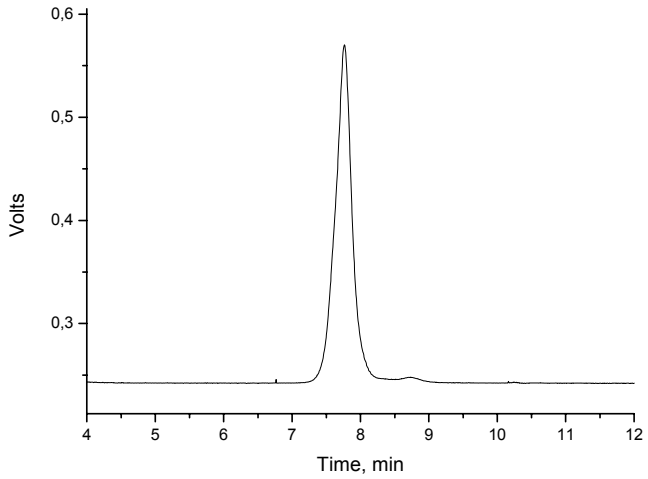

Figure 1.37 *The chromatogram obtained by analytical SEC of octamer* ***4****.*

The structure of the final product **4** was also confirmed by MALDI-TOF mass spectrometry, Figure 1.38. The octamer is characterized by the pick observed at 10378.0, which is attributed to the protonated octamer ($[MH]^+$ calculated for $C_{670}H_{743}N_{48}O_{51}SiZn$).

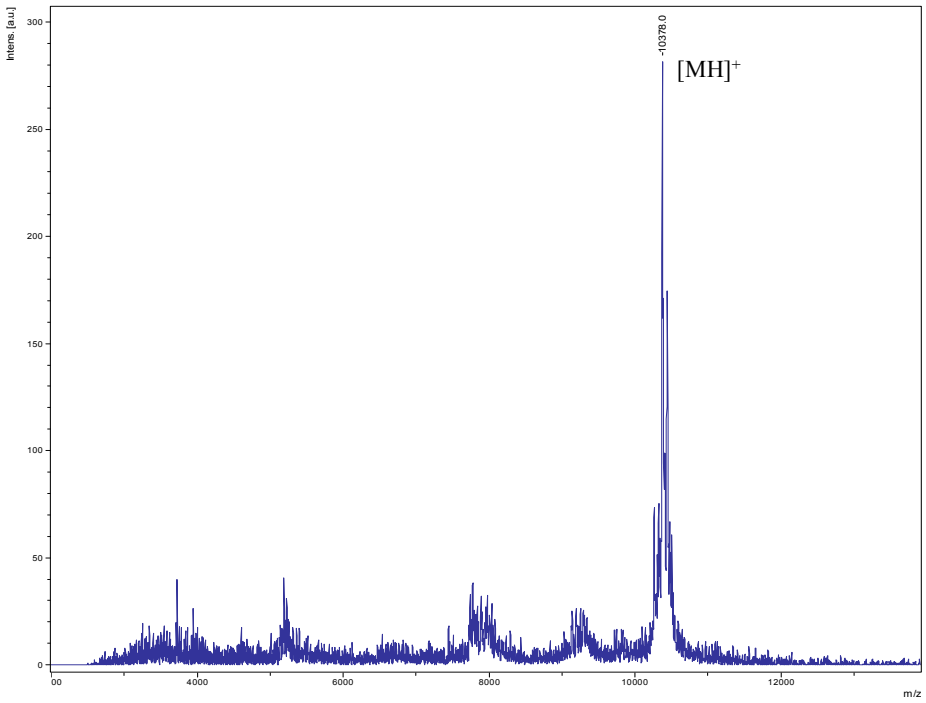

Figure 1.38 *The spectrum MALDI-TOF of octamer* ***4****.*

2 STRUCTURAL AND PHOTOCHEMICAL STUDIES OF MODIFIED OLIGONUCLEOTIDES WITH PENDANT PORPHYRINS

In naturally occurring light-harvesting complexes, biopolymer scaffolds hold pigments at intermolecular distances that optimize photon capture, electronic coupling, and energy transfer. The design of our system was guided by desire to exert control over the position and distance of porphyrins along the oligonucleotidic scaffold. To this end our uridine-porphyrin conjugates were subjected to a comprehensive conformational analysis by using NMR spectroscopy and to photophysical studies by using absorption and fluorescence spectroscopy.

2.1. CHARACTERIZATION BY NMR SPECTROSCOPY.

The NMR spectroscopy is a good starting point for determination of molecular conformation. The conformation of our modified oligonucleotidic arrays with pendant porphyrins largely depends on two types of interactions: π-π interactions between porphyrins and hydrogen bonding between uridines. These molecules have been designed such that they are adequately constrained to encourage intramolecular interactions and sufficiently flexible to be able to fold into a favourable conformation. Therefore, the geometrical dependence of interactions may be influenced by solvent in NMR analysis.

In line with this, monomer **1**, dimer **2**, tetramer **3** and octamer **4** were probed by NMR spectroscopy in collaboration with Dr. Yannick Coppel. The NMR spectra were initially measured in $CDCl_3$. As expected, with the oligomeric array growth the spectra were unsuitable for assignment and subsequent geometrical analysis. To overcome difficulties in assignment of NMR spectra we examined the solvent effect. On the basis of presumed hydrogen bonding interactions between uracil units we probed acetone-d_6 as a polar solvent. On the other hand, considering interaction between porphyrin macrocycles a poor peak separation could be overcome with magnetically anisotropic solvent benzene-d_6. After

examination of pure benzene-d_6 and acetone-d_6, as well as various combinations of acetone, benzene and chloroform in different ratios, acetone has shown to provide the best resolution of signals.

2.1.1. NMR analysis of monomer 1.

The ^{1}H NMR spectrum of **1** in chloroform-*d* (300 MHz, 297 K, *c*~ 3 mM) shows multiple resonances consistent with corresponding two constituent parts, modified uridine and the porphyrin, Figure 2.1.

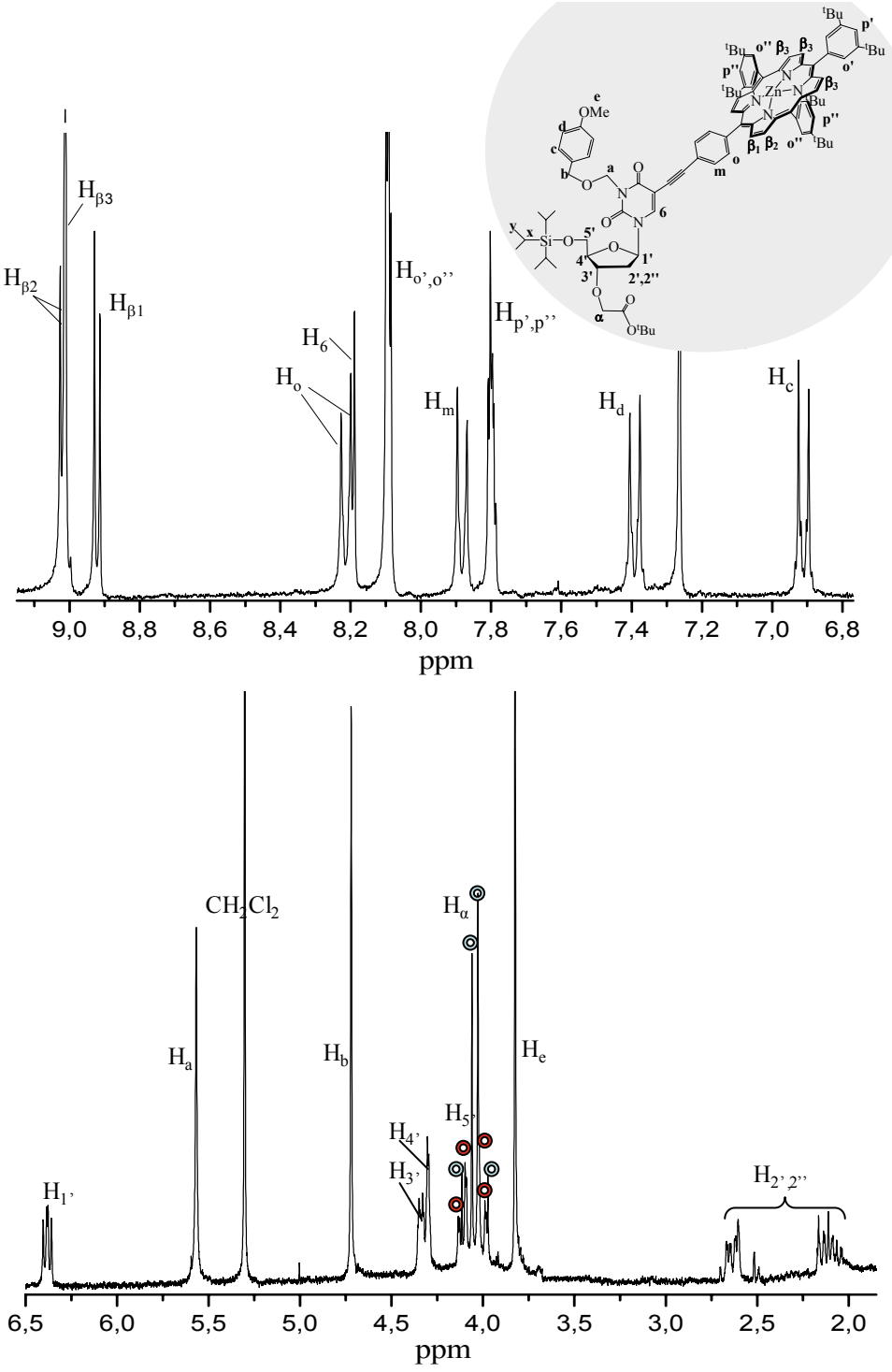

Figure 2.1 *^{1}H NMR spectrum of monomer **1** (chloroform-d, 300 MHz, 298 K).*

The β-pyrrolic protons that are flanked by di-*tert*-butylphenyl groups ($H_{\beta 3}$) give an unresolved singlet at 9.01 ppm, while two doublets are observed for the β-pyrrolic protons that are situated between the di-*tert*-butylphenyl group and phenylacetylene linker, $H_{\beta 2}$ and $H_{\beta 1}$ at 9.02 and 8.92 ppm, respectively. The protons on the phenylacetylene linker yielded the same splitting pattern. The resonances observed for the free uridine retained their characteristic features in the porphyrin-uridine conjugate. Generally, an inspection of the spectra has shown that $H_{1'}$ signals are usually the most downfield aliphatic signals and that the $H_{2'}$ are the most upfield. The 1'-proton appears as doublet of doublet at 6.38 ppm with a coupling constant $^3J_{H1'\text{-}H2''}$ and $^3J_{H1'\text{-}H2'}$ of 7.9 and 5.7 Hz, respectively, while the 2'- and 2''-protons yield two sets of splitting pattern at around 2.63 and 2.12 ppm with corresponding coupling constants of $^2J_{H2''\text{-}H2'}$= 13.8 Hz, $^3J_{H2'\text{-}H3}$= 5.6 Hz, $^3J_{H2'\text{-}H1}$= 8.1 Hz and $^2J_{H2'\text{-}H2''}$= 14.4 Hz, $^3J_{H2''\text{-}H1'}$= 6.6 Hz, $^3J_{H2''\text{-}H3'}$= 8.1 Hz.

All resonances in the NMR spectrum of monomer **1** in chloroform-*d* are well-resolved indicating well-defined conformational species. However, the NMR spectrum in acetone-d_6 (500 MHz, 298 K, *c*~ 3 mM) was also performed for comparation with higher order arrays, Figure 2.2. For comparison of the spectra performed in chloroform-*d* and acetone-d_6, the peak of *p*-metoxy group at N-3 was used as a reference. The signals in the overall spectrum in acetone-d_6 are better resolved than in chloroform-*d*. The splitting patterns are unchanged, but resonances of certain porphyrin and uridine protons are slightly shifted. The $H_{\beta 3}$ provides a singlet at 8.92 ppm, whereas $H_{\beta 2}$ and $H_{\beta 1}$ appear in the form of two doublets at 8.93 and 8.90 ppm. The two doublets of *orto* and *meta* protons at phenyl flanking the acetylene linker are shifted by 0.1 and 0.05 ppm downfield, probably due to orientation of porphyrin ring according to uridine. In line with this, the 1'-proton signal is shifted for 0.5 ppm upfield, while the signals of 3'-proton and 2'-proton (presumably one on the same side of the ribose as 3') are shifted downfield for 0.1 and 0.2 ppm, respectively. These observations signified interaction with acetone-d_6, hence the influence of this solvent effect on the resolution of signals in spectra of higher order arrays was envisaged.

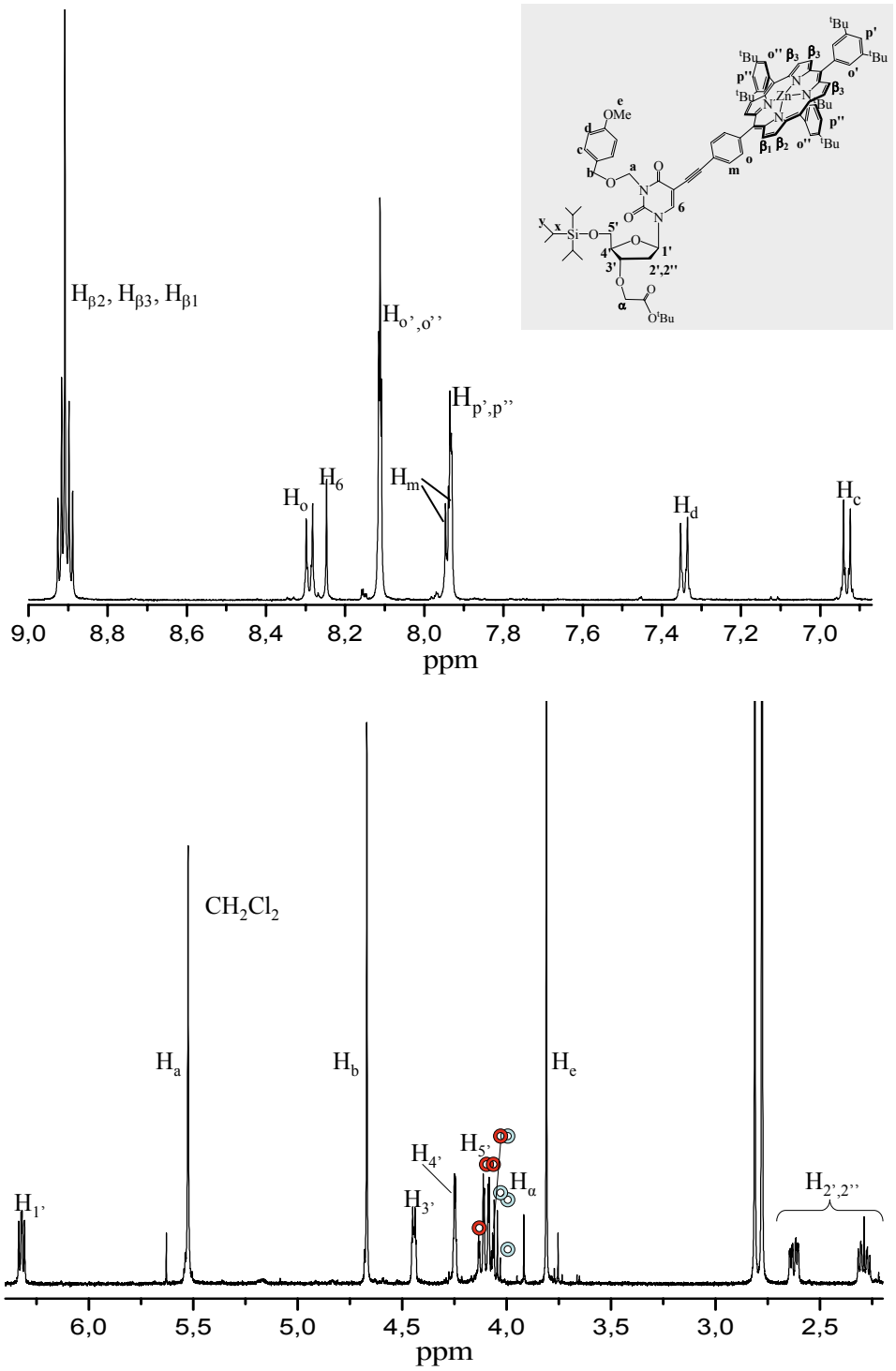

Figure 2.2 *^{1}H NMR spectrum of monomer* ***1*** *(*acetone-d_6*, 500 MHz, 298 K).*

2.1.2. NMR analysis of dimer 2.

The ^{1}H NMR spectrum of the dimer was employed to examine the geometry of the molecule with two porphyrin-uridine units. In relation to monomer **1**, dimer **2** consists of two differently modified uridine moieties functionalized with two large, aromatic, rigid porphyrin macrocycles with different π electron ring currents. The zinc porphyrin is appended to the lower and the free-base porphyrin to the upper uridine. Two uridine-porphyrin units are joined by ether-ester type of linker between C-3' of the upper unit and C-5' of the lower unit.

The initial NMR spectrum of dimer **2** was performed in chloroform-*d* (500 MHz, 288 K, *c*~ 3 mM), Figure 2.3. The temperature of 288 K was chosen by variable temperature experiment, because it provides well dispersed spectra. At the lower temperatures the resonances were broader and some signals overlapped indicating a dynamic process within the dimer.

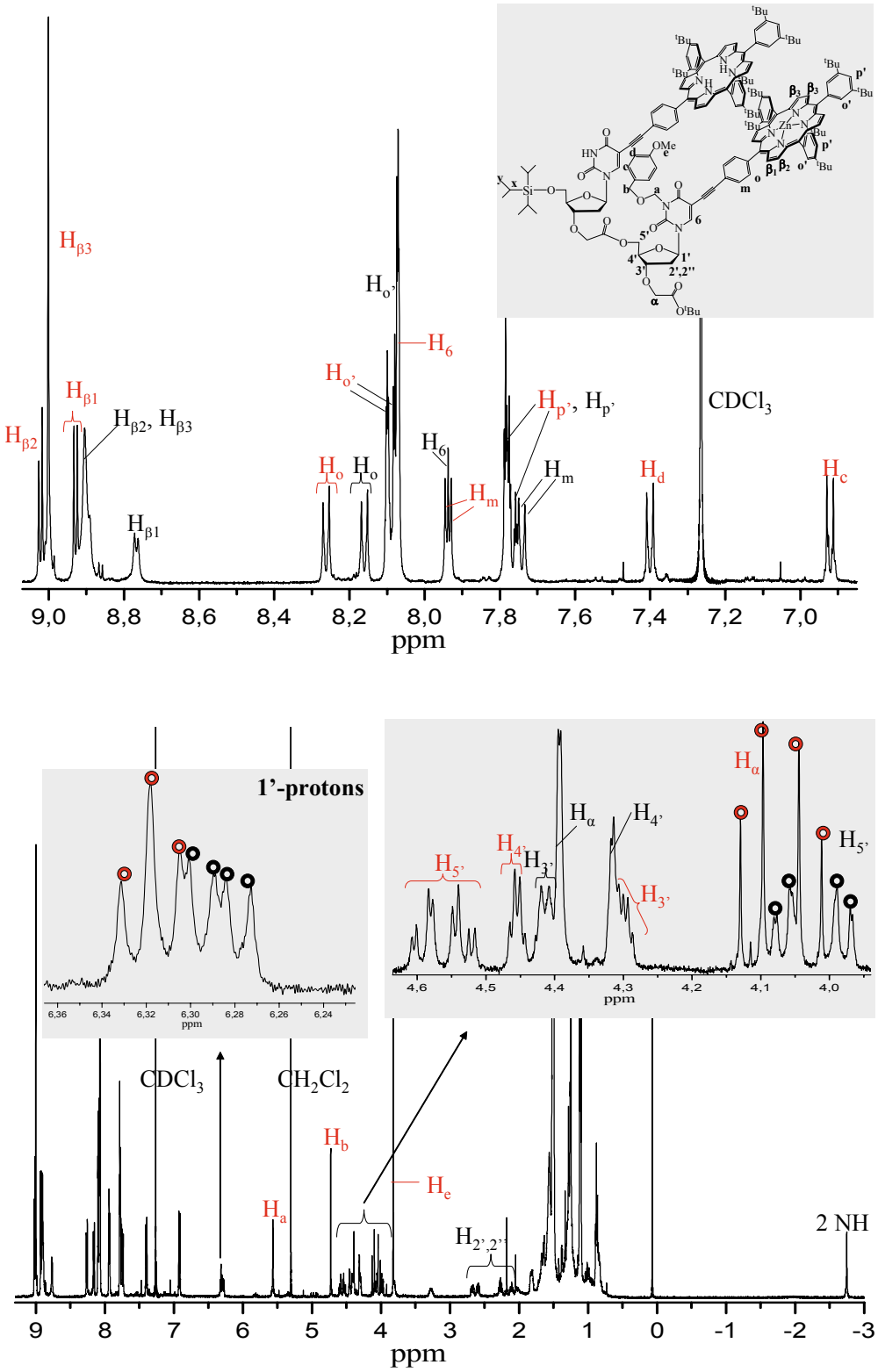

Figure 2.3 *^{1}H NMR spectrum of dimer **2** (chloroform-d, 500 MHz, 288 K), with chemical shift assignments for the uridine-free-base porphyrin unit in black and for uridine-zinc porphyrin unit in red. Upper-low field region, lower-the whole spectrum. In the left inset-resonances for $H_{1'}$, in the right inset-multi-signal region of sugar moieties.*

The nature of the dimer in two nonequivalent uridine-porphyrin units is nicely reflected in the NMR spectrum showing two set of resonances. The resonances for the lower uridine-zinc porphyrin unit are deshielded relative to those for uridine-free-base porphyrin unit due to the π-electron ring current. The β-pyrrolic protons of the zinc porphyrin exhibit two doublets at 9.02 and 8.92 ppm, whereas $H_{\beta 3}$ appears as a singlet at 8.99 ppm. In the case of the free-base porphyrin, $H_{\beta 1}$ is separated from overlapped $H_{\beta 2}$ and $H_{\beta 3}$ signals. The multiple protons of the sugar moieties appear without any general regulation, as they are non-equivalent. The 1'-proton of the lower unit with the zinc porphyrin appears as a triplet at 6.31 ppm with the coupling constant ^3J= 6.5 Hz, whereas 1'-proton of the upper unit appears as a doublet of doublet at 6.28 ppm with coupling constants $^3J_{H1'-H2'}$ and $^3J_{H1'-H2''}$ of 8.0 and 5.0 Hz. The methylene protons at C-3' position of the upper unit exhibit an AB system at 4.39 ppm, whereas those of the lower unit appear as a sharp well-defined AB system at 4.07 ppm. The 5'-protons from both units appear as a doublet of doublet.

In the context of shifted resonances for monomer **1** in acetone-d_6, the ^{1}H resonances of dimer **2** were also examined in this solvent (500 MHz, 293 K, c= 2.6 mM). This temperature was chosen by variable temperature experiment, because it provided the best dispersion and visibility of resonances. At the lower temperatures the signals for phenyl protons (*orto* and *meta* to the *meso*-carbon) of the upper unit and $H_{5'}$ and $H_{3'}$ of both upper and lower units are shifted downfield (around 0.05 ppm at 253 K). Generally, at 253 K relative to 293 K signals are broader and poorly resolved because they undergo coalescence phenomena. These observations suggest the involvement of some dynamic processes that are in the intermediate exchange region (between fast and slow). The detailed assignment of the spectrum in acetone at 293 K is presented in Figure 2.4.

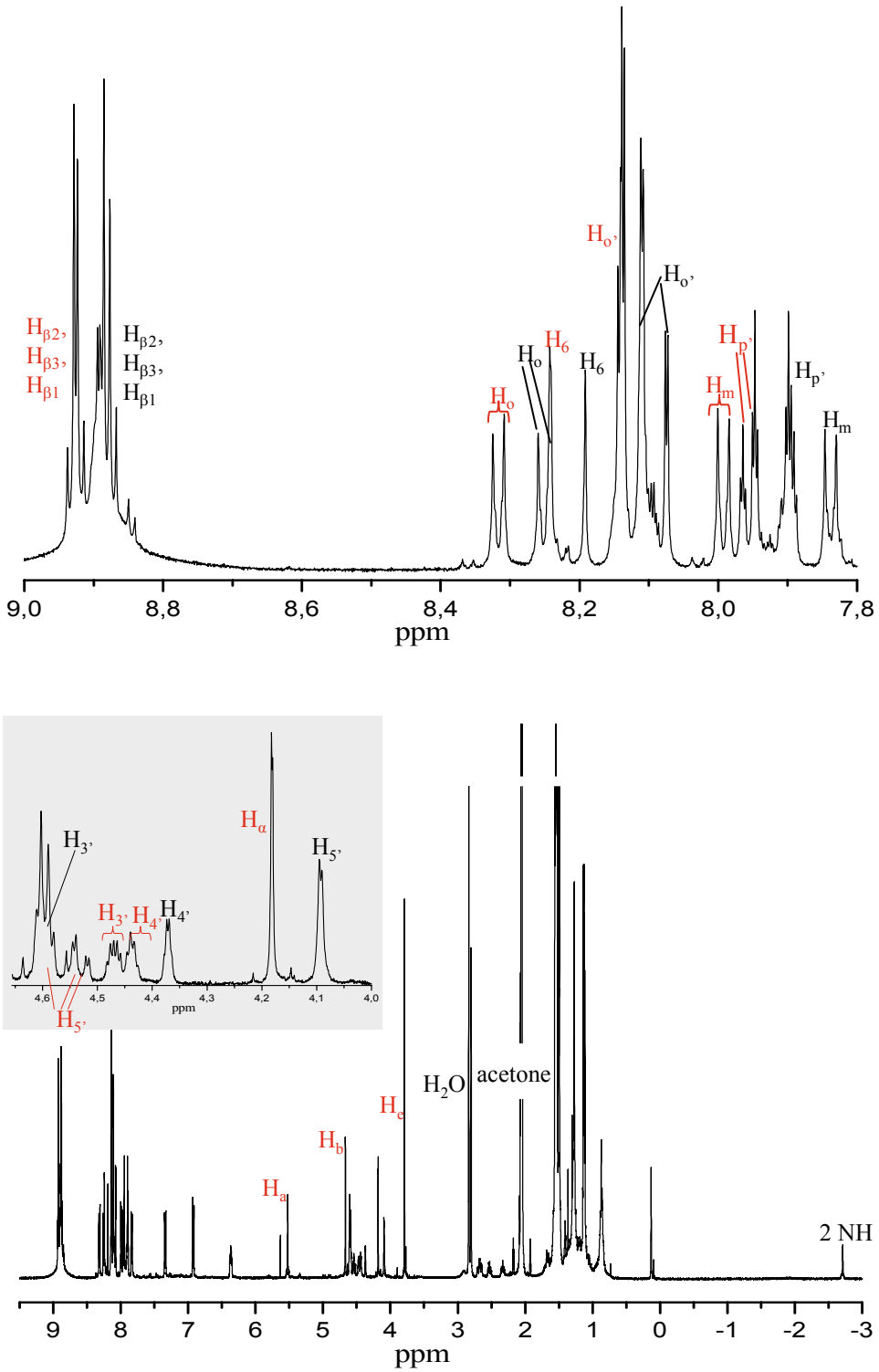

Figure 2.4 *^{1}H NMR spectrum of dimer **2** (acetone-d_6, 500 MHz, 293 K), with chemical shift assignments for uridine-free-base porphyrin unit in black and for uridine-zinc porphyrin unit in red. Upper-low field region, lower-the whole spectrum. In the inset multi-signal region of sugar moieties.*

The overall spectrum shows general downfield trend caused by significant reorganization in acetone, and clearly visible splitting patterns that indicate a fast exchange of the different conformations of the dimer. The characteristic pattern of β-pyrrolic protons changed, and the signals of the zinc porphyrin shifted upfield, closer to well-dispersed signals of the free-base porphyrin. The signals of *meso*-substituted groups of both porphyrins are shifted downfield for about 0.1 ppm. It is noteworthy that the larger shifts in the low field region of the spectrum belong to H-6 protons, namely 0.3 ppm for the lower unit and 0.2 ppm for the upper unit. Given observations suggest that porphyrin macrocycles are in a slipped cofacial orientation with a certainly small offset. Aside from the low field region in the spectra obtained in chloroform and acetone, a comparison of the multi-signal region at approximately 4.5 ppm was problematic due to a scattered signals for $H_{3'}$, $H_{4'}$, $H_{5'}$ and methylene protons of both units.

In principle the improvement of the spectrum in acetone-d_6 relating to chloroform-*d* is significant in that all signals are sufficiently resolved to proceed to the next step of the structure assignment processes by using COSY homonuclear experiments and NOE correlations. The NOE correlations are crucial in determination of the precise structural relationships between protons within the oligomers, because it provides information about spatial proximity of the units. The NOE experiment disclosed that the β-pyrrolic protons, phenyl protons (*orto* and *meta* to the *meso*-carbon) and H-6 proton of the lower unit, and phenyl protons, H-6 proton and di-*tert*-butylphenyl protons (*orto* to the *meso*-carbon) of the upper unit interact with one or both protons from the triisopropylsilyl protecting group at C-5' of the upper unit, Figure 2.5.

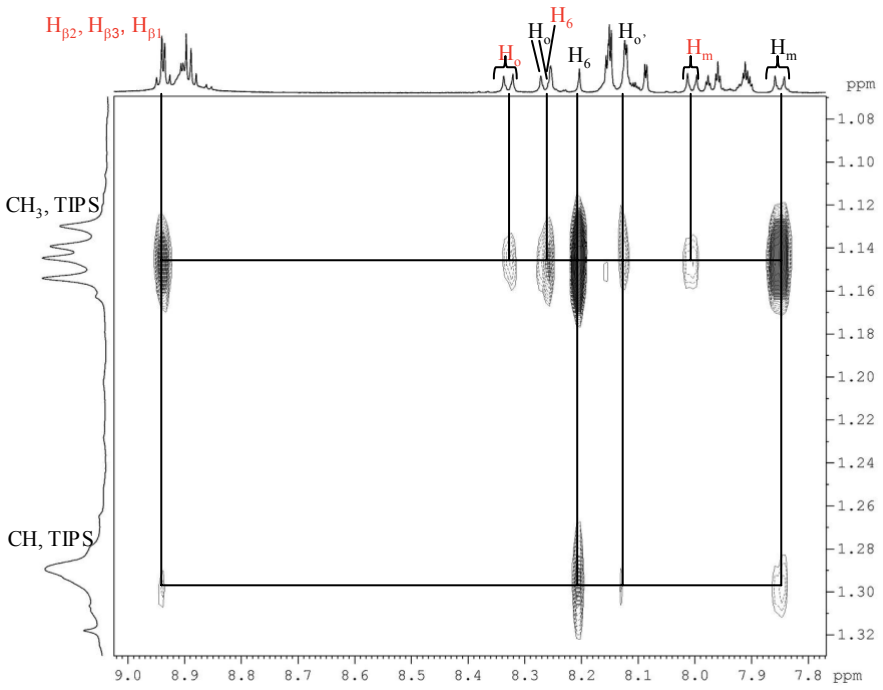

Figure 2.5 *The region of the ROESY collected at 288 K in acetone-d_6. The lines trace connectivity between upper and lower units, and protons of triispropylsilyl (TIPS) group at C-5' of the upper unit. The chemical shifts of the lower (uridine-zinc porphyrin) unit are labeled in red.*

The strong correlation of β-pyrrolic protons of the lower unit (zinc porphyrin) and H_m of the upper unit (free-base porphyrin) with TIPS protons suggest that porphyrins are close, but not in the symmetric face-to-face orientation. Significant NOE correlations were also found between H-6 protons and ribose protons within each unit. The H-6 protons interact more strongly with 1' and 2' protons than with 3' and 5' protons. Besides, H-6 protons do not interact with 4' protons. These NOE data indicate that H-6 protons at uracil moieties are oriented in the direction of the sugar ring; hence, the glycosidic angle is *anti*. All of these observations for the proximity in space of protons in dimer **2** are depicted in Figure 2.6.

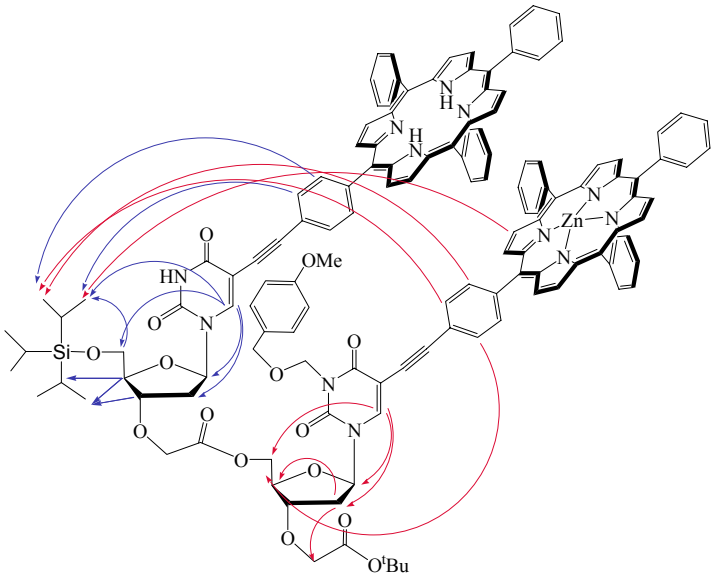

Figure 2.6 *Significant NOE correlations observed from the ROESY spectrum of dimer* ***2*** *in acetone-d_6; red arrows for protons at uridine-zinc porphyrin unit, blue arrows for protons at the other unit. Di-tert-butyl groups at three meso-phenyls at each unit are omitted for clarity.*

2.1.3. NMR analysis of tetramer 3.

In the case of the tetramer, the ^{1}H NMR spectrum in chloroform-*d* was unsuitable for assignment of the sugar signals and generally problematic due to the lack of fine details. The signals in the spectrum were broad and mainly overlapped. Most noticeable was increased number of magnetically equivalent uridine-free-base porphyrin units, which resulted with problematic attribution. To study possible aggregation phenomena and in an attempt to minimize implied attractive electrostatic interactions between the porphyrin macrocycles and/or hydrogen bonding between the uracil units, we examined the influence of different solvents. Hence, the spectrum of tetramer **3** was probed in acetone-d_6, which should compete with hydrogen bonding, and, on the other hand, in benzene-d_6 assuming that interactions between aromatic porphyrins disable fast exchange process. The solvent effect was examined at the temperature of 293 K with the tetramer solution of concentration around 3 mM, Figure 2.7.

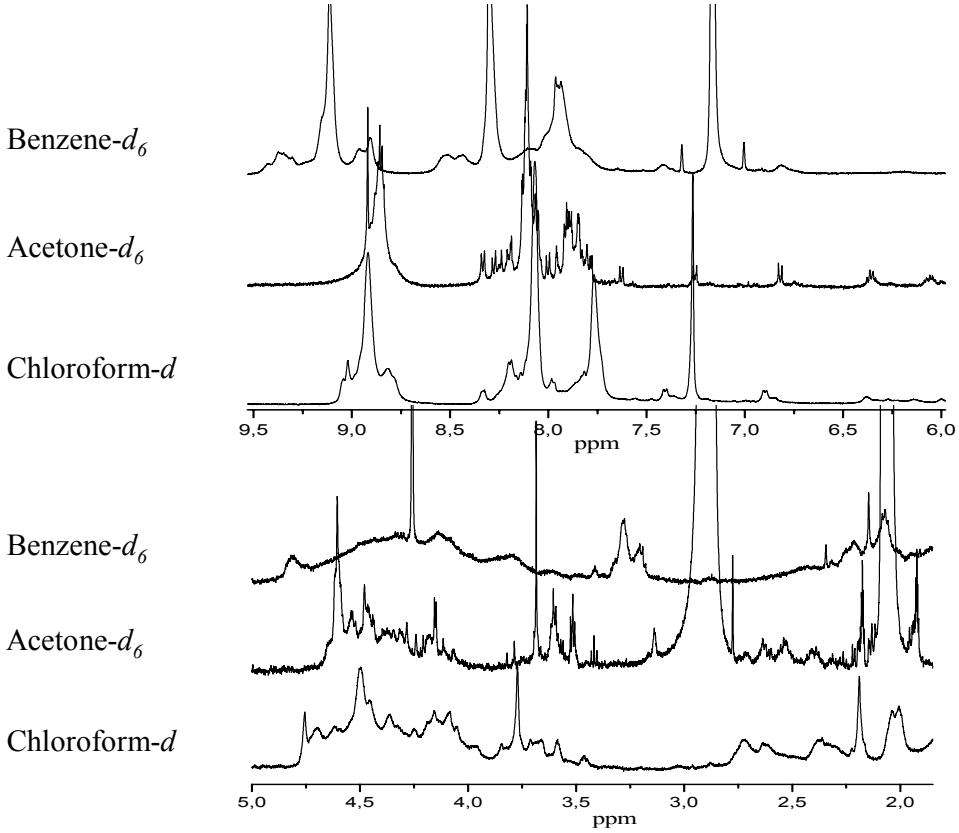

Figure 2.7 *Solvent effect on ^{1}H NMR spectra (500 MHz, 293 K) of tetramer **3**.*

The unexpectedly different appearance in the presented spectra undoubtedly shows that the tetramer interacts with these solvents. Furthermore, the obtained spectra supported the hypothesis of hydrogen bonding driven conformation of the molecule. Apart the β-pyrrolic resonances, the best resolution of signals was obtained in acetone-d_6. In order to enhance resolution of β-pyrrolic proton signals we examined mixtures of acetone-d_6 and chloroform-*d* (500 MHz, 293 K, *c*~ 3 mM). An increased volume ratio of chloroform in acetone solution caused significant line broadening, until in pure chloroform the spectrum is so broad that no peaks are identifiable.

These experiments proved that the conformational analysis of tetramer **3** should be performed in pure acetone-d_6. Before starting with the complete detailed structure assignment process by using a combination of one-dimensional and two-dimensional homonuclear and heteronuclear correlation experiments, we probed variable temperature and dilution experiments with tetramer **3** in acetone-d_6. The temperature was gradually decreased from 293 K (the temperature that was employed for the solvent examination) to 213 K. It is clearly visible that in the spectrum obtained at 293 K resonances are sharp and peaks well-resolved.

Besides, the spectra obtained at lower temperatures suggest an equilibration processes in the intermediate range. In attempt for further improvement of the appearance in the low field region of the spectrum measured at 293 K, the solution was heated up to 323 K. The spectra at temperatures higher then 293 K show no significant temperature dependence, suggesting that the well-defined tetramer spectrum can be obtained at around 300 K, Figure 2.8.

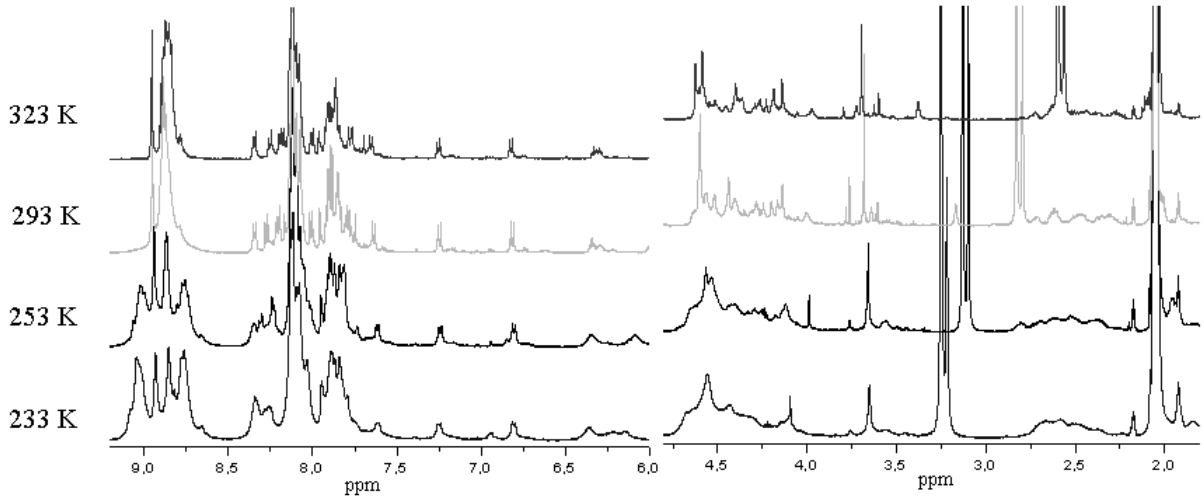

Figure 2.8 *Representative ^{1}H NMR spectra obtained in variable temperature experiment of tetramer **3** in acetone-d_6.*

The influence of concentration on the effective size of the tetramer in solution was studied by using diffusion NMR spectroscopy. By measuring translational motion of the tetramer in acetone-d_6, its diffusion coefficient was determined, reflecting effective molecular size and shape of the molecule in solution. The diffusion experiment was performed in concentrations of 5 mM and 1 mM of the tetramer in acetone-d_6 (500 MHz, 293 K). The experimental results are displayed as a 2D matrix with chemical shifts plotted along one axis and diffusion coefficient plotted along the vertical line in Figure 2.9.

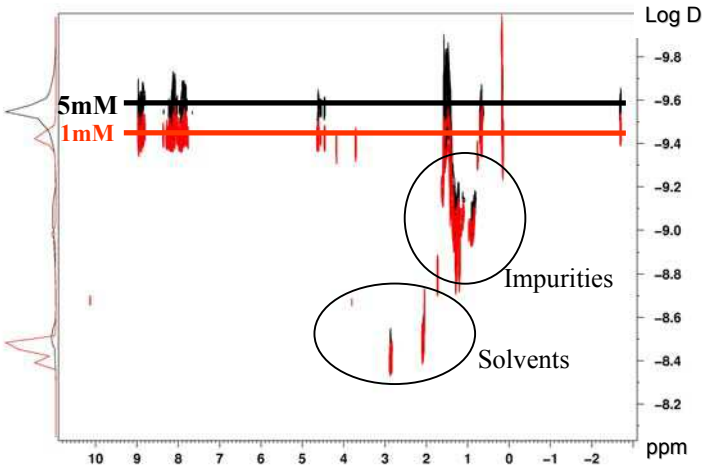

Figure 2.9 *2D DOSY spectrum showing two different species of the tetramer in two different concentrations in acetone-d_6.*

Each horizontal line represents a distinct diffusion coefficient and, hence, all the peaks on this horizontal line correlate with signals in the chemical shift dimension, and relate to spectroscopically separated molecular species. The molecules with smallest size relate to the solvent, since they have highest diffusion coefficient. The signals in the middle are attributed to impurities with smaller molecular weight than the tetramer. The diffusion coefficient of both species, solvent and impurities, do not differ significantly with concentration. On the other hand, the significant difference in diffusion coefficient was obtained for the tetramer. In the solution of 5 mM concentration, the corresponding tetramer specie diffuses less then the tetramer specie in 1 mM solution. Consequently, the diffusion coefficients of tetramer species in 5 mM and 1 mM solution are 2.8 x 10^{-10} m^2 s^{-1} and 3.9 x 10^{-10} m^2 s^{-1}, respectively. These studies show that aggregation takes place for high concentrations such as 5 mM, and that lower concentrations such as 1 mM has to be used to get the spectrum of non-aggregated tetramer.

At this stage, when the best conditions for NMR analysis were defined, a structural analysis was performed by using homonuclear correlation experiments, namely COSY and ROESY, and heteronuclear correlations emphasizing one C-H bond couplings (HSQC) and long range couplings (HMBC). All these internuclear correlations were employed in complete assignment of the ^{1}H NMR spectrum of tetramer **3** in acetone-d_6 (500 MHz, 303 K, c= 1.6 mM), Figure 2.10.

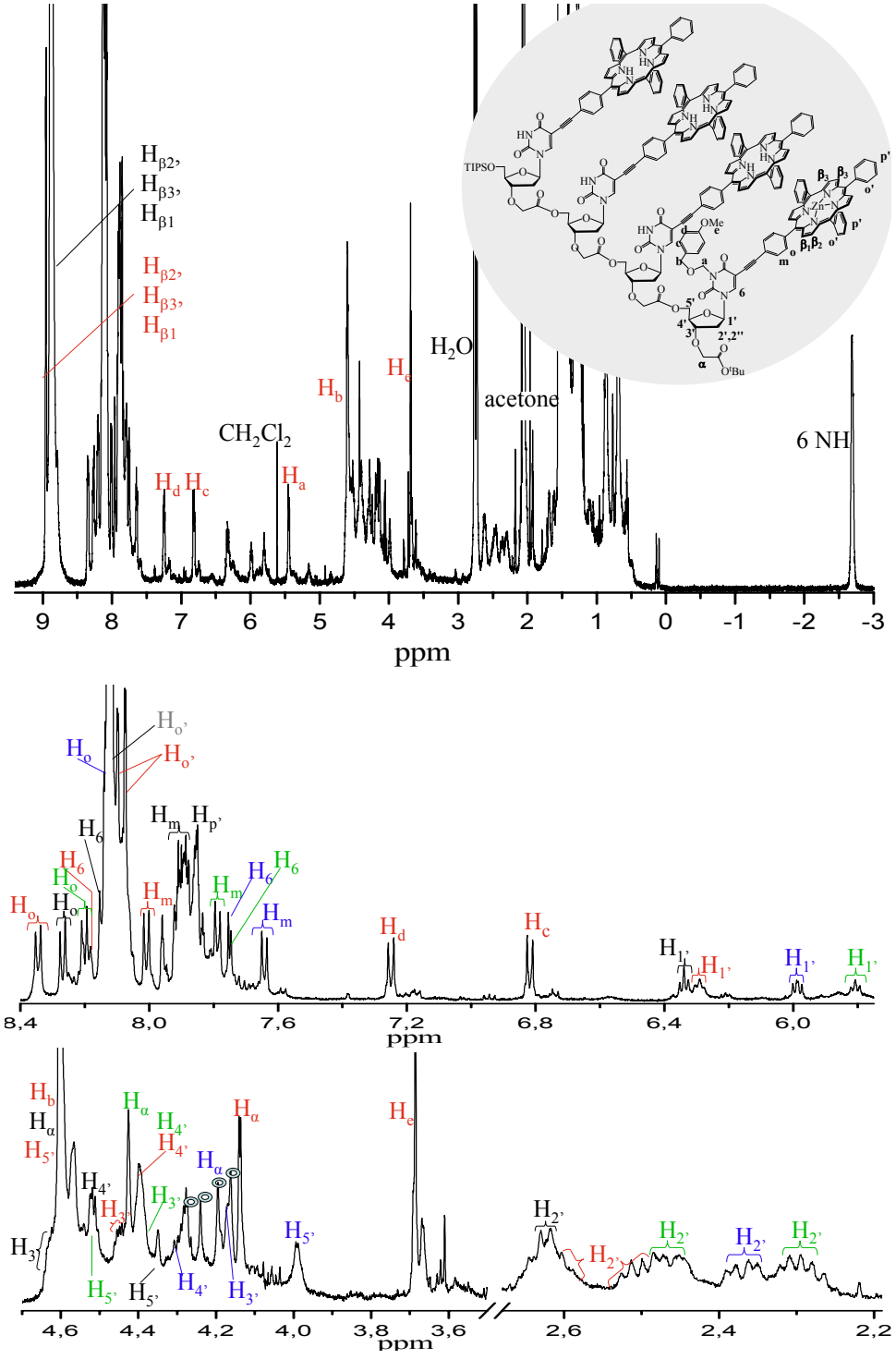

Figure 2.10 *^{1}H NMR spectrum of tetramer **3** in acetone-d_6 (500 MHz, 303 K, c= 1.6 mM) with complete chemical shift assignments: for first uridine-zinc porphyrin unit in red, for second in black, third in green and fourth in blue. Upper-low field region, lower-the whole spectrum. In the inset multi-signal region of sugar moieties.*

The NOE correlations were crucial in determination of structural relations between four individual uridine-porphyrin units of tetramer **3**. The significant NOEs observed in each unit are those between H-6 and 3'-protons. This characteristic and strong interactions indicate that the glycosidic angle between the ribose and uracil base is *anti*. Hence, in employed conditions our system exists in one preferable conformational form. As well precious interactions are those observed between H-6 of the lower unit and the methylene protons of the neighboring upper unit; this interaction is logically absent for the last unit in the array. Both fundamental NOE correlations are depicted in Figure 2.11.

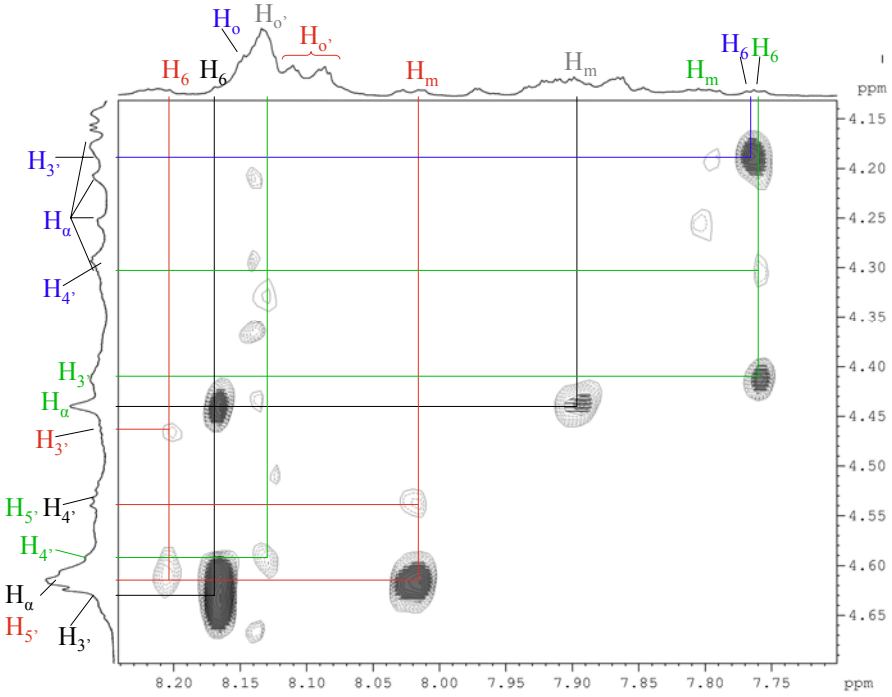

Figure 2.11 *The region of ROESY collected at 303 K in acetone-d_6. The lines trace connectivity between protons. The chemical shifts of first uridine-zinc porphyrin unit are labeled in red, while those of second, third and fourth in black, green and blue respectively.*

The first uridine-zinc porphyrin unit shows more intramolecular contacts than any other unit in the array. Another characteristic feature of this unit is interactions with the protons two units further. In other words, the NOE experiment disclosed that the β-pyrrolic protons of the zinc porphyrin interact with the methylene protons (H_α) of first and second neighboring units. The *meta*-phenyl protons (H_m) of each unit, apart the last one in the backbone, provide interactions with 4'-protons and the methylene protons from the

neighboring upper unit. These characteristic interactions of H-6 and H_m with the neighboring unit protons, in the last unit are replaced by the interactions with triisopropylsilyl group. The characteristic NOE correlations were also found between H-6 protons and 3'-protons within the same unit. The repetitive effect of the interactions characteristic for all four units indicates a well-defined conformation of corresponding porphyrin-uridine conjugate. All NOE effects that were observed are depicted in Figure 2.12.

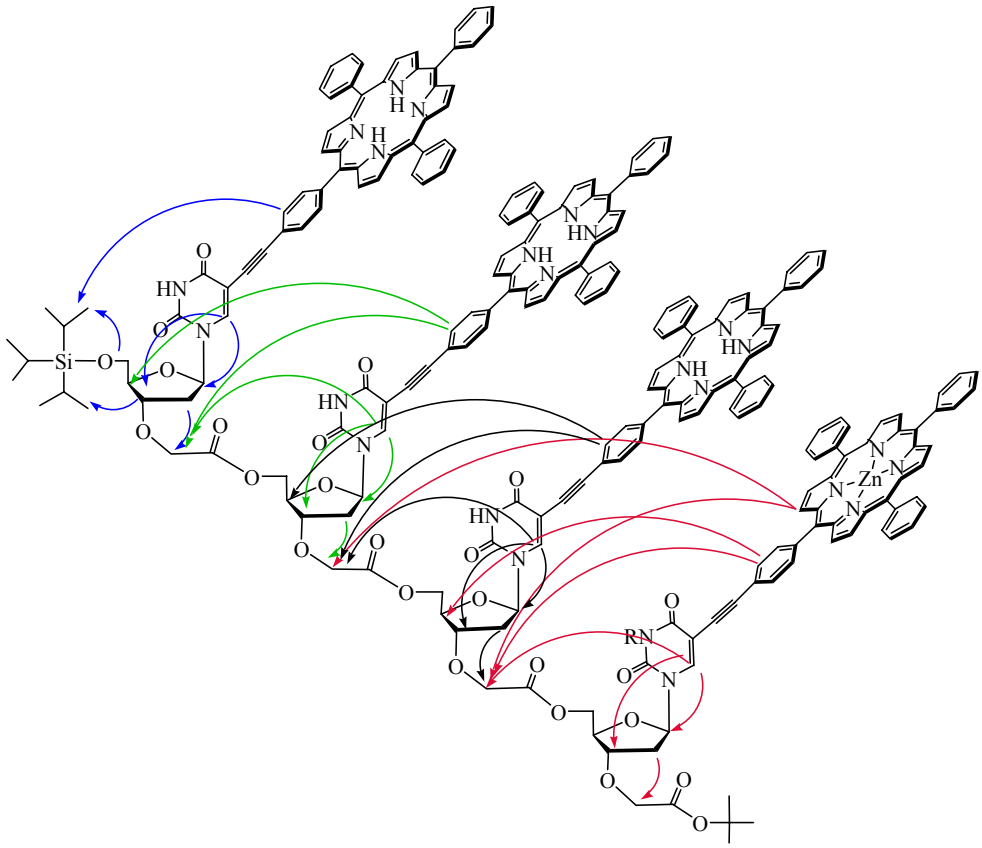

Figure 2.12 *NOE correlations observed from the ROESY spectrum of tetramer* ***3*** *in acetone-d_6, depicted by arrows; red arrows for first unit, black for second, blue and green for third and fourth. The di-tert-butyl groups at three meso-phenyls are omitted for clarity.*

Furthermore, proton 1' appears as a triplet, showing quasi similar coupling constants with both protons 2' and 2". This led us to estimate a pseudorotation angle of 70°, indicating a C4'-exo conformation of the sugar. However, this conformation usually does not correspond to a minimum of energy for the sugar of DNA. Another possibility to explain similar coupling constants with both protons 2' and 2" concerns the existence of an equilibrium between C2'-endo and C3'-endo conformations in fast exchange on the NMR time-scale at room

temperature. NMR experiments were carried out at variable temperature. At low temperature, the signals of the porphyrinic protons decoalesce showing two sets of β-pyrrolic protons. Similar observations are made for the signals corresponding to the sugar moieties and especially the $H_{1'}$ protons, indicating molecular motions within the tetramer. These results testify in favor of the existence of a dynamic process between C3'-endo and C2'-endo conformations.

2.1.4. NMR analysis of octamer 4.

An initial ^{1}H NMR spectrum of octamer **4** was measured in chloroform-*d* (500 MHz, 293 K, *c*~ 1 mM). As expected, the spectrum presented broad, non-defined resonances indicating a fast exchange process at the NMR time scale or aggregation. In attempt to increase mobility a temperature variable experiment was performed in 1,1,2,2-tetrachloroethane-d_2. After having gradually increased temperature to 373 K, no improvements were noticed. The lines did not narrow but remained rather broad. The dilution studies (0.99 mM to 0.25 mM) in acetone-d_6 at 293 K revealed no significant improvement in signal appearance. Following these observations the conclusion of fast equilibrating mixture with probably multiple associating modes was implied, Figure 2.13.

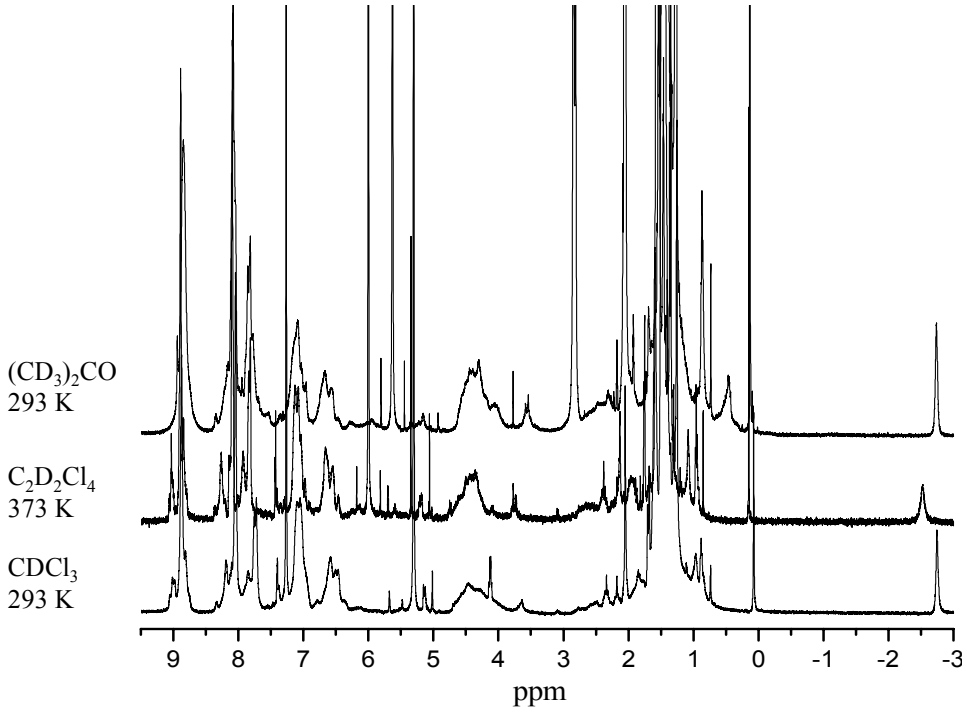

Figure 2.13 *Solvent effect in representative ^{1}H NMR spectra (500 MHz, c= 0.99 mM) of octamer **4** obtained at delineated temperatures.*

2.2. PRELIMINARY PHOTOCHEMICAL STUDIES OF THE PORPHYRINIC ARRAYS.

Following the natural pattern in light-harvesting antennae, we are attempted to reproduce sophisticated natural functions in our porphyrinic arrays. One of the attractive features in mimicry of natural energy transport phenomena is a fine control of structures in regular and well-arranged architectures of porphyrinic arrays. Thus, a fundamental challenge in the photophysics of porphyrinic arrays is the elucidation of the excitation energy transfer between porphyrinic chromophores. The energy migration process in porphyrinic arrays depends on Coulombic and electronic interactions between the chromophores, and interactions depend on the interconnection length and the relative configuration between adjacent pigments.[101,129,160,161] An explanation of such effects was first given by Kasha in terms of Coulombic interactions between neighbouring chromophores with isoenergetic electronic transitions.[162,163] The magnitude of such interactions depends on distance and spatial orientation, which are the basis of the through-space Förster energy transfer mechanism.[164-166]

Therefore, the pronounced differences in the optical absorption and emission spectra between the arrays of different range and corresponding simple porphyrins (zinc and free-base porphyrins) could relate with the results of structural analysis obtained by NMR spectroscopy, considering the distance between the porphyrins, their mutual orientation and conformation of oligonucleotidic backbone. All our principal systems, dimer **2**, tetramer **3** and octamer **4**, were subjected to examination of collective interactions between two or more closely similar or identical porphyrinic units. These systems comprise one zinc porphyrin appended to the terminal uridine in the oligonucleotidic backbone, while the others uridines in the backbone have pendant free-base porphyrins. The electronic interactions and the photoinduced energy transfer in the porphyrinic array appended to oligonucleotidic backbone were examined by UV-visible spectroscopy and steady-state fluorescence spectroscopy.

2.2.1. Characterization by UV-visible spectroscopy.

The electronic absorption spectra are a characteristic feature of the porphyrins, because of the broad range of optical absorption covering the entire visible spectrum. However, only the Soret band is particularly sensitive to electronic interactions between the porphyrins because of the extremely large transition dipole moment. On the other hand, Q-bands of the porphyrins have much lower transition dipole and are correspondingly much less sensitive to electronic interactions. Spectral changes in the Soret band absorption spectrum can therefore be used as an indication of the magnitude of electronic interporphyrinic interactions.

The absorption spectra of dimer **2**, tetramer **3** and octamer **4**, as well of zinc porphyrin **13** and free-base porphyrin **12** were measured in dichloromethane at room temperature. The adherence to Lambert-Beer's law was verified by quantitative analysis, which implied an absorbance recording of the corresponding porphyrinic array solution after successive addition of small aliquots from its stock solution of well-defined concentration. If probed solutions adhere to the law, the molar absorption coefficient can be calculated from the slope of the linear dependence of the absorption on concentration of the porphyrin solution at each wavelength. In this manner, the molar absorption coefficient can be calculated for the Soret band and for each absorption maxima of the Q-bands, by changing the concentration of the stock solution. The examined concentrations of the porphyrin solution were adjusted to absorbance, which recommendatory should cover the range between 0.5 and 1.2, and, in principle, this corresponds to concentration around 10^{-6} M for the Soret band, and around 10^{-5} M for the Q-bands. The calculated molar extinction coefficients for each compound at all absorption maxima are presented in Table 2.1. In addition, Figure 2.14 presents one spectrum for each, dimer **2**, tetramer **3** and octamer **4**, as well for zinc porphyrin **13** and free-base porphyrin **12**.

Free-base porphyrin **12**		Zinc porphyrin **13**	
λ_{max} (nm)	ε (M^{-1} cm^{-1})	λ_{max} (nm)	ε (M^{-1} cm^{-1})
421	506 800	422	558 100
517	18 600		
553	10 900	549	21 500
592	5 600	588	6 200
647	5 600		

Dimer **2**		Tetramer **3**		Octamer **4**	
λ_{max} (nm)	ε (M^{-1} cm^{-1})	λ_{max} (nm)	ε (M^{-1} cm^{-1})	λ_{max} (nm)	ε (M^{-1} cm^{-1})
422	795 600	422	1 559 600	422	2 285 100
517	18 800	517	54 800	518	87 400
552	29 000	553	48 300	553	70 600
592	11 900	592	22 300	592	33 500
647	5 500	647	16 000	648	27 300

Table 2.1 *Electronic absorption maxima and corresponding molar extinction coefficients.*

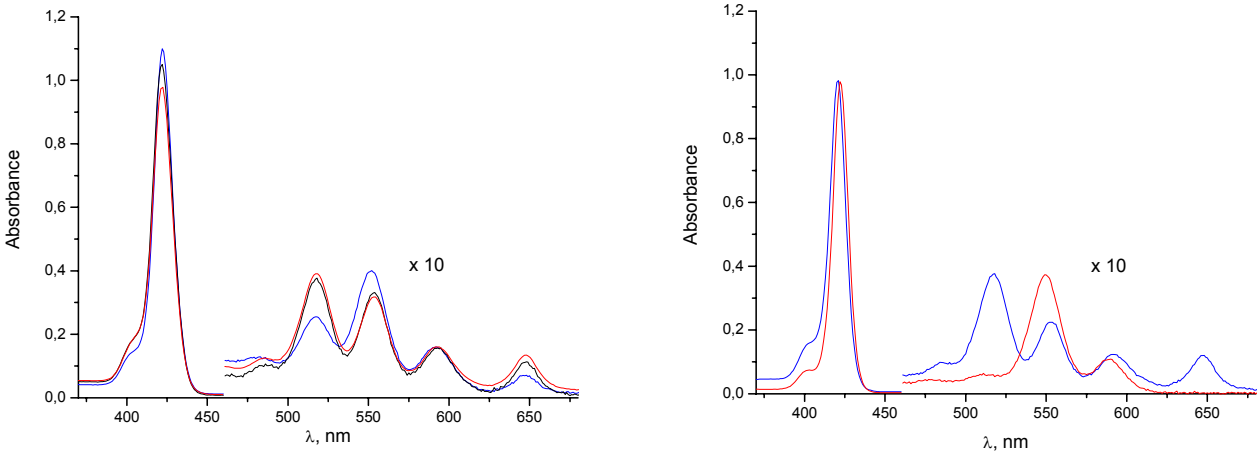

Figure 2.14 *UV-visible absorption spectra (CH_2Cl_2, 297 K) of: on the left hand side - dimer **2** (blue line) at c= 1.41 x 10^{-6} M, tetramer **3** (black line) at c= 7.21 x 10^{-7} M and octamer **4** (red line) at c= 3.98 x 10^{-7} M; on the right hand side - free-base porphyrin **12** (blue line) at c= 1.94 x 10^{-6} M and zinc porphyrin **13** (red line) at c= 1.75 x 10^{-6} M.*

Although, in general, the shape of the spectra of all compounds is similar to one another, the useful spectral differences relating to the type (zinc and free-base) and a number of porphyrinic units are clearly visible. In the absorption spectra, the typical Q-band system of a free-base porphyrin involves four distinct vibronic bands, and of a zinc porphyrin only two bands. The dimer provides Q-bands which correspond to juxtaposition of one free-base and one zinc porphyrin. The spectral changes of the octamer relating to the tetramer are small, but significant in slightly intensified Q-bands at 518 and 648 nm because the ratio free-base porphyrin/zinc porphyrin is elevated. Hence, the spectral properties are in great agreement with the fact that tetramer and octamer comprise one zinc porphyrin for three and seven free-base porphyrinic units respectively. An inspection of the molar extinction coefficients of the Soret bands suggests an absence of an additive effect and existence of electronic communication between the porphyrins along the arrays. To elucidate the presence of anticipated interaction, a comparison of the absorption spectra with the composite spectra generated by adding the spectra of the component porphyrins is presented in Figure 2.15.

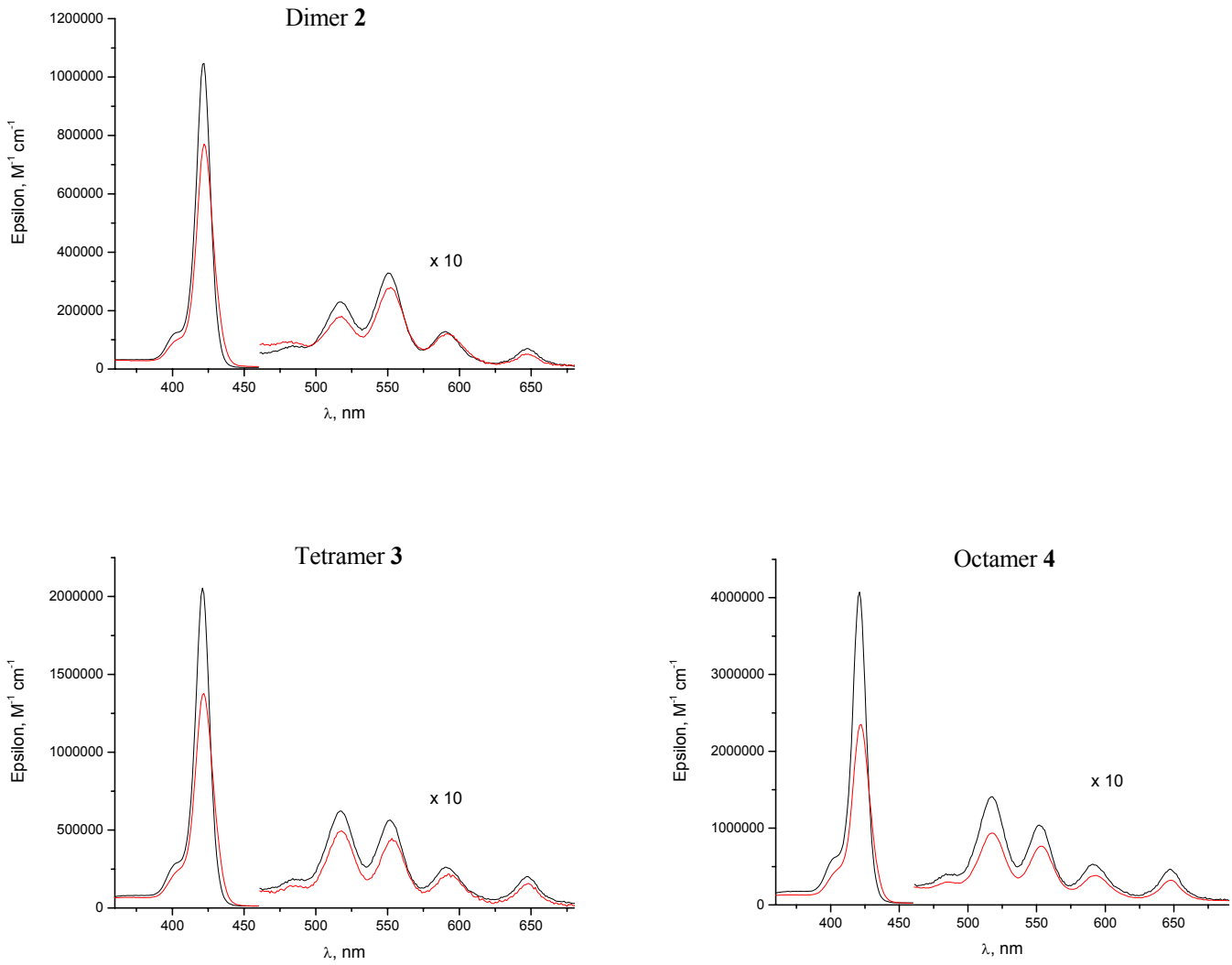

Figure 2.15 *Comparison of the absorption spectra (red line) of dimer **2**, tetramer **3** and octamer **4** with the composite spectra of the component porphyrins (black line).*

The shape of the spectra of all compounds is similar to composite spectra generated by adding the spectra of zinc porphyrin **13** and corresponding number of free-base porphyrin **12**. However, a broadening of the Soret band is observed for dimer **2**, tetramer **3** and octamer **4** relating to the composite spectra; a 1.1 nm half-width broadening is observed for the dimer, while for the tetramer and the octamer this value is 3.1 and 2.9 nm, respectively. These differences in the Soret absorption bands indicate electronic interporphyrinic communication. The Q-bands are virtually unchanged both in shape and in position relative to the spectra of the component parts, illustrating relatively weak electronic interaction. The difference in intensity of electronic interactions within the dimer and the higher order units has been

expected simply on the basis of the conformation of the oligonucleotidic backbone. The observed poor communication between the porphyrin chromophores along the oligonucleotidic backbone is in excellent agreement with the results obtained by using NMR spectroscopy. Thus, the porphyrin macrocycles are in non-coplanar conformation, yet presumably in a slipped cofacial orientation with a certainly small offset. We assume that this relatively close, but not symmetric orientation of the porphyrinic units is defined by preferable conformation of the porphyrin-uridine molecular system, which is already attained in the tetramer as it was suggested in the NMR analysis elaborated in the previous sub-chapter.

2.2.2. Energy transfer mechanisms.

In the system where the chromophores with energy donating and energy accepting features are present an energy transfer can occur such that the donor in its excited state returns to its ground state with simultaneous promotion of the acceptor to its excited state. The two main mechanisms of this energy transfer can occur by either through-bond (Dexter) or through-space (Förster), Figure 2.16.[164-167]

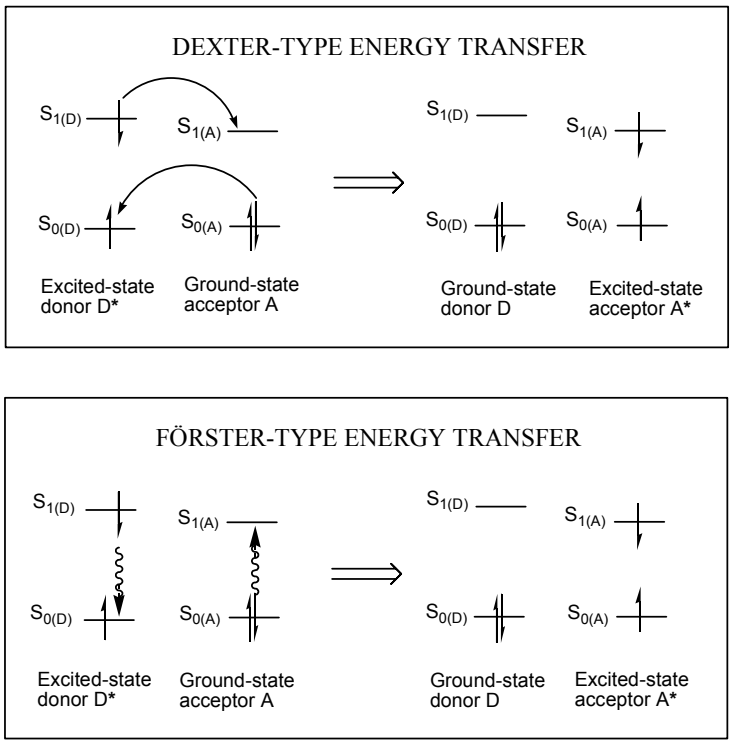

Figure 2.16 *The process of energy transfer involving the migration of excitation energy from the excited-state donor (D) to a nearby ground-state acceptor (A) by two main mechanisms.*

In the Dexter-type energy transfer mechanism, an electron exchange occurs from the S_1 state of the donor to the S_1 state of the acceptor, with a simultaneous exchange of an S_0 electron from acceptor to donor. This electron exchange requires strong D-A orbital overlap and is therefore a short-range (< 10 Å) interaction that diminishes exponentially with distance. In contrast, the Förster mechanism does not require electron exchange and is rather a through-space dipole-dipole interaction. In this case, D-A orbital overlap is not necessary, allowing the chromophores to be separated by a relatively large distance (10 – 100 Å). Hence, in

noncovalently linked donor-acceptor systems, the efficiency of Förster-type energy transfer has $1/r^6$ distance dependence, where r is the center-to-center distance between the donor and the acceptor. The transition dipole moments of the interacting chromophores play a large role in the energy transfer efficiency of the through-space mechanism. Therefore, this long-range energy transfer is expected to be efficient in systems in which the radiative transitions connecting the ground and the excited state of each partner have high oscillatory strength. The bridging moiety plays a crucial role in Dexter-type energy transfer, where rigidity and conjugation are the key parameters, whereas the properties of the chromophores themselves (transition dipole moments and spectral overlap of donor emission and acceptor absorption) as well as the interchromophoric distance play the more important role in Förster-type energy transfer. Strong interactions between the chromophores lead to optical spectra which are very different from the component spectra, while, on the other hand, weak coupling produces little or no alteration of the absorption spectra, but the luminescence properties may be quite different.

2.2.3. Photophysical studies by fluorescence spectroscopy.

The basic of photochemically active chomophores is that after absorption of a photon they enter a long-lived electronically excited state. Although, in principle, all the molecules are capable of electronic transitions in which electron is promoted from a ground state to a higher energy state, a vast majority of them collapses very quickly back to the ground state with evolution of heat.[98,160] On the other hand, if the electronic excited state of the molecule survives long enough, it can be transferred to other molecules, or it can be deactivated either thermally or by emission of a photon. In emission spectra of porphyrins, after excitation in the Soret band at around 420 nm, the excited S_2 state with a relatively long lifetime is reached. The detection wavelength dependence can be explained in terms of the emission from the vibrationally excited S_1 state, which is rapidly populated from the upper states.

The constitution of our porphyrinic arrays allowed us to study excited-state interactions of the porphyrins and to control the course of the excited energy flow. Hence, we assumed that the photonic energy absorbed by the terminal zinc porphyrin would be transferred towards the free-base porphyrins along the array. The existence of a photoinduced energy transfer in our porphyrin systems was examined by fluorescence spectroscopy.

Herein, the emission spectra of the porphyrinic arrays were recorded following the Soret band excitation in dichloromethane at room temperature. The emission spectra of a typical zinc(II) porphyrin show two bands at 600 and 650 nm, which are assigned to 0-0 and 1-0 vibronic transitions, while in the case of a typical free-base porphyrin emission spectra bands are at 650 and 710 nm. The comparison of the emission spectra of dimer **2**, tetramer **3** and octamer **4**, experimentally obtained by excitation at 422 nm, with the sum of the spectra of the component parts (free-base and zinc porphyrins), is presented in Figure 2.17. The overall emission data for all examined compounds were standardized relative to a reference optical density for the Soret band.

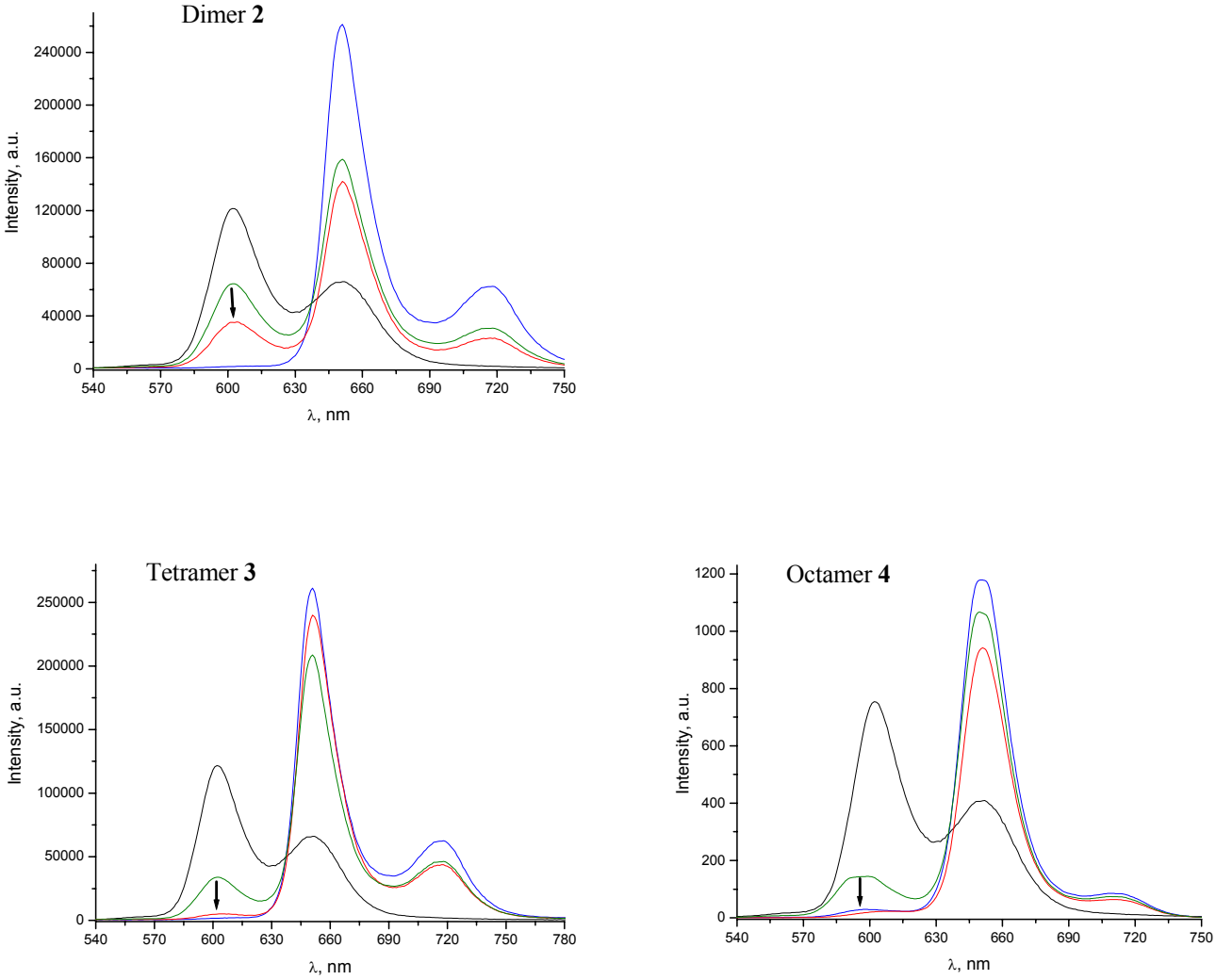

Figure 2.17 *The comparison of emission spectra of dimer **2**, tetramer **3** and octamer **4** (red line) with the sum of the component porphyrins spectra (green), zinc and free-base porphyrins, multiplied with $\varepsilon_{Zn}/(\varepsilon_{H2}+\varepsilon_{Zn})$ and $\varepsilon_{H2}/(\varepsilon_{H2}+\varepsilon_{Zn})$, considering the number of free-base porphyrins in each, dimer, tetramer and octamer. The reference emission spectra of the components: zinc (black) and free-base porphyrin (blue). All spectra were standardize to DO= 0.991.*

The presented spectral features show that emission from the zinc porphyrin diminishes in order of dimer, tetramer, octamer, and emission from the free-base porphyrin predominates. The emission spectrum of the dimer is characterized with significant residual emission from the zinc porphyrin, while the spectra of both tetramer and octamer indicate strong quenching of the zinc porphyrin. Throughout, the overall spectra of the tetramer and octamer show negligible differences suggesting similar interporphyrinic communication, which presumably

arises from preferable conformation of oligonucleotidic scaffold already defined in the tetramer.

To verify the hypothesis about a contribution of the zinc porphyrin excited state energy to emission of the energy acceptor, the free-base porphyrin, the fluorescence excitation spectra of the arrays were collected. The excitation spectra were obtained in dichloromethane by scanning the excitation from 350 to 800 nm with fixed emission at 710 nm, since at this wavelength dominates the emission of the free-base porphyrin. Appropriate justification of an energy transfer from the zinc porphyrin towards the free-base porphyrins arises from the comparison of the excitation spectra and the absorption spectra of dimer **2**, tetramer **3** and octamer **4**. The Q-state regions of the excitation and the absorption spectra are presented due to better visibility of the differences, Figure 2.18.

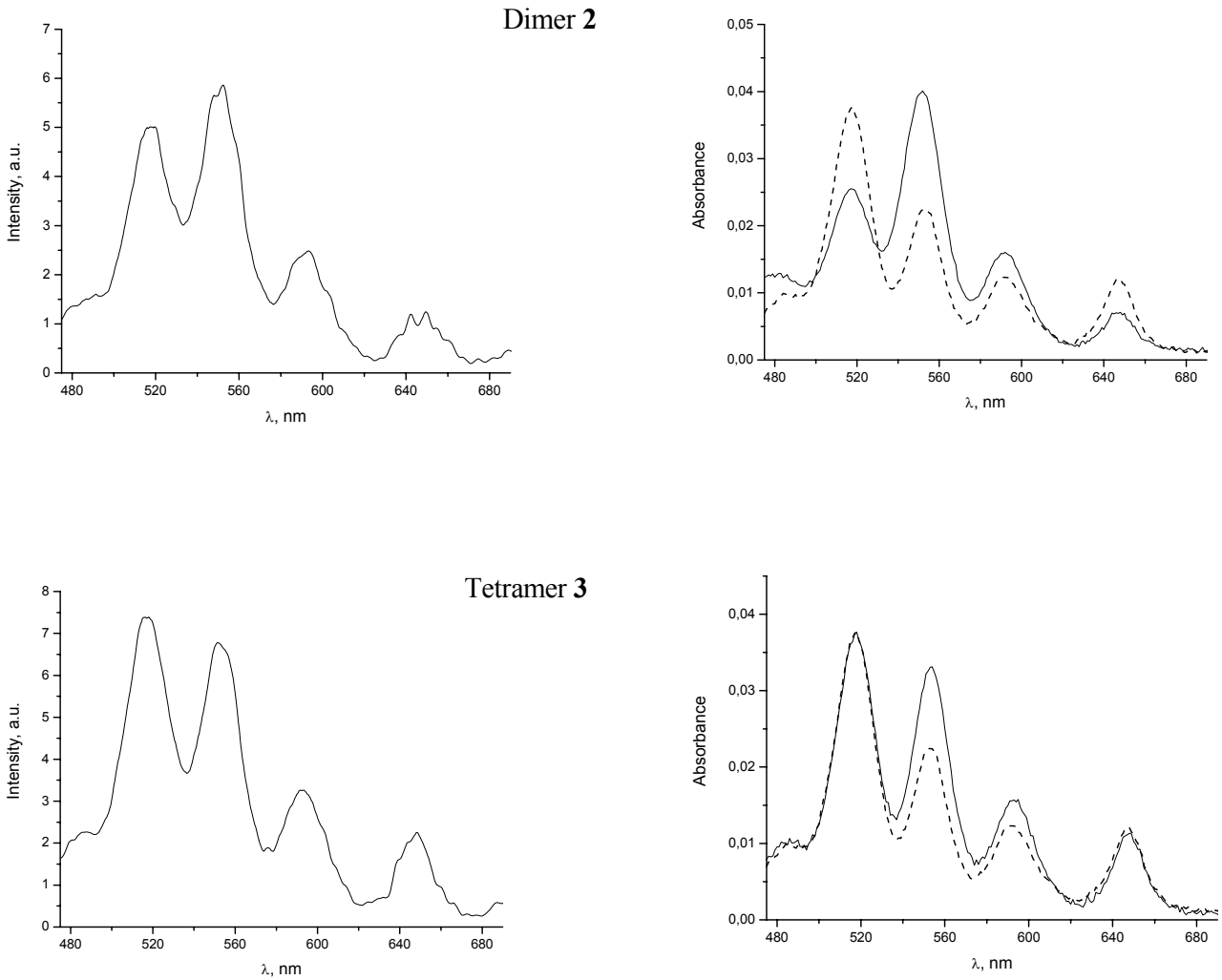

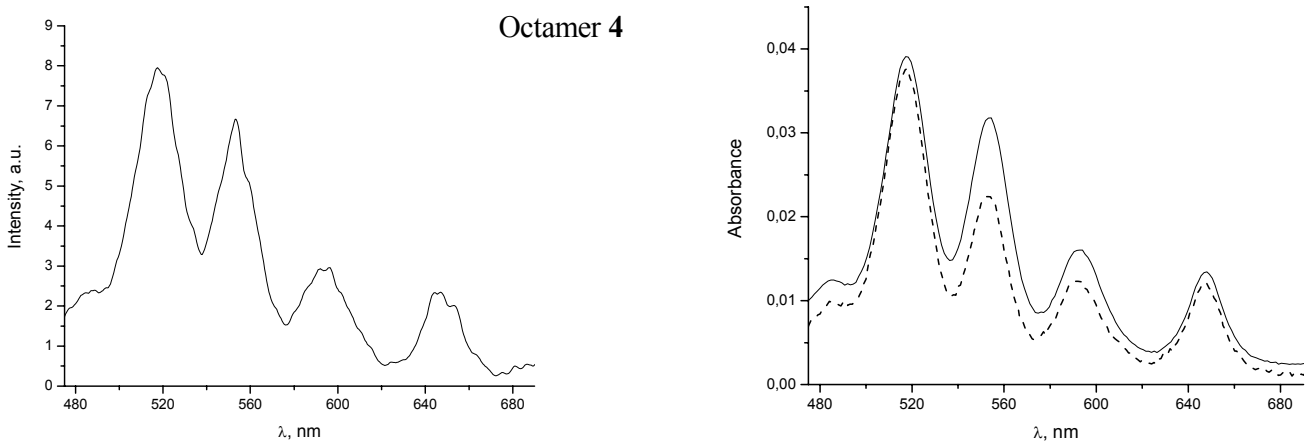

Figure 2.18 *The excitation spectra (λ_{em}= 710 nm) (left), and the absorption spectra (right) of dimer* ***2*** *(first row), tetramer* ***3*** *(middle row) and octamer* ***4*** *(last row) together with the absorption spectrum of the free-base porphyrin* ***12*** *(dashed line), in the Q-bands region.*

When no energy transfer takes place from the zinc porphyrin towards the free-base porphyrin, the observed excitation spectrum corresponds to the absorption spectrum of the free-base porphyrin only. The dimer comprises one unit of each, a zinc porphyrin as energy donor and a free-base porphyrin as energy acceptor, while the tetramer and octamer comprise a higher number of free-base porphyrins for only one zinc porphyrin. These structural dissimilarities lead to clear differences between the excitation spectra of the arrays and the absorption spectrum of the free-base porphyrin **12**. Nevertheless, juxtapositions of the excitation spectra and the absorption spectra of the corresponding array show close spectral matching. This indicates that the energy of the first singlet excited state from the zinc porphyrin contributes to the free-base porphyrin emission.

In conclusion, porphyrin-porphyrin electronic interactions along the arrays are present but weak as manifested by their slightly half-width broadening of Soret absorption bands. Initial fluorescence excitation and emission studies of porphyrin arrays covalently appended to oligonucleotidic scaffold indicate that an energy transfer occurs from the terminal zinc porphyrin towards the free-base porphyrins. The obtained spectral properties suggest that in the case of the tetramer and especially octamer, the energy is transferred with considerably greater efficiency than in the dimer. The porphyrinic macrocycles in the dimer are relatively

far apart, while in the tetramer we approached the preferable conformation of the porphyrin-uridine conjugates.

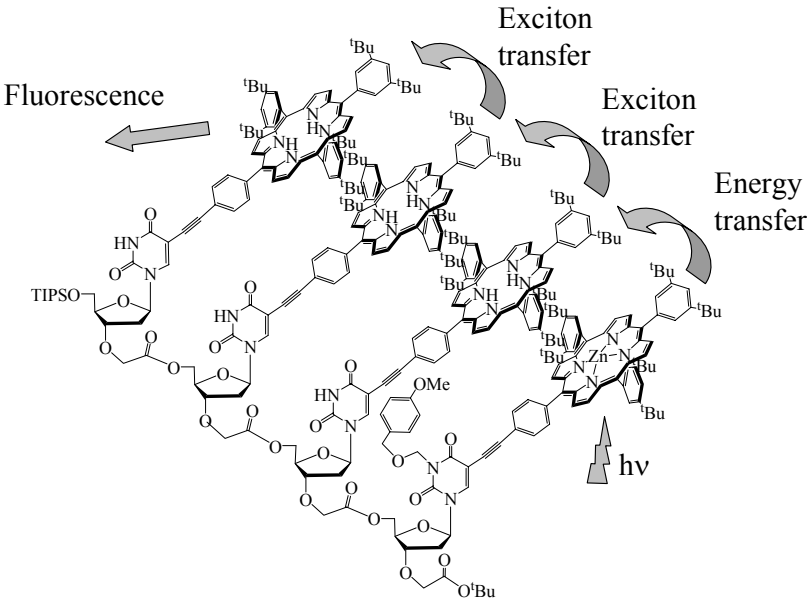

Figure 2.19 *The tetramer **3** as a representative of the oligodeoxyuridinic backbone with pendant porphyrins endowed with energy transfer capabilities.*

SUPRAMOLECULAR ASSEMBLIES: COORDINATION OF THE ZINC PORPHYRINIC ARRAYS WITH DABCO

Chemistry "beyond the molecule" is epitomized in nature by a plethora of relatively weak noncovalent interactions.[168,169] The three-dimensional structures of most biopolymers are controlled with noncovalent interactions, either between different parts of the same strand (as in protein α-helices) or between two separate strands (as in the DNA duplex and protein β-sheet). While nature has refined the construction of biopolymers, our mastery of the subtle noncovalent interactions as synthetic tools is in an early stage of development. Only in past two decades people begun to develop ways of mimicking the natural light-harvesting complexes by noncovalent assembly of porphyrin units aiming to obtain favoured spacing and orientation between the chromophores.[51,101,170-186] The construction of multi-chromophoric assemblies has led to resurgence of interest in coordination chemistry due to formation of ordered arrays directed through molecular recognition events.[187-191] As a modules in the construction of supramolecular assemblies porphyrins and metalloporphyrins can be exploited in two different ways: porphyrins can behave as donor building blocks insofar as they comprise *meso*-substituents, such as pyrridyl groups, which can act as ligands that can suitably coordinate to metal cations, while metalloporphyrins can act as acceptor building blocks as soon as the metal atom inside the porphyrin core has at least one axial site available for coordination. The interest in metalloporphyrins lays in the ease of exchange of various metals and ligands, which allow spatial control of porphyrin macrocycles. The coordination bond formed by metalloporphyrins has been explored in understanding how metal-ligand interactions are directing formation of supramolecular porphyrin arrays. In this respect a vast array of supramolecular systems have been prepared, such as, cyclic oligomers,[100,172,180,192] linear oligomers[31,193,194] and polymers,[195-197] squares,[198] tapes,[199,200] and other geometries.[173,201,202]

3.1. PREPARATION AND CHARACTERIZATION OF ZINC PORPHYRIN ARRAYS.

The divalent zinc metal was employed for the construction of metalloporphyrinic arrays. Zinc(II) porphyrin was chosen because it exhibits a number of advantages over other metals: it can easily be prepared from free-base porphyrin, it has good affinity for nitrogen donor ligands and forms with them five-coordinate complexes which have suitable binding constants for measurement by UV-visible titration, it has excellent photochemical properties and relative stability.[100,192]

In both dimer **2** and tetramer **3**, the zinc porphyrin is appended to the first uridine and the free-base porphyrins to the every other uridine in the arrays. According to this, for dimer **2** one porphyrin and for tetramer **3** three porphyrins underwent metallation process.

3.1.1. Synthesis of zinc porphyrin arrays, 30 and 31.

The synthetic routes to dimer **30** and tetramer **31** entails insertion of the zinc(II) ion into cavities of the free-base porphyrins of dimer **2** and tetramer **3**, according to Figures 3.1 and 3.2, respectively.

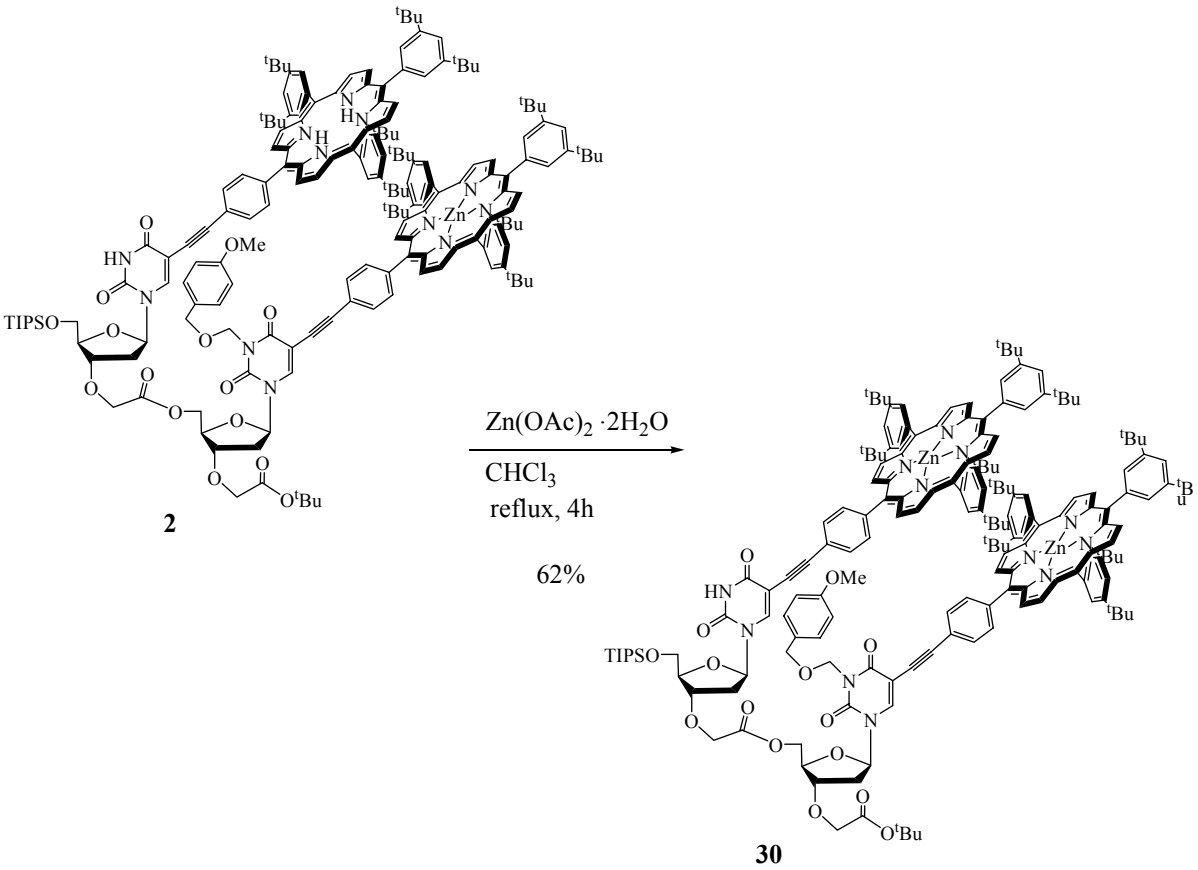

Figure 3.1 *Preparation of full zinc dimer* ***30****.*

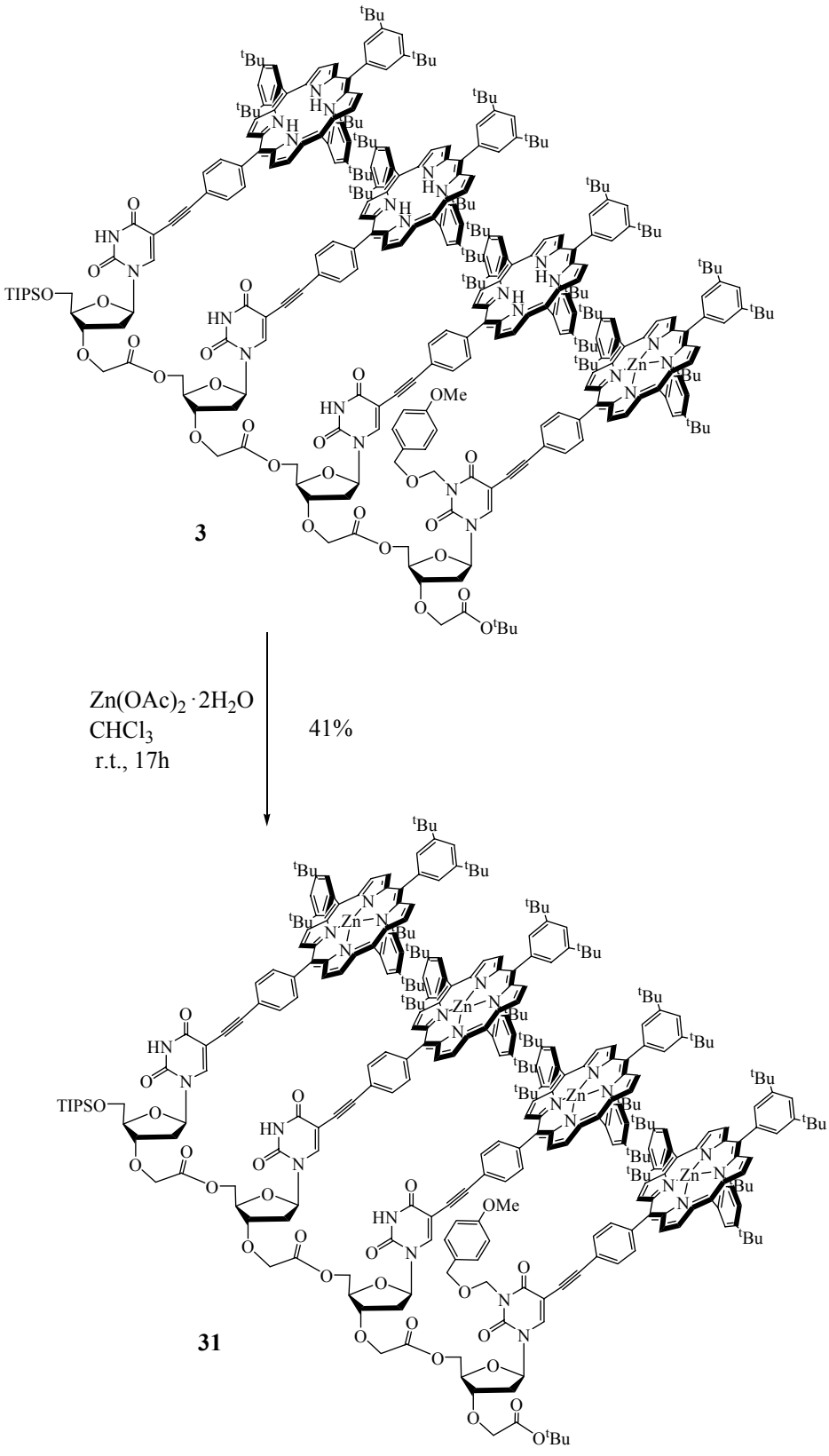

Figure 3.2 *Preparation of full zinc tetramer* ***31****.*

The free-base porphyrins of dimer **2** and tetramer **3** were metallated with Zn(II) in $CHCl_3$ as a solvent at reflux or room temperature within 4 or 17 hours, respectively. Metallation of both compounds, **2** and **3**, was performed in the presence of 2 equivalents of Zn(II) acetate dihydrate per porphyrin. The reaction yield decreases due to side reactions, especially at higher temperatures. In order to minimize the formation of byproducts, metallation of tetramer **3** was performed at room temperature. The mild experimental conditions enhanced the integrity of corresponding zinc porphyrin array **31**, thus obtained in 41% yield. The reaction progress was followed by thin-layer chromatography (TLC) and UV-visible absorption spectroscopy. On the TLC plates free-base and zinc porphyrin arrays are characterized with almost identical retention factors. However, by TLC an evolution of byproducts could be visualized. The insertion of Zn(II) into porphyrin macrocycle was corroborated by absorption spectroscopy. In the absorption spectra the presence of two Q-bands instead of four signified completion of metallation process. After purification, the further evidence of successful metallation was provided by ^{1}H NMR due to disappearance of the signals of the inner NH at -2.70 ppm.

3.1.2. Characterization of zinc porphyrin arrays by ^{1}H NMR spectroscopy.

Zinc porphyrins of both dimer **30** and tetramer **31** were characterized by ^{1}H NMR spectroscopy with important diagnostic shifts for β-pyrrolic protons and disappearance of signals of inner nitrogen protons at -2.70 ppm, Figure 3.3.

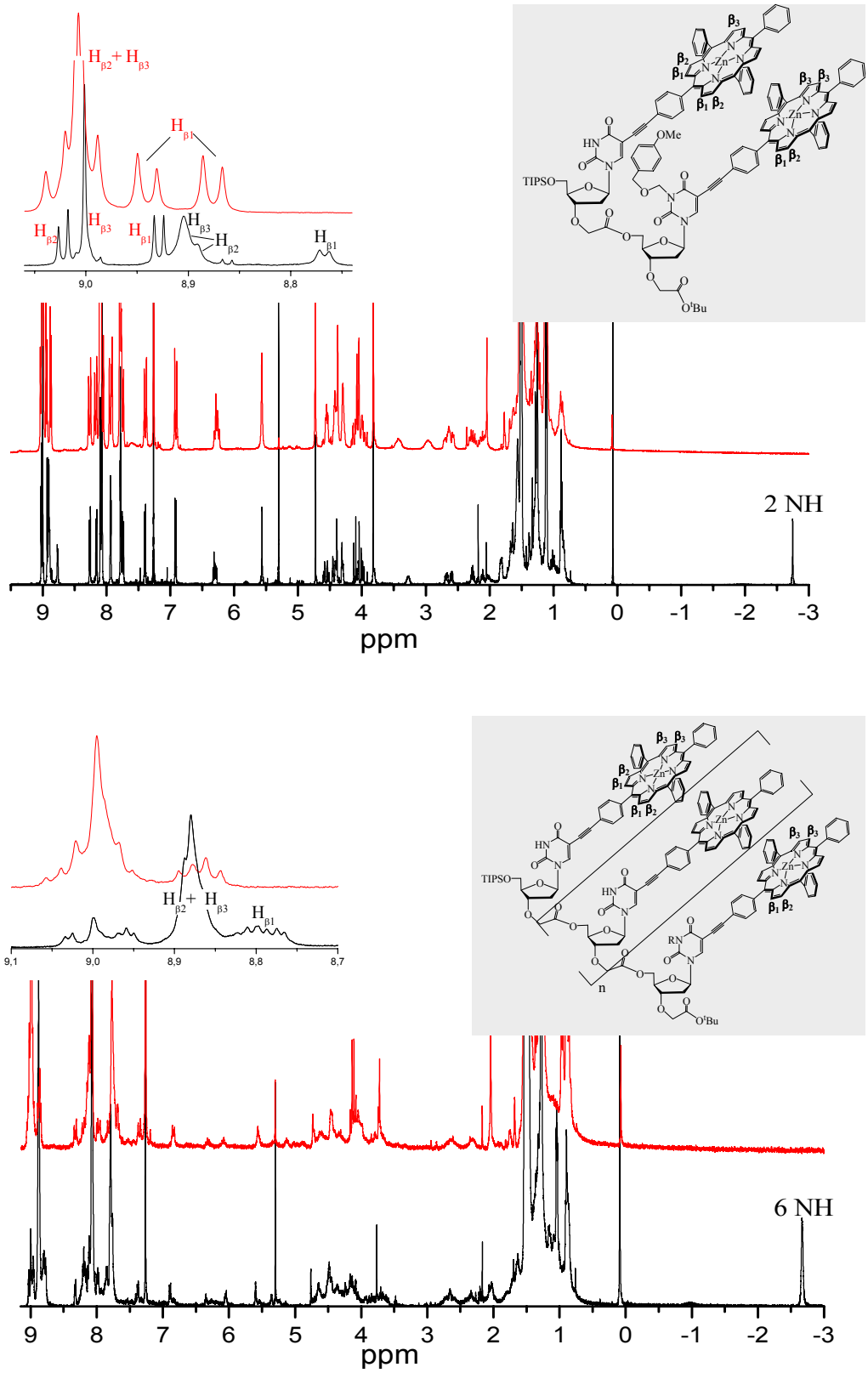

Figure 3.3 *Comparison of ^{1}H-NMR spectra (250 MHz, $CDCl_3$, 298 K) of dimer* ***2*** *and tetramer* ***3*** *(black) with zinc porphyrin* ***30*** *and* ***31*** *(red), respectively, for dimer (up) and tetramer (down). In the inset low field region is shown with chemical shift assignments for the free-base porphyrins (black) and the zinc porphyrins (red). The tert-butyls are omitted for clarity.*

With metallation of the free-base porphyrins, resonances of porphyrin cores underwent weak changes, while substituents at porphyrin rings and uridine moieties were not affected. The spectra of zinc porphyrin arrays exhibit distinctive features according to absence of free-base porphyrin β-pyrrolic resonances. That is to say that only the protons corresponding to the freshly metallated free-base porphyrin protons were subjected to transformations caused by the local ring current change. The splitting pattern of the β-pyrrolic protons for all porphyrins in the arrays is practically unchanged, i.e. $H_{\beta 1}$ situated beside phenylacetylene is separated from signals of $H_{\beta 2}$ and $H_{\beta 3}$. The dimer **30** provides a pair of doublets for $H_{\beta 1}$ since the two porphyrinic components are surrounded with slightly different environment. On the other hand, tetramer **31** shows β-pyrrolic resonances that are poorly separated due to increased number of magnetically equivalent porphyrin units. As expected, the spectrum of the tetramer is more complicated than that of the dimer. The signals of nucleotidic protons are not affected by insertion of the zinc into the porphyrinic macrocycles, neither for dimer **30** nor for tetramer **31**. Taken together, these small variations in the local environment of porphyrin macrocycles suggest that no structural change in the oligonucleotidic array was related to metallation.

3.1.3. Characterization of zinc porphyrin arrays by UV-visible spectroscopy.

The straightforward confirmation of the zinc(II) ion in porphyrinic macrocycles was realized by UV-visible spectroscopy. The electronic absorption spectrum of a typical zinc porphyrin consists of the strong transition to the second excited state ($S_0 \rightarrow S_2$), the Soret band at about 420 nm, and the two weak transitions to the first excited state ($S_0 \rightarrow S_1$), the Q-bands at about 550 and 590 nm. The two Q-bands in the absorption spectrum of a zinc porphyrin are the consequence of an identical x and y directions of Q(0-0) and Q(0-1) dipole transitions.[125,129]

The absorption spectra of dimer **30** and tetramer **31** were measured in dichloromethane at room temperature, and at concentration around 6.5×10^{-7} M for the Soret band and 1.5×10^{-5} M for the Q-bands. In general, the shape of the spectra of both compounds is similar to one another and similar to the one of the simple zinc porphyrin **13**. The wavelengths of the Soret absorption maxima for dimer and tetramer arrays are, however, slightly red-shifted relative to the composite spectra generated by adding the spectra of the component zinc porphyrins. The Soret band of dimer **30** is shifted for 2 nm, and of tetramer **31** for 4 nm. In addition, wavelengths of the Q-bands are also red-shifted in the case of the tetramer. To elucidate the

presence of anticipated electronic interactions between the chromophores along the arrays, molar extinction coefficients for corresponding absorption maxima as well as comparison of the absorption spectra with the composite spectra generated by adding the spectra of the component porphyrins are presented below in Table 3.1 and in Figure 3.4. The absorption spectra of dimer **30** and tetramer **31** were acquired at concentrations of 6.5 x 10^{-7} M and 1.5 x 10^{-5} M, respectively, in dichloromethane at room temperature.

	λ_{max} (nm)	ε (M^{-1} cm^{-1})
Zinc porphyrin **13**	422	558 000
	549	21 500
	588	6 200
Dimer **30**	422	1 009 000
	550	45 600
	589	14 400
Tetramer **31**	424	1 918 000
	551	87 200
	592	30 100

Table 3.1 *Electronic absorption maxima and corresponding molar extinction coefficients.*

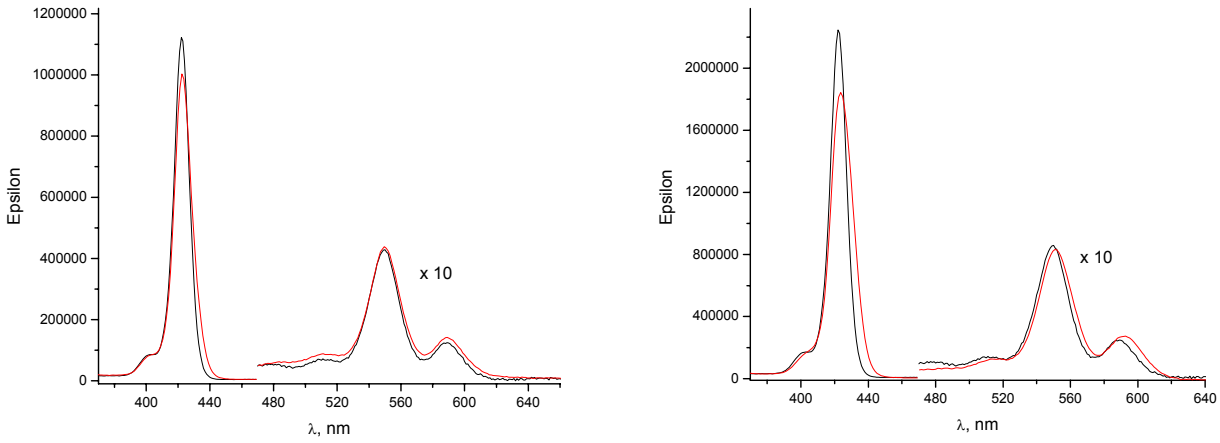

Figure 3.4 *Absorption spectra (red line) of dimer **30** (left) and tetramer **31** (right). Composite spectra of the component porphyrins (black line).*

From the delineated spectral features, we could presume an absence of the additive effect and existence of electronic communication between the porphyrins. In this respect,

broadening of the Soret band was evidenced from comparison of the dimer or tetramer spectra with the sum of the spectra of the component porphyrins, Figure 3.4. The Soret band of dimer **30** is slightly broadened with full width at half maximum (fwhm) of 13.0 nm, and for tetramer **31** of 15.4 nm. In comparison of those values with fwhm of 11.2 nm, yielded by adding the spectra of components, the presence of electronic interactions could be assumed. Generally, in the case of porphyrins, the Soret band is particularly sensitive to electronic interporphyrinic interactions due to the extremely large transition dipole moment. On the other hand, Q bands have much lower transition dipole and are correspondingly much less sensitive to electronic interactions.

3.2. COORDINATION OF THE ZINC MULTIPORPHYRINIC ARRAYS WITH DABCO: SPECTROSCOPIC STUDIES.

This chapter is based on the use of host-guest interactions for the formation of supramolecular assemblies between the multiporphyrinic arrays and small bidentate ligand, (1,4-diazabicyclo[2.2.2]octane (DABCO)) through axial coordination. We chose DABCO as a ligand because it's high basicity (pK_a= 8.7) was expected to lead to stable complexes, although some other linear bidentate ligands would probably behave the same way. It was assumed that coordination of this rigid bifunctional ligand to porphyrins will preorganized oligonucleotidic backbone and by that directed porphyrins to adopt parallel orientation. The synthesized molecular systems are amenable to preorganization, because their architecture is based on combination of rigid and flexible linkers. The architecture of multiporphyrinic systems is important because the covalent connectivity between the interacting centres dictates the geometry of resulting assembly and the relative orientation of chromophores dictates the strength of the interaction with ligands. As already noted, the geometry of porphyrins in supramolecular assembly is crucial in design of artificial light-harvesting complexes. [51,101,170-186]

3.2.1. Coordination of DABCO probed by UV-visible titration.

UV-visible absorption titrations were carried out to probe the structure and stability of zinc porphyrin-DABCO complexes. They were performed in dichloromethane at room temperature by adding small aliquots of DABCO solution of discrete concentration to the solution of the porphyrinic array. The approximate concentration of the zinc porphyrin solution was determined by peak absorbance which should be in the range between 0.9-1.0. The several DABCO solutions in dichloromethane with exact concentrations were prepared. 3 ml of the porphyrin solution was placed in a cuvette and the absorption spectrum was recorded. 1-10 μL aliquots of accurately determined DABCO solution were sequentially added to the porphyrin solution and the spectra were recorded after each addition.

3.2.2. Methods for analysis of titration data.

Data obtained by UV-visible titrations were analysed by using the values of the absorbance at fixed wavelengths and by simultaneous fitting of the whole series of spectra collected at 1 nm intervals using the software SPECFIT.[203-205]

The first method for determination of binding constant by analysis of titration data at selected wavelength is exclusively useful for the complexes with stoichiometry 1/1.[206] This analysis was processed by using the commonly available spreadsheet software Origin version 61. The basic equations for the formation of 1:1 complex based on concentrations of host, guest and a complex at equilibrium are defined as follows:

$$H + G \rightleftharpoons H*G \quad (1)$$

$$K_a = \frac{[HG]}{[H] * [G]} \quad (2)$$

$$[H]_o = [H] + [HG] \quad (3)$$

$$[G]_o = [G] + [HG], \quad (4)$$

where H is a host and G is a guest; $[H]_o$ and $[G]_o$ are total concentrations of host and guest at the initial state; [H], [G] and [HG] are concentrations of host, guest and complex at the final stage, namely, at equilibrium. The combination of equations (1)-(4), which describe the relationships between defined parameters, leads to equation (5).

$$K_a = \frac{[HG]}{([H]_o - [HG]) * ([G]_o - [HG])} \quad (5)$$

Parameters are classified as follows: variables defined as experimental conditions: $[H]_o$, $[G]_o$; variables dependent on equilibrium: [H], [G], [HG]; parameters to be determined: K_a.

In our experimental conditions, explained in the former paragraph, the concentration of the host was assumed to be constant as the overall volume of the guest in the cuvette at the end of titration is neglectable. On the basis of this consideration, concentration of host-guest complex at equilibrium depends on a mole fraction of host-guest complex in equilibrium mixture and on concentration of host, equation (6).

$$[HG] = F_c * [H]_o \quad (6)$$

Hence, equation (5) is transformed to equation (7) by using equation (6).

$$K_a = \frac{F_c * [H]_o}{([H]_o - F_c * [H]_o) * ([G]_o - F_c * [H]_o)} \quad (7)$$

Finally, the equation used for calculation of association or binding constants of the strong 1:1 complexes is expressed by equation (8), which is derived from equation (7) by substraction of denominator and numerator by $[H]_o$.

$$K_a = \frac{F_c}{(1-Fc) * ([G]_o - F_c * [H]_o)} \quad (8)$$

Here, F_c is a mole fraction of host-guest complex in equilibrium mixture and is calculated by: $F_c = \Delta Abs / (A_{complex} - A_o)$, explained just below,

ΔAbs is the difference in absorbance observed for the complex and that observed in the host molecule: $\Delta Abs = A_{observed} - A_o$,

$A_{observe}$ is absorbance measured after each addition of DABCO,

$[H]_o$ is known total concentration of host (porphyrin),

$[G]_o$ is known concentration of guest (ligand, DABCO).

In the case of complexation measured by UV-visible spectroscopy, concentrations and absorbances of species are related by the following equations (9)-(12). As a premise, the length of the cell is fixed to be 1 cm. In our case, absorbance of the guest molecule was not considered since DABCO doesn't absorb in the region where the host molecule and host-guest complex do.

$$A_{observed} = \varepsilon_{HG} * [HG] + \varepsilon_H * [H] \quad (9)$$

Equation (9) is transformed to equation (10) by using the equation (3).

$$A_{observed} = \varepsilon_{HG} * [HG] + \varepsilon_H * ([H]_o - [HG]) \quad (10)$$

Taken together, equations (10) and (6) lead to equation (11) which unveils the correlation between a mole fraction of a complex in equilibrium mixture and:

$A_{complex} = \varepsilon_{HG} * [H]_o$, absorbance of complex,

$A_o = \varepsilon_H * [H]_o$, an initial absorbance of host molecule (before addition of DABCO).

$$A_{observed} = F_c * (\varepsilon_{HG} * [H]_o) + \varepsilon_H * [H]_o - F_c * (\varepsilon_H * [H]_o) \qquad (11)$$

From here, it is feasible to elucidate F_c, equation (12), hence to calculate binding constant, equation (8).

$$F_c = \frac{A_{observed} - A_o}{A_{complex} - A_o} \qquad (12)$$

In addition, all UV-visible titrations were analysed using the SPECFIT, which uses a global analysis system with expanded factor analysis and Marquardt least-squares minimization to obtain globally optimized parameters. The advantages of this method relating to the previously explained is that the complete titration data can be fitted simultaneously to various combinations of stoichiometric binding models and that spectral changes in the whole spectra can be analysed at the same time and within the complete titration.

3.2.3. Complexation of DABCO by simple porphyrin 13.

Before examining the supramolecular complexes of DABCO with the porphyrin arrays, the properties of simple porphyrin **13**, further monomer, were investigated. This system was employed as a reference since the zinc center can coordinate only to one nitrogen of DABCO.

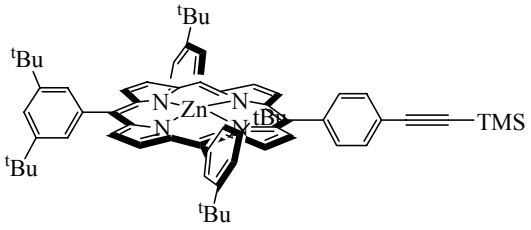

13

The coordination of DABCO to monomer **13** was probed by UV-visible titration, by using the coordination shift of the Soret absorption as well as the Q-bands. The Soret band absorption was measured at the concentration of 1.75 x 10^{-6} M which corresponds to peak absorbance of 1.05 at 422 nm. Under these dilute conditions binding of DABCO resulted in a shift of the Soret band from 422 to 432 nm. The clean isosbesticity of these spectra demonstrates that the spectroscopically active species in the solution are simple porphyrin **13** and one type of its complex with DABCO. Any further changes in the absorption spectra of this model system were not observed, even with addition of many more equivalents of DABCO, Figure 3.5.

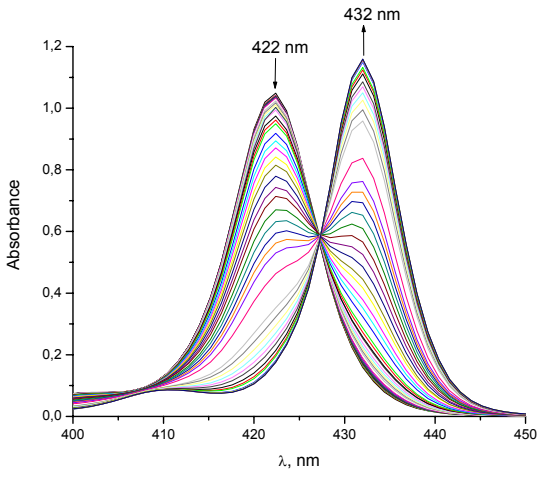

Figure 3.5 *UV-visible titration of simple porphyrin* ***13*** *with DABCO in* CH_2Cl_2 *at r.t..*

Spectrophotometric titration was repeated at concentration of 4.27 x 10^{-5} M, which corresponds to peak absorbance of 0.97 at 549 nm. At this wavelength the coordination shift of the Q-band was followed. Spectral changes of the monomer on addition of DABCO involved a progressive decline of bands characteristic for the simple porphyrin and appearance of the new bands indicating that new porphyrinic species were formed. Such behaviour corroborated the presence of two colored species (free **13** and monomer-DABCO complex) in equilibrium.

The titrations data were analysed with both methods delineated previously, by using the selected wavelengths and by fitting the whole spectra using SPECFIT. The first method could be applied only to the model system of zinc porphyrins that forms a 1/1 complex with DABCO. Hence, the binding constant for 1/1 monomer/DABCO complex calculated by this method was found to be 1.7 x 10^5 M^{-1} (log K_{11}= 5.23). Multivariate global factor analysis of the whole series of spectra showed that the titration can be analysed in terms of two colored species, free **13** and 1/1 stoichiometric model. The excellent fit of the titration data to the 1/1 binding model (Figure 3.6) provided the stoichiometric binding constant of log K_{11}= 5.27 ± 0.01.

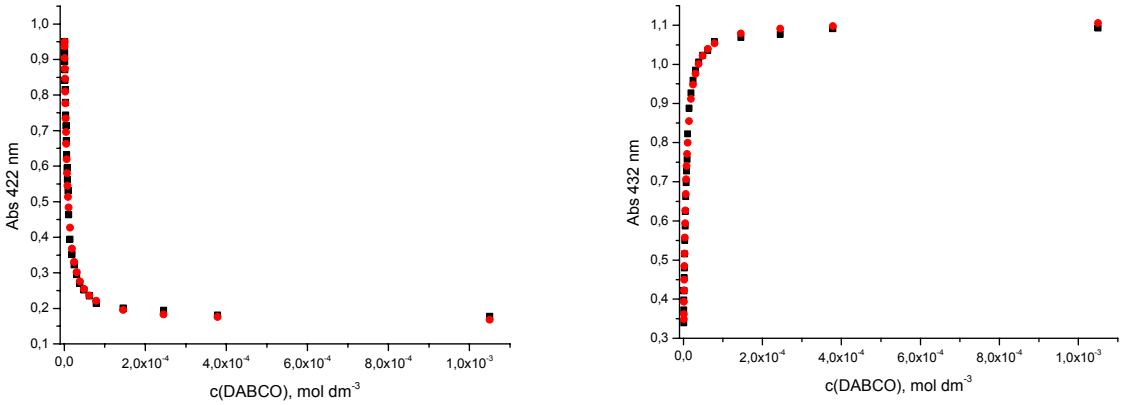

Figure 3.6 *UV-visible titration data (change in absorbance at two wavelengths, 422 and 432 nm) for the binding of simple porphyrin* ***13*** *with DABCO, fitted to the calculated curves for the only reliable equilibrium which corresponds to 1/1 complex.*

The excellent fit of experimental and calculated data and great agreement in the binding constants obtained by data analysis corroborated that the formation of the 1/1 monomer/DABCO complex was the only process in the titration. Hence, simple porphyrin **13**

as the acceptor unit complemented the donor ligand, DABCO, by coordination of electron deficient zinc to the one nitrogen of the base, Figure 3.7.

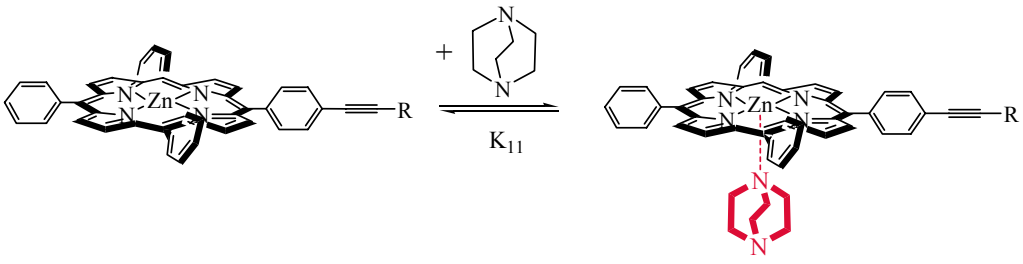

Figure 3.7 *Representation of the equilibria obtained in the binding of DABCO to simple porphyrin* ***13****. For clarity reasons tert-butyls on meso-phenyls are omitted.*

The zinc porphyrin-DABCO systems have been widely studied by Sanders, Hunter, Anderson and co-workers. They found that a red shift in the Soret band for 10 nm is typical for the 1/1 complex.[48,193,207-214] In addition, they described that a simple zinc porphyrin at micromolar concentrations with DABCO forms exclusively 1/1 complex with corresponding binding constant of about 10^5 M^{-1}. Thus, our result is in excellent agreement with their pattern.

3.2.4. Complexation of DABCO by bis-porphyrinic tweezer 30.

After examining the complexation of the simple porphyrin with DABCO, we studied the binding of the same base to dimer **30**, the bis-porphyrinic tweezer appended to an appropriate position of the flexible uridinic scaffold by the rigid acetylene group.

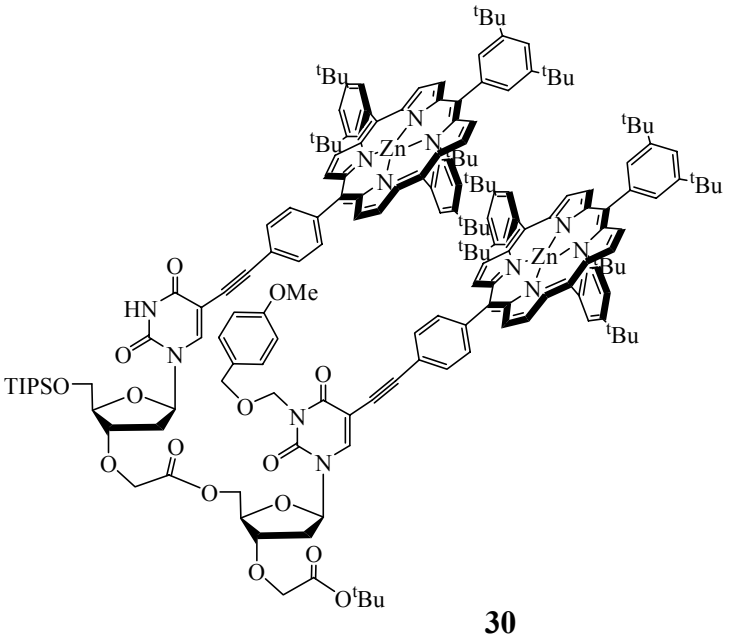

30

The titration of the dimer with DABCO was measured by using the coordination shift of the Soret absorption as well as the Q-bands. The Soret band absorption was measured at the concentration of 1.04 x 10^{-6} M which corresponds to an absorbance of 0.95 at 422 nm. The titration was performed in two parts to be analysed in terms of two-state equilibria. The first part of the titration was processed until 2 equivalents of DABCO were added per porphyrin. The complete titration that involved an addition of DABCO until 6000 equivalents per porphyrin was performed separately, Figure 3.8.

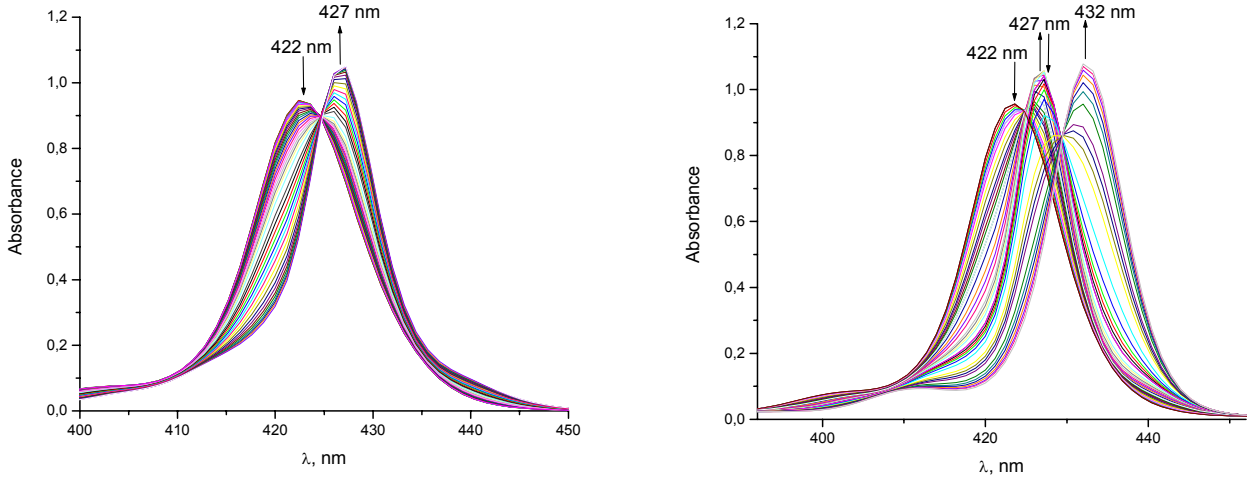

Figure 3.8 *UV-visible titration of bis-porphyrinic tweezer **30** with DABCO in CH_2Cl_2 at r.t.; on the left hand side first part of the titration and on the right the complete titration.*

The clean isosbesticity of spectra obtained in the first part of the titration demonstrates that the only colored species present in solution are free dimer **30** and one type of its complex with DABCO. The observed spectral changes are quite similar to those obtained in the titration of monomer **13**. However, there are some minor spectral changes, i.e. smaller red shift of the Soret peak, from 422 to 427 nm, as well as intensified and sharpened form of the titration spectrum. A shift in the Soret band of 5 nm is exactly two times smaller then the shift obtained for the 1/1 monomer/DABCO complex. Accordingly, it was reasonable to anticipate formation of the intramolecular 1/1 sandwich complex. On addition of more DABCO, intensity of the absorption band at 427 nm decreased, and a new absorption band appeared at 432 nm. As observed in the titration spectrum of monomer **13**, the Soret absorption at 432 nm is typical for the simple 1/1 porphyrin/DABCO complex. On the basis of the changes in absorption spectra, the possible two consecutive two-state equilibria with corresponding stepwise constants in the binding of DABCO to bis-porphyrinic tweezer **30** are shown in Figure 3.9.

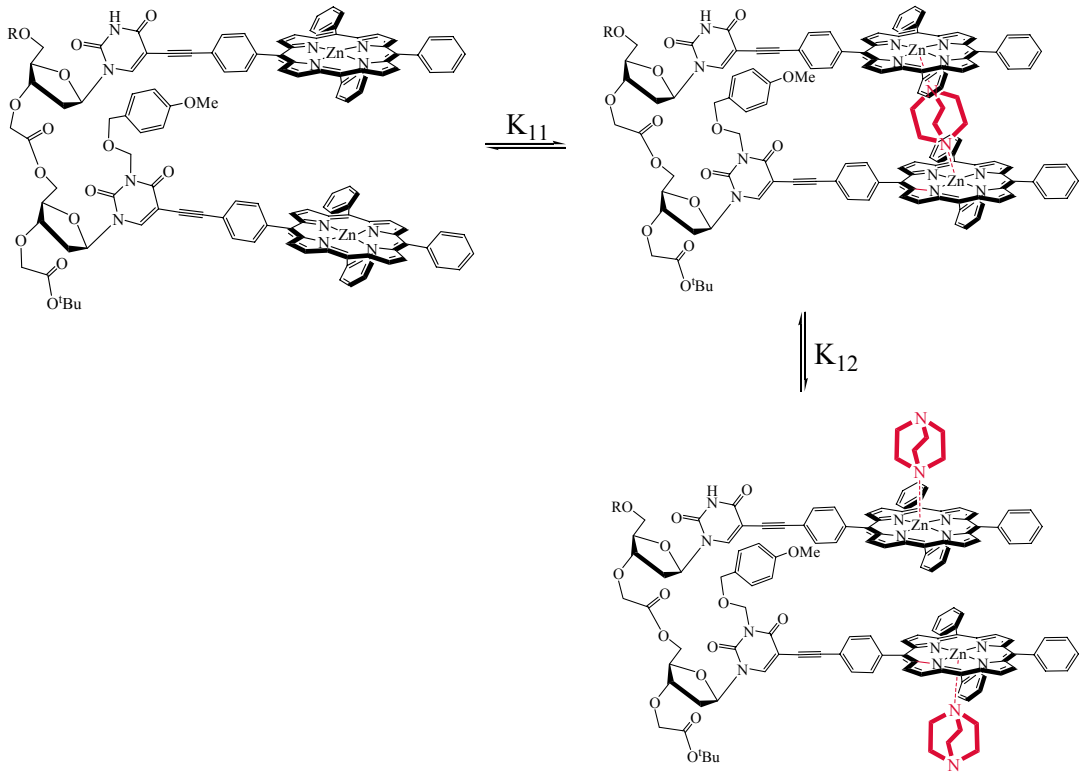

Figure 3.9 *Representation of the proposed equilibria involved in the binding of DABCO to bis-porphyrinic tweezer* ***30****. For clarity reasons tert-butyls on meso-phenyls are omitted.*

Spectrophotometric titration of dimer **30** with DABCO was repeated at concentration of 2.17 x 10^{-5} M, which corresponds to absorbance of 0.98 at 549 nm. At this wavelength the coordination shift of the Q-band was probed. Spectral changes in the titration spectrum involved a progressive decline of the bands characteristic for the free dimer and appearance of new red-shifted bands. This titration spectrum with sharp isosbestic points indicated the presence of an independent spectroscopically active species.

The first method for calculation of the binding constant by using titration data at selected wavelengths was applied only to the first part of the titration characterized by sharp isosbestic point. This analysis could be performed because the complexation by 1/1 binding model was envisaged in the first equilibrium. The binding constant for the 1/1 dimer/DABCO complex was found to be 7.4 x 10^{6} M^{-1} (log K_{11}= 6.87). The formation of this type of a complex was verified by analysis of the whole set of spectra which correspond to the first part of the titration by using SPECFIT. The analysis resulted with only one possible 1/1 complex with corresponding binding constant log K_{11}= 6.42 ± 0.03. It is interesting to note that calculated log K_{11} for 1/1 dimer/DABCO complex is more than one order of magnitude higher

than log K_{11} for 1/1 monomer/DABCO complex. Taken together, these results strongly support formation of 1/1 dimer/DABCO sandwich complex through the chelate effect. The whole spectra obtained by the complete titration was analysed in terms of three possible colored species: free dimer **30**, 1/1 sandwich complex, and 1/2 open complex (Figure 3.9). Fitting of the titration data revealed that 1/1 and 1/2 binding models for dimer/DABCO are only possible, Figure 3.10.

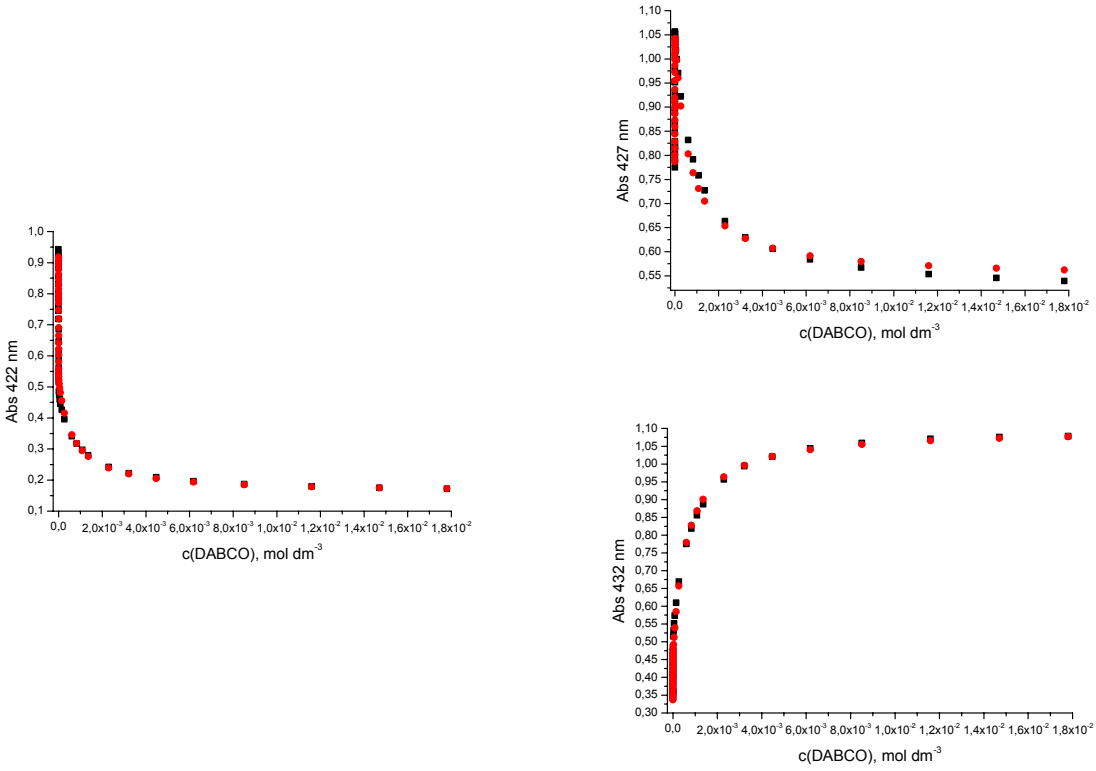

Figure 3.10 *UV-visible titration data (change in absorbance at three wavelengths, 422, 427 and 432 nm) for the binding of bis-porphyrinic tweezer* ***30*** *with DABCO, fitted to the calculated curves for the equilibria in Figure 3.9.*

Fitting to 1/1 binding isotherm yielded the stoichiometric binding constant log K_{11}= 6.65 ± 0.08, while the fit to 1/2 binding model provided log K_{12}= 3.21 ± 0.10. The calculated log K_{11} is almost identical to log K_{11} value obtained in the analysis of the first part of the titration. Moreover, calculated log K_{12} value is three orders of magnitude lower than log K_{11} value. Therefore, dissociation of the more stable chelated 1/1 complex is followed by coordination of second DABCO and by that formation of the 1/2 complex in which two DABCO molecules are coordinated to two porphyrins of the dimer. Both, 1/1 and 1/2

complexes involved in these consecutive two-state equilibria are in agreement with the species represented in Figure 3.9.

Similar formation of sandwich complexes was evidenced by Sanders, Hunter, Anderson and co-workers.[48,193,207-214] These studies show that sandwich complex formation is in concert with the parallel orientation of two porphyrin macrocycles. In this respect, the shifts in titration spectra are caused by proximity of the porphyrins and in this line increased interporphyrinic electronic interaction. The Soret band of the free dimer **30** has fwhm 15 nm, and the Soret band of the dimer/DABCO sandwich complex 11 nm. It is believed that this narrowing indicate a significant increase in the center-to-center distance between the two porphyrins, due to the insertion of DABCO into the bis-porphyrinic cavity. This hypothesis is in great agreement with the half width at half maximum of 13 nm for the 1/2 dimer DABCO open complex. The outer coordination of DABCO allows a shorter center-to-center distance between the porphyrins.

3.2.5. Complexation of DABCO by tetra-porphyrin 31.

Here we describe the binding properties of the last molecular system in this series. This system consists of four porphyrinic centres attached to flexible oligonucleotidic.

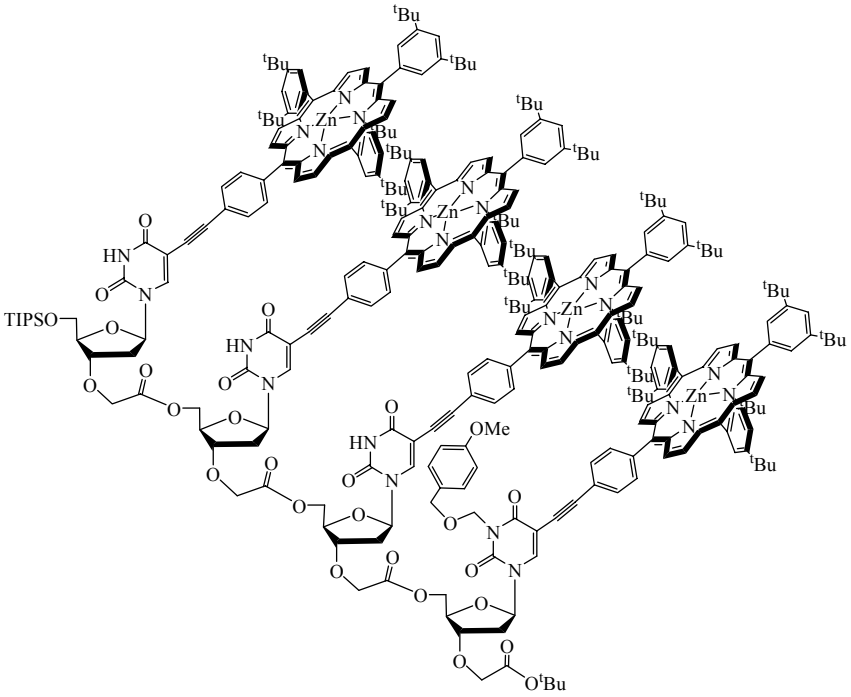

31

Again, the titration was probed by UV-visible absorption spectroscopy by using the coordination shift of the Soret absorption at the concentration of 6.64 x 10^{-7} M which corresponds to peak absorbance of 0.97 at 424 nm. Due to variety of possible binding patterns in such complex system the titration was performed in two parts to allow separate analysis of the first part of the titration, which would presumably provide a complex with the 1/1 stoichiometry. The first part of the titration processed until 1 equivalent of DABCO per porphyrin was added. The complete titration involved addition of DABCO up to 6500 equivalents of DABCO per porphyrin, Figure 3.11.

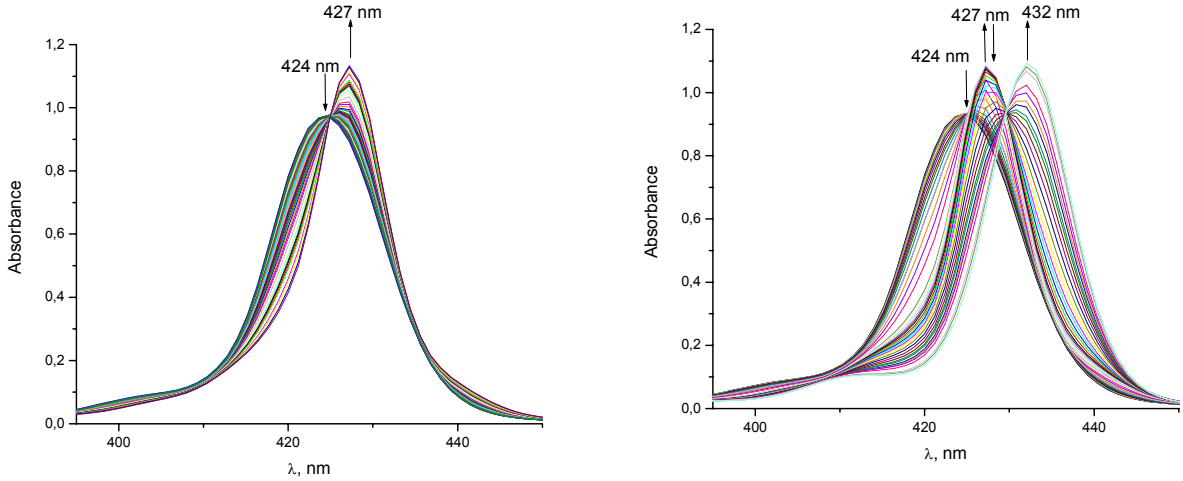

Figure 3.11 *UV-visible titration of tetra-porphyrin* ***31*** *with DABCO in CH_2Cl_2 at r.t.. The series of spectra at left hand side show the first phase of the titration process. Absorption spectra obtained by the complete titration are presented on the right hand side.*

The first part of the titration provided spectra with sharp isosbestic points. This set of spectra can be analysed in terms of only two spectroscopically active species, namely free **31** and one type of its complex with DABCO. The observed spectral changes are quite similar to those observed in the first part of the bis-porphyrinic tweezer titration, which present formation of the 1/1 sandwich complex. However, there are some minor differences, i.e. smaller batochromic shift of the Soret peak (precisely 5.0 nm and 2.5 nm in titrations of **30** and **31**, respectively) and different positions of the Soret absorption maxima. Accordingly, we could presume that the main process in the first part of the tetramer titration is the formation of intramolecular chelated complexes with stoichiometry 1/1 or 1/2. After the first red shift of the Soret band to 427 nm, which was following the initial addition of DABCO, addition of more DABCO caused another batochromic shift to the new absorption maximum at 432 nm. The Soret absorption at 432 nm characterizes the 1/1 monomer/DABCO and the 1/2 dimer/DABCO open complexes. The fact that two phases in the tetra-porphyrin titration show an isosbesticity is an indication that, under the dilute conditions used in the UV-visible titration, the concentration of any intermediate colored specie which may be involved during the formation or the destruction of the assembly is negligible. Thus, the overall titration is characterized by two principal equilibria in the separated ligand concentrations, which presumably correspond to three spectroscopically active species. According to the previous results obtained in the monomer and the dimer titrations, we assumed that the sharp isosbestic

point in the first phase of the tetramer titration supports the formation of chelated complex with the overall binding constant K_{12}. In line with that, an addition of incremental amounts of DABCO in the last part of the titration supports the destruction of chelated complex and the formation of open complex with corresponding stoichiometric constant K_{14}. All these proposed equilibria involved in the binding of DABCO to tetra-porphyrin **31** are presented in Figure 3.12.

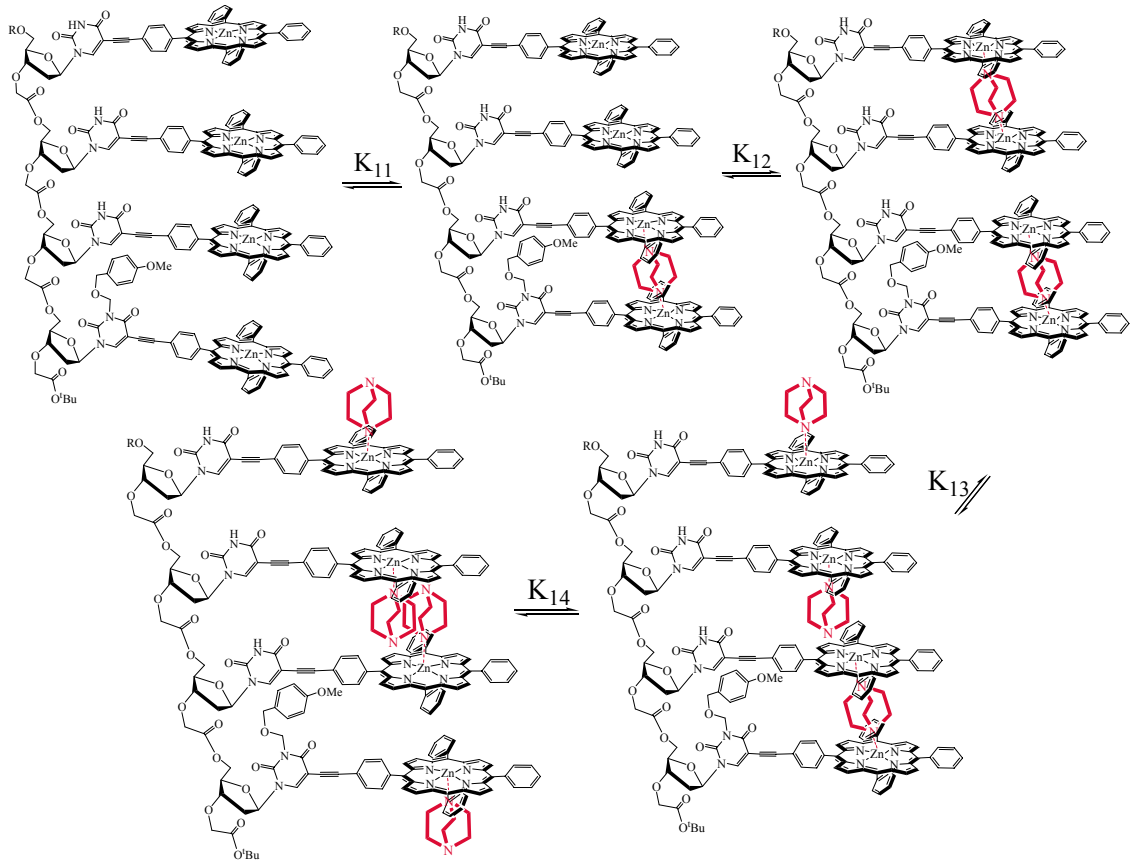

Figure 3.12 *Representation of the proposed equilibria involved in the binding of DABCO to tetra-porphyrin* ***31****.*

To minimize the number of variables in the fitting procedures, we decided to analyse the first part of the tetramer titration characterized by clean isosbestic point, separately. Processing of the titration data by SPECFIT provided the best correlation of experimental and calculated values for the formation of 1/1 complex with corresponding binding constant log K_{11}= 6.42 ± 0.90. It is interesting to note that calculated K_{11} value for 1/1 tetramer/DABCO complex is exactly identical to the binding constant for 1/1 dimer/DABCO complex. These strongly support that the formation of 1/1 tetramer/DABCO chelated complex is a main

process in the first part of the titration, as presented in Figure 3.12. Thereof we could start with far more complicated analysis of the whole series of spectra obtained in the complete titration. Processing of titration data by multivariate global factor analysis by using SPECFIT resulted with the best correlation of experimental and calculated values for the formation of porphyrin-DABCO complexes with the following stoichiometries: 1/1, 1/2, 1/3, 1/4 (Figure 3.12). Such stoichiometry is the logic consequence of the following facts: the first part of the titration with sharp isosbestic point presents the formation of 1/1 tetramer/DABCO complex; after the first part, the titration passed over non-isosbestic phase towards new isosbestic point characterized by the Soret at 432 nm, which is typical for an open complex. Hence, the variables calculated by the fitting of the data are the following binding constants for the complexes presented in Figure 3.12:

$$\text{Tetramer} + \text{DABCO} \rightleftharpoons (\text{Tetramer})_1 \cdot (\text{DABCO})_1 \qquad K_{11} \qquad \log K_{11} = 6.97 \pm 0.14$$

$$(\text{Tetramer})_1 \cdot (\text{DABCO})_1 + \text{DABCO} \rightleftharpoons (\text{Tetramer})_1 \cdot (\text{DABCO})_2 \qquad K_{12} \qquad \log K_{12} = 5.24 \pm 0.33$$

$$(\text{Tetramer})_1 \cdot (\text{DABCO})_2 + \text{DABCO} \rightleftharpoons (\text{Tetramer})_1 \cdot (\text{DABCO})_3 \qquad K_{13} \qquad \log K_{13} = 3.64 \pm 0.42$$

$$(\text{Tetramer})_1 \cdot (\text{DABCO})_3 + \text{DABCO} \rightleftharpoons (\text{Tetramer})_1 \cdot (\text{DABCO})_4 \qquad K_{14} \qquad \log K_{14} = 2.39 \pm 0.47$$

The binding constant of the 1/1 tetramer/DABCO complex is in excellent agreement with the constant of the 1/1 dimer/DABCO complex. These complexes are relating to intramolecular interactions between two porphyrins, which are induced by two binding sites of DABCO. The calculated K_{12} for the 1/2 tetramer/DABCO complex is somewhat lower then K_{11} obtained for the 1/1 dimer/DABCO chelated complex, but significantly higher than K_{12} obtained for the 1/2 dimer/DABCO open complex. This strongly suggests formation of bis-chelated 1/2 tetramer/DABCO complex, in which two bis-porphyrins are involved in binding with DABCO. Small differences of experimental values are presumably diagnostic for preorganization of the porphyrins in the conformationally more restricted tetra-porphyrin **31**. Continuation of DABCO addition leads to the formation of the 1/3 complex. The third DABCO molecule could not be bound between the two porphyrins in the middle, neither to any of two bis-porphyrins involved in sandwich complexes. Accordingly, this phase of the titration is characterized with the destruction of the one chelated complex to allow binding of DABCO from the outer side of the array. The binding constant obtained for the 1/3 tetramer/DABCO complex is in excellent agreement with the constant for the 1/2 dimer/DABCO open complex. In the last phase of the titration the second chelated complex

was separated by binding of the fourth DABCO molecule, hence, the fully open complex of the tetra-porphyrinic array was formed. The binding constant calculated for this complex is one order of magnitude smaller from the previous K_{13}.

The overall titration is characterized by two principal equilibria, one concerning formation and the other destruction of the bis-chelated complex 1/2, in separated ligand concentrations, namely 10^{-3} M and 10^{-1} M. This difference in the ligand concentration range is consistent with the calculated binding constants. An excellent fit of the titration data and the proposed binding models (Figure 3.12) is presented graphically in Figure 3.13.

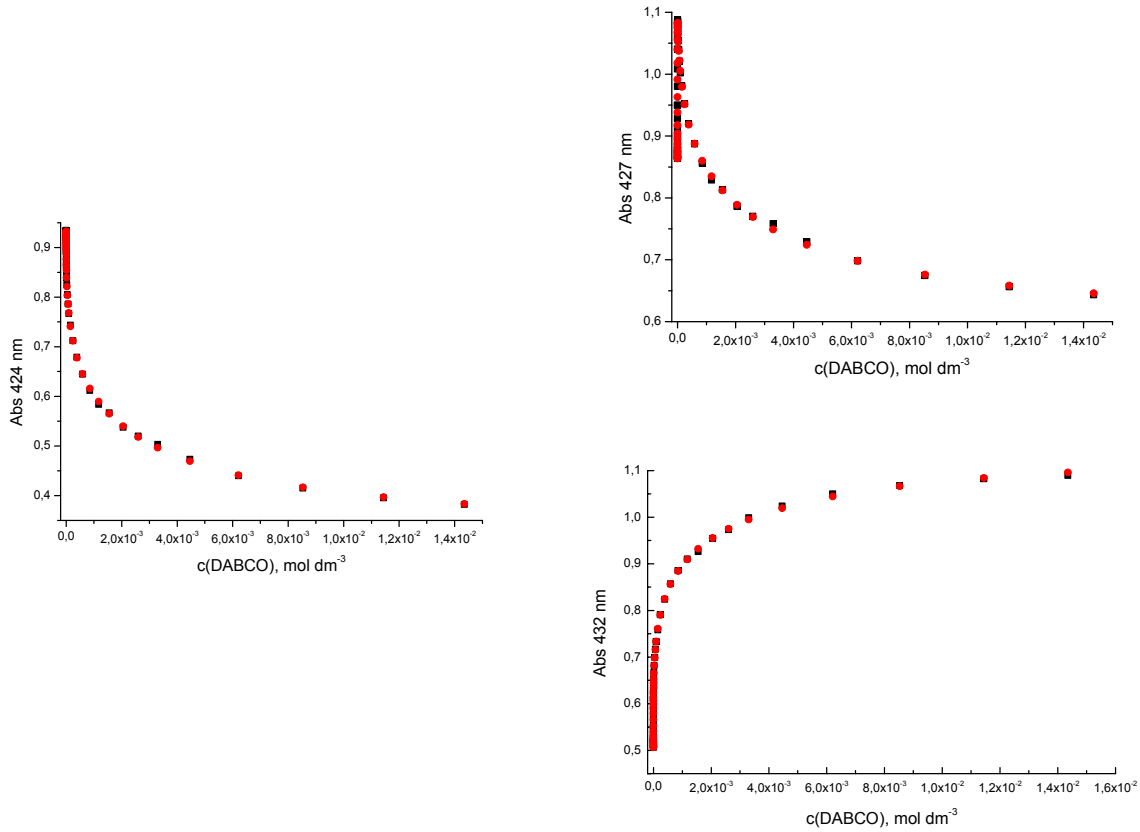

Figure 3.13 *UV-visible titration data (change in absorbance at three wavelengths, 424, 427 and 432 nm) for the binding of tetra-porphyrin* ***31*** *with DABCO, fitted to the calculated curves for the equilibria in Figure 3.12.*

3.3. CONCLUSION.

We have studied the formation of molecular assemblies of the simple zinc porphyrin **13**, bis-porphyrinic tweezer **30** and tetra-porphyrin **31** with the rigid, bidentate ligand DABCO by using UV-visible absorption titration. The binding constants of all assemblies were calculated by using SPECFIT, a multivariate global factor analysis of the whole series of spectra, and the results are summarized in Table 3.2.

	log K_{11}	**log K_{12}**	**log K_{13}**	**log K_{14}**
Simple porphyrin **13**	5.27 ± 0.01			
Bis-porphyrin **30**	6.65 ± 0.08	3.21 ± 0.10		
Tetra-porphyrin **31**	6.97 ± 0.14	5.24 ± 0.33	3.64 ± 0.42	2.39 ± 0.47

Table 3.2 *Binding constants for the complexes formed between monomer zinc porphyrin* ***13****, dimer* ***30*** *or tetramer* ***31*** *and DABCO.*

We were able to characterize all assemblies in terms of stability constants of all logically possible stoichiometric binding models. The spectral changes in titrations at micromolar concentrations together with the quality of correlations between experimental and calculated values for all possible combinations of stoichiometric binding models allowed us to distinguish the operative binding mode for each zinc porphyrin array. The values of all stoichiometric binding constants (Table 3.2) show that chelated complexes are two times more stable than corresponding open complexes formed upon addition of DABCO. Moreover, to highlight the promptness of binding, the following Figure 3.14 shows the coordination shift data of the Soret absorption in titrations of **13**, **30** and **31** until addition of 8 equivalents of DABCO per porphyrin.

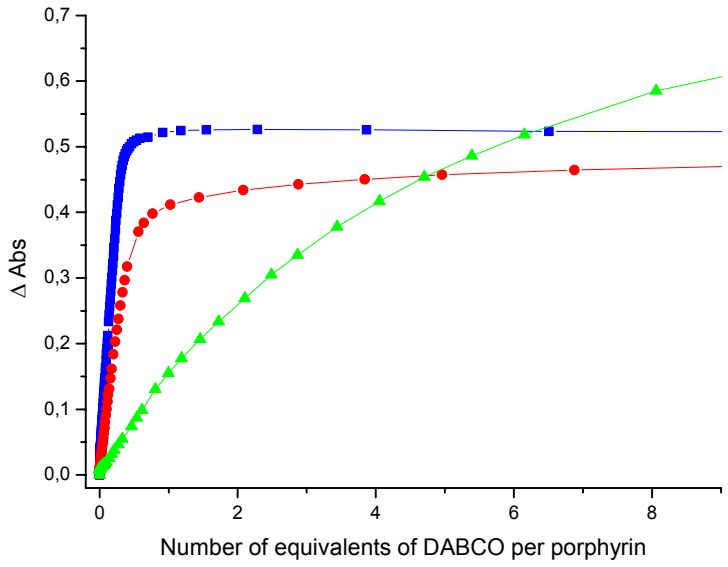

Figure 3.14 *Titration curves for titrations of the simple zinc porphyrin* ***13*** *(green), bis-porphyrinic tweezer* ***30*** *(red) and tetr-porphyrin* ***31*** *(blue) with DABCO in CH_2Cl_2, following the changes in Soret peak absorbance.*

The maximum difference in absorbance is reached at the point where formation of the complex is completed. The titration curve of the simple zinc porphyrin is reaching the straight line at addition of around 100 equivalents of DABCO. The profile of the titration curves for the bis-porphyrin and the tetra-porphyrin is relatively similar. However, the corresponding 1/1 chelated complexes form with addition of around four and two equivalents of DABCO, respectively. An appropriate justification of these observations is that straight line of slope for the tetra-porphyrin is reached earlier than for the bis-porphyrin. That is to say, preorganization increases with the number of uridine-porphyrin units. On the other hand, destruction of the 1/1 dimer/DABCO chelated complex started with addition of 600 equivalent of DABCO, and destruction the 1/2 tetramer/DABCO bis-chelated complex with 1300 equivalents of DABCO. These results indicate that the overall binding constant for the 1/2 tetramer/DABCO bis-chelated complex is two times higher than for the 1/1 dimer/DABCO chelated complex, what is in agreement with calculated values presented in Table 3.2.

It was anticipated that the formation of supramolecular assemblies of zinc porphyrin arrays favours conformations in which neighbouring porphyrin macrocycles are coplanar, and thus affects an increase of interporphyrin electronic interactions. The observed changes in UV-visible spectra accompanying the formation and the destruction of chelated complexes

with addition of DABCO demonstrate that there is indeed increased electronic overlap in obtained assemblies.

4

SELF-ASSEMBLING PROCESSES BETWEEN URIDINE-PORPHYRIN CONJUGATES AND PORPHYRIN-MODIFIED TRIAZINES

Biomolecules represent one of the most fascinating areas of supramolecular architectures, particularly the self-assembly of two single-stranded oligonucleotides into a double stranded helix driven by many intermolecular and intramolecular forces, Figure 4.1.

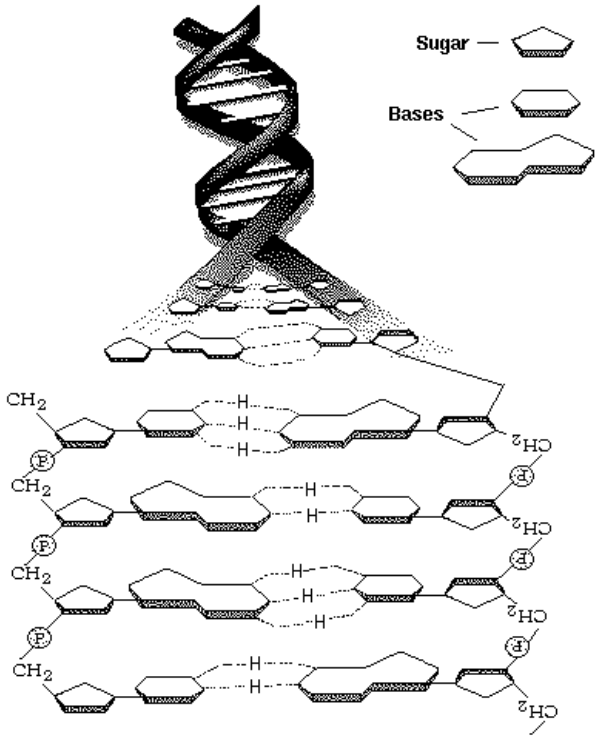

Figure 4.1 *A view inside DNA molecule.*

The recognition between the two single stranded oligonucleotides includes aromatic π-stacking interactions, hydrophobic forces, van der Waals forces, and hydrogen bonding interactions.[215] Among these, the self-complementary Watson-Crick hydrogen bonding

interactions[216] that dictate specific base-pairing are arguably the most crucial for establishing the fidelity required for efficient storage, replication and transcription of genetic information. From the base-pairing patterns elucidated by Watson and Crick two different base-pairs are available, Figure 4.2. The adenine-thymine/uracil (AT or AU) couple (K_a ~ 10^2 M^{-1} in chloroform)[217,218] is weaker than the guanine-cytosine (GC) counterpart (K_a ~ 10^3-10^5 M^{-1} in chloroform).[219-221]

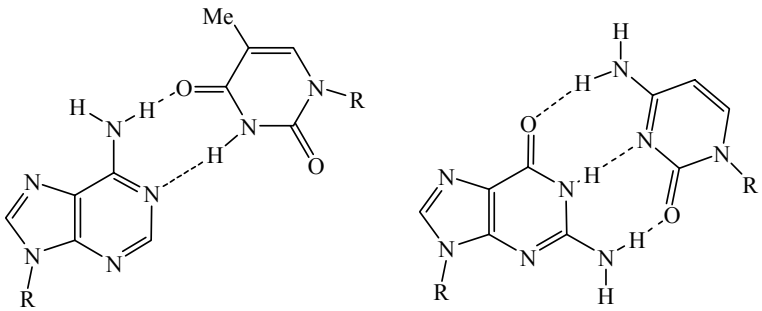

Watson-Crick (AT) Watson-Crick (GC)

Figure 4.2 *Canonical Watson-Crick base-pairing modes.*

The complementary hydrogen bonding concept embodied in DNA inspired preparation of various synthetic superstructures using nucleic acid bases ("nucleobases").[222-229] In this context, the preparation of synthetic receptors that specifically bind to various nucleobases is still a goal for the future. An unifying feature of such receptors is to complement the chemical characteristics of the target nucleobases. Hence, the contribution of multiple recognition capabilities from both complementary molecules is desired in terms of their propensity to self-assemble and stabilize distinct supramolecular structures. However, besides the other interactions, such as π-stacking and electrostatic interactions, hydrogen bonding has been by far the most popular action force in designing a receptor molecule, because of its strength, directionality, and specificity. To this end, the prevalent strategy in preparation of receptors is to make use of natural base pairing model, that is, to place multiple hydrogen bonding moiety in the receptor. This problem inspired a number of research group to prepare various structures that can both recognize specific counterpart and act as an artificial photosynthetic reactor. Some of these systems, produced as the result of this effort, are shown in Figure 4.3.

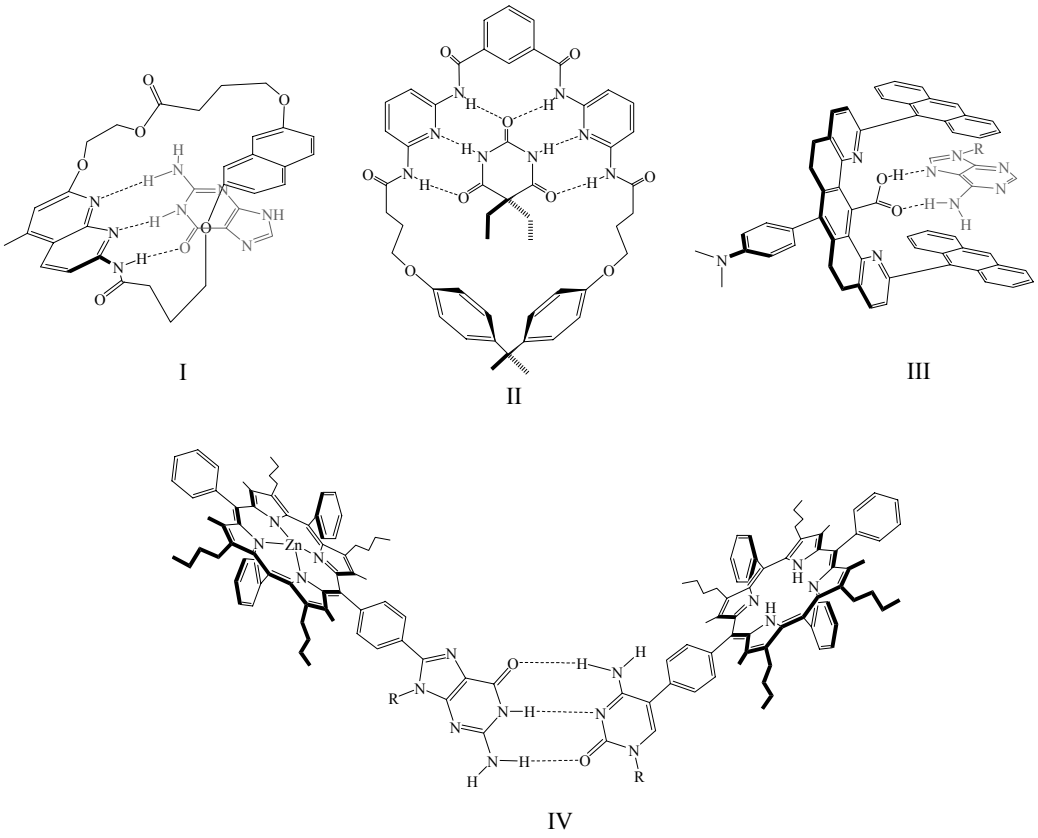

Figure 4.3 *Some molecular receptors assembled through various hydrogen-bonding motifs. Receptors I and II, III, and IV were prepared by the research groups of Hamilton,*[230,231] *Zimmerman,*[232] *and Sessler,*[233] *respectively.*

Macrocyclic receptor I, reported by Hamilton, contains napthyridine binding unit that is complement to guanine. This system also contains a naphthalene linker that allows π-stacking interactions with the targeted nucleobase.[230] In accord with its design, this receptor was found to bind guanine (K_a= 5.3 x 10^2 M^{-1} in chloroform). From the same group, it is worth to mention multichromophore assembly II based on a barbiturate recognition motif and two 2,6-diamidopyridine units reported in 1990 (K_a= 1.4 x 10^6 M^{-1} in chloroform).[231] Using a similar strategy, Zimmerman and coll. prepared molecular tweezer III that binds to adenine through sandwich-like π-stacking and hydrogen bonding (K_a= 2.5 x 10^4 M^{-1} in chloroform).[232] In order to mimic light-harvesting antenna units of natural systems, Sessler et al. prepared GC couple IV that brings free-base and zinc porphyrins within close proximity.[233]

Our contribution into this fascinating branch of supramolecular chemistry comes from the desire to construct novel uracil base receptors endowed with specific recognition abilities. In order to enclose accessible three-point hydrogen-bonding sequence of the uracil base in the

recognition process, as a template in the construction of the artificial receptor we employed cyanuric chloride. Cyanuric chloride is an important bridge molecule in the synthesis of variously functionalized triazine, due to its three chlorine atoms that can be substituted sequentially by different nucleophiles. The triazine skeleton has shown to be a powerful tool in the formation of stable supramolecular structures due to specific recognition capabilities with multiple electronegative nitrogen atoms.[234-238] The stepwise substitution of cyanuric chloride by using different amines, including the porphyrin-amine, afforded mono- and bis-porphyrinic triazine systems equipped with various hydrogen bonding patterns. The uracil base employed in the formation of our supramolecular systems is the nucleobase of our uridine derivatives bearing porphyrins.

4.1. SYNTHESIS AND CHARACTERIZATION OF THE MONO- AND BIS-PORPHYRINIC TRIAZINE SYSTEMS.

The synthesis of the porphyrin-modified triazines was based on two essential building blocks: cyanuric chloride, which provides a scaffold, and the porphyrin-amine. The employed strategy allows one-pot functionalization of cyanuric chloride and its combinatorial construction, due to unequal susceptibility of three chlorine atoms on substitution.[239,240] The stepwise substitution of chlorines pursues at different temperatures and, therefore, provides possibility to apply three different amines. In our synthesis of the triazine derivatives two amines were employed, porphyrin-amine **36** and piperidine. The simultaneous presence of two amines in the reaction mixture over a range of temperatures resulted with two triazine derivatives as the reaction products. The corresponding porphyrin-amine **36** was prepared by convergent synthesis of porphyrin-phenol **34** and *N*-Boc-3-bromo-propanamine **33**.

4.1.1. Preparation of *N*-Boc-3-bromo-propanamine 33.

The desired compound **33** was prepared in two steps starting from 3-amino-propan-1-ol by the synthetic methods presented in Figure 4.4.

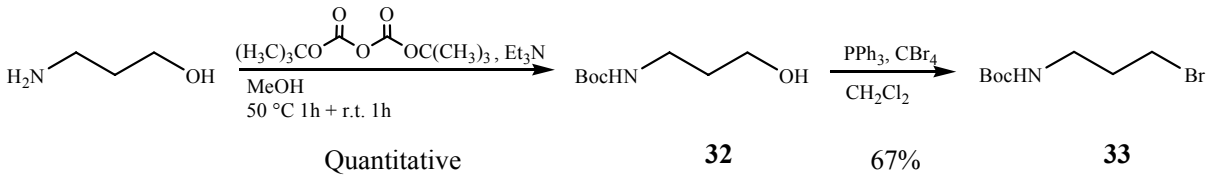

Figure 4.4 *Synthetic path employed in the preparation of N-Boc-3-bromo-propanamine **31**.*

The first step in the synthesis comprised protection of the terminal amine with Boc group (*tert*-butyloxycarbonyl) in the presence of the corresponding anhydride and triethylamine as a base.[241] The Boc group was appropriate protection because it is easily removed under acidic conditions, and in the same time stable towards most nucleophiles and bases. The desired product **32** in the form of the colorless oil was obtained in the quantitative yield.

The next step included activation of position-1 to substitution by conversion of the alcohol **32** to the corresponding bromide **33**. The conversion to bromide was performed with triphenylphosphine (PPh_3) and tetrabromomethane (CBr_4) in dichloromethane stabilized with amylene under mild conditions.[242,243] After stirring over-night at room temperature the product was isolated by chromatography on silica-gel in 67% yield. The product was characterized by ^1H NMR spectroscopy.

4.1.2. Preparation of porphyrin-phenol 34.

The porphyrin bearing three di-*tert*-butylphenyl groups and one phenol at the *meso* positions was prepared following the procedure developed by J. S. Lindsey.[89-95] In terms of targeted A_3B porphyrin a mixed aldehyde condensation was prompted harnessing 3,5-di-*tert*-butyl-benzaldehyde (**10**) and 4-hydroxybenzaldehyde. To obtain desired arrangement of functional groups around the porphyrin ring, the condensation involved 3 equivalents of benzaldehyde **10**, 1 equivalent of 4-hydroxybenzaldehyde and 4 equivalents of pyrrole, Figure 4.5.

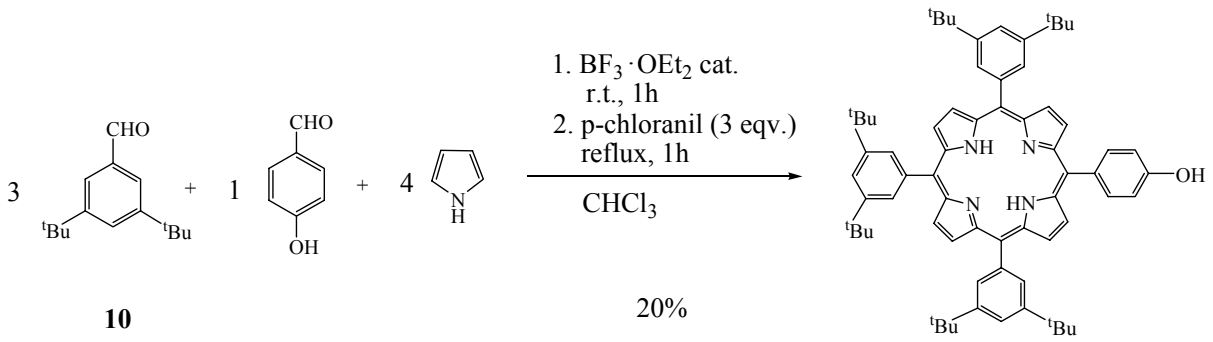

10 **34**

Figure 4.5 *Synthesis of porphyrin-phenol **34** by mixed aldehyde condensation under reaction conditions developed by J. S. Lindsey.*

Chloroform was charged with benzaldehydes, pyrrole and boron trifluoride etherate under argon atmosphere. The concentration of the benzaldehydes and pyrrole were equimolar (10^{-2} M), and the concentration of the acid catalyst, boron trifluoride etherate ($BF_3 \cdot OEt_2$), 3.3 x 10^{-3} M. After one hour at room temperature the reaction mixture was charged with an

oxidant 2,3,5,6-tetrachlorobenzoquinone (*p*-chloranil) an allowed to stir at reflux for one hour. Neutralization of the acid catalyst with triethylamine was performed prior to evaporation of the solvent. The product isolation comprised a passage of the concentrated crude reaction mixture over chromatography columns. The repetitive column chromatography on silica-gel afforded porphyrin **34** in 20% yield. An appropriate justification of the porphyrin-phenol was provided from ^{1}H NMR spectroscopy.

4.1.3. Synthesis of porphyrin-amine 36.

The porphyrin-amine **36** was synthesized by the procedure outlined in Figure 4.6. The synthesis began by elongation of porphyrin-phenol **34** using aliphatic constituent with protected amine (**33**). Once the aliphatic moiety was appended to the porphyrin macrocycle, the protecting group from the primary amine was cleaved, and the porphyrin-amine was generated.

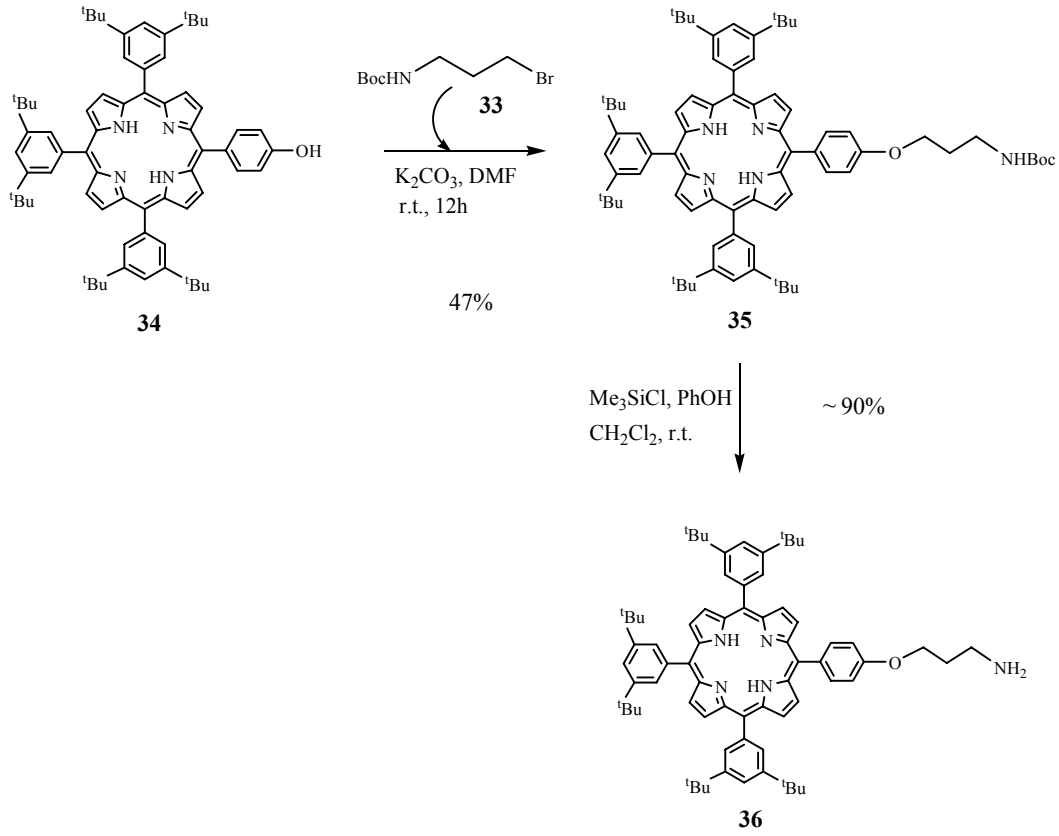

Figure 4.6 *Synthesis of porphyrin-amine* ***36****.*

O-Alkylation of the porphyrin-phenol was performed under mild basic conditions. Isolation of the product imposed neutralization and purification by column chromatography on silica-gel affording compound **35** in 47% yield.

The last step towards porphyrin-amine **36** included removal of the Boc group. The hydrolysis of Boc group is usually performed under anhydrous acidic conditions. Herein, the Boc group was removed under mild conditions using HCl generated *in situ* by the reaction of trimethylsilyl chloride (TMSCl) and phenol, Figure 4.7.[244] Initially generated phenolic TMSCl weakens the O-H bond of the phenol, and in this respect acidic proton triggers off the cleavage of Boc. That has been achieved by separately prepared 1 M solution of TMSCl and phenol in dichloromethane.

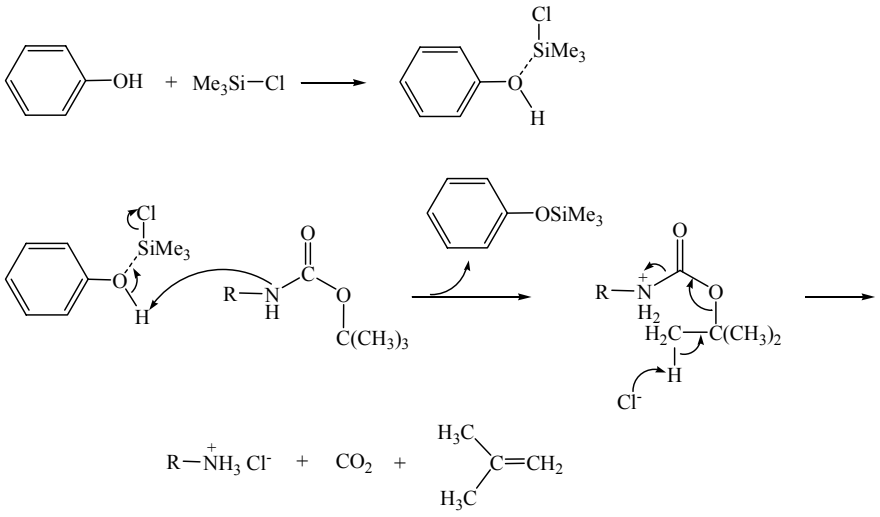

Figure 4.7 *Mechanism of deprotection of the Boc group.*

The reaction mixture was quenched with triethylamine after 6 hours of stirring at room temperature. The crude product was purified over silica-gel column affording porphyrin-amine **36** in high yield.

The product was characterized by ^{1}H NMR spectroscopy, Figure 4.8. The spectrum reflects the characteristic multiple resonances of the porphyrinic ring together with the well-resolved signals of the aliphatic branch. The β-pyrrolic protons appear as one singlet at 9.01 ppm and one AB system at 9.00 ppm. The protons of the aliphatic branch appended to putative *meso*-phenol appear as two triplets and one quintet-triplet for H_b in the following

order: H_a at 4.43 ppm with coupling constant ^3J= 5.8 Hz, H_c at 3.31 ppm with coupling constant ^3J= 6.7 Hz and H_b at 2.34 ppm with coupling constant ^3J= 6.2 Hz.

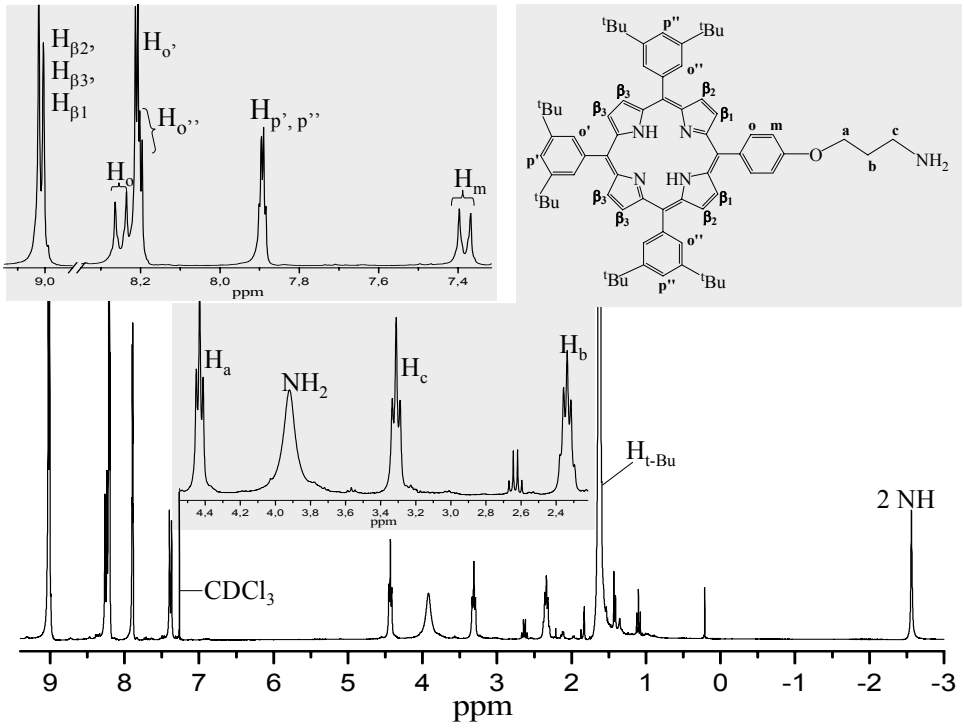

Figure 4.8 *^1H NMR spectrum ($CDCl_3$, 300 MHz) of porphyrin-amine **36**.*

4.1.4. Preparation of the mono- and bis-porphyrinic triazine derivatives.

Stepwise amination of cyanuric chloride with porphyrine-amine **36** and piperidine afforded simple triazine-porphyrin (**39**) and triazine bridged porphyrin dyad (**40**) in a one-pot protocol. Although our initial attention was devoted to the preparation of triazine-bridged porphyrin dyad, the formation of the simple triazine-porphyrin was advisable. The reaction course toward formation of both triazine derivatives by the stepwise addition of the amine is presented in Figure 4.9. The progress of the overall reaction was readily monitored by TLC due to noticeable difference in polarity between the starting porphyrin-amine, intermediate monochlorotriazine, and the final amine products.

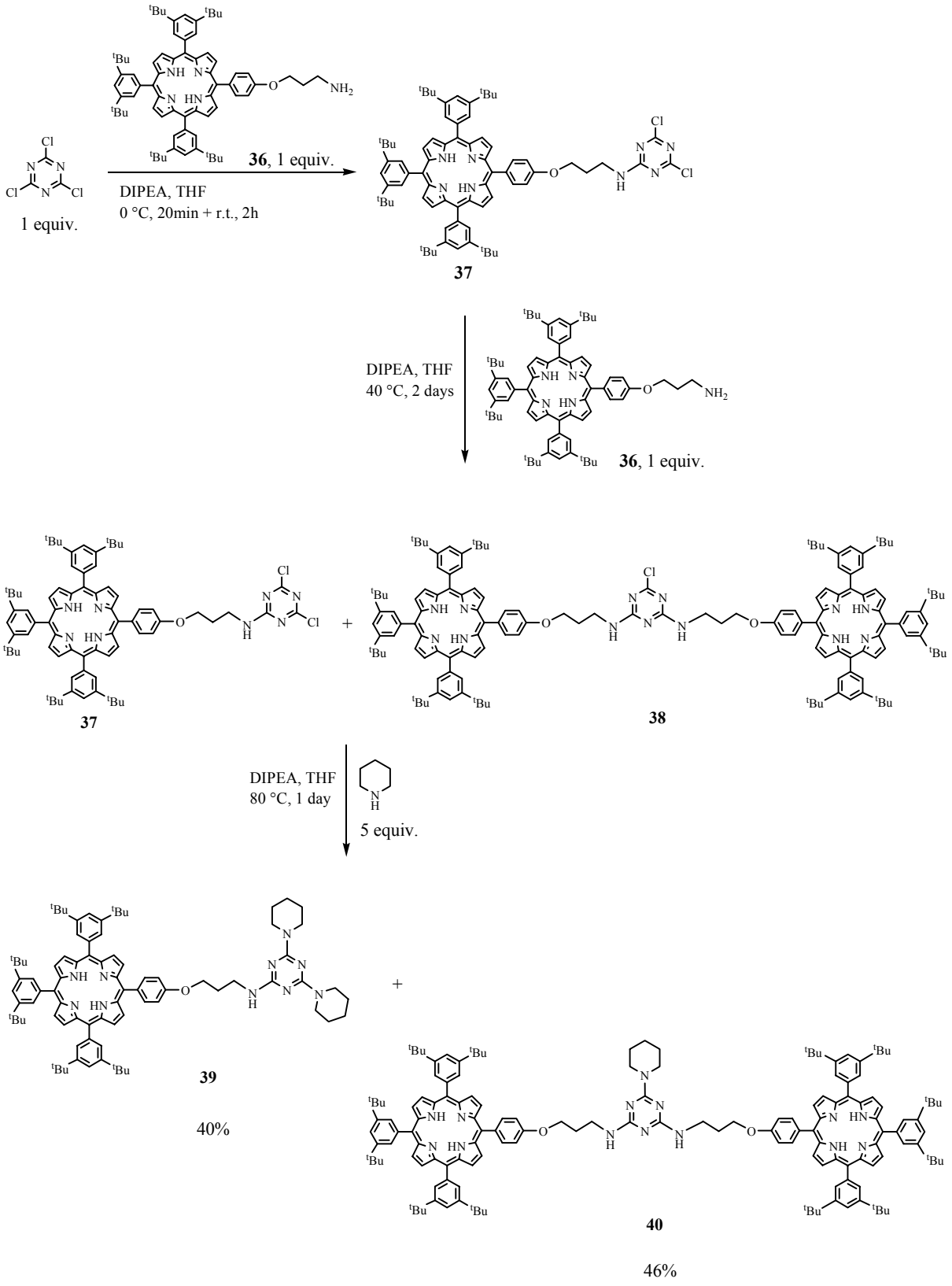

Figure 4.9 *Synthesis of simple triazine-porphyrin* ***39*** *and triazine-bridged porphyrin dyad* ***40****.*

The reaction was started with 1 equivalent of cyanuric chloride, 1 equivalent of porphyrin-amine **36** and 1.2 equivalents of diisopropylethylamine (DIPEA) in THF at 0 °C. The time course of the reaction was examined by TLC analysis (dichloromethane/methanol (8.5:1.5)) following the disappearance of the porphyrin-amine. After 20 minutes at 0 °C and 2 hours at room temperature the formation of the monoadduct **37** was found to be complete. Since monoadduct **37** is rather reactive the second equivalent of the porphyrin-amine together with DIPEA (2.4 equivalents in two portions) was added aiming to the formation of the dyad **40**. Monitoring the reaction by TLC (petroleum ether/ethyl acetate (7.5:2.5)) indicated appearance of compound **38**, and the presence of unreacted monoadduct **37**. Although, presumably the addition of supplementary equivalent of the porphyrin-amine would lead uniquely toward dyad **40**, in our case it was preferred to obtain as well in this one-pot synthesis simple triazine-porphyrin **39**. Finally, the complete substitution of chlorine atoms was performed by using an excess of piperidine in the presence of DIPEA. Aqueous workup followed by column chromatography on silica-gel afforded mono-porphyrinic triazine **39** and bis-porphyrinic triazine **40** in 40% and 46% yield, respectively. Both products were characterized by ^{1}H NMR and UV-visible spectroscopy, and mass spectrometry. Positive ion DCI/NH_3 mass spectra of **39** showed the mass peak at 1269.9, calculated: 1269.8, while MALDI-TOF analysis of **40** provided the mass peak at 2209.4, calculated: 2209.1.

The structural difference between the two triazine derivatives is nicely reflected in their ^{1}H NMR spectra, Figure 4.10. The spectrum of **40** displays one set of signals due to symmetric triazine skeleton. All resonances of the porphyrin dyad are slightly deshilded relative to the monoadduct, because of the second porphyrinic ring. The splitting pattern of the porphyrinic protons at both derivatives is consistent with that observed for porphyrin-amine **36**. The H_a protons of the aliphatic branches appear as triplets, H_b protons as quintet-triplet, and H_c overlap with H_x of piperidines. From juxtaposition of the spectra it is evident that the number of piperidine units in **39** and **40** is not equal. Moreover, an overall integration of both spectra clearly reveals porphyrin/piperidine ratios, 1/2 and 2/1 for **39** and **40** respectively.

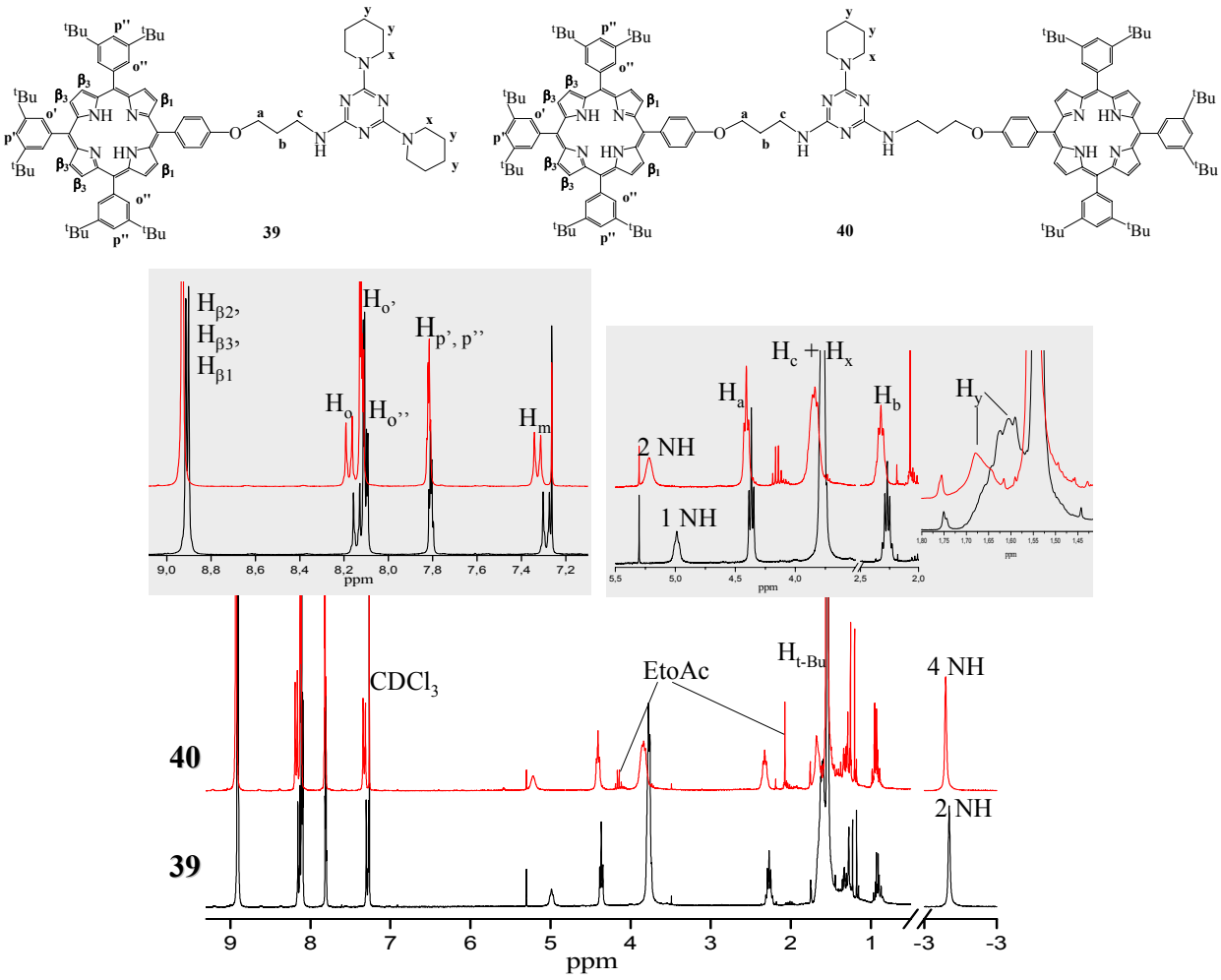

Figure 4.10 *^{1}H NMR spectra ($CDCl_3$, 300 MHz) of simple triazine-porphyrin **39** and triazine-bridged porphyrin dyad **40**.*

The UV-visible spectra of **39** and **40** were recorded in dichloromethane at room temperature. Their adherence to Lambert-Beer's law was verified by quantitative analysis, which implied an absorbance recording of the solutions after successive addition of small aliquots from the stock solutions of well-defined concentration. If probed solutions with certain concentration adhere to the law, the molar absorption coefficient can be calculated from the slope of a linear dependence of the absorption on concentration, at each wavelength. In this manner, the molar absorption coefficients were calculated for the Soret band and for each absorption maxima of the Q-bands. The examined concentrations of the porphyrin solution were adjusted to absorbance which recommendatory should cover the range between 0.5 and 1.2., and, in principle, this corresponds to concentration of around 10^{-6} M for the Soret band, and around 10^{-5} M if the absorption of the Q-bands is measured. Therefore, the

calculated values of molar extinction coefficients of **39** and **40** are presented in Table 4.1. In addition, in Figure 4.11 are presented the spectra of both **37** and **38**, obtained at exact concentration.

Simple triazine-porphyrin **39**		Triazine-bridged porphyrin dyad **40**	
λ_{max} (nm)	ε (M^{-1} cm^{-1})	λ_{max} (nm)	ε (M^{-1} cm^{-1})
421	599 000	421	868 900
518	21 000	518	36 600
554	12 800	554	22 400
593	6 300	593	11 100
648	6 700	648	11 900

Table 4.1 *Electronic absorption maxima and corresponding molar extinction coefficients calculated from the slope of linear dependence of the absorption on concentration.*

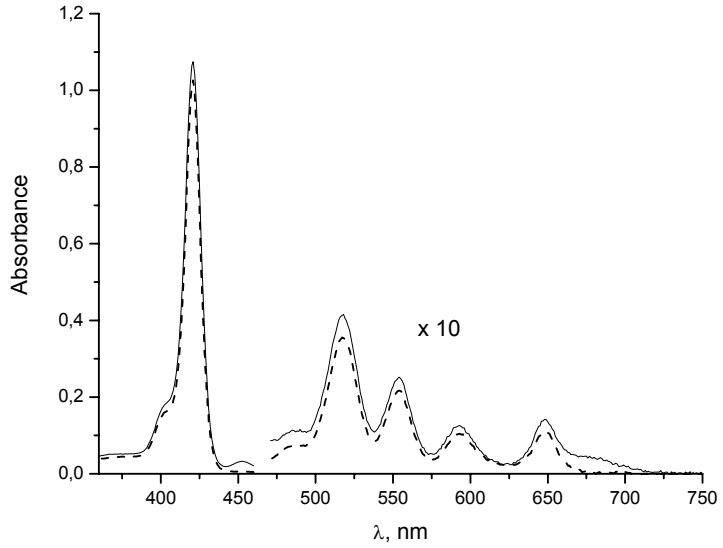

Figure 4.11 *UV-visible absorption spectra of **39** (solid line) at concentration of 1.74 x 10^{-6} M and **40** (dashed line) at concentration of 1.26 x 10^{-6} M, in dichloromethane at 298 K.*

The shape of both spectra is similar to one another showing the Soret band at 421 nm and four Q-bands characteristic of the free-base porphyrins at 518, 554, 593, and 648 nm.

4.2. COMPLEXATION OF THE URIDINE-PORPHYRIN CONJUGATE (15) WITH THE TRIAZINE-PORPHYRIN DERIVATIVES.

Our studies were focused on recognition of the three-point hydrogen-bonding site at the uracil base of the uridine-porphyrin conjugates by synthesized triazin-based derivatives **39** and **40**, as well as on the influence of the porphyrins on this intermolecular recognition. We anticipated that juxtaposition of corresponding uridine and triaminotriazine in principle can lead to their mutual recognition through complementary triply hydrogen-bonding mode (ADA-DAD). The studies performed to calculate the association constant for the complex of 1-cyclohexyluracil (ADA binding motif) with 2,6-bis(acetylamino)pyridine endowed with DAD binding motif revealed weak association with the value of around 10^2 M^{-1} in chloroform.[219] On the other hand, for assemblies such as cytosine-guanine (AAD · DDA), reported constants range between 10^4 and 10^5 M^{-1}.[245] Such difference in stability was explained by Jorgensen and coll. on the basis of the arrangement of hydrogen bond donor and acceptor in two molecules forming a complex, more then 20 years ago.[220,245] They showed that stabilization arises from electrostatic attraction between positively and negatively polarized atoms in adjacent H-bonds, whereas destabilization is likewise the result of electrostatic repulsion between two positively or negatively polarized atoms, Figure 4.12. Thus, formation of the C · G assembly involves two attractive and two repulsive secondary interactions, whereas in the U · DAP all the secondary interactions are repulsive.

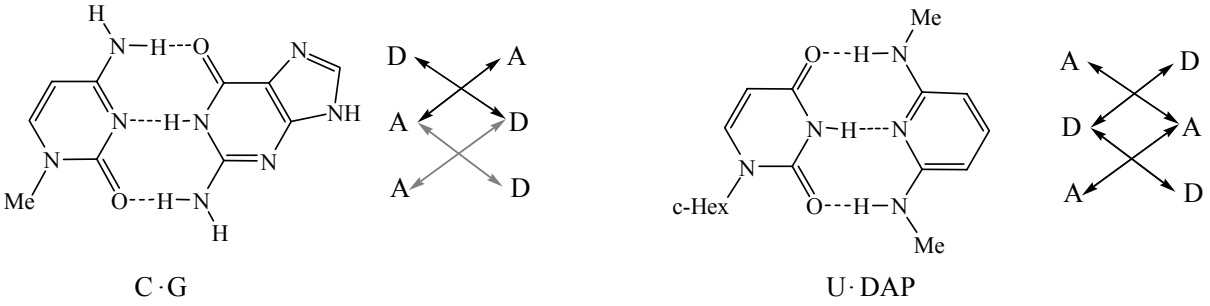

Figure 4.12 *Attractive (grey arrows) and repulsive (black arrows) secondary interactions involved in the 1-methylcytosine · 9-methylguanine (C · G) assembly and in the 1-cyclohexyluracil with 2,6-bis(acetylamino)pyridine (U · DAP) assembly.*

Zimmerman and co-workers studied the difference in thermodynamic stability of a series of dimeric complexes with ADA · DAD, AAD · DDA, and AAA· DDD arrays with 0, 2, and 4 favourable secondary interactions, respectively, in order to test Jorgensen's hypothesis on secondary interactions.[246-248] The stability constants found to be in order of values 10^2, 10^3-10^4, and 10^5 M^{-1} in chloroform, are fully in line with Jorgensen's model. The same behaviour was observed in two hydrogen-bonded complexes, where alternating hydrogen-bonded systems (AD · DA) are destabilized and, on the other hand, systems based on homo-combinations (AA · DD) stabilized by secondary interactions.[248,249]

In the formation of our supramolecular systems from uridine-porphyrin conjugates and porphyrin-modified triazines, the simultaneous operation of hydrogen bonding recognition and π-π interactions was envisaged. It is noteworthy to mention that the choice of solvent is an important factor for the formation of assemblies based on hydrogen bonding. Individual bases do not pair to a large extent in protic solvents due to strong competition for all-important hydrogen-bonding donor and acceptor sites. Thus, for the most part, the complexations of individual nucleobase derived systems are carried out in aprotic organic solvents. We bypassed the general insolubility of nucleobases in these solvents using uridine functionalized with the lipophilic porphyrin. Therefore, the formation of supramolecular assemblies of uridine tethered to porphyrin with porphyrinic trazine systems have been studied in non-polar aprotic solvents. Complexation studies were performed by ^{1}H NMR spectroscopy in chloroform-*d* and by UV-visible spectroscopy in dichloromethane.

4.2.1. Complexation of the uridine-porphyrin conjugate (15) with the triazine-bridged porphyrin dyad (40).

In principle, due to the various hydrogen bonding sites in triazine derivative **40**, the structures of the assemblies with uridine derivative **15** that presumably may be obtained are shown in Figure 4.13. While triazine derivative **40** has a binding motif DAD or dyad DA, uridine **15** has a complementary motif ADA of AD.

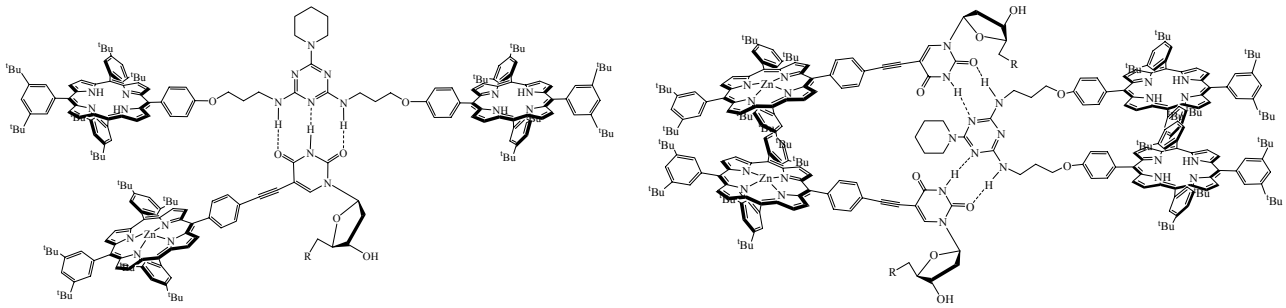

Figure 4.13 *The complexes that may be obtained in recognition process between **15** and **40**.*

Before triazine receptor **40** and uridine-porphyrin conjugate **15** were employed in complexation studies, an examination of concentration-dependent changes was performed by ^{1}H NMR spectroscopy in chloroform-*d*. Dilution of the triazine receptor **40** was preformed in concentration range from 13 to 0.86 mM in chloroform-*d*. The revealed concentration-independent chemical shifts indicated that **40** most likely does not form self-assembly in this concentration range. An examination of **15** was performed in concentration range from 20 mM to 0.98 mM. Upon decrease of the concentration the signals of the imide proton moved upfield, until the concentration of around 4 mM was reached, Figure 4.14. Hence, homodimerization of **15** could be neglected up to this concentration.

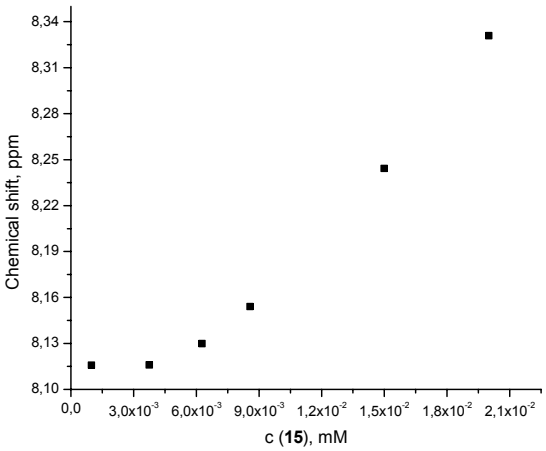

Figure 4.14 *The chemical shift summary obtained by ^{1}H NMR dilution study of* ***15*** *in chloroform-d following the signal of the imide proton.*

Further studies were performed under conditions where self-association of **15** was negligible. The recognition abilities of the receptor **40** were first investigated in solution with the complementary molecule **15** by NMR spectroscopy. A series of solutions were prepared by varying the ratio between **40** and **15**, and keeping the sum of their concentrations constant at 2 mM. The partial ^{1}H NMR spectra of these mixtures, and both compounds in the free form are presented in Figure 4.15. The spectra revealed broader signals for β-pyrrolic protons when the two compounds were mixed. Moreover, it is obvious that broadening and overlapping can be observed when the proportion of **38** is increased, reflecting a dynamic process within the porphyrins upon clearly indicated formation of a supramolecular complex. The characteristic changes were observed for imide proton, which moved slightly downfield from 8.13 ppm in free **15** to 8.19 ppm in the 2/1 mixture of **15** and **40**. In addition, the 1'-proton of the sugar was shifted considerably, from 6.30 to 6.87 ppm. The NH protons of triazine **40** showed up as a splitted pattern, which may be attributed to a differentiation of the two sites induced by conformational changes upon complexation. The NOE experiment was performed aiming to detailed attribution of all dispersed signals in aliphatic region. Unfortunately, no information about intermolecular proximity of the units could be detected with certainty.

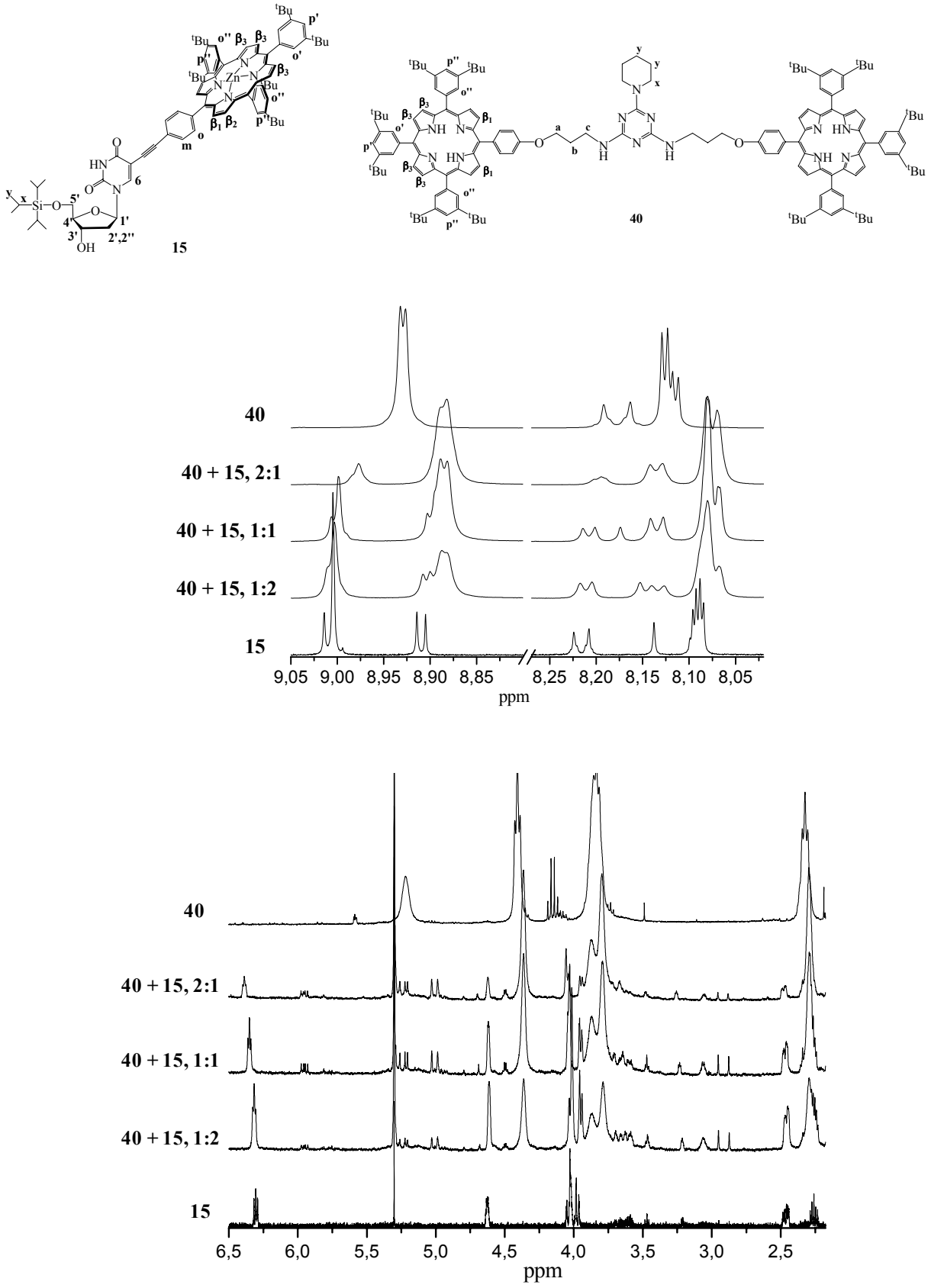

Figure 4.15 *^{1}H NMR spectra of mixtures of **40** and **15** (2 mM) in chloroform-d at 298 K.*

In principal, unlike a notable broadening and coalescence of the porphyrinic signals, the majority of the signals in the spectra are sharp. This was expected as the free-base porphyrins are attached to the triazine by a flexible linker that allows free rotation. This hypothesis is supported by notable broadening and coalescence of the signals observed in the spectra with increased portions of **40** according to **15**. Indeed, a rotational freedom of the porphyrins after complex formation leads to their slow equilibration on the NMR time scale. The same effect can be observed for the H_c and H_b protons of the linker between the triazine ring and the porphyrins. The flexible linkage, to some extent, might allow the porphyrins to adopt a favourable conformation for recognition with **15**. The signals in the aliphatic region of the spectra can be attributed to different orientation of the components involved in a supramolecular complex. Furthermore, it is surprising that even the signals of the sugar stayed sharp, but shifted in the bound state beside the fact that they appear to be far removed from the hydrogen-bonding recognition site. Taken together, these observations indicate that a favorable conformation is obtained in the presence of higher molar amount of **15**, while an opposite case indicates destabilization of a complex.

At this stage, before abstracting the association constant, determination of the stoichiometry of this favourable complex was required. This was readily achieved from NMR data by means of the method of continuous variation, putative Job's plot method, Figure 4.16.[250,251] It involved a series of solutions containing **15** and **40** in various proportions so that complete range of mole ratios was sampled ($0< ([\mathbf{15}]_t/[\mathbf{15}]_t+[\mathbf{40}]_t) <1$), by keeping the total concentration of each solution constant at 2 mM.

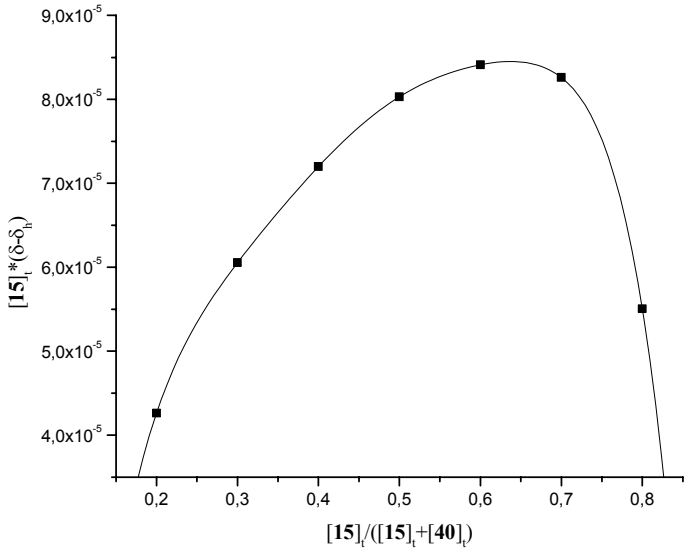

Figure 4.16 *The Job's plot for the association of **15** and **40**.*

The y-coordinate was defined with the property proportional to corresponding complex, namely $[\mathbf{15}]_t \cdot (\delta - \delta_h)$, where $[\mathbf{15}]_t$ is total concentration of the free **15**, δ is observed chemical shift and δ_h is chemical shift of **15** in the free **15**. All combinations displayed the maximum at mole fraction of approximately 0.66. Thus, the stoichiometry for the predominant supramolecular complex of **15** with **40** was established to be 2/1. Instead of the expected triply hydrogen bonded complex with stoichiometry 1/1, we obviously obtained the 2/1 **15**/**40** doubly hydrogen bonded complex (Figure 4.13).

The quantitative assessment of the strength of the proposed **15**/**40** complex with 2/1 stoichiometry was primarily performed by NMR titration method. However, dilute conditions were required for assessing the association constant, and therefore UV-visible absorption was the first choice, because the zinc porphyrins do not absorb in some regions of the spectra where the free-base porphyrins do. In this case, the advantage of low concentrations was the justification of the approximation towards the true thermodynamic equilibrium constant based on activities.

The UV-visible titration was performed by addition of porphyrin-uridine conjugate **15** to the solution of triazine-bridged free-base porphyrin dyad **40**. In this way, the binding constant could be readily determined, because the free-base porphyrin dyad **40** absorbs light in the range between 600 and 700 nm significantly stronger than zinc porphyrin **15**, Figure 4.17.

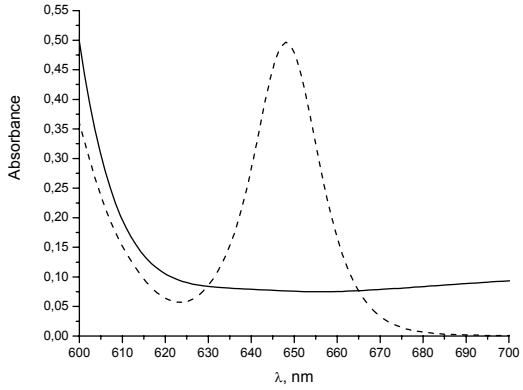

Figure 4.17 *UV-visible spectra of* ***40*** *(dashed line) and* ***15*** *(solid line) measured at the concentration of 4.60 x 10^{-5} M and 4.63 x 10^{-4} M, respectively, in the region where titration was followed.*

The titration was probed in dichloromethane at room temperature by addition of the small aliquots of **15** (c= 8.10 x 10^{-3} M) into the solution of **40**. The concentration of the solution of **40** was determined by peak absorbance of 0.5 for the Q-band at 648 nm. Hence, the Q-band absorption of **40** was measured at the concentration of 4.62 x 10^{-5} M which corresponds to peak absorbance of 0.5 at 648 nm. The titration was carried out by monitoring the spectral changes associated with incremental addition of **15** covering the concentration range of 1.30 x 10^{-5} M to 2.00 x 10^{-3} M, Figure 4.18.

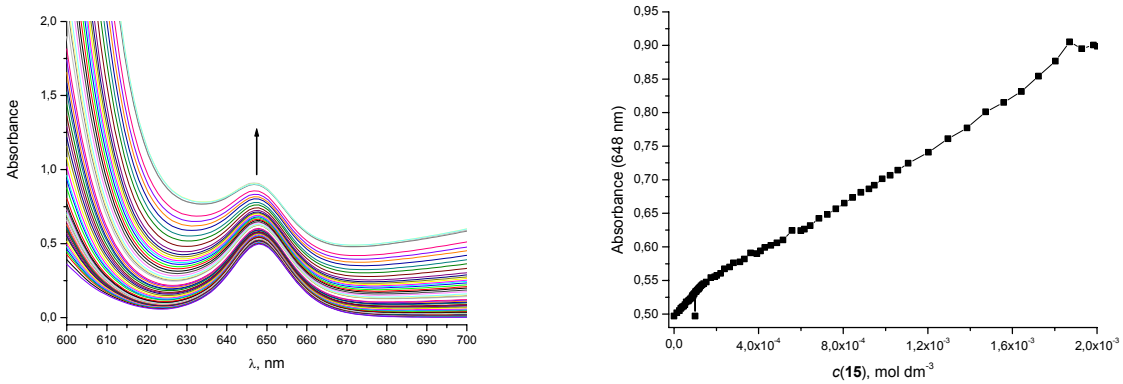

Figure 4.18 *Overlay of the visible spectra recorded by addition of* ***15*** *to dichloromethane solution of* ***40*** *(4.62 x 10^{-5} M). At the right hand side, a plot of absorbance of* ***40*** *as a function of added* ***15*** *at 648 nm.*

A comparison of the obtained spectra indicates small spectroscopic changes upon addition of porphyrin-uridine conjugate **15**. The UV-visible titration data were analysed both by using the values of the absorbance at fixed wavelengths and by simultaneous fitting of the whole series of spectra collected at 1 nm intervals using the software SPECFIT.[203-205]

The factor analysis of the complete titration data by using SPECFIT suggested the presence of four dominant spectroscopically active species. Due to the fact that both **40** and **15** absorb in examined region of the spectra, the co-existence of two different complexes could be expected. However, eigenvalue of one of the complexes is in the same order of magnitude with the line describing one of the free species, while eigenvalue of the second complex is two orders of magnitude lower. Taken together, these results suggested that only one complex is dominant. Further on, in the calculation process of the titration data, the spectra of **40** and **15** were introduced as the fixed data. Processing of the titration data by SPECFIT by the model with 1/1 stoichiometry did not provide any reasonable result. Processing of the titration data by the model with postulated 1/1 and 1/2 stoichiomety for **40**/**15** resulted with the following values:

$\log K_{11} = -0.77 \pm 2.70$

$\log K_{12} = 4.95 \pm 0.11$

The obtained $\log K_{11}$ is far too low to be even estimated in the concentration range of the performed titration experiment. Therefore, it is highly uncertain that 1/1 complex of **40** with **15** exists at these experimental conditions. In addition, calculated UV-visible spectrum of this complex is negative in the range from 675 to 690 nm and calculated ε values are unexpectedly high in comparison to the other species in the solution. Taken together, all these observations strongly testify against the existence of the 1/1 stoichiomery for the **40**/**15** assembly. On the other hand, all the values obtained for the 1/2 stoichiometry strongly support the existence of such complex. Finally, processing of the titration data gave the best correlation of experimental and calculated values for the formation of exclusively 1/2 stoichiometry complex. The 1/2 stoichiometry is in excellent agreement with the results of the Job's plot. The obtained binding constant for 1/2 **40**/**15** complex was $\log K_{12} = 5.85 \pm 0.04$ ($K_{12} = 7.08 \times 10^5$ M^{-2}). The fit of the experimental data to the calculated values for the formation of the 1/2 stoichiometry complex of triazine-bridged porphyrin dyad **40** with uridine-porphyrin conjugate **15** is presented in Figure 4.19.

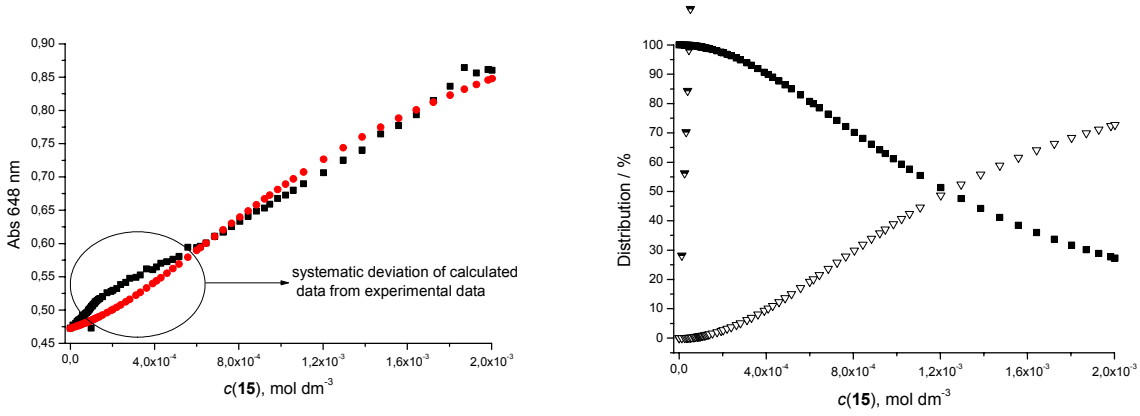

Figure 4.19 *UV-visible titration data, presented as a plot of absorbance at 648 nm, as a function of addition of* ***15*** *(0 to 2 x* 10^{-3} *M) to* ***40****, and fitted to the calculated curves by 1/2 binding model.*

All obtained data support formation of the 1/2 stoichiometry for **40**/**15** complex as the only possible complex between triazine-bridged porphyrin dyad **40** and uridine-porphyrin conjugate **15**. Agreement of the experimental and calculated data delineated above shows systematic deviation in the concentration range from 0 to 6.16 x 10^{-4} M. At the same time, it is clearly visible from the plot of the distribution that this concentration range is below 20% complexation ratio, hence, this deviation is not relevant for evaluation of the association constant. The most probable cause of systematic deviation is the experimental error that appears frequently at such low percentages of the complex formation. To get highest possible accuracy of calculated association constant (log K_{12}) from the available experimental data, the part of the titration data implying the complexation ratio between 20 and 80% were processed separately. That part of the titration corresponds to a concentration range of **15** from 5.16 x 10^{-4} to 2 x 10^{-3} M. In that analysis, all the binding models that could be logically formed within complexation of **40** with **15** (1/1 only; 1/1 and 1/2) were involved simultaneously. Again, the only acceptable result was obtained exclusively for the 1/2 **40**/**15** complex. The obtained value for the association constant is log K_{12}= 5.78 ± 0.06 (K_{12}= 6.03 x 10^5 M^{-2}), and corresponding graph obtained by fitting is presented in Figure 4.20.

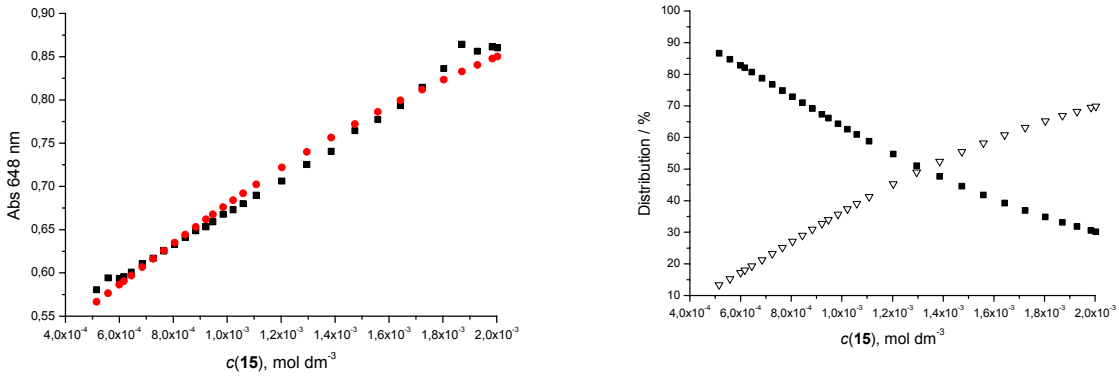

Figure 4.20 *UV-visible titration data, presented as a plot of absorbance at 648 nm, as a function of addition* ***15*** *(5.16 x 10^{-4} to 2 x 10^{-3} M) to* ***40****, and fitted to the calculated curves by 1/2 binding model.*

In principle, the association constant of the common AD/DA complexes predicted by Sartorius and Schneider was found to be about 60 M^{-1} in chloroform.[249] In order to explain the relatively high association constant that was obtained for the **15**/**40** complex, it has to be noted that molecular recognition interactions are equilibria processes affected by secondary forces, and directed toward stabilization of the intermolecular complexes. In this dynamic process preorganization has a key role, leading to the favourable conformation and the stable complex. Thereof, we can suggest the existence of significant contribution of the porphyrins arranged in favourable orientation to stabilization of the supramolecular assembly. We suppose that in this recognition process the two free-base porphyrin arms at the triazine could swing towards zinc porphyrins appended to the uridine, as provided in Figure 4.21.

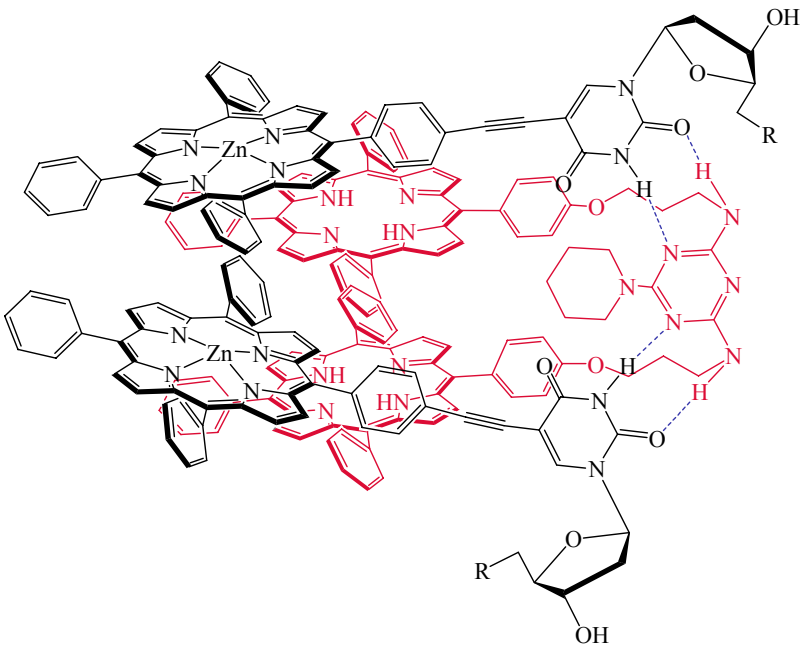

Figure 4.21 *The proposed structure of the supramolecular assembly obtained by the recognition process between uridine-porphyrin conjugate* ***15*** *and triazine-bridged porphyrin dyad* ***40****.*

4.2.2. Complexation of the uridine-porphyrin conjugate (15) with the simple triazine-porphyrin (39).

In order to examine the influence of the absence of one porphyrin appended to triazine ring and loss of one binding site on binding properties, mono-porphyrinic triazine was applied to complexation process with uridine-porphyrin conjugate **15**. The mono-porphyrinic triazine is structural analogue of bis-porphyrinic triazine **40**, in which one porphyrin appended to triazine ring was replaced by a piperidine. For the supramolecular assembly of **39** and **15** we could expect the structure presented in Figure 4.22.

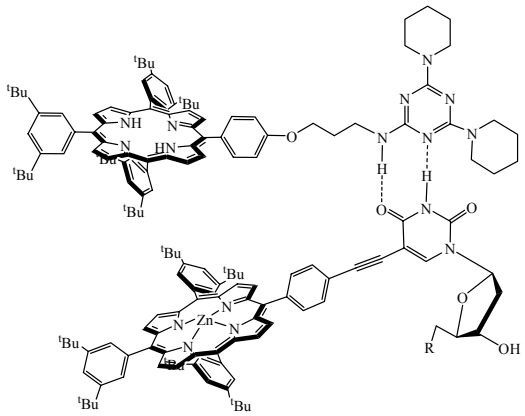

Figure 4.22 *The proposed structure of the supramolecular complex of **15** with **39**.*

Dilution studies of receptor **39** monitored by proton NMR in chloroform-*d* revealed concentration independent chemical shifts indicating that the dimerization can be ignored. A series of solutions were prepared by varying the ratio between **39** and **15**, and keeping the sum of their concentrations constant, and monitored by proton NMR spectroscopy. The partial spectra from that series, as well as the spectra of both compounds in the free form are presented in Figure 4.23. Well defined and resolved signals in the spectra reveal fast equilibration on the NMR time scale, indicating the well-defined conformation of the species in solution. The characteristic changes were observed for imide proton, which moved slightly from 8.13 ppm in the free **15** to 8.18 ppm in the 2/1 mole ratio mixture of **15** and **39**. The same deshilding effect was observed for all the sugar protons, although in smaller proportions. On the other hand, the β-pyrrolic protons and the *meso*-aryls protons of the free-base

porphyrin of **39** in the mixtures moved toward high field. A NOE experiment was also performed for this complex, but did not reveal any intermolecular interactions. Although minor, the complexation-induced shifts, both downfield and upfield, are similar to those observed in the complexation process between **40** and **15**. Therefore, these spectral changes illustrate the recognition process.

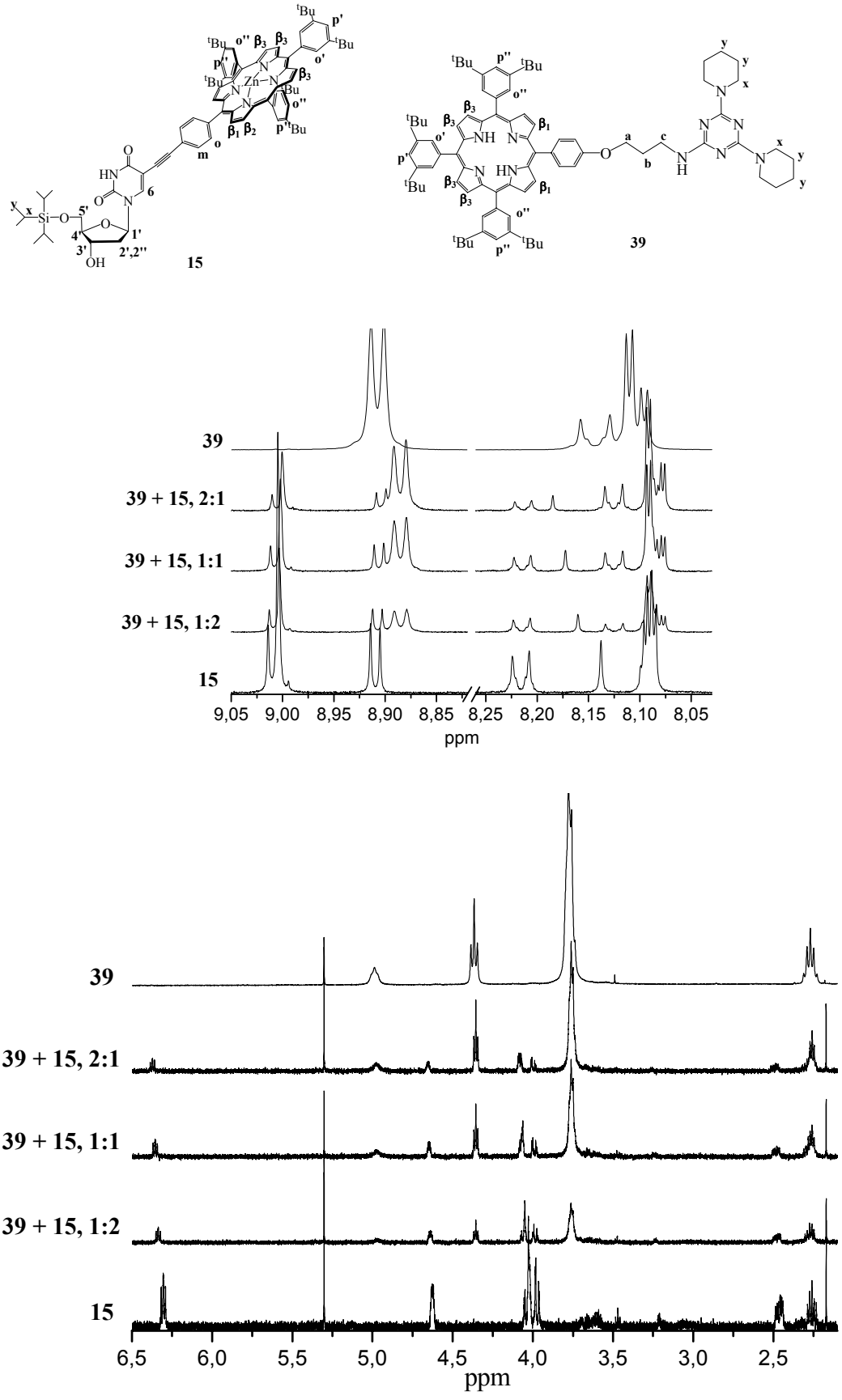

Figure 4.23 *^{1}H NMR spectra of mixtures of **39** and **15** (2 mM) in chloroform-d at 298 K.*

The stoichiometry of the **15**/**39** complex was determined by Job's plot method in chloroform-*d* under conditions of invariant total concentration of 2 mM by proton NMR spectroscopy using the relevant uridine-porphyrin protons, Figure 4.24.

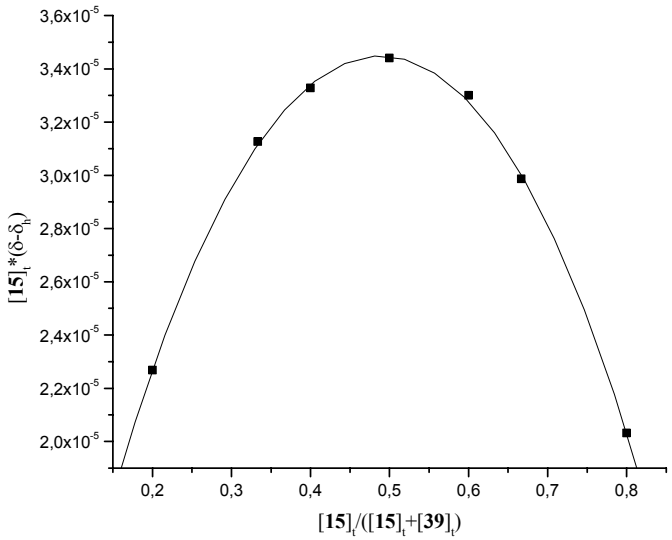

Figure 4.24 *Job's plot indicating the formation of the 1/1 supramolecular complex of* ***15*** *with* ***39****.*

This approach reveals that the relative concentrations of **15**/**39** complex approach the maximum when the mole fraction of **15** is approximately 0.5. Such finding is consistent with a 1/1 stoichiometry for the complex **15**/**39**, as it was expected on the basis of the results obtained for the complex of **15**/**40**. Indeed, despite the minor spectroscopic changes in NMR spectra, the formation of the supramolecular complex was evidenced.

For the constant a value of few hundreds was anticipated due to the association constant obtained for the complex of **15** with bis-porphyrinic triazine **40**, which involves two-side double hydrogen-bonding. In addition, the stability of the supramolecular assembly between adenine and uridine derivatives has been found to be around 10^2 M^{-1}.[220,245,249] The quantitative binding studies were first attempted by using the proton NMR titration method, which unfortunately did not afford reliable results because of low resolution of the relevant signals. Therefore, as in the previous case of the complex **15**/**40**, UV-visible titration binding experiment of **15** with mono-porphyrinic triazine **39** was performed in dichloromethane. As well, the titration was performed by addition of **15** to the solution of **39**. The binding constant could be readily determined, because the free-base porphyrin **39** absorbs light in the range

between 600 and 700 nm significantly stronger than zinc porphyrin **15**. However, in the context of here expected lower stability of the complex, higher concentration had to be used to measure the self-association constant. Therefore, since in dilution study of uridine-porphyrin conjugate **15** performed by proton NMR the self-association was revealed, the kinetic experiment was performed upon addition of aliquots from the stock solution (*c*= 5.08 x 10^{-3} M) into dichloromethane. The obtained spectra evidenced no spectroscopic change in the time period of 1 hour, pointing that if present in the stock solution self-assembly of **15** dissociate fast upon dilution, Figure 4.25.

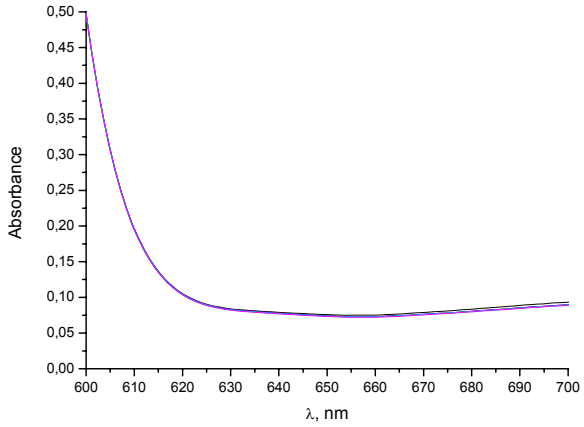

Figure 4.25 *Kinetics of uridine-porphyrin conjugate **15** upon addition of aliquots from the stock solution (c= 5.08 x 10^{-3} M) into dichloromethane.*

The titration was probed in dichloromethane at room temperature by addition of small aliquots of **15** (*c*= 4.14 x 10^{-2} M) into the solution of **39**. The concentration of the free-base porphyrin **39** solution was determined by peak absorbance of 0.5 for the Q-band at 648 nm. Hence, the Q-band absorption was measured at the concentration of 9.78 x 10^{-5} M. The titration was carried out by monitoring the spectral changes associated with addition of **15**, covering the concentration range of 8.27 x 10^{-5} M to 1.00 x 10^{-2} M, Figure 4.26.

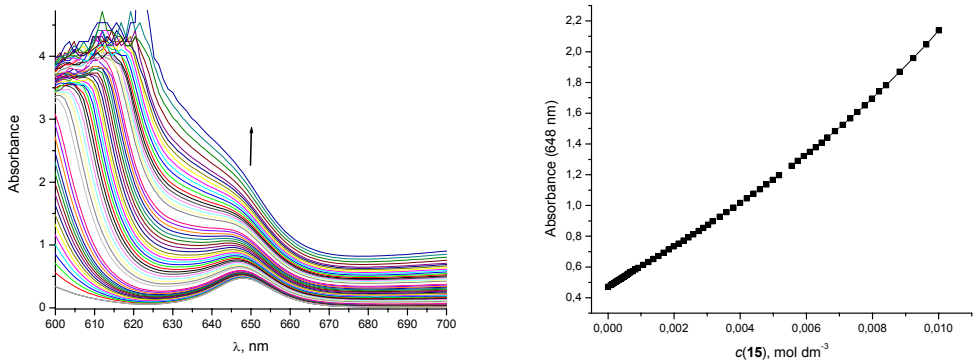

Figure 4.26 *Overlay of the visible spectra recorded by addition of* ***15*** *to dichloromethane solution of* ***39*** *(9.78 x* 10^{-5} *M). At the right hand side, a plot of absorbance of* ***39*** *as a function of added* ***15*** *at 648 nm.*

The analysis of the titration data by using the values of the absorbance at fixed wavelengths by using SPECFIT resulted with very small values for association constant together with poor fit of the experimental and calculated values. In the first line, an explanation can be inquired in clearly visible perforation of the sensitivity of an instrument (Abs>2) in the monitored region, and even at the wavelength of 648 nm. However, in employed concentration range we only extended the complexation ratio below ~10%. It can be assumed that association constant is smaller then 10 M^{-1} and therefore hardy measurable due to associated large error. Such low binding ability of **15** to **39** is in agreement with the association constant value obtained for the 1/1 stoichiometry of **15**/**40** complex. Generally, it is surprising that such discrepancies in binding properties of mono- and bis-porphyrinic triazine **39** and **40** with **15** can result from such minor structural differences, namely replacement of one free-base porphyrin with one piperidine at triazine skeleton.

4.3. Conclusion.

We prepared rationally designed porphyrin-modified hydrogen-bonding structures based on uridine and triazine, in which both hydrogen-bonding and π-stacking can operate simultaneously. For the **15**/**40** complex with stoichiometry 2/1 we obtained unexpectedly high association constant, while for the only possible 1/1 stoichiometry of the **15**/**39** complex considerably lower value was estimated. An explanation of such behavior can be search in absence of one porphyrin ring, and the fact that only two hydrogen bonds can possibly be established. These differences in binding abilities of **15** towards structurally modified triazines imply a strong presumption that the driving force for the binding uridine-porphyrin conjugate **15** is not governed only by hydrogen bonding but also by π-stacking interactions. Therefore, it can be assumed that insertion of porphyrin rings can influence the stability of complexes based on hydrogen bonding.

Although the binding selectivity needs to be further improved, the study presented here serves for the potential noncovalently assembled system through which photoinduced energy transfer might be facilitated. Moreover, and perhaps more importantly, the porphyrin-modified triazine receptors can be applied to assemble higher-order arrays for the elaboration of photonic and electronic wires. Besides, introduction of a magnesium(II) cation into the porphyrin core of the triazine receptors aiming to an electro-chemical control of the luminescence still remind to be elucidated.

III – CONCLUSIONS AND OUTLOOKS

In this work we have synthesized oligonucletidic scaffold with pendant porphyrins for the formation of the organized porphyrin arrays. The synthesis is based on the oligomerization process of the porphyrin-uridine conjugates, which are coupled by using ether-ester type of linker between O-3' of the upper unit and O-5' of the lower unit. The monomer (**1**) was prepared by stepwise functionalization of 2'-deoxyuridine at both 3'- and 5'-positions of the ribose and at the 5-position of the uracil base with the corresponding porphyrin. The selective cleavage of the protecting groups at 3'- and 5'-positions allowed convergent strategy of the oligomerization, providing dimer (**2**), tetramer (**3**), and octamer (**4**). All porphyrin-uridine conjugates of different range were characterized by ^{1}H NMR spectroscopy, UV-visible and fluorescence spectroscopy, mass spectrometry, and elemental analysis or analytical size-exclusion chromatography.

Whereas in the natural light-harvesting antennae complexes an efficient energy transfer is based on α-helical polypeptides, in our systems the required parallel orientation of the pigments was anticipated in respect to the conformational features of oligonucleotides. The architecture of our modified oligodeoxyuridinic backbone with pendant porphyrins is based on combination of rigid and flexible linkers, namely, porphyrins are appended to an appropriate position of the uridine by the rigid acetylenic linker, while the interuridinic linkage is flexible.

The preliminary conformational studies were performed by using NMR spectroscopy. The different solvents were probed due to the possible influence of two main secondary interactions (π-π between the porphyrins and hydrogen bonding between the uracil nucleobases). The spectra of monomer (**1**) and dimer (**2**) measured in the chloroform-*d* were well-resolved, but acetone-d_6 was more suitable for well-assignment. The observations from the comparison of those spectra signified the positive interaction of our compounds with acetone. The spectra of tetramer (**3**) measured in chloroform-*d* were insufficiently resolved for an assignment, but in acetone-d_6 a considerable improvement in resolution was found. The spectra of both dimer **2** and tetramer **3**, obtained in the acetone-d_6, showed that the environment of each uridine and, consequently, each appended porphyrin is different. The NOE effect of both dimer **2** and tetramer **3** showed some regularity in interactions between each lower unit and its neighbouring units of the porphyrin-uridine arrays. In principle, our molecular systems exist in one preferable conformational form. Some characteristic and strong interactions, among which are those of the H-6 protons and the *meso*-phenylethyne protons, indicate that the porphyrins are organized, that they are in proximity, but not in direct face-to-face orientation. Besides, the interactions indicate that the glycosidic angle between

the ribose and the uracil base is *syn*. Hence, the use of modified oligonucleotides as scaffold with the goal of formation of organized porphyrinic arrays was largely justified.

The further insight in spacing of the porphyrins within the corresponding oligonucleotidic wires was obtained by performing preliminary photochemical studies by using UV-visible and fluorescence spectroscopy. It was found that the mutual porphyrinic electronic interactions along the arrays are weak as manifested by slightly red-shifted Soret absorption bands. The fluorescence emission and excitation studies indicated that excited-state energy of the terminal zinc-porphyrin is funnelled along the free-base porphyrin arrays. The obtained spectral properties suggested that in the case of the tetramer **3**, and especially octamer **4**, the energy absorbed by the zinc-porphyrin is transferred with considerably greater efficiency than in the dimer **2**. Thereof, the porphyrin macrocycles in the dimer are relatively further away than in the tetramer, and especially in the octamer. However, the intramolecular electronic interactions within the porphyrin arrays in these systems may be categorized into through-space (Förster-type) interactions. Considering the results obtained by using NMR spectroscopy, it can be assumed that the preferable parallel conformation form of the oligodeoxyuridinic scaffold with pendant porphyrins is reached with the tetramer.

Within our interest in obtaining parallel orientation of the porphyrins, the range of oligodeoxyuridines with pendant zinc(II)-porphyrins was subjected to coordination with the bidentate base such as DABCO. The complexation of the simple zinc(II)-porphyrin (**13**), dimer (**30**) and tetramer (**31**) with DABCO was studied by using the UV-visible titration. The assemblies were characterized in terms of stability constants for all possible stoichiometric binding models to examine the effectivness of the oligomerization degree on complexation. It was found that the coordination of DABCO is favoured as one goes toward tetramer (**31**). Besides, the values of all stoichiometric binding constants showed that the chelated complexes are two times more stable then corresponding open complexes, which were formed upon addition of incremental amounts of DABCO. The spectroscopic changes in the UV-visible spectra of titrations demonstrated an increased electronic interaction along the porphyrinic arrays, presumably due to a rapprochement of the porphyrins imposed by conformational pre-organization within the oligonucleotidic backbone.

The second approach to a self-assembly of our uridine-porphyrin conjugates was based on the construction of an appropriate receptor that complement the chemical characteristics of the target nucleobase. Thereby, from cyanuric chloride and the synthesized porphyrin-amine **36**, the triazine-bridged porphyrin dyad (**40**) and the simple triazine-porphyrin (**39**) were prepared. These triazine derivatives provide recognition abilities through

various hydrogen bonding regions. The quantitative studies of the supramolecular structures of the monomeric uridine-porphyrin conjugate (**15**) with the triazine derivatives evidenced an influence of aromatic interactions between the porphyrins on their stability. The stoichiometry for the predominant supramolecular complex of **15** and the triazine-bridged porphyrin dyad in equilibrium was found to be 2/1. Hereafter, processing of the titration data gave the best correlation of experimental and calculated values for the formation of exclusively this complex. The value of the corresponding association constant (K_{12}= 6.0 x 10^5 M^{-2}) signifies a contribution of the porphyrins on stabilization of that supramolecular complex. On the other hand, the molecular recognition interaction of **15** with the simple triazine-porphyrin resulted in the formation of 1/1 stoichiometry complex. The association constant for this complex was estimated to be smaller then 10 M^{-1}.

The revealed contribution of porphyrins to intermolecular recognition based on hydrogen bonding concept can be employed in efficient mimicry of light-harvesting antennae. The whole range of the prepared uridine-porphyrin conjugates can form noncovalently assembled systems with the triazine derivatives endowed with porphyrins. In those molecular systems the sequence of metallated and free-base porphyrins can be chosen as desired, depending on potential applications. Thus, the porphyrinic array appended to the oligonucleotidic backbone can be fully metallated with zinc(II) if aiming to antenna effect. The supramolecular complex formed between such molecular system endowed with zinc-porphyrin array and triazine-bridged free-base porphyrin dyad, as it is presented below, can facilitate a photoinduced energy transfer within the supramolecular complex. In such complexes, the energy absorbed by the zinc-porphyrin appended to the oligonucleotidic backbone can be transferred toward the triazine-bridged free-base porphyrins, and therefore contribute to an emission of the free-base porphyrins.

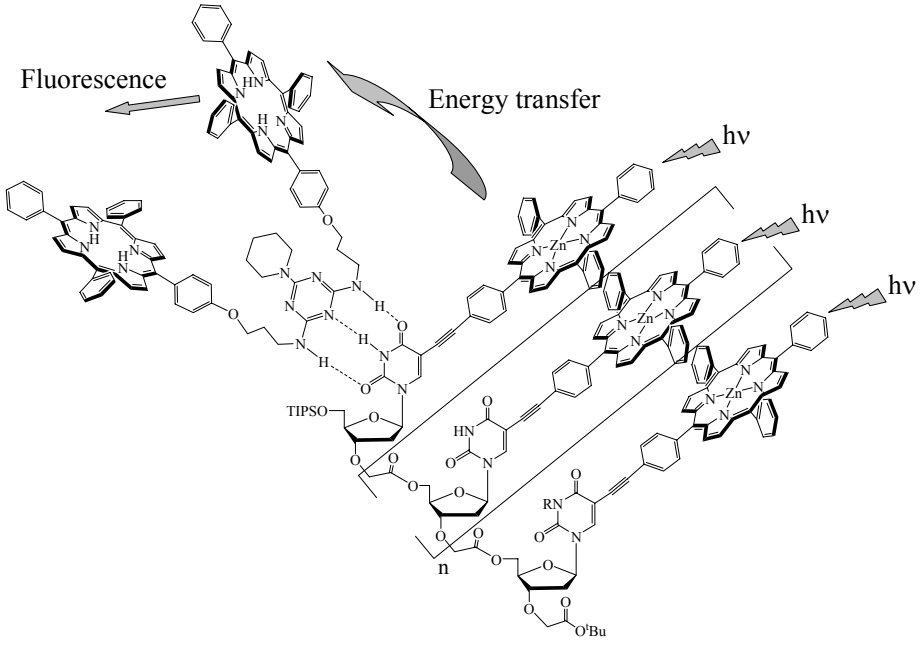

The different sequence of zinc-porphyrin and free-base porphyrins along the porphyrinic array appended to oligonucleotidic backbone and insertion of magnesium(II) ion in the cavities of the free-base porphyrins at triazine can enable to combine antenna effect and bi-functionality of the magnesium(II) porphyrin. The energy absorbed by the terminal zinc(II) porphyrin can be transmitted down the porphyrinic array constituted of free-base porphyrins. The emission of the luminescent free-base porphyrin would be switched on/off in a controlled manner, depending on the oxidation state of the magnesium(II) porphyrin at triazine. The magnesium(II) porphyrin in its oxidated non-luminescent form has a first singlet excited state that lies lower then the first singlet excited state of a free-base porphyrin, and is therefore a perfect switching site candidate. Hence, in molecular systems as such presented below a control of the energy transfer path *via* electrochemical control of the redox state of the magnesium(II) porphyrin should allow an on/off switching of the luminescence of the compound.

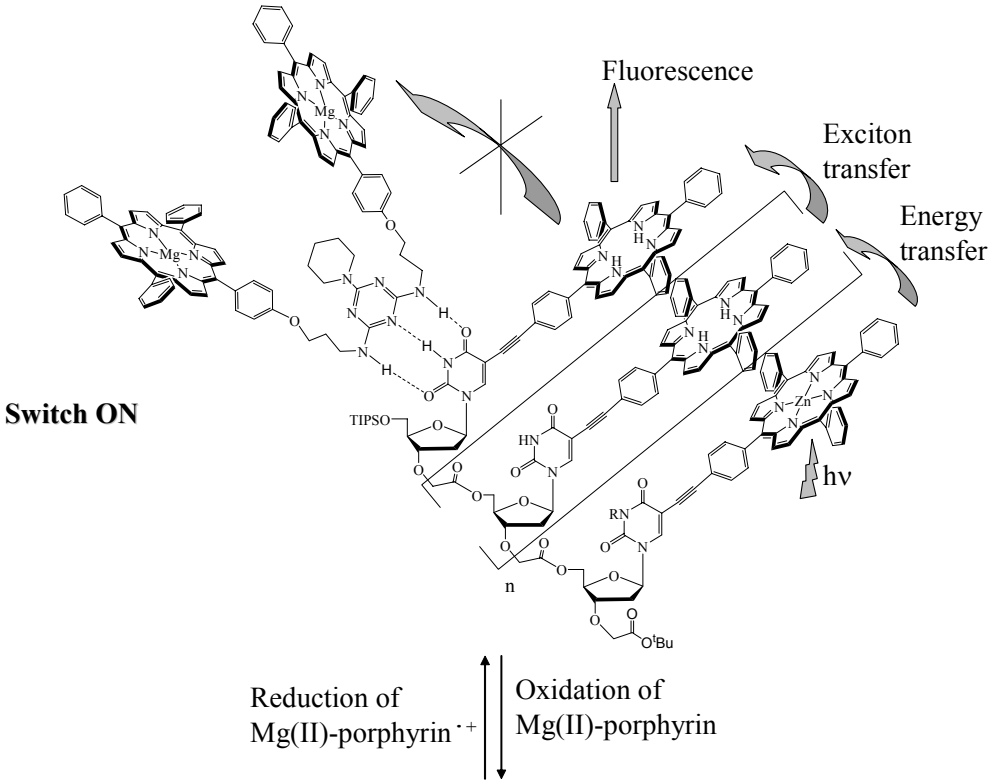

Reduction of Mg(II)-porphyrin$^{\cdot+}$ ⇕ Oxidation of Mg(II)-porphyrin

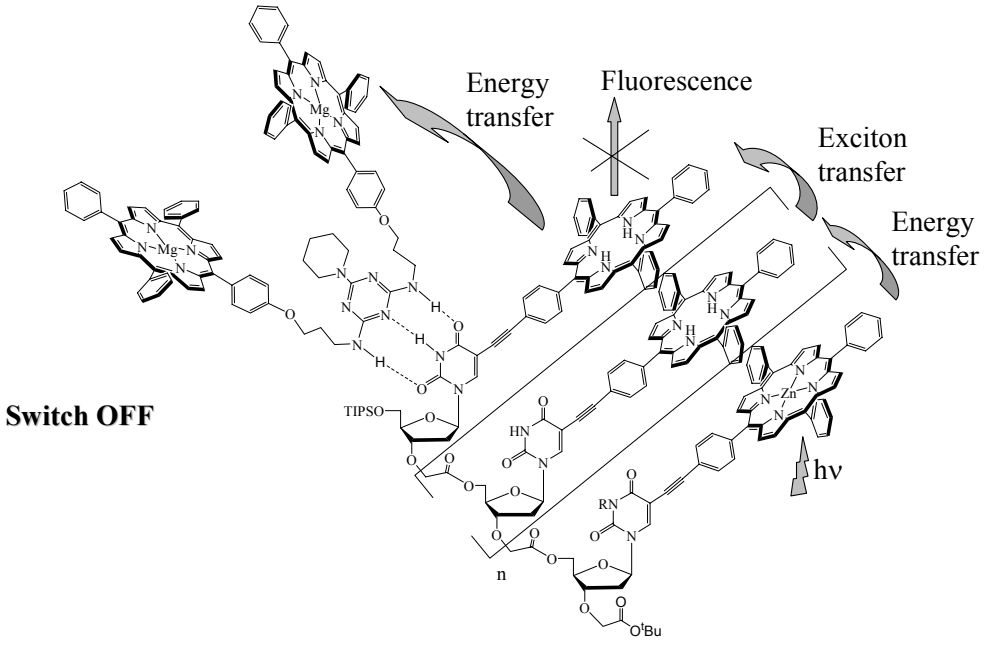

Dans ce travail, nous avons réalisé la synthèse de squelettes oligonucléotidiques comprenant des porphyrines pendantes pour la formation de réseaux porphyriniques organisés. La synthèse est fondée sur un processus d'oligomérisation de l'uridine fonctionnalise par une porphyrine. Les différents uridines sont couplées en utilisant des connexions de type éther-ester entre la position O-3' de l'unité du dessus et O-5' de l'unité du dessous. Le monomère (**1**) a été préparé grâce à une étape de fonctionnalisation de la 2'-désoxyuridine en positions 3' et 5' du ribose et la position 5 de la base uracile avec la porphyrine correspondante. La déprotection sélective en positions 3' et 5' permet l'utilisation d'une stratégie convergente pour l'oligomérisation, donnant naissance au dimère (**2**), au tétramère (**3**) et à l'octamère (**4**). Tous les différents systèmes porphyrine-uridine ont été caractérisés par spectroscopie RMN du proton, par spectroscopies UV-visible et de fluorescence, par spectrométrie de masse, par chromatographie d'exclusion stérique et par analyse élémentaire.

Tandis que dans les complexes naturels à effet d'antenne, le transfert d'énergie efficace est basé sur des polypeptides à hélice α, dans nos systèmes, l'orientation parallèle des pigments a été anticipée, eu égard aux caractéristiques conformationnels des oligonucléotides. L'architecture de notre squelette oligodésoxyuridinique modifié à porphyrines pendantes est basée sur une combinaison de liens rigides et flexibles : les porphyrines sont attachées à la position appropriée de l'uridine par un lien rigide de type acétylénique, tandis que le lien interuridinique est flexible.

Des études conformationnelles préliminaires ont été réalisées en utilisant la méthode de spectroscopie RMN. Différents solvants ont été utilisés en raison d'une probable influence de deux interactions secondaires (de type π-π entre les porphyrines et de type liaisons hydrogène entre les nucléobases uraciles). Les spectres du monomères (**1**) et du dimère (**2**) enregistrés dans le chloroforme deutéré ont été bien résolus, mais l'acétone deutérée s'est avérée être un meilleur solvant pour l'assignation des protons. Les observations résultant des comparaisons des spectres ont mis en évidence l'interaction positive de nos composés avec l'acétone. Les spectres du tétramère (**3**) enregistrés dans le chloroforme deutéré n'ont pas été suffisamment bien résolus pour que les protons puissent être assignés, en revanche, dans l'acétone deutérée, une amélioration considérable de la résolution a été observée. Les spectres du dimères (**2**) et du tétramère (**3**), obtenus dans l'acétone deutérée, ont révélé que l'environnement de chaque uridine, et par conséquent, de la porphyrine qui y est attaché, est différent. L'effet NOE du dimère (**2**) et du tétramère (**3**) montre quelques régularités dans les interactions entre chaque unité et leurs unités voisines en sein du réseau porphyrine-uridine.

En principe, nos systèmes moléculaires existent sous une conformation préférentielle. Des interactions fortes et caractéristiques, parmi lesquelles celles des protons H-6 et des protons *méso*-phénylèthyne, révèlent que les porphyrines sont organisées. Elles sont à proximités les unes des autres, mais elles n'adoptent pas une orientation directement en face-à-face. En outre, les interactions indiquent que l'angle glycosidique entre le ribose et la base uracile est *syn*. Ainsi, l'utilisation d'oligonucléotides modifiés en tant que squelette, dans l'optique de former des réseaux de porphyrines organisés, a été largement justifiée.

La preuve supplémentaire de l'agencement parallèle des porphyrines au sein des fils oligonucléotidiques, a été obtenue grâce à des études préliminaires de photochimie en utilisant les spectroscopies UV-visible et de fluorescence. Il a été démontré qu'il existe des interactions électroniques entre les porphyrines, à travers le réseau, ce qui se manifeste par un léger effet bathochrome pour la bande d'absorption de Soret. Les études d'émission et d'excitation ont révélé que l'énergie de l'état excité de la porphyrine de zinc terminale est canalisée le long du réseau porphyrinique base-libre. Les propriétés spectrales obtenues ont suggèrent que dans le cas du tétramère (**3**), et plus spécialement dans celui de l'octamère (**4**), l'énergie absorbée par la porphyrine de zinc est transférée avec une plus grande efficacité que peur le dimère (**2**). Par conséquent, les macrocycles porphyriniques dans le dimère sont plus éloignés que dans le tétramère et encore plus que dans l'octamère. Cependant, les interactions électroniques intramoléculaires dans le réseau porphyrinique de ces systèmes peuvent entrer dans la catégorie des interactions qui ont lieu à travers l'espace (de type Förster). En considérant les résultats obtenus par spectroscopie RMN, il est possible de prétendre que la conformation préférentielle attendue du squelette oligodésoxyuridinique à porphyrines pendantes a été obtenue avec le tétramère.

Ayant pour intérêt d'obtenir une orientation parallèle des porphyrines, les oligodésoxyuridines à porphyrines de zinc(II) pendantes ont été coordinées avec une base bidentate tel que le DABCO. La complexation de la porphyrine de zinc(II) simple (**13**), du dimère (**30**) et du tétramère (**31**) avec le DABCO a été étudiée en utilisant une méthode de titration par UV-visible. Les ensembles ont été caractérisés en terme de constante de stabilité pour les complexes de toutes les stoechiométries possibles afin d'examiner l'influence du degré d'oligomérisation sur la complexation. Il a été démontré que la coordination du DABCO est plus favorable dans le cas du tétramère (**31**). En outre, les valeurs de toutes les constantes d'association ont montré que les complexes chelatés sont deux fois plus stables que les complexes « ouverts » correspondants, qui résultent de l'addition d'une quantité supplémentaire de DABCO. Les changements dans les spectres UV-visible des titrations

démontrent la présence d'interactions électroniques qui augmentent à travers le réseau porphyrinique, ce qui est probablement dû à un rapprochement des porphyrines, imposé par une pré-organisation à l'intérieur du squelette oligonucléotidique.

La seconde approche pour l'assemblage de nos systèmes uridine-porphyrine consiste en la construction d'un récepteur approprié qui complète les caractéristiques chimiques de la nucléobase cible. Ainsi, la dyade triazine-porphyrine pontée (**40**) ainsi que la simple triazine-porphyrine (**39**) ont été préparées à partir du chlorure de cyanure et de la porphyrine amine **36** précédemment synthétisée. Ces dérivés de triazine assurent des capacités de reconnaissance à travers des réseaux de liaisons hydrogène. Les études quantitatives des structures supramoléculaires du système monomérique uridine-porphyrine (**15**) avec les dérivés de triazine ont révélé l'influence d'interactions aromatiques entre les porphyrines sur leur stabilité. La stoechiométrie du complexe supramoléculaire prédominant de **15** et de la dyade triazine-porphyrine pontée à l'équilibre est de 2/1. Ensuite, les données de titration ont montré une meilleure corrélation entre les valeurs expérimentales et calculées pour la formation exclusive de ce complexe. La valeur de la constante d'association correspondante (K_{12}= 6,0 x 10^5 M^{-2}) signifie qu'il existe une contribution des porphyrines dans la stabilisation du complexe supramoléculaire. D'un autre côté, les interactions de reconnaissance moléculaire de **15** avec la triazine-porphyrine simple proviennent de la formation d'un complexe de stoechiométrie 1/1. Il a été estimé que la constante d'association de ce complexe est plus petite que 10 M^{-1}.

Cette contribution des porphyrines pour la reconnaissance intermoléculaire, basée sur le concept de liaisons hydrogène, peut être employée dans le but de mimer efficacement les antennes collectrices de lumière. Tous les systèmes uridine-porphyrine préparés peuvent former des systèmes assemblés de façon non covalente avec les dérivés de triazine dotés de porphyrines. Au sein de ces systèmes moléculaires, la séquence de porphyrines métallées et base-libre peut être choisie librement, en fonction des applications potentielles. Ainsi, le réseau porphyrinique accroché au squelette oligonucléotidique peut être entièrement métallé au zinc(II) si un effet d'antenne est désiré. Le complexe supramoléculaire formé par un tel système doté d'un réseau des porphyrines de zinc et d'une dyade triazine-porphyrine base libre pontée (représenté ci-dessous) est capable de faciliter un transfert d'énergie photoinduit grâce à processus intermoléculaire entre les porphyrines à l'état excité. Dans de tels complexes, l'énergie absorbée par la porphyrine de zinc attachée au squelette oligonucléotidique peut être transférée vers la triazine pontée aux porphyrines base-libre, et ainsi contribue à l'émission des porphyrine base-libre.

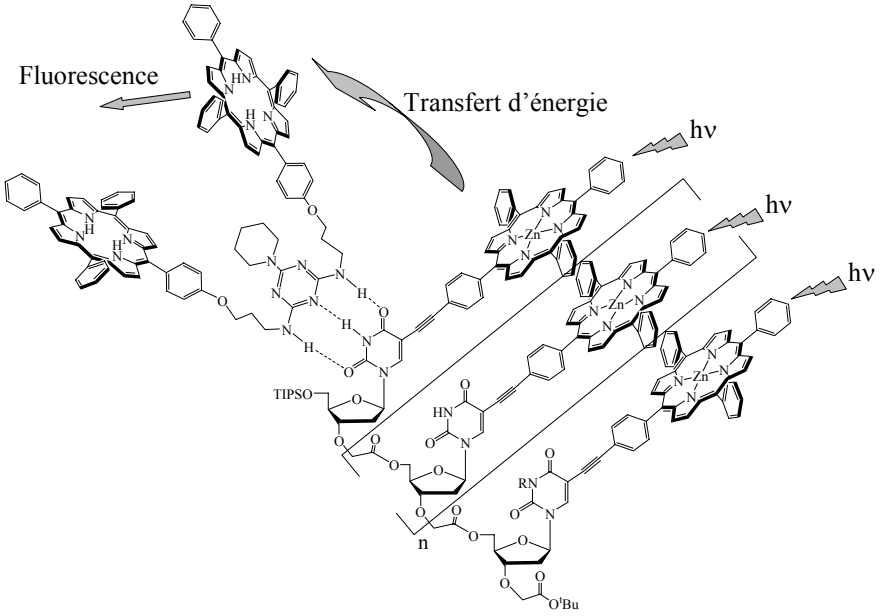

Les différentes séquences de porphyrine de zinc et de porphyrines base-libre le long du fil multi-porphyrinique ainsi que l'insertion de l'ion magnésium(II) dans les cavités des porphyrines base libre peut permettre de combiner l'effet d'antenne et la bi-fonctionnalité de la porphyrine de magnésium(II). L'énergie absorbée par la porphyrine de zinc(II) terminale peut être transmise par le réseau porphyrinique constitué des porphyrines base-libre. L'émission de la porphyrine base-libre aurait lieu ou non, de manière controlée (« switch moléculaire »), en fonction de l'état d'oxydation de la porphyrine de magnésium(II). La porphyrine-magnésium(II), dans sa forme oxydée non luminescente, possède un premier état excité singulet plus bas en énergie que le premier état excité singulet de la porphyrine base libre, et représente par conséquent l'interrupteur moléculaire redox idéal. En conséquence, dans des systèmes moléculaires tels que ceux représentés ci-dessous, un contrôle du chemin de transfert d'énergie, *via* un contrôle électrochimique de l'état d'oxydo réduction de la porphyrine de magnésium(II), devrait permettre d'activer ou de désactiver la luminescence du composé.

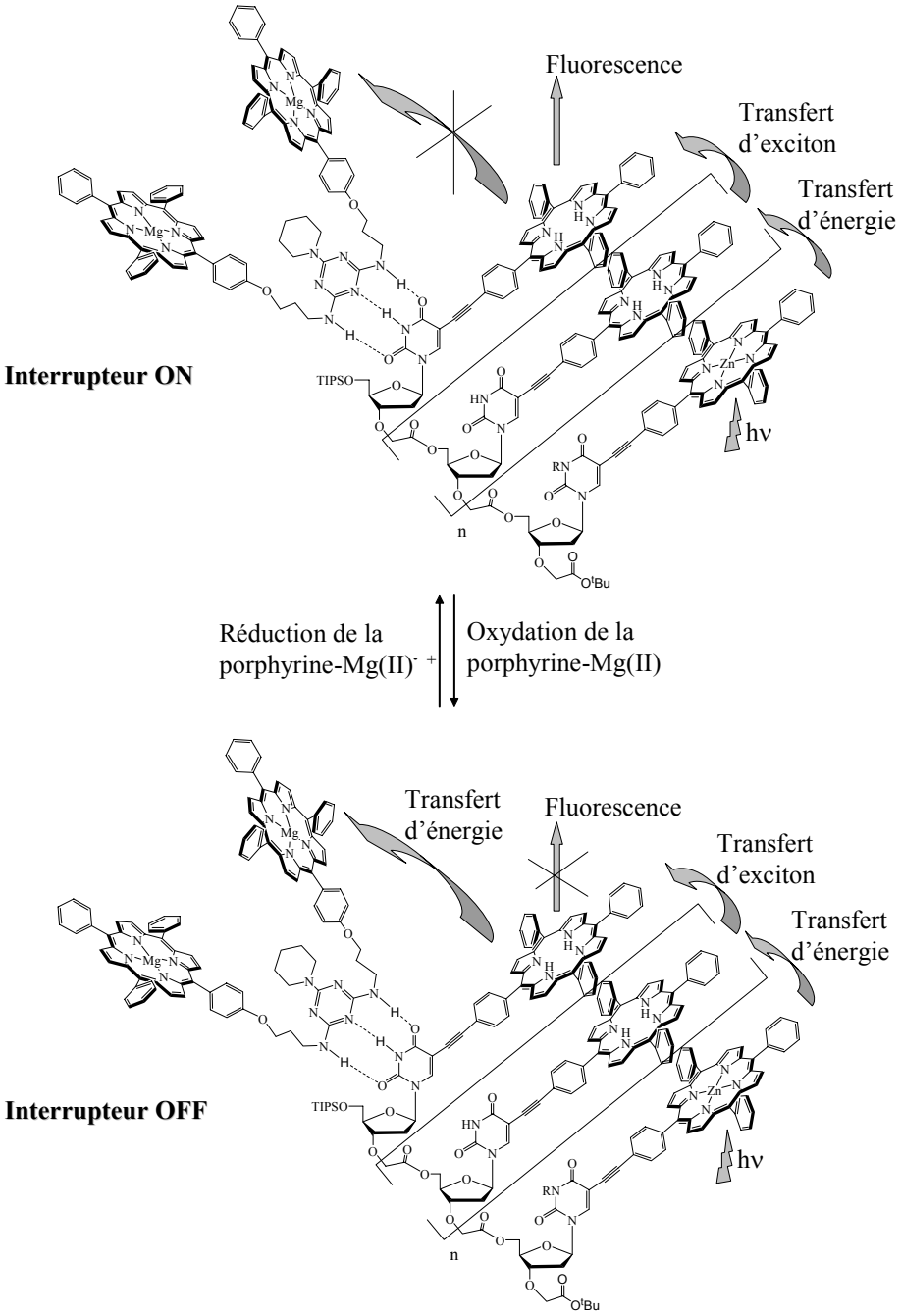
Fluorescence
Transfert d'exciton
Transfert d'énergie
Interrupteur ON
hν
Réduction de la porphyrine-Mg(II)•+
Oxydation de la porphyrine-Mg(II)
Transfert d'énergie
Fluorescence
Transfert d'exciton
Transfert d'énergie
Interrupteur OFF
hν

IV – EXPERIMENTAL SECTION

1. GENERAL.

All commercial products were used as received, except pyrrole used in the synthesis of porphyrins, which was filtrated through an aluminium micro-column. Almost all reactions were performed under an argon atmosphere. All solvents used in reactions were p.a. quality. All anhydrous solvents were prepared by distillation over an appropriated dehydrating agent under an argon atmosphere. Tetrahydrofuran (THF) was used as freshly distilled over sodium-benzophenone. Triethylamine was refluxed over and then distilled from CaH_2, and stored over 4 Å molecular sieves. Dimethylformamide (DMF), chloroform, dimethoxyethane (DME), and acetonitrile employed in the syntheses were dried and stored over 4 Å molecular sieves.

Analyses by thin layer chromatography were performed on a Merck silica-gel 60 F_{254}, and TLC plaques were visualized by UV-lamp at wavelengths of 254 and 365 nm. Unless otherwise noted, for column chromatography Merck silica-gel 60 (40-63 μm or 63-200 μm) was used. For gel-permeation or size-exclusion column chromatography Bio-Beads S-X1 Bio-Rad Laboratories were used in toluene.

The NMR spectra were recorded on Bruker spectrometers: Avance-300, ARX-250 and Avance 500. Chemical shifts are given in ppm (δ) upfield toward tetramethylsilane (TMS) used as an internal standard. The reference peak in the spectra was assigned to an employed solvent: $CDCl_3$ (7.26 ppm), $(CD_3)_2CO$ (2.05 ppm), C_6D_6 (7.16 ppm), CD_3OD (3.31 ppm), $C_2D_2Cl_4$ (5.99 ppm) or CD_2Cl_2 (5.32 ppm).

UV-visible spectra were obtained using a Perkin Elmer Lambda 25 or on a Varian Cary 100 Bio spectrophotometer in dichloromethane. Fluorescence spectra were recorded on a Perkin Elmer LS 55 spectrometer in dichloromethane.

The mass spectra were recorded in the "Laboratoire de spectrométrie de masse des macromolécules biologiques et des édifices supramoléculaires" at "Ecole européenne de chimie, polymères et matériaux" in Strasbourg and in the "Service commun de spectrométrie de masse" at the University Paul Sabatier in Toulouse.

Elemental analyses were carried out by the “Service de microanalyse” at “Laboratoire de Chimie de Coordination” in Toulouse. The purity of the higher order arrays has been assessed by analytical size-exclusion chromatography (SEC) with MINI-DAWN instrument purchased from Wyatt Technology using styrene-divinylbenzene copolymer columns eluting with THF.

2. SYHTHESES OF THE PRODUCTS.

5-Iodo-2'-deoxyuridine 5.

Silver sulfate (3.28 g, 10.52 mmol) was added to the clear brown solution of iodine (2.67 g, 10.52 mmol) in methanol (120 mL). The mixture was stirred for around 15 min before 2'-deoxyuridine (2.0 g, 8.76 mmol) was added. The reaction was continuing to stir at r.t. for 50 min, after which it was filtrated. The solid was washed with methanol. The volume of the filtrate was reduced upon evaporation. Recrystallization from methanol yielded **5** as pale yellow crystals (2.78 g, 7.85 mmol, 90%). TLC analysis was performed in ethyl acetate/methanol (9:1) as an eluent, R_f= 0.55. ^{1}H NMR (CD_3OD, 300 MHz): δ = 8.52 (s, 1H, H_6), 6.21 (t, 1H, $H_{1'}$, ^{3}J= 6.5 Hz), 4.40 (t, 1H, $H_{3'\text{-}4'}$, ^{3}J= 3.5 Hz), 4.38 (t, 1H, $H_{3'\text{-}2'}$, ^{3}J= 3.7 Hz), 3.92 (q, 1H, $H_{4'}$, ^{3}J= 3.2 Hz), 3.77 (dd, 2H, $H_{5'}$, ^{3}J= 2.9 Hz and ^{2}J= 11.9 Hz), 2.29 (ddd, 1H, $H_{2'}$, ^{3}J= 4.0 and 6.3 Hz and ^{2}J= 10.2 Hz), 2.21 (td, 1H, $H_{2'}$, ^{3}J= 6.8 and 13.3 Hz).

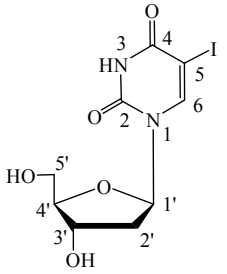

5

5'-*O*-Triisopropylsilyl-5-iodo-2'-deoxyuridine 6.

To the solution of 5-iodo-2'-deoxyuridine (**5**, 2.00 g, 5.65 mmol) in dry dimethylformamide (25 mL) were added imidazole (0.77 g, 11.3 mmol) and triisopropylsilylchloride (1.37 mL, 6.21 mmol). The solution was stirred at r.t. for 12 h and then evaporated to dryness. The dichloromethane solution of the crude product was washed with water. After evaporation of the solvent from the organic phase, the product was purified by column chromatography (SiO_2, ethylacetate/*n*-hexane (6:4 → 8:2), R_f= 0.57), affording **6** as a white solid (2.22 g, 4.35 mmol, 77%). ^{1}H NMR ($CDCl_3$, 300 MHz): δ = 8.32 (s, 1H, NH), 8.04 (s, 1H, H_6), 6.27 (dd, 1H, $H_{1'}$, ^{3}J= 5.7 and 7.9 Hz), 4.57 (m, 1H, $H_{3'}$), 4.06 (ddd, 1H, $H_{4'}$, ^{3}J= 2.7 and 5.3 Hz), 3.96

(ABM, 2H, $H_{5'}$, ^3J= 2.4 and 2.9 Hz and ^2J= 8.5 Hz), 2.42 (ddd, 1H, $H_{2'}$, ^3J= 2.6 and 5.7 Hz and ^2J= 13.5 Hz), 2.14 (ddd, 1H, $H_{2'}$, ^3J= 5.0 and 6.5 Hz and ^2J= 13.7 Hz), 1.19 (m, 3H, CH_{TIPS}), 1.11 (s, 9H, $CH_{3,TIPS}$), 1.09 (s, 9H, $CH_{3,TIPS}$). Elemental analysis (%) for $C_{18}H_{31}IN_2O_5Si$ (510.44): calcd C 42.35, H 6.12, N 5.49; found C 42.53, H 6.01, N 5.35.

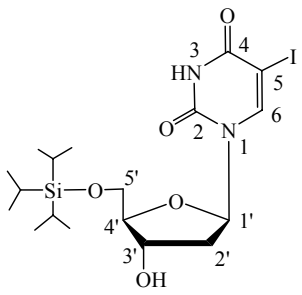

6

3,5-Di-*tert*-butyltoluene 7.

Tert-butyl chloride (120mL, 1.10 mol) was dissolved in toluene (60mL, 0.57 mol) under an argon atmosphere, and aluminium chloride (3.0 g, 22.8 mmol) was added in small portions to avoid overheating. $AlCl_3$ has to be stored under argon to minimize exposure to air. The reaction mixture was colourless at the beginning, and then it changed to orange and red with addition of $AlCl_3$. After addition of $AlCl_3$ was terminated, the solution was stirred during 48 h at r.t.. The reaction progress was followed by TLC (*n*-hexane as an eluent). The obtained clear orange solution was washed with 0.5 M HCl (2 x 100 mL). The combined aqueous phase was extracted with *n*-hexane before successive washing with water and saturated solution of $NaHCO_3$. All organic phases were combined and evaporated to dryness. The residue as a colourless oil was distilled under vacuum affording four fractions: at 58 °C m= 48.81 g, at 67 °C m= 24.41 g, at 75 °C m= 30.72 g, at 78 °C m= 65.42 g. Those fractions were characterized by ^1H NMR spectroscopy. The first two fractions contained a mixture of the byproducts, the third fraction contained the desired product **7** with small impurity, and the fourth provided pure **7**. Hence, compound **7** was obtained as colourless oil (96.14 g, 0.47 mol, 41%). ^1H-NMR ($CDCl_3$, 300 MHz): δ= 7.47 (t, 1H, ^4J= 1.7 Hz, $H_{p'}$), 7.26 (d, 2H, ^4J= 1.7 Hz, $H_{o'}$), 2.57 (s, 3H, CH_3), 1.54 (s, 18H, ^{t}Bu).

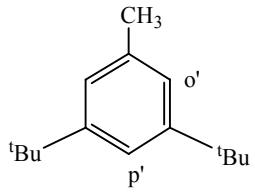

7

1-Monobromomethyl-3,5-di-*tert*-butyltoluene 8 and 1-dibromomethyl-3,5-di-*tert*-butyltoluene 9.

Bromination of the methyl group of **7** was provided with *N*-bromosuccinimide (NBS) in benzene under irradiation of the projector. Since 95.5 g of the starting material was disposed, the reaction was performed in four portions to reduce the volume subjected to irradiation. Thus, the solution of 3,5-di-*tert*-butyltoluene (**7**, 20.4 g, 0.10 mol) and NBS (26.1 g, 0.15 mmol) in benzene (45 mL) was subjected to irradiation of the projector of 150 W, and then heated to reflux for 2h. The reaction mixture at the beginning was colourless, then it progressively became orange, and after around 30 min it became colourless with white precipitate (NHS). This solid was removed by filtration, and the filtrate was evaporated to dryness and dried in vacuum. The same procedure was repeated three times yielding yellow oil. A value of the overall yield was not evaluated at this step, hence it was considered to be 100%. ^{1}H-NMR ($CDCl_3$, 300 MHz): δ= 7.39 (t, 1H, ^{4}J= 1.7 Hz, $H_{p'}$), 7.36 (t, 1H, ^{4}J= 1.6 Hz, $H_{p'}$), 7.23 (d, 4H, ^{4}J= 1.8 Hz, $H_{o'}$), 6.67 (s, 1H, $CHBr_2$), 4.52 (s, 2H, CH_2Br), 1.55 (s, 18H, ^{t}Bu). The proton NMR revealed the presence of monobromo derivative **8** in 38% and dibromo derivative **9** in 62% yield.

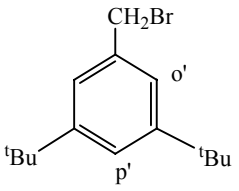

8

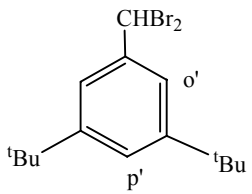

9

3,5-Di-*tert*-butylbenzaldehyde 10.

The mixture of two bromo derivatives (**8** and **9**, 95.5 g, 0.47 mol) and hexamethylenetetramine (HMTA, 183.4 g, 1.31 mol) were stirred to reflux in the solvent containing water/ethanol (1:1). After 3 h of reflux concentrated hydrochloric acid (86.5 mL) was added dropwise keeping the reaction temperature at reflux. The addition of HCl was regulated within 1 h, and then the reaction mixture was continuing heated at reflux for another 30 min. The organic phase was separated by decantation, and aqueous phase was extracted with three portions of CH_2Cl_2. The combined organic phase was washed successively with $NaHCO_3$ and water. Evaporation of the solvent afforded crude orange solid, which was then purified by column chromatography (SiO_2; Ø= 7 cm, h= 20 cm; ethylacetate/*n*-hexane (1:9)). The two fraction of the product were obtained and characterized by proton NMR. The first fraction provided pure **10** as a white solid (43.5 g, 0.20 mol), while the second fraction yielded mixture of the product as yellow solid. The latter was purified by recrystallization from *n*-hexane. Finally, the targeted aldehyde **10** was obtained in overall yield of 67% (68.3 g, 0.31 mol). ^{1}H-NMR ($CDCl_3$, 300 MHz): δ=10.01 (s, 1H, CHO), 7.73 (d, 2H, ^{4}J= 1.5 Hz, $H_{o'}$), 7.72 (t, 1H, ^{4}J= 1.7 Hz, $H_{p'}$), 1.37 (s, 18H, ^{t}Bu).

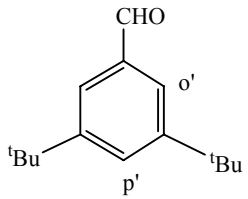

10

4-Trimethylsilylethynyl-benzaldehyde 11.

Freshly distilled triethylamine was deoxygenized by bubbling with argon prior being employed in the reaction. In such triethylamine bubbled during 3 h 4-bromo-benzaldehyde (5.84 g, 31.56 mmol) and trimethylsilyl-acetylene (5.84 mL, 41.03 mmol) were dissolved. After $Pd(PPh_3)_2Cl_2$ (0.55 g, 0.79 mmol) and CuI (0.30 g, 1.58 mmol) were added under an argon atmosphere the reaction flask was deaerated and flushed with argon. The reaction mixture was allowed to stir at r.t. overnight and then the solvent was removed by evaporation. The dark brown residue was dissolved in dichloromethane and successively extracted with EDTA disodium salt (2% solution), $Na_2S_2O_3$ (0.35 M), saturated solution of NH_4Cl, and

water. The solvent was evaporated and the crude product was purified by column chromatography (SiO_2; Ø= 5 cm, h= 16 cm; *n*-hexan/ethylacetate (9:1)), yielding the compound **11** as a brown solid (5.54 g, 27.38 mmol, 87%). ^{1}H-NMR ($CDCl_3$, 300 MHz): δ= 10.00 (s, 1H, CHO), 7.83 (d, 2H, ^{3}J= 7.8 Hz, H_o), 7.81 (d, 2H, ^{3}J= 7.7 Hz, H_m), 0.27 (s, 9H, $CH_{3,TMS}$).

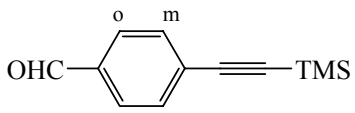

11

Free-base A_3B porphyrin 12.

After a three-necked, round-bottomed flask fitted with two septum ports and a reflux condenser with a gas inlet port was flushed with argon, it was charged with chloroform dried over molecular sieves (1.5 L). Subsequently, under continuous argon flow the both aldehydes, 3,5-di-*tert*-butylbenzaldehyde (**10**, 2.52 g, 11.52 mmol) and 4-trimethylsilylethynyl-benzaldehyde (**11**, 0.78 g, 3.84 mmol) were added, in an overall concentration of 10^{-2} M. Sock solution of BF_3 etherate was prepared separately by diluting the commercial $BF_3 \cdot OEt_2$ (1.2 mL) with chloroform (1.8 mL). Further, pyrrole (1.04 mL, 15.00 mmol) and $BF_3 \cdot OEt_2$ from freshly prepared stock solution (1.6 mL of 3.16 M, in 1.5 L 3.37 x 10^{-3} M) were added via syringe. The resulted solution was stirred for 1 h at r.t. under an argon atmosphere. The reaction progress was monitored by TLC (dichloromethane/*n*-hexane (3:7)) by removing the aliquots from the reaction mixture and oxidizing with DDQ. The oxidation of porphyrinogen to porphyrin was performed with addition of *p*-chloranil (2.83 g, 11.52 mmol). The solution was refluxed for 1 h, and then allowed to cool to r.t. while triethylamine was added (2 mL). The reaction mixture was concentrated, to the slurry SiO_2 was added and evaporation was continued to dryness. Such reaction procedure was repeated six times, and the combined crude product was purified by repetitive silica-gel column chromatography. The first column (SiO_2; Ø= 7 cm, h= 20 cm; *n*-hexan/dichloromethane (9:1 → 5:5)) was effectuated to separate porphyrins from the other polymers. The second was employed to separate targeted A_3B porphyrin from the other porphyrin isomers. The pure compound **12** was isolated as violet solid (4.35 g, 4.15 mmol, 18%). ^{1}H-NMR ($CDCl_3$, 300 MHz) : δ= 8.90 (s, 4H, $H_{\beta 3}$), 8.89 (d,

2H, ^{3}J= 3.8 Hz, $H_{\beta 2}$), 8.81 (d, 2H, ^{3}J= 4.8 Hz, $H_{\beta 1}$), 8.19 (d, 2H, H_o, ^{3}J= 8.1 Hz), 8.08 (d, 4H, ^{4}J= 1.8 Hz, $H_{o''}$), 8.07 (d, 2H, ^{4}J= 1.8 Hz, $H_{o'}$), 7.87 (d, 2H, ^{3}J= 8.1 Hz, H_m), 7.80 (td, 3H, ^{4}J= 1.8 and 3.9 Hz, $H_{p'+p''}$), 1.53 (s, 36H, ^{t}Bu), 1.52 (s, 18H, ^{t}Bu), 0.39 (s, 9H, H_{TMS}), -2.70 (s, 2H, NH). UV-visible (CH_2Cl_2): λ_{abs} (ε) = 421 nm (506 836 M^{-1} cm^{-1}), 517 nm (18 627 M^{-1} cm^{-1}), 553 nm (10 941 M^{-1} cm^{-1}), 592 nm (5 565 M^{-1} cm^{-1}), 647 nm (5 590 M^{-1} cm^{-1}). Fluorescence (CH_2Cl_2): λ_{em}= 650 and 709 nm.

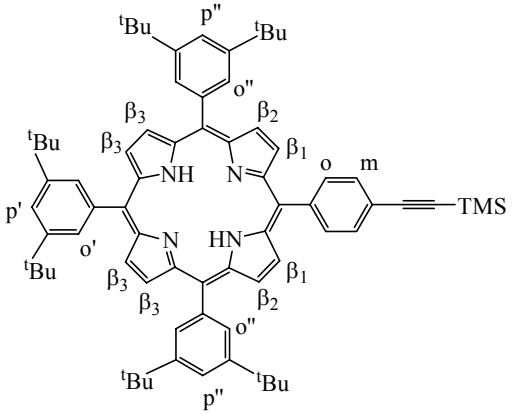

12

Zinc(II) porphyrin 13.

The solution of $Zn(OAc)_2 \cdot 2H_2O$ (0.1 M) was prepared separately by dissolving the corresponding salt (2.31 g, 10.54 mmol) in methanol (100 mL). Such solution was added to the mixture of free-base porphyrin **12** (5.52 g, 5.27 mmol) in chloroform (1380 mL) and obtained homogenous mixture was heated to reflux. The progress of metallation was monitored by UV-visible spectroscopy showing that the reaction was terminated after 4 h of reflux under an argon atmosphere. The solvent was removed by evaporation, the residue was dissolved in dichloromethane and obtained solution was extracted with water. The crude product was purified by column chromatography (SiO_2; Ø= 5 cm, h= 19 cm; *n*-hexan/dichloromethane (9:1 → 6:4)), yielding the zinc(II) porphyrin **13** as a dark red solid (5.56 g, 5.00 mmol, 95%). ^{1}H-NMR ($CDCl_3$, 300 MHz) : δ= 9.02 (s, 4H, $H_{\beta 3}$), 9.01 (d, 2H, ^{3}J= 3.6 Hz, $H_{\beta 2}$), 8.92 (d, 2H, ^{3}J= 4.7 Hz, $H_{\beta 1}$), 8.19 (d, 2H, H_o, ^{3}J= 8.1 Hz), 8.10 (d, 4H, ^{4}J= 1.7 Hz, $H_{o''}$), 8.09 (d, 2H, ^{4}J= 1.4 Hz, $H_{o'}$), 7.87 (d, 2H, ^{3}J= 8.1 Hz, H_m), 7.80 (td, 3H, ^{4}J= 1.8 and 6.3 Hz, $H_{p'+p''}$), 1.54 (s, 36H, ^{t}Bu), 1.53 (s, 18H, ^{t}Bu), 0.39 (s, 9H, H_{TMS}). Elemental

analysis (%) for $C_{73}H_{84}N_4SiZn$ (1110.95): calcd C 78.92, H 7.62, N 5.04; found C 78.37, H 7.82, N 4.79. UV-visible (CH_2Cl_2): λ_{abs} (ε) = 422 nm (558 097 M^{-1} cm^{-1}), 549 nm (21 483 M^{-1} cm^{-1}), 588 nm (6 159 M^{-1} cm^{-1}). Fluorescence (CH_2Cl_2): λ_{em}= 596, 643 nm.

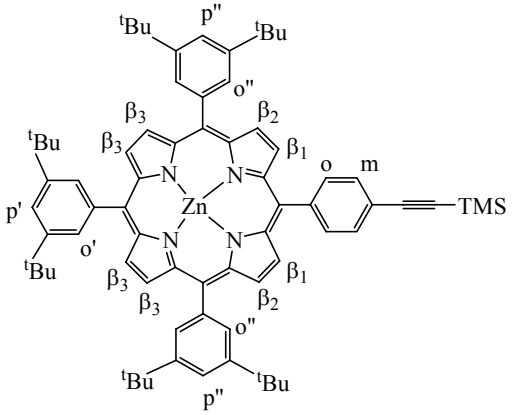

13

Zinc(II) porphyrin with terminal acetylene 14.

To the solution of the compound **13** (5.74 g, 5.17 mmol) in the mixture of solvents tetrahydrofuran/methanol (1:1) (160 mL) K_2CO_3 was added (2.86 g, 20.70 mmol) and the mixture was allowed to stir at r.t. for 4 h. The reaction progress was monitored by TLC in *n*-hexan/dichloromethane (7:3) as an eluent, R_f= 0.58. After evaporation to dryness, the residue was dissolved in dichloromethane and the obtained solution was neutralized with saturated solution of NH_4Cl by gradually by extraction, and then washed with water. The crude product isolated by the solvent removal was dried in vacuum overnight, and then purified by column chromatography (SiO_2; Ø= 5 cm, h= 20 cm; *n*-hexan/dichloromethane (9:1 → 5:5)), yielding the compound **14** as a violet solid (5.21 g, 5.01 mmol, 97%). ^{1}H-NMR ($CDCl_3$, 300 MHz) : δ= 9.05 (s, 4H, $H_{\beta3}$), 9.04 (d, 2H, ^{3}J= 3.5 Hz, $H_{\beta2}$), 8.96 (d, 2H, ^{3}J= 4.7 Hz, $H_{\beta1}$), 8.24 (d, 2H, H_o, ^{3}J= 8.3 Hz), 8.13 (d, 4H, ^{4}J= 1.9 Hz, $H_{o''}$), 8.12 (d, 2H, ^{4}J= 2.0 Hz, $H_{o'}$), 7.91 (d, 2H, ^{3}J= 8.0 Hz, H_m), 7.83 (td, 3H, ^{4}J= 1.8 and 3.8 Hz, $H_{p'+p''}$), 3.32 (s, 1H, $H_{acetylene}$), 1.56 (s, 36H, ^{t}Bu), 1.55 (s, 18H, ^{t}Bu).

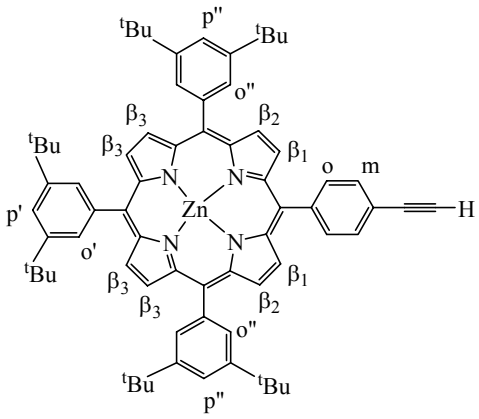

14

Porphyrin-uridine conjugate 15.

The reaction was performed in four batches due to yields acquired at this scale. Thus, 5'-*O*-triisopropylsilyl-5-iodo-2'-deoxyuridine (**6**, 0.31 g, 0.61 mmol) and zinc(II) porphyrin with terminal acetylene (**14**, 0.77 g, 0.74 mmol) were dissolved in triethylamine (15 mL), freshly distilled and deoxygenized by bubbling with argon during 3 h. To this solution $Pd(PPh_3)_2Cl_2$ (0.011 g, 0.015 mmol) and CuI (0.006 g, 0.031 mmol) were added under an argon atmosphere. The mixture was stirred at r.t. for 60 h and then the batches were combined and concentrated under a vacuum. The dark brown residue was dissolved in dichloromethane and successively extracted with EDTA disodium salt (2% solution), $Na_2S_2O_3$ (0.35 M), saturated solution of NH_4Cl, and water. The organic phase was concentrated and to the slurry SiO_2 was added, and then evaporated to dryness. The obtained composite was dried in vacuum overnight and then purified by silica-gel column chromatography (Ø= 5 cm, h= 19 cm; *n*-hexan/ethylacetate (8:2)), yielding the compound **15** as a violet solid (3.07 g, 2.16 mmol, 88%). ^{1}H-NMR ($CDCl_3$, 500 MHz) : δ= 9.00 (d, 2H, ^{3}J= 4.5 Hz, $H_{\beta2}$), 8.99 (s, 4H, $H_{\beta3}$), 8.90 (d, 2H, ^{3}J= 4.5 Hz, $H_{\beta1}$), 8.21 (d, 2H, H_o, ^{3}J= 8.5 Hz), 8.13 (s, 1H, H_6), 8.09 (dd, 6H, J= 2.0 and 4.0 Hz, $H_{o''}$), 7.87 (d, 2H, ^{3}J= 8.0 Hz, H_m), 7.79 (td, 3H, ^{4}J= 2.0 and 6.5 Hz, $H_{p'+p''}$), 6.30 (dd, 1H, $H_{1'}$, ^{3}J= 6.5 and 7.0 Hz), 4.62 (m, 1H, $H_{3'}$), 4.03 (m, 1H, $H_{4'}$), 3.97 (m, 2H, $H_{5'}$), 2.45 (ddd, 1H, $H_{2'}$, ^{3}J= 3.1 and 6.0 Hz and ^{2}J= 13.6 Hz), 2.26 (ddd, 1H, $H_{2'}$, ^{3}J= 5.8 and 7.3 Hz and ^{2}J= 13.9 Hz), 1.53 (s, 36H, ^{t}Bu), 1.52 (s, 18H, ^{t}Bu), 1.26 (s, 3H, CH_{TIPS}), 1.15 (d, 9H, $CH_{3,TIPS}$, ^{3}J= 3.5 Hz), 1.13 (d, 9H, $CH_{3,TIPS}$, ^{3}J= 3.6 Hz). Elemental analysis (%) for $C_{88}H_{106}N_6O_5SiZn$ (1421.30): calcd C 74.36, H 7.52, N 5.91; found C 74.21, H 7.72, N 5.21.

UV-visible (CH_2Cl_2): λ_{abs} (ε) = 423 nm (569 120 M^{-1} cm^{-1}), 549 nm (21 793 M^{-1} cm^{-1}), 589 nm (6 173 M^{-1} cm^{-1}).

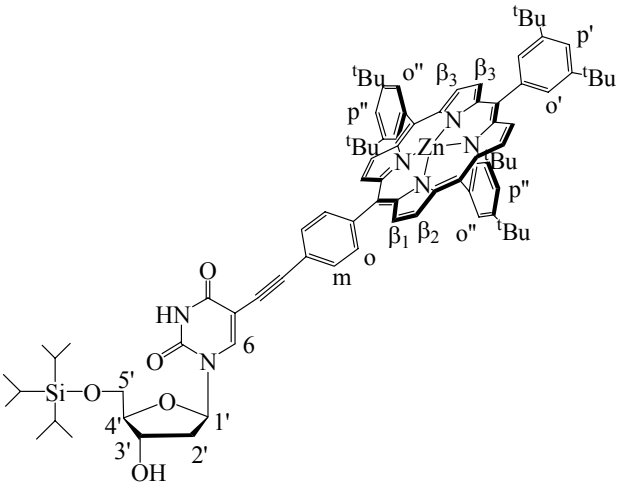

15

Methyltiomethyl *p*-metoxybenzyl ether 16.

A mixture of NaH (2.03 g, 50.66 mmol) in DME (25 mL) is placed in round-bottom flask equipped with an addition funnel filled with the solution of 4-metoxybenzylalcohol (3.50 g, 25.33 mmol) in DME (5 mL). The whole system was deaerated and flushed with argon. To the suspension of NaH, which was cooled using the ice-salt bath, the solution of the corresponding alcohol was added dropwise during 15 min under argon. To this reaction mixture were successively added NaI (3.84 g, 25.33 mmol) and chloromethyl methyl sulfide (2.20 mL, 25.33 mmol). After stirring at 0 °C for 1 h, the reaction mixture was allowed to warm to r.t. at which it was stirred for 5 h. The mixture was then poured into water under continuous stirring, and then the organic phase was separated and aqueous was extracted with ether. The combined organic extracts were evaporated and obtained yellow oil dried in vacuum. The crude product was purified by using short column of silica-gel (*n*-hexan/ethylacetate (9:1)) to afford pure methyltiomethyl ether **16** as clear yellow oil (4.52 g, 19.71 mmol, 90%). ^{1}H-NMR ($CDCl_3$, 300 MHz) : δ= 7.28 (AB, 2H, ^{3}J= 2.7 and 4.9 Hz, H_d), 6.90 (AB, 2H, ^{3}J= 2.7 and 4.9 Hz, H_c), 4.66 (s, 2H, H_a), 4.55 (s, 2H, H_b), 3.81 (s, 3H, H_e), 2.18 (s, 3H, H_f).

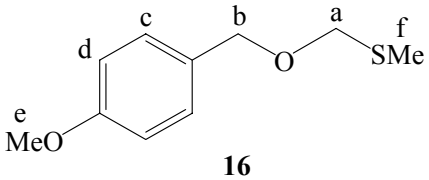

16

Chloromethyl *p*-metoxybenzyl ether 17.

The solution of *O*,*S*-acetal (**16**, 0.50 g, 2.52 mmol) in CH_2Cl_2 (10 mL) is placed in round-bottom flask equipped with an addition funnel filled with the solution of sulfuryl chloride (0.31 mL, 3.78 mmol) in CH_2Cl_2 (5 mL). The whole system was deaerated and flushed with argon. To the solution of **16**, which was cooled to -78 °C, the solution of SO_2Cl_2 was added dropwise during 30 min under argon. From a light protected obtained clear yellow solution was allowed to stir at the same temperature for another 1.5 h. Since the product **17** is rather unstable and decomposes on heating and storage, removing of the solvent via rotaevaporation and subsequent drying in vacuum should be done at room temperature and preferably protected from light. The compound **17** was obtained as pale yellow oil, which was used without further purification due; the yield was considered to be 70%. ^{1}H-NMR ($CDCl_3$, 300 MHz) : δ= 7.29 (AB, 2H, ^{3}J= 2.9 and 5.1 Hz, H_d), 6.90 (AB, 2H, ^{3}J= 2.7 and 5.0 Hz, H_c), 5.50 (s, 2H, H_a), 4.69 (s, 2H, H_b), 3.82 (s, 3H, H_e).

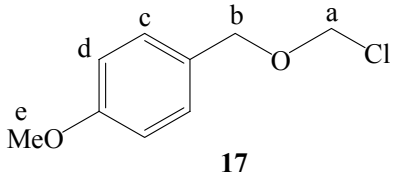

17

Porphyrin-uridine conjugate protected at *N*-3 18.

Porphyrin-uridine conjugate **15** (1.00 g, 0.70 mmol) was suspended in acetonitrile (50 mL) and obtained mixture was allowed to stir for 15 min. This homogeneous solution was deaerated and flushed with argon, and then cooled down to 0 °C. To this mixture DBU (0.23 mL, 1.55 mmol) was added and then chloromethyl *p*-metoxybenzyl ether (**17**, 0.26 mL, 1.41 mmol) was added in portions under argon atmosphere. After an addition was completed the

solution was stirred for another 3 h at 0 °C. The product formation was followed by TLC in *n*-hexan/ethylacetate (5:5) as an eluent, R_f= 0.52. After the reaction mixture was concentrated, the residue was dissolved in dichloromethane. This solution was washed with three portions of water, then evaporated and dried in vacuum overnight. The crude product was purified by column chromatography (SiO_2; Ø= 2 cm, h= 28 cm; *n*-hexan/ethylacetate (8:2 → 2:8)), yielding the compound **18** as a violet solid (0.88 g, 0.56 mmol, 80%). ^{1}H-NMR ($CDCl_3$, 300 MHz) : δ = 9.02 (d, 2H, ^{3}J= 4.6 Hz, $H_{\beta2}$), 9.00 (s, 4H, $H_{\beta3}$), 8.92 (d, 2H, ^{3}J= 4.7 Hz, $H_{\beta1}$), 8.22 (d, 2H, H_o, ^{3}J= 8.2 Hz), 8.13 (s, 1H, H_6), 8.09 (d, 4H, ^{4}J= 1.8 Hz, $H_{o''}$), 8.08 (d, 2H, ^{4}J= 1.8 Hz, $H_{o'}$), 7.89 (d, 2H, ^{3}J= 8.2 Hz, H_m), 7.79 (td, 3H, ^{4}J= 1.8 and 4.8 Hz, $H_{p'+p''}$), 7.38 (d, 2H, ^{3}J= 8.8 Hz, H_d), 6.90 (d, 2H, ^{3}J= 8.8 Hz, H_c), 6.30 (t, 1H, $H_{1'}$, ^{3}J= 6.5 Hz), 5.55 (s, 2H, H_a), 4.71 (s, 2H, H_b), 4.60 (m, 1H, $H_{3'}$), 4.00 (ABM, 2H, $H_{5'}$, ^{3}J= 1.9 and 2.4 Hz and ^{2}J= 8.9 Hz), 3.99 (m, 1H, $H_{4'}$), 3.82 (s, 3H, H_e), 2.46 (ddd, 1H, $H_{2'}$, ^{3}J= 3.0 and 5.7 Hz and ^{2}J= 13.5 Hz), 2.20 (ddd, 1H, $H_{2'}$, ^{3}J= 6.0 and 7.7 Hz and ^{2}J= 13.8 Hz), 1.54 (s, 36H, ^{t}Bu), 1.53 (s, 18H, ^{t}Bu), 1.26 (s, 3H, CH_{TIPS}), 1.18 (d, 9H, $CH_{3,TIPS}$, ^{3}J= 3.5 Hz), 1.15 (d, 9H, $CH_{3,TIPS}$, ^{3}J= 3.5 Hz). Elemental analysis (%) for $C_{97}H_{116}N_6O_7SiZn$ (1571.47): calcd C 74.14, H 7.44, N 5.35; found C 73.41, H 7.56, N 5.08 (+ 1ethylacetate).

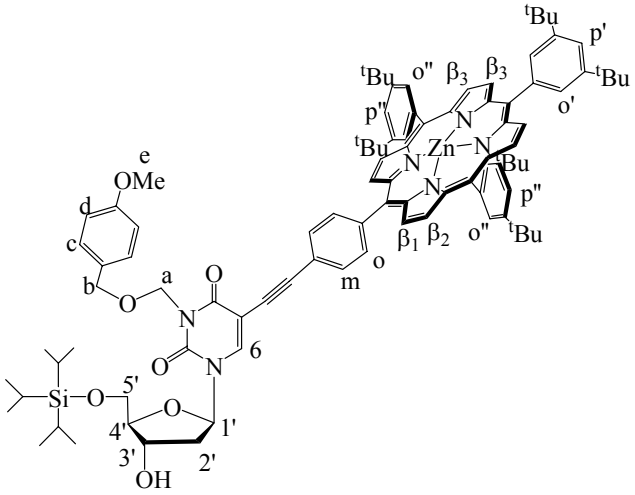

18

Monomer 1.

The whole system, round-bottom flask equipped with a magnetic stirring bar and an addition funnel was extra dried, deaerated and flushed with argon. The suspension of NaH (0.005 g, 0.12 mmol) in dry THF (2.0 mL) was cooled using an ice-salt bath, and then charged with the uridine-porphyrin conjugate **18** (0.10 g, 0.064 mmol). The mixture was stirred at 0 °C for 1 h and then at r.t. for 4 h to complete deprotonation. Again the reaction was cooled using an ice-salt bath and charged with TBAI (0.007 g, 0.0191 mmol), and then an addition funnel was filled with the solution of *tert*-butyl 2-bromoacetate (0.012 mL, 0.083 mmol) in dry THF (0.1 mL), which was added dropwise into the reaction under an argon atmosphere. The mixture was then stirred overnight, allowing it to slowly warm to r.t.. The product formation was followed by TLC in *n*-hexan/ethylacetate (7.5:2.5) as an eluent, R_f= 0.40. Removal of solvent via rotaevaporation afforded residue which was then dissolved in dichloromethane. The corresponding solution was washed with one portion of saturated solution of NH_4Cl and two portions of water, before it was evaporated to dryness. The crude product was purified by using column chromatography (SiO_2; Ø= 1 cm, h= 22 cm; *n*-hexan/ethylacetate (9:1 → 6:4)), to yield monomer **1** as a violet solid (0.067 g, 0.040 mmol, 62%) together with residual unreacted **18** (0.03 g, 0.020 mmol, 29%). ^{1}H-NMR ($CDCl_3$, 300 MHz) : δ = 9.02 (d, 2H, ^{3}J= 4.4 Hz, $H_{\beta2}$), 9.01 (s, 4H, $H_{\beta3}$), 8.92 (d, 2H, ^{3}J= 4.7 Hz, $H_{\beta1}$), 8.21 (d, 2H, H_o, ^{3}J= 8.4 Hz), 8.19 (s, 1H, H_6), 8.09 (d, 4H, ^{4}J= 2.0 Hz, $H_{o''}$), 8.08 (d, 2H, ^{4}J= 2.0 Hz, $H_{o'}$), 7.88 (d, 2H, ^{3}J= 8.2 Hz, H_m), 7.79 (td, 3H, ^{4}J= 1.8 and 4.7 Hz, $H_{p'+p''}$), 7.39 (d, 2H, ^{3}J= 8.8 Hz, H_d), 6.91 (d, 2H, ^{3}J= 8.7 Hz, H_c), 6.38 (dd, 1H, $H_{1'}$, ^{3}J= 7.9 and 5.7 Hz), 5.57 (s, 2H, H_a), 4.72 (s, 2H, H_b), 4.34 (m, 1H, $H_{3'}$), 4.30 (m, 1H, $H_{4'}$), 4.06 (dd, 2H, $H_{5'}$, ^{3}J= 2.0 and 3.0 Hz and ^{2}J= 9.0 Hz), 4.04 (AB, 2H, $CH_{2,\ ether}$, ^{2}J= 16.38 Hz), 3.82 (s, 3H, H_e), 2.63 (ddd, 1H, $H_{2'}$, ^{3}J= 1.9 and 5.6 Hz and ^{2}J= 13.8 Hz), 2.12 (ddd, 1H, $H_{2'}$, ^{3}J= 6.6 and 8.1 Hz and ^{2}J= 14.4 Hz), 1.53 (s, 36H, ^{t}Bu), 1.52 (s, 18H, ^{t}Bu), 1.51 (s, 9H, ^{t}Bu), 1.26 (s, 3H, CH_{TIPS}), 1.18 (d, 9H, $CH_{3,TIPS}$, ^{3}J= 3.3 Hz), 1.16 (d, 9H, $CH_{3,TIPS}$, ^{3}J= 3.4 Hz). ^{1}H-NMR ($(CD_3)_2CO$, 500 MHz, c= 2.966 x 10^{-7} M) : δ = 8.93 (d, 2H, ^{3}J= 4.6 Hz, $H_{\beta2}$), 8.90 (s, 4H, $H_{\beta3}$), 8.90 (d, 2H, ^{3}J= 4.6 Hz, $H_{\beta1}$), 8.29 (d, 2H, H_o, ^{3}J= 6.4 Hz), 8.24 (s, 1H, H_6), 8.11 (d, 4H, ^{4}J= 1.6 Hz, $H_{o''}$), 8.10 (d, 2H, ^{4}J= 1.8 Hz, $H_{o'}$), 7.94 (s, 2H, H_m), 7.93 (td, 3H, ^{4}J= 1.8 and 3.7 Hz, $H_{p'+p''}$), 7.34 (AB, 2H, ^{3}J= 2.8 and 4.8 Hz, H_d), 6.93 (AB, 2H, ^{3}J= 2.8 and 4.8 Hz, H_c), 6.32 (dd, 1H, $H_{1'}$, ^{3}J= 5.7 and 8.0 Hz), 5.52 (s, 2H, H_a), 4.67 (s, 2H, H_b), 4.44 (td, 1H, $H_{3'}$, ^{3}J= 2.0 and 5.7 Hz), 4.25 (m, 1H, $H_{4'}$), 4.10 (dd, 2H, $H_{5'}$, ^{3}J= 2.7 Hz and ^{2}J= 8.6 Hz), 4.05 (AB, 2H, $CH_{2,\ ether}$, J= 7.1 Hz), 3.81 (s, 3H, H_e), 2.62 (ddd, 1H, $H_{2'}$, ^{3}J= 2.0 and 5.8 Hz and ^{2}J= 14.1 Hz), 2.29 (ddd, 1H, $H_{2'}$, ^{3}J= 6.1 and 8.1 Hz and

^{2}J= 14.2 Hz), 1.56 (s, 36H, ^{t}Bu), 1.55 (s, 18H, ^{t}Bu), 1.49 (s, 9H, ^{t}Bu), 1.28 (s, 3H, CH_{TIPS}), 1.21 (d, 9H, $CH_{3,TIPS}$, ^{3}J= 4.6 Hz), 1.20 (s, 9H, $CH_{3,TIPS}$, ^{3}J= 4.6 Hz). Elemental analysis (%) for $C_{103}H_{126}N_6O_9SiZn$ (1685.61): calcd C 73.39, H 7.53, N 4.99; found C 73.13, H 7.44, N 4.62.

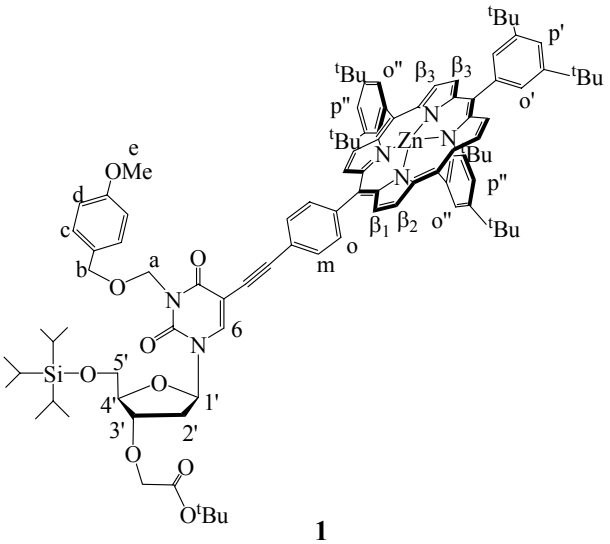

1

Monomer-alcohol 19.

Monomer **1** (1.00g, 0.59 mmol) was dissolved in THF (30 mL), and TBAF (2.0 mL, 1.19 mmol, 1M solution in THF) was added. The mixture was deareated and flushed with argon, and then left to stir at r.t. for 5 h under an argon atmosphere. The formation of the product was followed by TLC in *n*-hexan/ethylacetate (6.5:3.5) as an eluent, R_f= 0.44. The solvent was removed by evaporation and the residue was dissolved in dichloromethane. The obtained solution was washed with three portions of water, and organic phase was removed under reduced pressure. Finally the pure product was isolated by silica-gel column chromatography (Ø= 3 cm, h= 23 cm; *n*-hexan/ethylacetate (8:2)), to afford monomer-alcohol **19** as a violet solid (0.86 g, 0.565 mmol, 96%). ^{1}H-NMR ($CDCl_3$, 300 MHz) : δ= 9.05 (d, 2H, ^{3}J= 4.1 Hz, $H_{\beta 2}$), 9.04 (s, 4H, $H_{\beta 3}$), 9.00 (d, 2H, ^{3}J= 4.7 Hz, $H_{\beta 1}$), 8.25 (d, 2H, H_o, ^{3}J= 8.1 Hz), 8.13 (d, 4H, ^{4}J= 1.8 Hz, $H_{o''}$), 8.12 (d, 2H, ^{4}J= 1.8 Hz, $H_{o'}$), 8.04 (s, 1H, H_6), 7.94 (d, 2H, ^{3}J= 8.1 Hz, H_m), 7.83 (m, 3H, $H_{p'+p''}$), 7.36 (d, 2H, ^{3}J= 6.9 Hz, H_d), 6.89 (d, 2H, ^{3}J= 7.0 Hz, H_c), 6.04 (t, 1H, $H_{1'}$, ^{3}J= 6.4 Hz), 5.53 (s, 2H, H_a), 4.70 (s, 2H, H_b), 4.18 (td, 1H, $H_{3'}$, ^{3}J= 4.2 and 8.1 Hz), 4.00 (AB, 2H, $CH_{2,\ ether}$, ^{2}J= 16.5 Hz), 3.95-3.71 (m, 3H, $H_{4'}$+$H_{5'}$), 3.81 (s, 3H, H_e), 2.44 (ddd,

1H, $H_{2'}$, ^3J= 4.2 and 6.0 Hz and ^2J= 13.5 Hz), 2.27 (td, 1H, $H_{2'}$, ^3J= 6.3 Hz and ^2J= 13.2 Hz), 1.56 (s, 36H, ^{t}Bu), 1.55 (s, 18H, ^{t}Bu), 1.50 (s, 9H, ^{t}Bu).

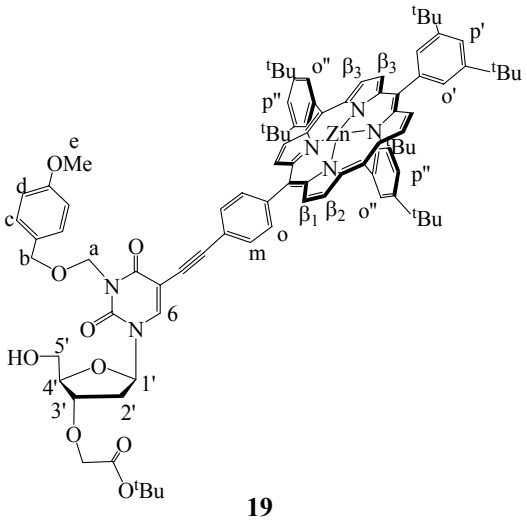

19

Monomer-acid 20.

Monomer **1** (1.00g, 0.59 mmol) was dissolved in CH_2Cl_2 stabilized with amylene (25 mL) and solution was cooled using an ice-salt bath, and then TFA (5.0 mL, 0.065 mol) was added. The mixture was flushed with argon, and then left to stir. After 1 h at 0 °C, the bath was removed and the mixture allowed to warm to r.t.. The reaction was stirred for 5 h at r.t. when it was judged complete by TLC analysis in the mixture of ethylacetate/methanol (8.5:1.5) with few drops of acetic acid (R_f (**20**)= 0.48). The reaction solution was diluted and successively washed with water until pH of an aqueous phase was 7. The solvent from the organic phase was removed by evaporation, and subsequently the crude product was dried in vacuum overnight. Finally the pure product was isolated by silica-gel column chromatography (Ø= 2 cm, h= 30 cm; ethylacetate + 0.1% of acetic acid and gradually increased methanol up to 5%), to yield monomer-acid **20** as a violet solid (0.63 g, 0.445 mmol, 75%). ^{1}H-NMR ($CDCl_3$, 300 MHz) : δ= 8.90 (d, 2H, ^3J= 4.3 Hz, $H_{\beta2}$), 8.89 (s, 4H, $H_{\beta3}$), 8.80 (d, 2H, ^3J= 4.8 Hz, $H_{\beta1}$), 8.21 (d, 2H, H_o, ^3J= 8.0 Hz), 8.22 (s, 1H, H_6), 8.08 (d, 4H, ^4J= 1.8 Hz, $H_{o''}$), 8.07 (d, 2H, ^4J= 2.2 Hz, $H_{o'}$), 7.88 (d, 2H, ^3J= 8.2 Hz, H_m), 7.79 (td, 3H, ^4J= 1.7 and 3.3 Hz, $H_{p'+p''}$), 6.38 (dd, 1H, $H_{1'}$, ^3J= 5.7 and 8.0 Hz), 4.39 (m, 1H, $H_{3'}$), 4.31 (m, 1H, $H_{4'}$), 4.23 (s, 2H, $CH_{2,\ ether}$), 4.06 (ABM, 2H, $H_{5'}$, ^3J= 1.4 and 3.0 Hz and ^2J= 9.6 Hz), 2.67 (ddd, 1H, $H_{2'}$, ^3J= 1.5 and 5.6 Hz and ^2J= 13.3 Hz), 2.18 (ddd, 1H, $H_{2'}$, ^3J= 6.4 and 7.9 Hz and ^2J= 14.3 Hz), 1.52 (s, 54H, ^{t}Bu),

1.26 (s, 3H, CH_{TIPS}), 1.19 (d, 9H, $CH_{3,TIPS}$, ^3J= 3.6 Hz), 1.16 (d, 9H, $CH_{3,TIPS}$, ^3J= 3.7 Hz), -2.7 (s, 2H, NH).

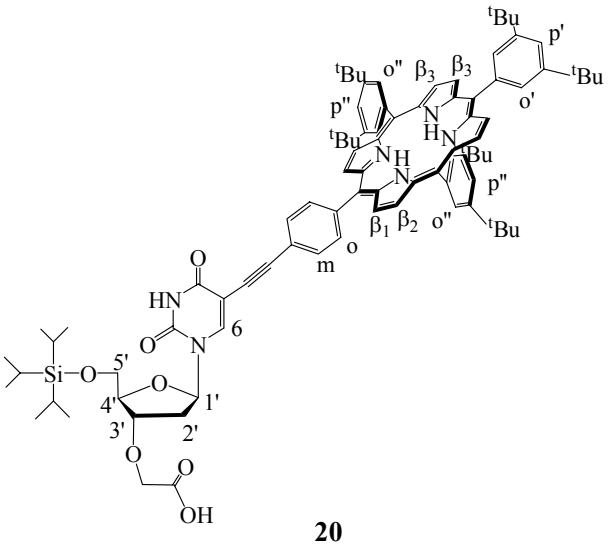

20

Dimer 2.

Monomer-alcohol **19** (0.66 g, 0.430 mmol) and monomer-acid **20** (0.61 g, 0.430 mmol) were dissolved in dichloromethane (without ethanol and dried over molecular sieves, 40 mL) and to this solution DMAP (0.11 g, 0.903 mmol) and DCC (0.12 g, 0.602 mmol) were added, respectively. The obtained mixture was allowed to stir at r.t. overnight under an argon atmosphere. The reaction progress was followed by TLC analysis examining the disappearance of the both starting materials and formation of the product (*n*-hexan/ethylacetate (6.5:3.5), R_f= 0.31). The solvent was removed to dryness via rotaevaporation and afforded residue was suspended in minimum volume of toluene. The slurry was placed in refrigerator for 3 h to precipitate DCU. The precipitated white solid was collected by filtration and washed with small portions of chilled toluene. The obtained filtrate was evaporated *in vacuo* and then left to dry in a vacuum overnight. The crude product was purified by using column chromatography (SiO_2; Ø= 3 cm, h= 30 cm; *n*-hexan/ethylacetate (8:2 → 6:4)) and preparative size exclusion chromatography (Bio-Beads, toluene), yielding dimer **2** as a violet solid (0.92 g, 0.314 mmol, 73%). ^{1}H-NMR ($CDCl_3$, 500 MHz, *c*= 3.027 x 10^{-3} M) : δ= 9.01 (d, 2H, ^3J= 4.6 Hz, *Zn*-$H_{\beta2}$), 8.99 (s, 4H, *Zn*-$H_{\beta3}$), 8.92 (d, 2H, ^3J= 4.7 Hz, *Zn*-$H_{\beta1}$), 8.89 (s, 4H, *2H*-$H_{\beta3}$), 8.88 (d, 2H, ^3J= 4.6 Hz, *2H*-$H_{\beta2}$), 8.76 (d, 2H, ^3J= 4.7 Hz, *2H*-

$H_{\beta 1}$), 8.25 (d, 2H, *Zn*-H_o, ^{3}J= 8.5 Hz), 8.16 (d, 2H, *2H*-H_o, ^{3}J= 8.0 Hz), 8.10 (t, 4H, ^{4}J= 1.3 Hz, *Zn*-$H_{o'}$), 8.08 (d, 2H, ^{4}J= 1.8 Hz, *Zn*-$H_{o'}$), 8.07 (d, 6H, ^{4}J= 1.8 Hz, *2H*-$H_{o'}$), 8.06 (s, 1H, *2H*-H_6), 7.93 (d, 2H, ^{3}J= 8.0 Hz, *Zn*-H_m), 7.92 (s, 1H, *Zn*-H_6), 7.78 (td, 5H, ^{4}J= 1.5 and 3.5 Hz, $H_{p'}$), 7.76 (t, 1H, ^{4}J= 2.0 Hz, $H_{p'}$), 7.75 (d, 2H, ^{3}J= 8.0 Hz, *2H*-H_m), 7.39 (d, 2H, ^{3}J= 9.0 Hz, H_d), 6.92 (d, 2H, ^{3}J= 8.5 Hz, H_c), 6.31 (t, 1H, *Zn*-$H_{1'}$, ^{3}J= 6.5 Hz), 6.28 (dd, 1H, *2H*-$H_{1'}$, ^{3}J= 8.0, ^{4}J=5.0 Hz), 5.57 (s, 2H, H_a), 4.73 (s, 2H, H_b), 4.55 (ABM, 2H, *2H*-$CH_{2,\ ether}$, ^{3}J= 3.5 and 4.3 Hz and ^{2}J= 7.8 Hz), 4.45 (q, 1H, *Zn*-$H_{4'}$, ^{3}J= 4.0 Hz), 4.41 (d, 1H, *2H*-$H_{3'}$, ^{3}J= 5.5 Hz), 4.39 (s, 2H, *Zn*-$CH_{2,\ ether}$), 4.31 (m, 1H, *2H*-$H_{4'}$), 4.29 (m, 1H, *Zn*-$H_{3'}$), 4.07 (AB, 2H, *Zn*-$H_{5'}$, ^{2}J= 16.5 Hz), 4.02 (ABM, 2H, *2H*-$H_{5'}$, ^{3}J= 1.0 and 1.8 Hz and ^{2}J= 10.0 Hz), 3.82 (s, 3H, H_e), 2.68 (ddd, 1H, *2H*-$H_{2'}$, ^{3}J= 3.0 and 5.5 Hz and ^{2}J= 14.3 Hz), 2.60 (ddd, 1H, *Zn*-$H_{2'}$, ^{3}J= 5.3 and 6.8 Hz and ^{2}J= 13.8 Hz), 2.27 (dd, 1H, *Zn*-$H_{2'}$, ^{3}J= 7.5 Hz and ^{2}J= 14.3 Hz), 2.11 (ddd, 1H, *2H*-$H_{2'}$, ^{3}J= 6.2 and 8.6 Hz and ^{2}J= 13.9 Hz), 1.53 (s, 72H, ^{t}Bu), 1.52 (s, 36H, ^{t}Bu), 1.51 (s, 9H, ^{t}Bu), 1.25 (s, 3H, CH_{TIPS}), 1.12 (d, 9H, $CH_{3,TIPS}$, ^{3}J= 4.0 Hz), 1.11 (d, 9H, $CH_{3,TIPS}$, ^{3}J= 3.5 Hz), -2.70 (s, 2H, NH). ^{1}H-NMR ($(CD_3)_2CO$, 500 MHz, c= 2.6 x 10^{-3} M) : δ= 8.92 (m, 8H, *Zn*-$H_{\beta 2}$+$H_{\beta 1}$+$H_{\beta 3}$), 8.88 (m, 8H, *2H*- $H_{\beta 2}$+$H_{\beta 1}$+$H_{\beta 3}$), 8.31 (d, 2H, *Zn*-H_o, ^{3}J= 8.2 Hz), 8.25 (d, 2H, *2H*-H_o, ^{3}J= 8.5 Hz), 8.24 (s, 1H, *Zn*-H_6), 8.20 (s, 1H, *2H*-H_6), 8.14 (d, 2H, *Zn*-$H_{o'}$, ^{4}J= 2.0 Hz), 8.13 (d, 3H, *Zn*-$H_{o'}$, ^{4}J= 1.8 Hz), 8.11 (d, 4H, ^{4}J= 1.6 Hz, *2H*-$H_{o'}$), 8.07 (d, 2H, ^{4}J= 1.7 Hz, *2H*-$H_{o'}$), 8.00 (d, 2H, ^{3}J= 8.3 Hz, *Zn*-H_m), 7.96 (t, 1H, ^{4}J= 1.8 Hz, *Zn*-$H_{p'}$), 7.94 (t, 2H, ^{4}J= 1.8 Hz, *Zn*-$H_{p'}$), 7.89 (td, 3H, ^{4}J= 1.8 and 3.7 Hz, *2H*-$H_{p'}$), 7.83 (d, 2H, ^{3}J= 8.3 Hz, *2H*-H_m), 7.34 (d, 2H, ^{3}J= 8.8 Hz, H_d), 6.92 (d, 2H, ^{3}J= 8.7 Hz, H_c), 6.36 (m, 2H, $H_{1'}$-*Zn*+*2H*), 5.52 (s, 2H, H_a), 4.66 (s, 2H, H_b), 4.60 (AB, 2H, *Zn*-$H_{5'}$, ^{2}J= 16.5 Hz), 4.60 (d, 1H, *2H*-$H_{3'}$, ^{3}J= 5.6 Hz), 4.52 and 4.44 (m, 1H, *Zn*-$H_{3'}$), 4.47 (q, 1H, *Zn*-$H_{4'}$, ^{3}J= 3.1 Hz), 4.37 (m, 1H, *2H*-$H_{4'}$), 4.18 (s, 2H, *Zn*-$CH_{2,\ ether}$), 4.09 (m, 2H, *2H*-$H_{5'}$), 3.79 (s, 3H, H_e), 2.70 (m, 1H, *2H*-$H_{2'}$), 2.66 (m, 1H, *Zn*-$H_{2'}$), 2.53 (ddd, 1H, *2H*-$H_{2'}$, ^{3}J= 6.3 and 7.0 Hz and ^{2}J= 14.0 Hz), 2.33 (ddd, 1H, *Zn*-$H_{2'}$, ^{3}J= 6.1 and 8.5 Hz and ^{2}J= 14.2 Hz), 1.56 (s, 27H, *Zn*-^{t}Bu), 1.54 (s, 27H, *Zn*-^{t}Bu + 9H, *2H*-^{t}Bu), 1.53 (s, 27H, *2H*-^{t}Bu), 1.50 (s, 18H, *2H*-^{t}Bu), 1.49 (s, 9H, ^{t}Bu), 1.27 (s, 3H, CH_{TIPS}), 1.13 (d, 9H, $CH_{3,TIPS}$, ^{3}J= 4.7 Hz), 1.12 (d, 9H, $CH_{3,TIPS}$, ^{3}J= 4.7 Hz), -2.71 (s, 2H, NH). Analysis by NMR included as well COSY and ROESY experiments in the both solvents, $CDCl_3$ and $(CD_3)_2CO$. Elemental analysis (%) for $C_{184}H_{214}N_{12}O_{15}SiZn$ (2927.21): calcd C 75.50, H 7.37, N 5.74; found C 75.49, H 7.69, N 5.35. UV-visible (CH_2Cl_2): λ_{abs} (ε) = 422 nm (795 631 M^{-1} cm^{-1}), 517 nm (18 801 M^{-1} cm^{-1}), 552 nm (29 005 M^{-1} cm^{-1}), 592 nm (11 856 M^{-1} cm^{-1}), 647 nm (5 457 M^{-1} cm^{-1}). Fluorescence (CH_2Cl_2): λ_{em}= 597, 651 and 710 nm. MALDI-TOF MS: *m/z*= 2927.9 ([M^+] calcd 2927.2).

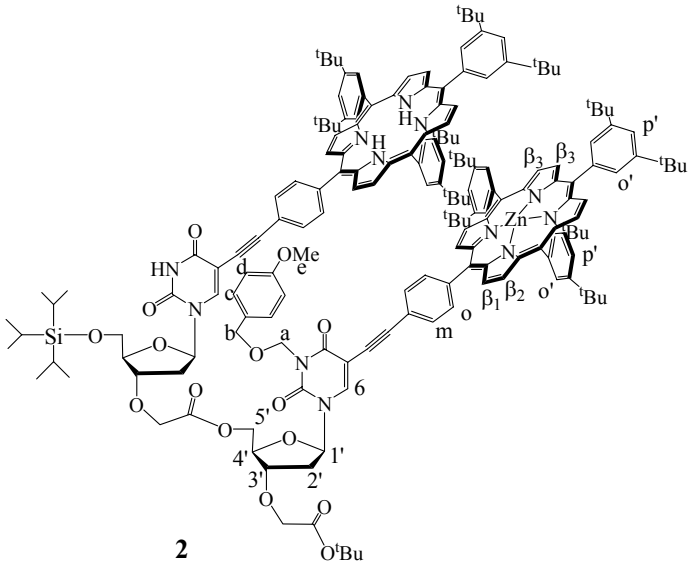

2

Dimer-alcohol 21.

Dimer **2** (0.32g, 0.11 mmol) was dissolved in THF (10 mL), and TBAF (0.22 mL, 0.22 mmol, 1M solution in THF) was added. The mixture was deareated and flushed with argon, and then left to stir at r.t. for 4 h under an argon atmosphere. The formation of the product was followed by TLC in *n*-hexan/ethylacetate (4.5:5.5) as an eluent, R_f= 0.52. The solvent was removed by evaporation and the residue was dissolved in dichloromethane. The obtained solution was washed with two portions of water, and organic phase was removed under reduced pressure. Finally the pure product was isolated by silica-gel column chromatography (Ø= 2 cm, h= 30 cm; *n*-hexan/ethylacetate (7:3)), to afford dimer-alcohol **21** as a violet solid (0.27 g, 0.097 mmol, 89%). ^{1}H-NMR ($CDCl_3$, 300 MHz) : δ= 9.07 (d, 2H, ^{3}J= 4.7 Hz, *Zn*-$H_{\beta 2}$), 9.04 (s, 4H, *Zn*-$H_{\beta 3}$), 9.00 (d, 2H, ^{3}J= 4.7 Hz, *Zn*-$H_{\beta 1}$), 8.93 (s, 4H, *2H*-$H_{\beta 3}$), 8.92 (d, 2H, ^{3}J= 4.6 Hz, *2H*-$H_{\beta 2}$), 8.81 (d, 2H, ^{3}J= 4.7 Hz, *2H*-$H_{\beta 1}$), 8.33 (d, 2H, *Zn*-H_o, ^{3}J= 8.1 Hz), 8.18 (d, 2H, *2H*-H_o, ^{3}J= 8.3 Hz), 8.15 (t, 4H, ^{4}J= 1.8 Hz, *Zn*-$H_{o'}$), 8.13 (d, 2H, ^{4}J= 1.8 Hz, *Zn*-$H_{o'}$), 8.11 (d, 6H, ^{4}J= 1.7 Hz, *2H*-$H_{o'}$), 8.00 (d, 2H, ^{3}J= 8.3 Hz, *Zn*-H_m), 7.97 (s, 1H, *Zn*-H_6), 7.83 (m, 3H, $H_{p'}$), 7.80 (m, 3H, $H_{p'}$), 7.77 (s, 1H, *2H*-H_6), 7.74 (d, 2H, ^{3}J= 8.0 Hz, *2H*-H_m), 7.38 (d, 2H, ^{3}J= 8.6 Hz, H_d), 6.91 (d, 2H, ^{3}J= 8.6 Hz, H_c), 6.03 (m, 2H, $H_{1'}$), 5.55 (s, 2H, H_a), 4.73 (s, 2H, H_b), 4.20 (m, 12H, $CH_{2,\ ether}$, $H_{4'}$, $H_{3'}$, $H_{5'}$-*Zn* and *2H*), 3.79 (s, 3H, H_e), 2.56 (m, 2H, $H_{2'}$), 2.26 (m, 2H, $H_{2'}$), 1.55 (s, 72H, ^{t}Bu), 1.53 (s, 36H, ^{t}Bu), 1.52 (s, 9H, ^{t}Bu), -2.67 (s, 2H, NH).

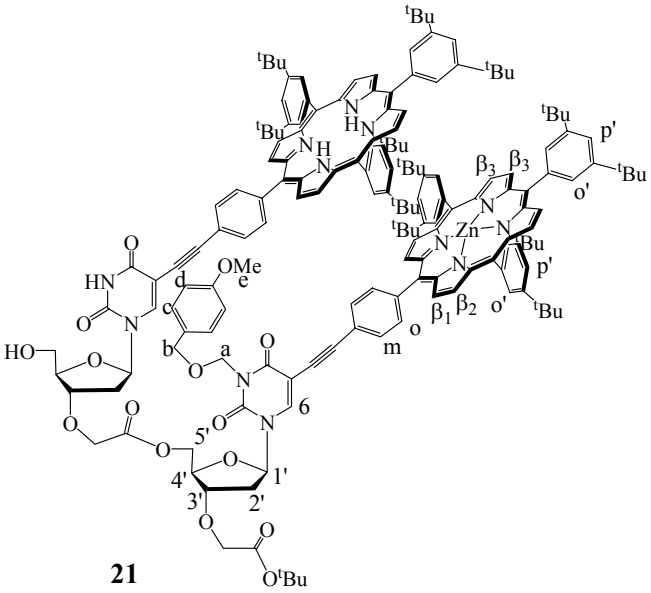

21

Dimer-acid 22.

Dimer **2** (0.42g, 0.14 mmol) was dissolved in CH_2Cl_2 stabilized with amylene (10 mL) and solution was cooled using an ice-salt bath, and then TFA (2.0 mL, 0.026 mol) was added. The mixture was flushed with argon, and then left to stir. After 1 h at 0 °C, the bath was removed and the mixture allowed to warm to r.t.. The reaction was stirred for 6 h at r.t. when it was judged complete by TLC analysis in the mixture of ethylacetate/methanol (9.5:0.5) with few drops of acetic acid (R_f= 0.32). The reaction solution was diluted and successively washed with water until pH of an aqueous phase was 7. The solvent from the organic phase was removed by evaporation, and subsequently the crude product was dried in vacuum overnight. Finally the pure product was isolated by silica-gel column chromatography (Ø= 2 cm, h= 30 cm; ethylacetate + 0.1% of acetic acid and gradually increased methanol up to 15%), to yield dimer-acid **22** as a violet solid (0.28 g, 0.11 mmol, 73%). ^{1}H-NMR ($CDCl_3$, 500 MHz) : δ= 8.86 (m, 16H, $H_{\beta2}$ $H_{\beta3}$ $H_{\beta1}$-*Zn* and *2H*), 8.25 (m, 3H, H_o+H_6), 8.21 (d, 2H, H_o, ^{3}J= 8.3 Hz), 8.08 (m, 12H, $H_{o'}$), 8.06 (s, 1H, H_6), 7.94 (d, 2H, ^{3}J= 8.1 Hz, H_m), 7.88 (d, 2H, ^{3}J= 8.2 Hz, H_m), 7.78 (m, 6H, $H_{p'}$), 6.36 (m, 2H, $H_{1'}$), 4.22 (m, 12H, $CH_{2,\ ether}$, $H_{4'}$, $H_{3'}$, $H_{5'}$-*Zn* and *2H*), 2.60 (m, 2H, $H_{2'}$), 2.34 (m, 2H, $H_{2'}$), 1.52 (s, 27H, ^{t}Bu), 1.51 (s, 27H, ^{t}Bu), 1.50 (s, 36H, ^{t}Bu), 1.49 (s, 18H, ^{t}Bu), 1.27 (s, 3H, CH_{TIPS}), 1.14 (d, 9H, $CH_{3,TIPS}$, ^{3}J= 2.5 Hz), 1.12 (d, 9H, $CH_{3,TIPS}$, ^{3}J= 2.6 Hz), -2.70 (s, 4H, NH).

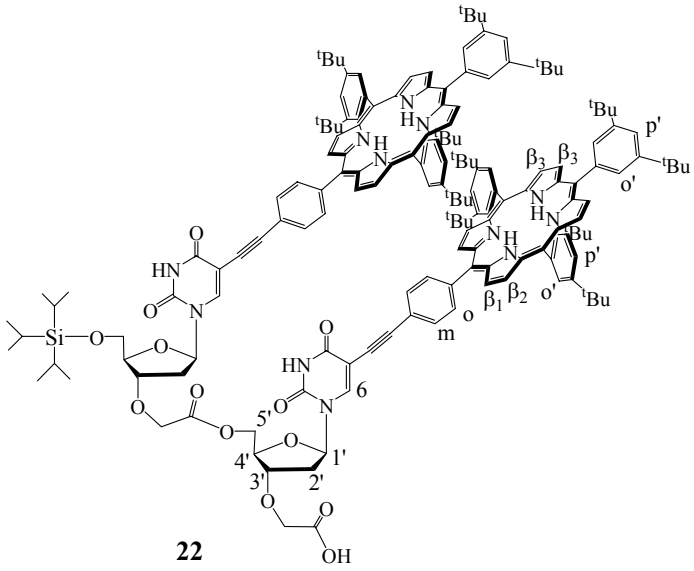

22

Tetramer 3.

Dimer-alcohol **21** (0.23 g, 0.082 mmol) and dimer-acid **22** (0.28 g, 0.105 mmol) were dissolved in dichloromethane (without ethanol and dried over molecular sieves, 15 mL) and to this solution DMAP (0.031 g, 0.256 mmol) and DCC (0.026 g, 0.124 mmol) were added, respectively. The obtained mixture was allowed to stir at r.t. under an argon atmosphere for 2 days, when TLC analysis showed the unreacted residues of alcohol and acid. Therefore additional portions of DMAP (0.023 g, 0.186 mmol) and DCC (0.026, 0.124 mmol) were added, and the reaction was continued stirring for another day. The time course for the reaction was examined by following the formation of the product (*n*-hexan/ethylacetate (4.5:5.5), R_f= 0.43) and disappearance of the both starting materials, despite the fact that several spots were characterizing the reaction mixture. The solvent was removed to dryness via rotaevaporation and afforded residue was suspended in minimum volume of toluene. The slurry was placed in refrigerator for 3 h to precipitate DCU. The precipitated white solid was collected by filtration and washed with small portions of chilled toluene. The obtained filtrate was evaporated *in vacuo* and then left to dry in a vacuum overnight. The crude product was purified by using few silica-gel column chromatography and gel permeation chromatography in toluene. With the first the first silica-gel column (Ø= 2 cm, h= 35 cm; *n*-hexan/ethylacetate (9:1) → ethylacetate) the mixture of the product with impurities characterized by similar retention factors (including the residual starting dimer-alcohol) was separated. The gel-

permeation chromatography afforded separation of two mixtures, one containing tetramer and the other with dimer-alcohol. The second column on silica-gel (Ø= 2 cm, h= 35 cm; *n*-hexan/ethylacetate (9:1 → 3:7)) provided pure tetramer. The further purification was performed aiming to isolate the higher quantity of the product. Finally, tetramer **3** was obtained as a violet solid (0.16 g, 0.03 mmol, 36%). ^{1}H-NMR ($CDCl_3$, 500 MHz, c= 3.0 x 10^{-3} M) : δ= 9.02 (d, 2H, ^{3}J= 4.5 Hz, *Zn*-$H_{\beta2}$), 8.99 (s, 4H, *Zn*-$H_{\beta3}$), 8.95 (d, 2H, ^{3}J= 5.0 Hz, *Zn*-$H_{\beta1}$), 8.88 (d, 6H, ^{3}J= 4.0 Hz, *2H*-$H_{\beta2}$), 8.87 (s, 12H, *2H*-$H_{\beta3}$), 8.77 (d, 6H, ^{3}J= 4.5 Hz, *2H*-$H_{\beta1}$), 8.32 (d, 2H, *Zn*-H_o, ^{3}J= 7.5 Hz), 8.19 (t, 4H, *2H*-H_o, ^{3}J= 7.6 Hz), 8.16 (d, 2H, *2H*-H_o, ^{3}J= 8.5 Hz), 8.12 (m, 6H, *Zn*-$H_{o'}$), 8.07 (s, 18H, *2H*-$H_{o'}$), 8.00 (s, 1H, *Zn*-H_6), 7.98 (d, 2H, ^{3}J= 7.5 Hz, *Zn*-H_m), 7.85 (d, 6H, ^{3}J= 7.5 Hz, *2H*-H_m), 7.78 (s, 12H, $H_{p'}$), 7.76 (s, 1H, *2H*-H_6), 7.38 (d, 2H, ^{3}J= 6.8 Hz, H_d), 6.89 (d, 2H, ^{3}J= 6.8 Hz, H_c), 6.35 (t, 1H, *Zn*-$H_{1'}$, ^{3}J= 6.8 Hz), 6.05 (m, 3H, *2H*-$H_{1'}$), 5.60 (s, 2H, H_a), 4.76 (s, 2H, H_b), 4.65 (m, 3H, *2H*-$H_{4'}$), 4.48 (s, 2H, *Zn*-$CH_{2,\ ether}$), 4.46 (m, 1H, *Zn*-$H_{4'}$), 4.35 (m, 3H, *2H*-$H_{3'}$), 4.17 (m, 8H, *Zn* and *2H*-$H_{5'}$), 3.77 (s, 3H, H_e), 2.66 (m, 3H, *2H*-$H_{2'}$), 2.34 (m, 2H, *Zn*-$H_{2'}$), 2.03 (m, 3H, *2H*-$H_{2'}$), 1.53 (s, 84H, ^{t}Bu), 1.51 (s, 132H, ^{t}Bu), 1.49 (s, 9H, ^{t}Bu), 1.28 (s, 3H, CH_{TIPS}), 1.05 (d, 9H, $CH_{3,TIPS}$, ^{3}J= 3.5 Hz), 1.04 (d, 9H, $CH_{3,TIPS}$, ^{3}J= 3.5 Hz), -2.74 (s, 6H, NH). ^{1}H-NMR ($(CD_3)_2CO$, 500 MHz, c= 1.56 x 10^{-3} M) : δ= 8.95 (m, 8H, *Zn*-$H_{\beta2}$+$H_{\beta1}$+$H_{\beta3}$), 8.87 (m, 24H, *2H*-$H_{\beta2}$+$H_{\beta1}$+$H_{\beta3}$), 8.34 (d, 2H, *Zn*-H_o, ^{3}J= 7.9 Hz), 8.26 (d, 2H, *2H(A)*-H_o, ^{3}J= 8.0 Hz), 8.18 (s, 1H, *Zn*-H_6), 8.15 (s, 1H, *2H(A)*-H_6), 8.13 (d, 2H, *2H(C)*-H_o, ^{3}J= 1.9 Hz), 8.09 (d, 3H, *Zn*-$H_{o'}$, ^{4}J= 1.4 Hz), 8.07 (d, 3H, *Zn*-$H_{o'}$, ^{4}J= 1.7 Hz), 8.00 (d, 2H, ^{3}J= 8.1 Hz, *Zn*-H_m), 7.89 (m, 4H, *2H(A)*-H_m), 7.85 (m, 12H, $H_{p'}$), 7.78 (d, 2H, ^{3}J= 7.9 Hz, *2H(D)*-H_m), 7.75 (s, 1H, *2H(C)*-H_6), 7.74 (s, 1H, *2H(D)*-H_6), 7.64 (d, 2H, ^{3}J= 8.0 Hz, *2H(C)*-H_m), 7.25 (d, 2H, ^{3}J= 8.5 Hz, H_d), 6.81 (d, 2H, ^{3}J= 8.4 Hz, H_c), 6.34 (t, 1H, *2H(A)*-$H_{1'}$, ^{3}J= 6.8 Hz), 6.29 (t, 1H, *Zn*-$H_{1'}$, ^{3}J= 6.8 Hz), 5.98 (t, 1H, *2H(C)*-$H_{1'}$, ^{3}J= 6.7 Hz), 5.80 (t, 1H, *2H(D)*-$H_{1'}$, ^{3}J= 6.8 Hz), 5.52 (s, 2H, H_a), 4.63 (m, 1H, *2H(A)*-$H_{3'}$), 4.60 (m, 2H, *2H(A)*-$CH_{2,\ ether}$), 4.60 (m, 4H, $H_{5'}$-*Zn* and *2H(A)*), 4.51 (s, 1H, *2H(A)*-$H_{4'}$), 4.45 (m, 1H, *Zn*-$H_{3'}$), 4.42 (s, 2H, *2H(D)*-$CH_{2,\ ether}$), 4.40 (s, 1H, *Zn*-$H_{4'}$), 4.39 (m, 1H, *2H(D)*-$H_{3'}$), 4.30 (m, 2H, *2H(D)*-$H_{5'}$), 4.21 (AB, 2H, *2H(C)*-$CH_{2,\ ether}$, ^{2}J= 16.4 Hz), 4.18 (m, 2H, *2H(D)*-$H_{5'}$), 4.14 (d, 2H, *Zn*-$CH_{2,\ ether}$, J= 2.1 Hz), 3.99 (s, 1H, *2H(D)*-$H_{4'}$), 4.60 (s, 2H, H_b), 3.68 (s, 3H, H_e), 3.67 (s, 1H, *2H(C)*-$H_{4'}$), 3.23 (s, 2H, *2H(C)*-$H_{5'}$), 2.72 (m, 1H, *2H(A)*-$H_{2'}$), 2.62 (ddd, 1H, *2H(A)*-$H_{2'}$, ^{3}J= 6.2 and 7.1 Hz and ^{2}J= 13.3 Hz), 2.60 (m, 1H, *Zn*-$H_{2'}$), 2.50 (ddd, 1H, *Zn*-$H_{2'}$, ^{3}J= 6.3 and 6.9 Hz and ^{2}J= 13.1 Hz), 2.46 (m, 1H, *2H(D)*-$H_{2'}$), 2.37 (dd, 1H, *2H(C)*-$H_{2'}$, ^{3}J= 5.4 Hz and ^{2}J= 13.9 Hz), 2.30 (ddd, 1H, *2H(D)*-$H_{2'}$, ^{3}J= 6.4 and 7.2 Hz and ^{2}J= 13.6 Hz), 1.93 (m, 1H, *2H(C)*-$H_{2'}$), 1.50 (br s, 216H, ^{t}Bu), 1.47 (s, 9H, *Zn*-$^{t}Bu_{terminal}$), 1.27 (s,

3H, CH_{TIPS}), 0.68 (m, 9H, $CH_{3,TIPS}$), -2.69 (s, 6H, NH). Analysis by NMR included as well: temperature variable experiments in acetone, dilution studies at 293 K in acetone, COSY and ROESY experiments in the both solvents, $CDCl_3$ and $(CD_3)_2CO$, and DOSY in acetone (Chapter 2). Analytical SEC: flow rate 1.0 mL/min, *t*= 13.0 min. UV-visible (CH_2Cl_2): λ_{abs} (ε) = 422 nm (1 559 590 M^{-1} cm^{-1}), 517 nm (54 837 M^{-1} cm^{-1}), 553 nm (48 349 M^{-1} cm^{-1}), 592 nm (22 288 M^{-1} cm^{-1}), 647 nm (15 973 M^{-1} cm^{-1}). Fluorescence (CH_2Cl_2): λ_{em}= 601, 651 and 709 nm. MALDI-TOF MS: *m/z*= 5408.1 ([M+H^+] calcd 5411.4).

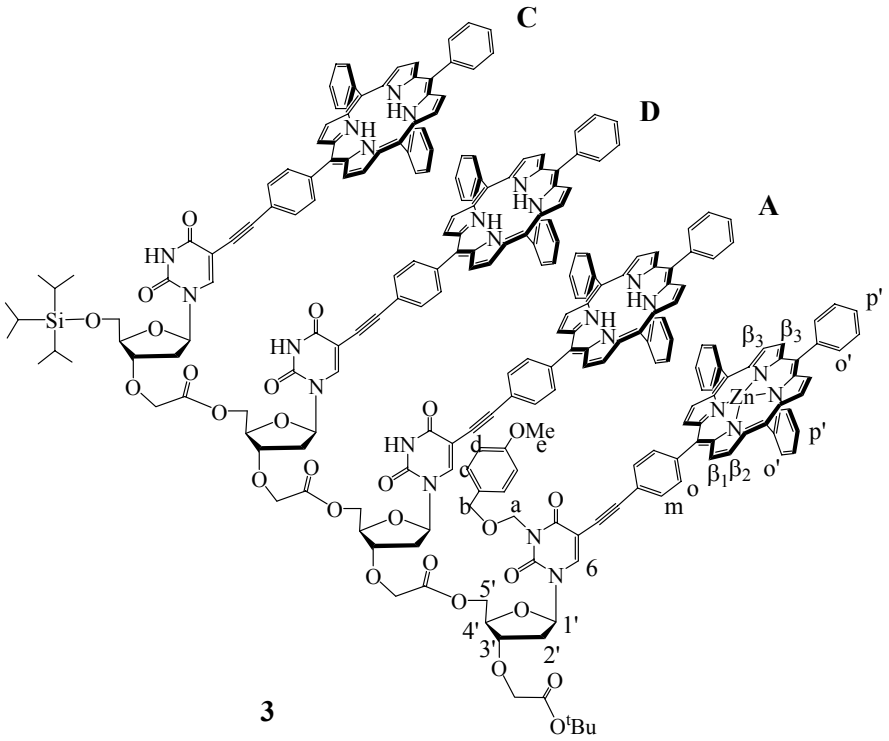

N.B. *Tert*-butyl groups at porphyrins are omitted for clarity.

Tetramer-alcohol 23.

Tetramer **3** (0.08g, 0.015 mmol) was dissolved in THF (2.5 mL), and TBAF (0.03 mL, 0.03 mmol, 1M solution in THF) was added. The mixture was deareated and flushed with argon, and then left to stir at r.t. for 12 h under an argon atmosphere. The reaction course was difficult to follow by TLC (*n*-hexan/ethylacetate (4.0:6.0)), because the tetramer and the tetramer-alcohol are characterized with similar retention factor. The solvent was removed by evaporation and the residue was dissolved in dichloromethane. The obtained solution was washed with two portions of water, and organic phase was removed under reduced pressure.

Finally the pure product was isolated by silica-gel column chromatography (Ø= 1 cm, h= 24 cm; *n*-hexan/ethylacetate (8:2 → 2:8)), to afford tetramer-alcohol **23** as a violet solid (0.067 g, 0.013 mmol, 87%). ^{1}H-NMR ($CDCl_3$, 300 MHz) : δ= 9.10 (d, 2H, ^{3}J= 4.7 Hz, *Zn*-$H_{\beta 2}$), 9.06 (s, 4H, *Zn*-$H_{\beta 3}$), 9.00 (d, 2H, ^{3}J= 4.7 Hz, *Zn*-$H_{\beta 1}$), 8.93 (s, 16H, *2H*-$H_{\beta 2}$+$H_{\beta 3}$), 8.83 (d, 3H, ^{3}J= 4.7 Hz, *2H*-$H_{\beta 1}$), 8.82 (d, 3H, ^{3}J= 4.7 Hz, *2H*-$H_{\beta 1}$), 8.37 (d, 2H, *Zn*-H_o, ^{3}J= 8.1 Hz), 8.20 (m, 6H, *2H*-H_o), 8.17 (m, 6H, *Zn*-$H_{o'}$), 8.10 (s, 21H, *2H*-$H_{o'}$+ H_6), 8.04 (s, 1H, H_6), 8.03 (d, 2H, ^{3}J= 7.5 Hz, *Zn*-H_m), 7.90 (d, 2H, ^{3}J= 8.0 Hz, *2H*-H_m), 7.81 (m, 15H, *Zn* and *2H*-$H_{p'}$ + *2H*-H_m), 7.77 (m, 2H, *2H*-H_m), 7.40 (d, 2H, ^{3}J= 8.6 Hz, H_d), 6.90 (d, 2H, ^{3}J= 8.7 Hz, H_c), 6.30 (t, 1H, *Zn*-$H_{1'}$, ^{3}J= 6.1 Hz), 6.10 (t, 1H, *2H*-$H_{1'}$, ^{3}J= 6.3 Hz), 5.82 (t, 1H, *2H*-$H_{1'}$, ^{3}J= 6.2 Hz), 5.60 (s, 2H, H_a), 4.78 (s, 2H, H_b), 4.34 (m, 22H, *2H* and *Zn*-$H_{4'}$+$H_{5'}$+$H_{3'}$+$CH_{2,\ ether}$), 3.77 (s, 3H, H_e), 2.63 (m, 3H, *2H*-$H_{2'}$), 2.31 (m, 2H, *Zn*-$H_{2'}$), 2.07 (m, 3H, *2H*-$H_{2'}$), 1.55 (s, 84H, ^{t}Bu), 1.53 (s, 132H, ^{t}Bu), 1.46 (s, 9H, ^{t}Bu), -2.67 (s, 6H, NH).

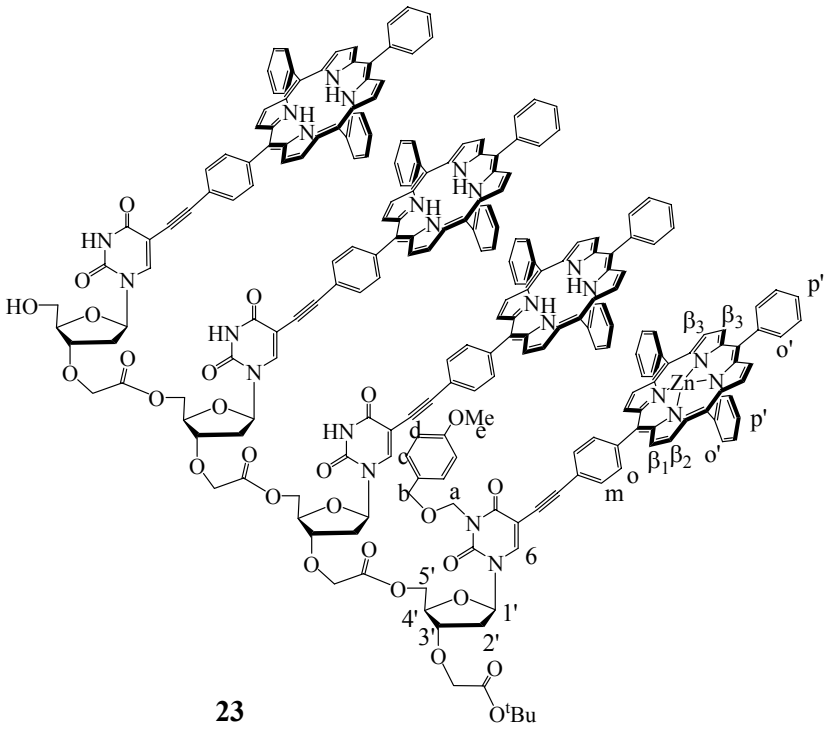

23

N.B. *Tert*-butyl groups at porphyrins are omitted for clarity.

Tetramer-acid 24.

Tetramer **3** (0.095g, 0.018 mmol) was dissolved in CH_2Cl_2 stabilized with amylene (2.5 mL) and solution was cooled using an ice-salt bath, and then TFA (0.25 mL, 6.49 mmol) was added. The mixture was flushed with argon, and then left to stir. After 1 h at 0 °C, the bath was removed and the mixture allowed to warm to r.t.. The reaction was stirred at r.t. for 11 h when it was judged to be complete by TLC analysis (ethylacetate/methanol (9:1) with few drops of acetic acid). The reaction solution was diluted and successively washed with water until pH of an aqueous phase was 7. The solvent from the organic phase was removed by evaporation, and subsequently the crude product was dried in vacuum overnight. Finally the pure product was isolated by silica-gel column chromatography (Ø= 1 cm, h= 19 cm; ethylacetate + 0.1% of acetic acid and gradually increased methanol up to 15%), to yield tetramer-acid **24** as a violet solid (0.07 g, 0.0137 mmol, 78%). ^{1}H-NMR ($CDCl_3$, 300 MHz) : δ= 8.93 (m, 32H, $H_{\beta2}$+$H_{\beta3}$+$H_{\beta1}$), 8.26 (m, 8H, H_o+H_6), 8.10 (s, 25H, $H_{o'}$+H_6), 8.03 (s, 2H, H_6), 8.01 (d, 2H, ^{3}J= 6.8 Hz, H_m), 7.92 (m, 6H, H_m), 7.80 (d, 12H, $H_{p'}$, J= 6.0 Hz), 6.30 (br s, 4H, $H_{1'}$), 4.51 (m, 22H, $H_{4'}$+$H_{5'}$+$H_{3'}$+$CH2_{, ether}$), 2.66 (m, 8H, $H_{2'}$), 1.53 (br s, 216H, ^{t}Bu), 1.30 (s, 3H, CH_{TIPS}), 1.09 (m, 18H, $CH_{3,TIPS}$), -2.67 (s, 8H, NH).

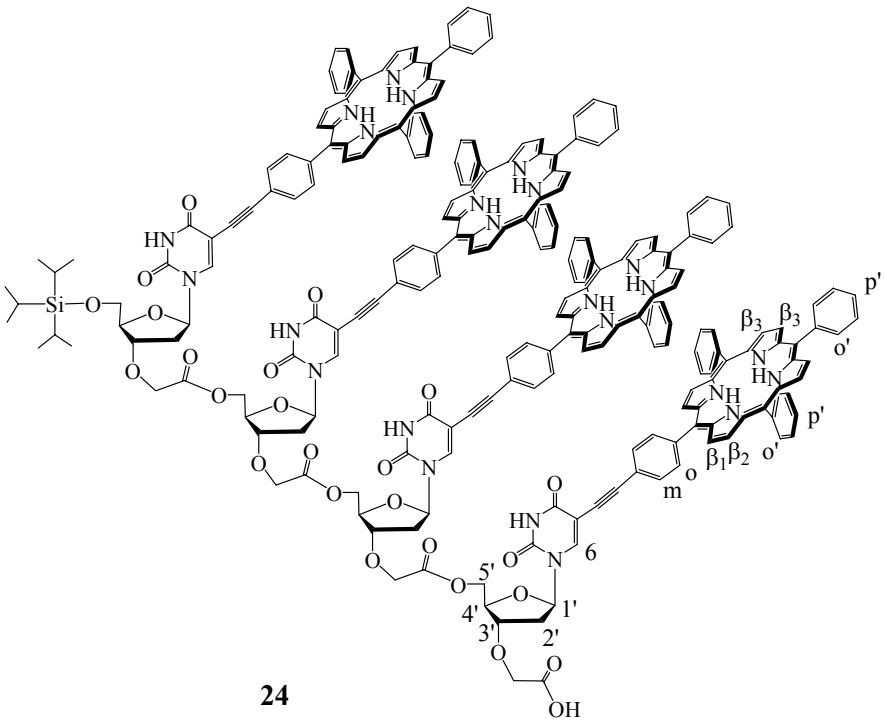

24

N.B. *Tert*-butyl groups at porphyrins are omitted for clarity.

Octamer 4.

Tetramer-alcohol **23** (0.07 g, 0.0133 mmol) and tetramer-acid **24** (0.07 g, 0.0137 mmol) were dissolved in dichloromethane (without ethanol and dried over molecular sieves, 4 mL) and to this solution DMAP (0.0036 g, 0.0292 mmol) and DCC (0.0041 g, 0.02 mmol) were added, respectively. The obtained mixture was allowed to stir at r.t. under an argon atmosphere for 2 days, when TLC analysis showed the unreacted residues of alcohol and acid. Therefore additional portions of DMAP (0.0024 g, 0.0199 mmol) and DCC (0.0027, 0.0133 mmol), as well as HOBt (0.00036 g, 0.00265 mmol) were added, and the reaction was continued stirring for another day. Subsequently a progress of the reaction was evidenced by TLC, but still the reaction was not completed. Hence, another portions of DMAP (0.00162 g, 0.0133 mmol), DCC (0.0027, 0.0133 mmol) and HOBt (0.00072 g, 0.0053 mmol) were added. The reaction course was extremely difficult to follow by TLC analysis (*n*-hexan/ethylacetate (4.2:5.8)), because the product on TLC plates characterizes a long trail. However, the reaction was stopped after 4 d of stirring at r.t. The solvent was removed to dryness via rotaevaporation and afforded residue was suspended in minimum volume of toluene. The slurry was placed in refrigerator for 3 h to precipitate DCU. The precipitated white solid was collected by filtration and washed with small portions of chilled toluene. The obtained filtrate was evaporated *in vacuo* and then left to dry in a vacuum overnight. The crude product was purified by using a dozen of gel-permeation chromatography in toluene and silica-gel column chromatography (63-200 μm, *n*-hexan/ethylacetate). The product was obtained in extremely poor yield due to extensive process toward pure octamer **4** (5.52 mg, 0.53 μmol, 4%). Analysis by NMR (500 MHz) included: temperature variable experiments in $C_2D_2Cl_4$ at c= 9.64 x 10^{-4} M from 273 to 373 K and dilution studies in acetone-d_6 from 1.0 x 10^{-3} M to 2.5 x 10^{-4} M. Analytical SEC: flow rate 1.0 mL/min, t= 7.77 min. UV-visible (CH_2Cl_2): λ_{abs} (ε) = 422 nm (2 285 060 M^{-1} cm^{-1}), 518 nm (87 426 M^{-1} cm^{-1}), 553 nm (70 556 M^{-1} cm^{-1}), 592 nm (33 548 M^{-1} cm^{-1}), 648 nm (27 315 M^{-1} cm^{-1}). Fluorescence (CH_2Cl_2): λ_{em}= 651 and 711 nm. MALDI-TOF MS: *m/z*= 10378.0 ([$M+H^+$] calcd 10377.8).

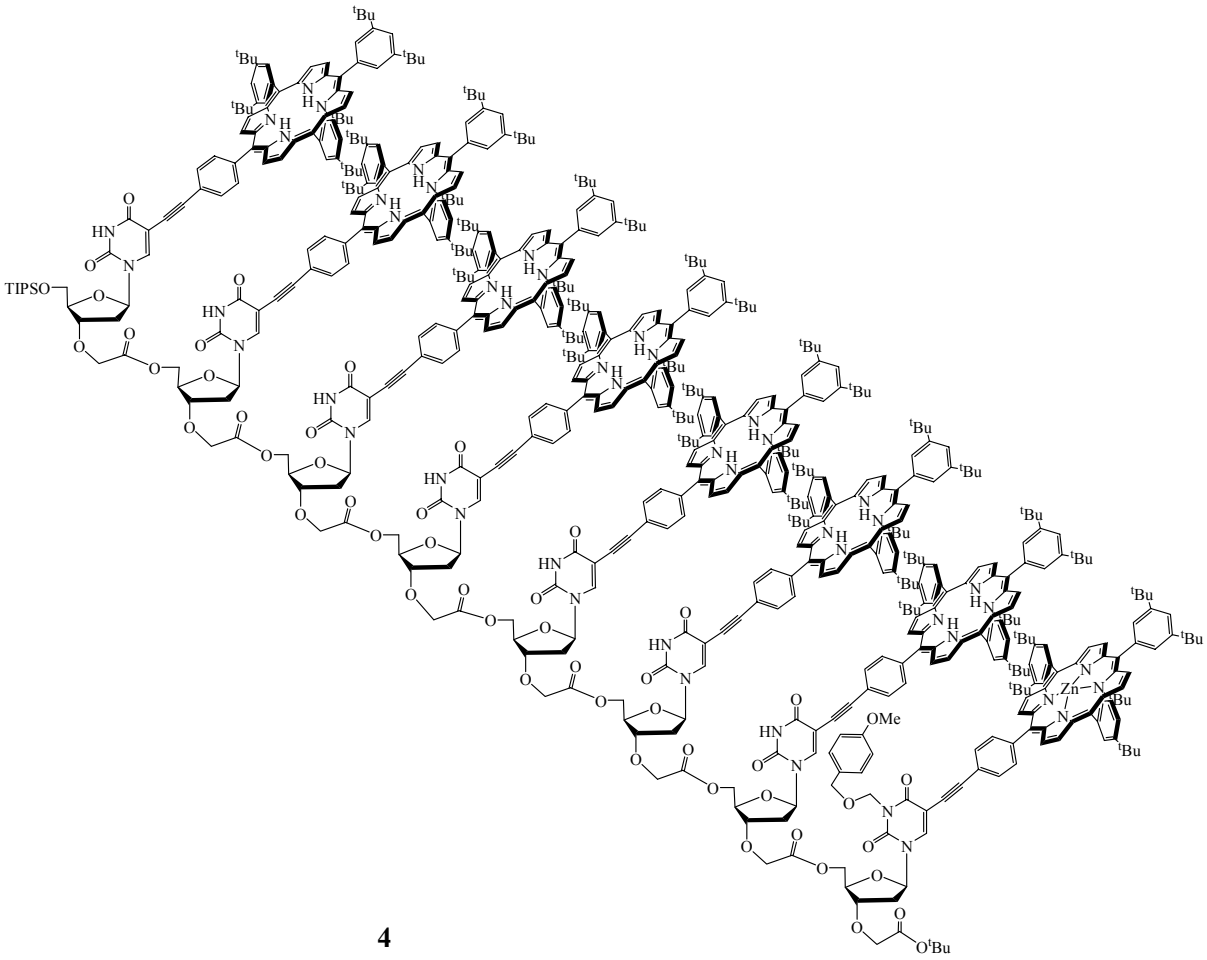

4

Zinc(II) porphyrin dyad 30.

The solution of $Zn(OAc)_2 \cdot 2H_2O$ (0.11 M) was prepared separately by dissolving the corresponding salt (0.0042 g, 0.019 mmol) in methanol (0.18 mL). Such solution was added to the mixture of dimer **2** (0.028 g, 0.0096 mmol) in chloroform (7 mL), and such obtained homogenous mixture was flushed with argon and heated to reflux. The progress of metallation was monitored by UV-visible spectroscopy showing that the reaction was terminated after 4 h of reflux under an argon atmosphere. The solvent was removed by evaporation, the residue was dissolved in dichloromethane and the solution was washed with water. The crude product was purified by column chromatography (SiO_2; Ø= 1 cm, h= 10 cm; *n*-hexan/ethylacetate (7:3)) yielding **30** (0.018 g, 0.0059 mmol, 62%). ^{1}H-NMR ($CDCl_3$, 250 MHz) : δ= 9.02 (d, 2H, ^{3}J= 4.7 Hz, $H_{\beta 2}$), 9.00 (s, 8H, $H_{\beta 3}$), 8.99 (d, 2H, ^{3}J= 4.7 Hz, $H_{\beta 2}$), 8.94 (d, 2H, ^{3}J= 4.7 Hz, $H_{\beta 1}$), 8.87 (d, 2H, ^{3}J= 4.7 Hz, $H_{\beta 1}$), 8.26 (d, 2H, H_o, ^{3}J= 8.2 Hz), 8.17 (d, 2H, H_o, ^{3}J= 8.1 Hz), 8.11 (d, 4H, ^{4}J= 1.7 Hz, $H_{o'}$), 8.09 (d, 8H, ^{4}J= 1.7 Hz, $H_{o'}$), 8.05 (s, 1H, H_6), 7.94 (d, 2H, ^{3}J=

8.2 Hz, H_m), 7.91 (s, 1H, H_6), 7.79 (s, 6H, $H_{p'}$), 7.75 (d, 2H, ^3J= 8.4 Hz, H_m), 7.39 (d, 2H, ^3J= 8.7 Hz, H_d), 6.91 (d, 2H, ^3J= 8.7 Hz, H_c), 6.29 (t, 1H, $H_{1'}$, ^3J= 6.7 Hz), 6.26 (t, 1H, $H_{1'}$, ^3J= 6.9 Hz), 5.57 (s, 2H, H_a), 4.73 (s, 2H, H_b), 4.55 (ABM, 2H, $CH_{2,\ ether}$, ^3J= 3.8 and 5.1 Hz and ^2J= 8.1 Hz), 4.42 (m, 2H, $H_{4'}$+H_3), 4.38 (s, 2H, $CH_{2,\ ether}$), 4.30 (m, 2H, $H_{4'}$+H_3), 4.06 (AB, 2H, $H_{5'}$, ^2J= 14.2 Hz), 4.05 (m, 2H, $H_{5'}$), 3.82 (s, 3H, H_e), 2.64 (m, 2H, $H_{2'}$), 2.27 (q, 1H, $H_{2'}$, ^3J= 7.0 Hz), 2.11 (m, 1H, $H_{2'}$), 1.52 (s, 108H, ^{t}Bu), 1.50 (s, 9H, ^{t}Bu), 1.26 (s, 3H, CH_{TIPS}), 1.14 (d, 9H, $CH_{3,TIPS}$, ^3J= 1.3 Hz), 1.11 (d, 9H, $CH_{3,TIPS}$, ^3J= 1.4 Hz). UV-visible (CH_2Cl_2): λ_{abs} (ε) = 422 nm (1 008 610 M^{-1} cm^{-1}), 550 nm (45 606 M^{-1} cm^{-1}), 589 nm (14 398 M^{-1} cm^{-1}). MALDI-TOF MS: *m/z*= 2989.9 ([M^+] calcd 2990.6).

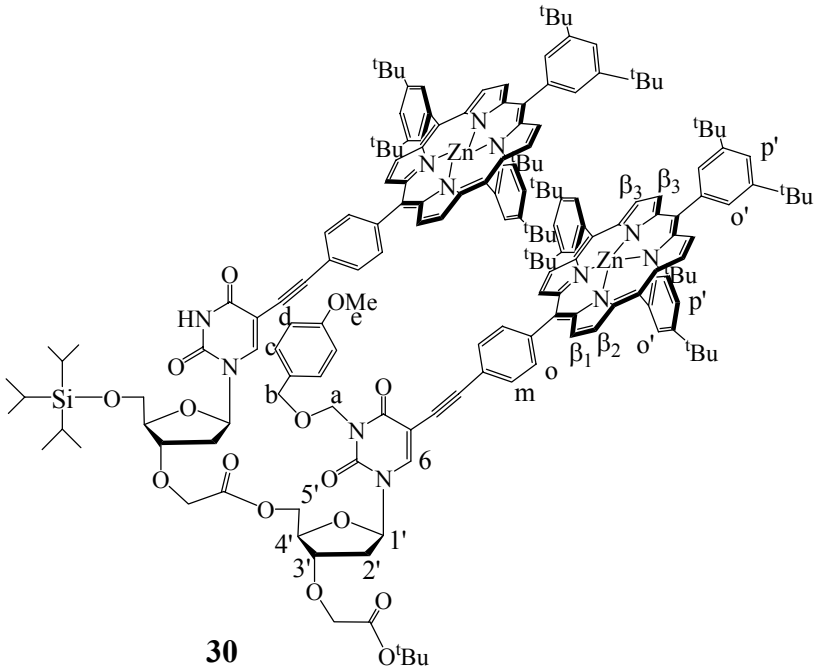

30

Zinc(II) porphyrin array 31.

The solution of $Zn(OAc)_2 \cdot 2H_2O$ (0.11 M) was prepared separately by dissolving the corresponding salt (0.00225 g, 0.0102 mmol) in methanol (0.1 mL). Such solution was added to the mixture of tetramer **3** (0.00923 g, 0.00171 mmol) in chloroform (2.4 mL), and such obtained homogenous mixture was flushed with argon and allowed to stir at r.t.. The progress of metallation was monitored by UV-visible spectroscopy showing that the reaction was terminated after 17 h. At the end of reaction the mixture was characterized at TLC plates with five separated spots, some of which are having a retention factor similar to the starting

material. The solvent was removed by evaporation, the residue was dissolved in dichloromethane and the solution was washed with water. The crude product was purified by using gel-permeation chromatography in toluene followed by silica-gel column chromatography. With the gel-permeation chromatography the mixture with the product was separated. The silica-gel column (Ø= 1 cm, h= 9 cm; *n*-hexan/ethylacetate (7:3) → 10% of methanol in ethylacetate) afforded pure zinc porphyrin tetramer. The further purification was performed aiming to isolate the higher quantity of the product, finally yielding **31** (0.0039 g, 0.6994 μmol, 41%). ^{1}H-NMR ($CDCl_3$, 250 MHz) : δ= 9.04 (d, 2H, ^{3}J= 4.7 Hz, $H_{\beta2}$), 9.00 (m, 22H, $H_{\beta2}$+$H_{\beta3}$), 8.88 (d, 4H, ^{3}J= 4.7 Hz, $H_{\beta1}$), 8.85 (d, 4H, ^{3}J= 4.6 Hz, $H_{\beta1}$), 8.32 (d, 2H, H_o, ^{3}J= 7.9 Hz), 8.20 (d, 2H, H_o, ^{3}J= 8.1 Hz), 8.13 (m, 4H, H_o), 8.07 (m, 26H, $H_{o'}$+H_6), 8.00 (s, 1H, H_6), 7.96 (d, 2H, ^{3}J= 7.6 Hz, H_m), 7.82 (d, 2H, ^{3}J= 8.3 Hz, H_m), 7.73 (m, 17H, $H_{p'}$+H_m+H_6), 7.35 (d, 2H, ^{3}J= 8.4 Hz, H_d), 6.84 (d, 2H, ^{3}J= 8.6 Hz, H_c), 6.32 (t, 2H, $H_{1'}$, ^{3}J= 6.3 Hz), 6.07 (m, 2H, $H_{1'}$), 5.56 (s, 2H, H_a), 4.73 (s, 2H, H_b), 4.61 (m, 3H, $H_{4'}$), 4.45 (m, 6H, $CH_{2,\ ether}$+$H_{3'}$+$H_{4'}$), 4.32 (m, 3H, $H_{3'}$), 4.08 (m, 10H, $H_{5'}$+$CH_{2,\ ether}$), 3.72 (s, 3H, H_e), 2.63 (m, 3H, $H_{2'}$), 2.31 (m, 2H, $H_{2'}$), 2.03 (m, 3H, $H_{2'}$), 1.50 (br s, 225H, ^{t}Bu), 1.26 (s, 3H, CH_{TIPS}), 0.91 (m, 18H, $CH_{3,TIPS}$). UV-visible (CH_2Cl_2): λ_{abs} (ε) = 424 nm (1 917 880 M^{-1} cm^{-1}), 551 nm (87 181 M^{-1} cm^{-1}), 592 nm (30 148 M^{-1} cm^{-1}). MALDI-TOF MS: *m/z*= 5601.7 ([$M+H^+$] calcd 5601.5).

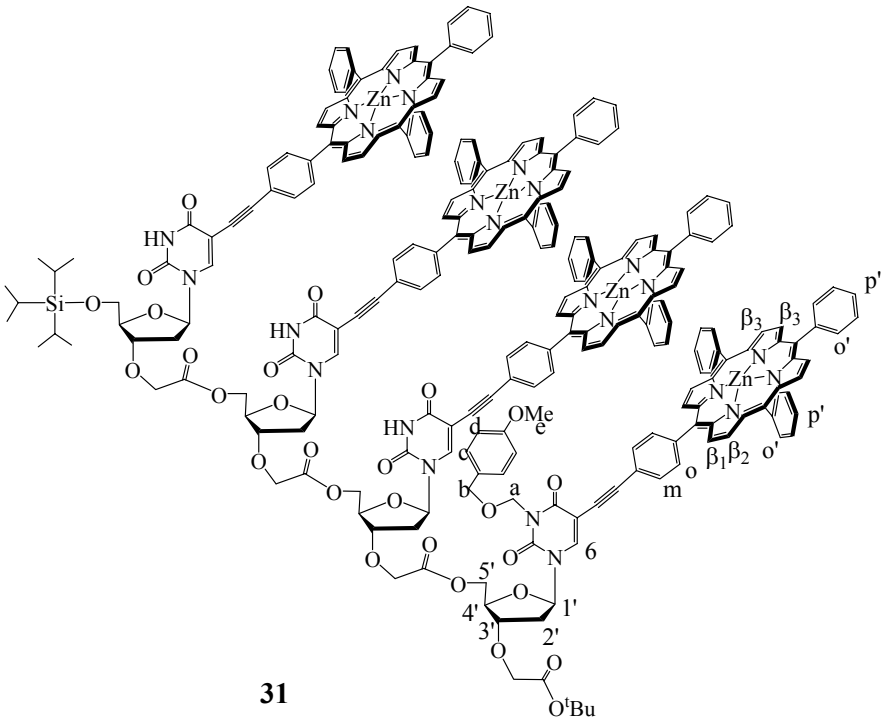

31

N.B. *Tert*-butyl groups at porphyrins are omitted for clarity.

***N*-Boc-3-hydroxy-propanamine 32.**

Triethylamine (9.8 mL, 70.4 mmol) and di-*tert*-butyloxycarbonate (6.62 g, 30.4 mmol) were added, respectively, to the solution of 3-amino-propan-1-ol (1.825 g, 24.3 mmol) in methanol (250 mL). The mixture was deaerated and flushed with argon, and heated to reflux under an argon atmosphere. After 1 h of stirring at reflux, an oil bath was removed and the mixture allowed to cool to r.t. and continued stirring for 1 h at this temperature. The solvent was removed via rotaevaporation to dryness, and subsequently the crude product was purified by silica-gel column chromatography (Ø= 3 cm, h= 13 cm, dichloromethane/methanol (9:1)) affording the desired product **32** (4.26 g, 24.3 mmol, quantitative) as a colourless oil. ^{1}H-NMR ($CDCl_3$, 300 MHz) : δ= 5.01 (s, 1H, NH), 3.59 (m, 2H, H_c), 3.19 (q, 2H, H_a, ^{3}J= 6.3 Hz), 2.16 (s, 1H OH), 1.61 (q, 2H, H_b, ^{3}J= 6.3 Hz), 1.38 (s, 9H, ^{t}Bu).

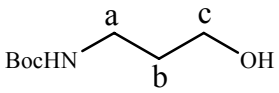

32

***N*-Boc-3-bromo-propanamine 33.**

The compound **32** (4.26 g, 24.3 mmol) was dissolved in dichloromethane (40 mL) stabilized with amylene and dried over molecular sieves. This solution was charged with CBr_4 (11.59 g, 34.95 mmol) and PPh_3 (7.33 g, 27.96 mmol), and then left to stir at r.t. and under an argon atmosphere overnight. The solvent was removed by evaporation and the residue as yellow oil was dried in a vacuum. A purification by column chromatography (SiO_2, Ø= 3 cm, h= 15 cm, dichloromethane/methanol (9:1)) yielded pure **33** (3.88 g, 16.29 mmol, 67%) as a clear yellow oil. ^{1}H-NMR ($CDCl_3$, 300 MHz) : δ= 4.68 (s, 1H, NH), 3.43 (t, 2H, H_c, ^{3}J= 6.6 Hz), 3.26 (q, 2H, H_a, ^{3}J= 6.4 Hz), 2.03 (q, 2H, H_b, ^{3}J= 6.6 Hz), 1.43 (s, 9H, ^{t}Bu).

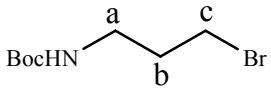

33

Porphyrin-phenol 34.

After a three-necked, round-bottomed flask fitted with two septum ports and a reflux condenser with a gas inlet port was flushed with argon, it was charged with chloroform dried over molecular sieves (1.5 L). Subsequently, under continuous argon flow two aldehydes, 3,5-di-*tert*-butylbenzaldehyde (**10**, 2.83 g, 12.98 mmol) and 4-hydroxybenzaldehyde (0.53 g, 4.32 mmol) were added, in an overall concentration of 10^{-2} M. Sock solution of BF_3 etherate was prepared separately by diluting commercially available $BF_3 \cdot OEt_2$ (1.2 mL) with chloroform (1.8 mL). Further, pyrrole (1.2 mL, 17.35 mmol) and $BF_3 \cdot OEt_2$ from freshly prepared stock solution (1.6 mL of 3.16 M, in 1.5 L 3.37 x 10^{-3} M) were added via syringe. The resulted solution was stirred for 1 h at r.t. under an argon atmosphere. The reaction progress was monitored by TLC (dichloromethane/*n*-hexane (7:3), R_f= 0.35) by removing the aliquots from the reaction mixture and oxidizing with DDQ. The oxidation of porphyrinogen to porphyrin was performed with addition of *p*-chloranil (3.19 g, 12.97 mmol). The solution was refluxed for 1 h, and then allowed to cool to r.t. while triethylamine was added (1 mL). The reaction mixture was concentrated, to the slurry SiO_2 was added and evaporation was continued to dryness. Such prepared crude product was purified by repetitive column chromatography on silica-gel. The first column (SiO_2; Ø= 5 cm, h= 20 cm; *n*-hexan/dichloromethane (6:4) → dichloromethane)) was effectuated toward porphyrins separation from polymers. The second was employed to isolate the targeted A_3B porphyrin **34** (0.84 g, 0.865 mmol, 20%) from the other isomers. ^{1}H-NMR ($CDCl_3$, 300 MHz) : δ= 8.89 (s, 4H, $H_{\beta 3}$), 8.86 (d, 4H, ^{3}J= 4.6 Hz, $H_{\beta 2}$+$H_{\beta 1}$), 8.09 (d, 2H, H_o, ^{3}J= 8.6 Hz), 8.08 (d, 4H, ^{4}J= 1.8 Hz, $H_{o''}$), 8.07 (d, 2H, ^{4}J= 1.8 Hz, $H_{o'}$), 7.79 (td, 3H, ^{4}J= 1.8 and 3.7 Hz, $H_{p'+p''}$), 7.21 (d, 2H, ^{3}J= 8.6 Hz, H_m), 1.52 (s, 18H, ^{t}Bu), 1.51 (s, 36H, ^{t}Bu), -2.71 (s, 2H, NH).

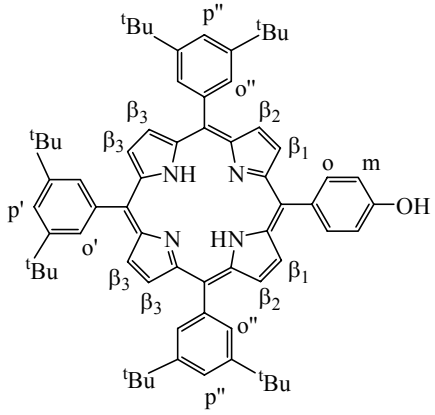

34

***O*-(*N*-Boc-aminopropanyl) porphyrin-phenol 35.**

Porphyrin-phenol (**34**, 0.4 g, 0.414 mmol) was dissolved in DMF (20 mL) and to the solution K_2CO_3 (0.126 g, 0.911 mmol) was added. The mixture was stirring for 1 h, then charged with *N*-Boc-3-bromo-propanamine (**33**, 0.099 g, 0.414 mmol) and continued to stir overnight at r.t. and under an argon atmosphere. The reaction course was followed by TLC analysis (dichloromethane/*n*-hexane (7:3)). The solvent was removed *in vacuo*, the residue was dissolved in dichloromethane and the obtained solution was neutralized by extraction with saturated solution of NH_4Cl. The combined organic phase was evaporated and the crude product purified by silica-gel column chromatography (Ø= 2 cm, h= 20 cm; *n*-hexan/dichloromethane (4:6)) affording *O*-alkylated porphyrin-phenol **35** (0.22 g, 0.194 mmol). ^{1}H-NMR ($CDCl_3$, 300 MHz) : δ= 8.90 (s, 4H, $H_{\beta3}$), 8.89 (s, 4H, $H_{\beta2}$+$H_{\beta1}$), 8.15 (d, 2H, H_o, ^{3}J= 8.4 Hz), 8.10 (d, 4H, ^{4}J= 1.8 Hz, $H_{o''}$), 8.09 (d, 2H, ^{4}J= 1.8 Hz, $H_{o'}$), 7.80 (td, 3H, ^{4}J= 2.0 and 3.8 Hz, $H_{p'+p''}$), 7.28 (d, 2H, ^{3}J= 8.4 Hz, H_m), 4.93 (s, 1H, NH), 4.33 (t, 2H, H_c, ^{3}J= 5.9 Hz), 3.51 (q, 2H, H_a, ^{3}J= 6.2 Hz), 2.19 (q, 2H, H_b, ^{3}J= 6.0 Hz), 1.55 (s, 18H, ^{t}Bu), 1.54 (s, 36H, ^{t}Bu), 1.52 (s, 9H, ^{t}Bu), -2.68 (s, 2H, NH).

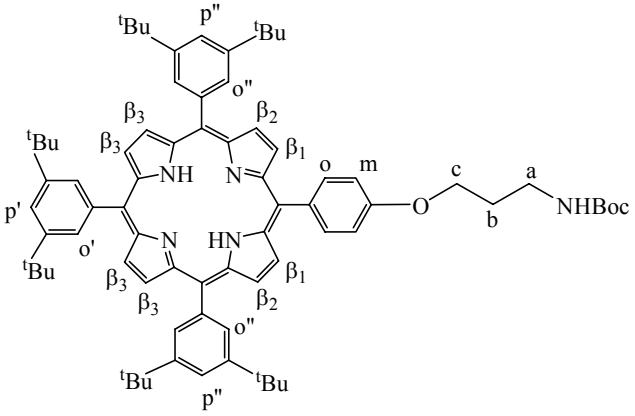

35

Porphyrin-amine 36.

The 1 M solution of TMSCl (1 mL, 7.88 mmol) and phenol (0.74 g, 7.88 mmol) in dichloromethane (8 mL) was prepared and charged with the compound **35** (0.20 g, 0.1778 mmol). The mixture was stirred at r.t. under an argon atmosphere for 6 h, and then quenched with triethylamine and washed with water. The combined organic phase was evaporated to

dryness and the residue applied to column chromatography purification (SiO_2, methanol (0 →10%) in dichloromethane) affording porphyrin-amine **36** (0.169 g, 0.165 mmol, 93%) as dark-violet solid. ^{1}H-NMR ($CDCl_3$, 300 MHz) : δ = 9.01 (s, 4H, $H_{\beta3}$), 9.00 (s, 4H, $H_{\beta2}$+$H_{\beta1}$), 8.25 (d, 2H, H_o, ^{3}J= 8.6 Hz), 8.21 (d, 4H, ^{4}J= 1.8 Hz, $H_{o''}$), 8.20 (d, 2H, ^{4}J= 1.9 Hz, $H_{o'}$), 7.89 (td, 3H, ^{4}J= 1.7 and 3.3 Hz, $H_{p'+p''}$), 7.38 (d, 2H, ^{3}J= 8.6 Hz, H_m), 4.43 (t, 2H, H_c, ^{3}J= 5.8 Hz), 3.92 (s, 1H, NH), 3.31 (t, 2H, H_a, ^{3}J= 6.7 Hz), 2.34 (t, 2H, H_b, ^{3}J= 6.2 Hz), 1.63 (s, 18H, ^{t}Bu), 1.62 (s, 36H, ^{t}Bu), -2.73 (s, 2H, NH).

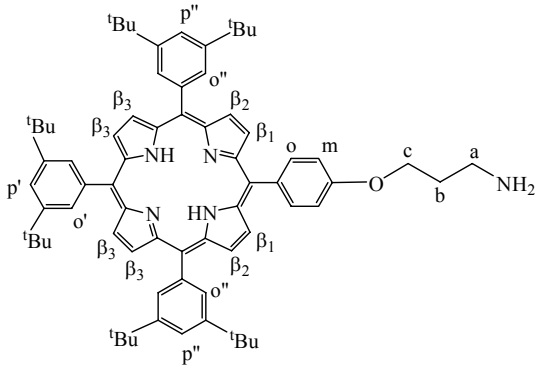

36

Simple porphyrin triazine 39 and triazine-bridged porphyrin dyad 40.

To a solution of porphyrin-amine **36** (0.04 g, 0.0391 mmol) in THF (3 mL) cooled at 0 °C were added cyanuric chloride (0.0073 g, 0.0391 mmol) and DIPEA (8.35 μL, 0.0469 mmol) under an argon atmosphere. After the mixture was stirred at this temperature for 20 min, the solution was allowed to warm to r.t. The reaction course followed by TLC (dichloromethane/methanol (8.5:1.5)) evidenced that after 2 h porphyrin **36** was no longer present (R_f(**36**)= 0.27). Another portion of porphyrin-amine **36** (0.04 g, 0.0391 mmol) was then added with DIPEA (8.35 μL, 0.0469 mmol), and the time course for the product formation was monitored by TLC (petroleum ether/ethylacetate (8:2), R_f(**38**)= 0.27). After 1 h of stirring at 40 °C a TLC analysis of the reaction mixture evidenced the presence of porphyrin-amine **36** and monoadduct **37**, thus a supplementary portion of DIPEA (8.35 μL, 0.0469 mmol) was added and the mixture continued to stir at 40 °C under an argon atmosphere. The TLC analysis indicated a complete disappearance of the starting porphyrin-amine **36** in an overall 2 days of stirring at 40 °C. Finally, an excess of piperidine (20 μL,

0.203 mmol) was added together with DIPEA (20 µL, 0.115 mmol), and the mixture was heated to reflux. After 1 d of stirring at reflux the TLC analysis indicated a complete conversion to the targeted **39** and **40** (petroleum ether/ethylacetate (8:2), R_f(**39**)= 0.50 and (6:4), R_f(**40**)= 0.34). The solvent was evaporated and the residue subjected to silica-gel column chromatography purification (Ø= 1 cm, h= 22 cm; petroleum ether/ethylacetate (9:1 → 6:4)) yielding simple porphyrinic triazine **39** (0.0197 g, 0.0155 mmol, 40%) and traizine-bridged porphyrin dyad **40** (0.0395 g, 0.0179 mmol, 46%). ^{1}H-NMR (**39**, $CDCl_3$, 300 MHz) : δ= 8.91 (s, 4H, $H_{\beta3}$), 8.90 (s, 4H, $H_{\beta2}$+$H_{\beta1}$), 8.14 (d, 2H, H_o, ^{3}J= 8.6 Hz), 8.11 (d, 4H, ^{4}J= 1.8 Hz, $H_{o''}$), 8.09 (d, 2H, ^{4}J= 1.8 Hz, $H_{o'}$), 7.81 (t, 2H, ^{4}J= 1.9 Hz, $H_{p''}$), 7.80 (t, 1H, ^{4}J= 2.0 Hz, $H_{p'}$), 7.29 (d, 2H, ^{3}J= 8.6 Hz, H_m), 4.50 (s, 1H, NH), 4.36 (t, 2H, H_c, ^{3}J= 6.0 Hz), 3.78 (m, 10H, H_a and H_x), 2.27 (q, 2H, H_b, ^{3}J= 6.3 Hz), 1.61 (q, 12H, H_y, ^{3}J= 4.9 Hz), 1.54 (s, 36H, ^{t}Bu), 1.53 (s, 18H, ^{t}Bu), -2.67 (s, 2H, NH). ^{1}H-NMR (**40**, $CDCl_3$, 300 MHz) : δ= 8.93 (s, 8H, $H_{\beta3}$), 8.92 (s, 8H, $H_{\beta2}$+$H_{\beta1}$), 8.17 (d, 4H, H_o, ^{3}J= 8.6 Hz), 8.12 (d, 8H, ^{4}J= 1.8 Hz, $H_{o''}$), 8.11 (d, 4H, ^{4}J= 1.8 Hz, $H_{o'}$), 7.82 (t, 3H, ^{4}J= 1.6 Hz, $H_{p'}$), 7.81 (t, 3H, ^{4}J= 1.7 Hz, $H_{p'}$), 7.32 (d, 4H, ^{3}J= 8.6 Hz, H_m), 5.22 (s, 2H, NH), 4.41 (t, 4H, H_c, ^{3}J= 5.7 Hz), 3.73 (m, 8H, H_a and H_x), 2.32 (t, 4H, H_b, ^{3}J= 5.8 Hz), 1.68 (m, 6H, H_y), 1.55 (s, 36H, ^{t}Bu), 1.54 (s, 72H, ^{t}Bu), -2.65 (s, 4H, NH). UV-visible (**39**, CH_2Cl_2): λ_{abs} (ε) = 421 nm (598 956 M^{-1} cm^{-1}), 518 nm (20 988 M^{-1} cm^{-1}), 554 nm (12 836 M^{-1} cm^{-1}), 593 nm (6 312 M^{-1} cm^{-1}), 648 nm (6 736 M^{-1} cm^{-1}). UV-visible (**40**, CH_2Cl_2): λ_{abs} (ε) = 421 nm (868 871 M^{-1} cm^{-1}), 518 nm (36 588 M^{-1} cm^{-1}), 554 nm (22 423 M^{-1} cm^{-1}), 593 nm (11 078 M^{-1} cm^{-1}), 648 nm (11 870 M^{-1} cm^{-1}). DCI/NH_3 MS (**39**): *m/z*= 1269.9 ([M^+] calcd 1269.8). MALDI-TOF MS (**40**): *m/z*= 2209.4 ([M^+] calcd 2209.1).

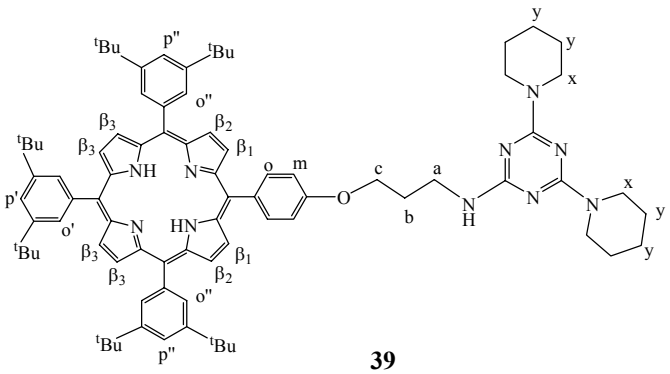

39

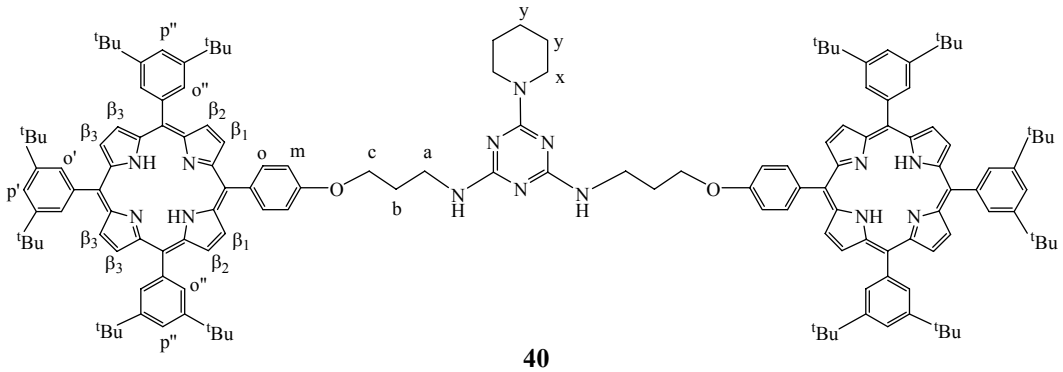

40

V - REFERENCES

1. A. Andronov, J. M. J. Fréchet, *Chem. Commun.* **2000**, 1701 and references cited therein.
2. X. Hu, A. Damjanović, T. Ritz, K. Schulten, *Proc. Natl. Acad. Sci. U. S. A.* **1998**, *95*, 5935.
3. G. McDermott, S. M. Prince, A. A. Freer, A. M. Hawthornthwaite-Lawless, M. Z. Papiz, R. J. Cogdell, N. W. Isaacs, *Nature* **1995**, *374*, 517.
4. S. M. Prince, M. Z. Papiz, A. A. Freer, G. McDermott, A. M. Hawthornthwaite-Lawless, R. J. Cogdell, N. W. Isaacs, *J. Mol. Biol.* **1997**, *268*, 412.
5. T. Pullerits, V. Sundström, *Acc. Chem. Res.* **1996**, *29*, 381.
6. S. Karrasch, P. A. Bullough, R. Ghosh, *EMBO J.* **1995**, *14*, 631.
7. W. Kühlbrandt, *Nature* **1995**, *374*, 497.
8. H. Zuber, *Trends Biochem. Sci.* **1986**, *11*, 414.
9. N. Krauss, W.-D. Schubert, O. Klukas, P. Fromme, H. T. Witt, W. Saenger, *Nat. Struct. Biol.* **1996**, *3*, 965.
10. A. N. Glazer, *Biochim. Biophys. Acta* **1984**, *768*, 29.
11. W. Kühlbrandt, D. N. Wang, Y. Fujiyoshi, *Nature* **1994**, *367*, 614.
12. R. Huber, *Angew. Chem. Int. Ed. Engl.* **1989**, *28*, 848.
13. X. Hu, K. Schulten, *Physics Today* **1997**, *50*, 28.
14. R. J. Cogdell, P. Fyfe, S. Barrett, S. M. Prince, A. A. Freer, N. W. Isaacs, P. McGlynn, C. Hunter, *Photosynth. Res.* **1996**, *48*, 55.
15. T. Monger, W. Parson, *Biochim. Biophys. Acta* **1977**, *460*, 393.
16. R. van Grondelle, J. Dekker, T. Gillbro, V. Sundstrom, *Biochim. Biophys. Acta* **1994**, *1187*, 1.
17. J. Deisenhofer, O. Epp, K. Miki, R. Huber, H. Michel, *Nature* **1985**, *318*, 618.
18. J. Deisenhofer, H. Michel, *Angew. Chem. Int. Ed. Engl.* **1989**, *28*, 829.
19. L. Germeroth, F. Lottspeich, B. Robert, H. Michel, *Biochemistry* **1993**, *32*, 5615.
20. T. Walz, R. Gosh, *J. Mol. Biol.* **1997**, *265*, 107.
21. J. Aagaard, W. Sistrom, *Photochem. Photobiol.* **1972**, *15*, 209.
22. X. Hu, D. Xu, K. Hamer, K. Schulten, J. Loepke, H. Michel, *Protein Sci.* **1995**, *4*, 1670.
23. A. P. Shreve, J. K. Trautman, H. A. Frank, T. G. Owens, A. C. Albrecht, *Biochim. Biophys. Acta* **1991**, *1058*, 280.
24. H.-M. Wu, N. R. S. Reddy, G. J. Small, *J. Phys. Chem. B* **1997**, *101*, 651.
25. S. Hess, M. Chachisvilis, K. Timpmann, M. R. Jones, G. J. S. Fowler, C. N. Hunter, V. Sundstrom, *Proc. Natl. Acad. Sci. U. S. A.* **1995**, *92*, 12333.
26. K. J. Visscher, H. Bergstrom, V. Sundstrom, C. N. Hunter, R. van Grondelle, *Photosynth. Res.* **1989**, *22*, 211.
27. A. Kimura, T. Kikitani, T. Yamoto, *J. Phys. Chem. B* **2000**, *104*, 9276.
28. L. R. Milgrom, *The Colours of Life: An Introduction to the Chemistry of Porphyrins and Related Compounds*, OUP, Oxford, 1997; *The Porphyrins*, ed. D. Dolphin, Academic Press, New York, 1978.
29. C. M. Drain, R. Fischer, E. G. Nolen, J. M. Lehn, *J. Chem. Soc., Chem. Commun.* **1993**, 243.
30. C. M. Drain, J. M. Lehn, *J. Chem. Soc., Chem. Commun.* **1994**, 2313.
31. H. L. Anderson, *Inorg. Chem.* **1994**, *33*, 972.
32. P. J. Stang, J. Fan, B. Olenyuk, *Chem. Commun.* **1997**, 1453.
33. M.-S. Choi, T. Yamazaki, I. Yamazaki, T. Aida, *Angew. Chem. Int. Ed.* **2004**, *43*, 150.
34. G. M. Dubowchik, A. D. Hamilton, *J. Chem. Soc., Chem. Commun.* **1987**, 293.

35. C. M. Drain, K. C. Russell, J.-M. Lehn, *Chem. Commun.* **1996**, 337.
36. H. A. M. Biemans, A. E. Rowan, A. Verhoeven, P. Vanoppen, L. Letterini, J. Foekema, A. P. H. J. Schenning, E. W. Meijer, F. C. De Schryver, R. J. M. Nolte, *J. Am. Chem. Soc.* **1998**, *120*, 11054.
37. K. Chichak, N. R. Brand, *Chem. Commun.* **2000**, 1211.
38. R. Takahashi, Y. Kobuke, *J. Am. Chem. Soc.* **2003**, *125*, 2372.
39. T. Hori, N. Aratani, A. Takagi, T. Matsumoto, T. Kawai, M.-C. Yoon, Z. S. Yoon, S. Cho, D. Kim, A. Osuka, *Chem. Eur. J.* **2006**, *12*, 1319.
40. J. Li, A. Ambroise, S. I. Yang, J. R. Diers, J. Seth, C. R. Wack, D. F. Bocian, D. Holten, J. S. Lindsey, *J. Am. Chem. Soc.* **1999**, *121*, 8927.
41. O. Mongin, A. Schuwey, M. A. Vallot, A. Gossauer, *Tetrahedon Lett.* **1999**, *40*, 8347.
42. P. G. Van Patten, A. P. Shreve, J. S. Lindsey, R. J. Danohoe, *J. Phys. Chem. B* **1998**, *102*, 4209.
43. S. Prathapan, T. E. Johnson, J. S. Lindsey, *J. Am. Chem. Soc.* **1993**, *115*, 7519.
44. J. Seth, V. Palaniappan, T. E. Johnson, S. Prathapan, J. S. Lindsey, D. F. Bocian, *J. Am. Chem. Soc.* **1994**, *116*, 10578.
45. N. Solladié, M. Gross, J.-P. Gisselbrecht, C. Sooambar, *Chem. Commun.* **2001**, 2206.
46. A. Nakano, A. Osuka, I. Yamazaki, T. Yamazaki, Y. Nishimura, *Angew. Chem. Int. Ed.* **1998**, *37*, 3023.
47. A. Nakano, T. Yamazaki, Y. Nishimura, I. Yamazaki, A. Osuka, *Chem. Eur. J.* **2000**, *6*, 3254.
48. C. C. Mak, N. Bampos, J. K. M. Sanders, *Angew. Chem. Int. Ed.* **1998**, *37*, 3020.
49. N. Solladié, C. Sooambar, H. Herschbach, J.-M. Strub, E. Leize, A. Van Dorsselaer, A. M. Talarico, B. Ventura, L. Flamigni, *New J. Chem.* **2005**, *29*, 1504.
50. N. Solladié, A. Hamel, M. Gross, *Tetrahedron Lett.* **2000**, *41*, 6075.
51. V. Troiani, Ph. D. Thesis 2004, Groupe de Synthèse de Systèmes Porphyriniques du Dr. N. Solladié, Université Louis Pasteur, Strasbourg, France.
52. J. Lebreton, A. De Mesmaeker, A. Waldner, *Synlett* **1993**, 54.
53. S. Wendeborn, C. Jouanno, R. M. Wolf, A. De Mesmaeker, *Tetrahedon Lett.* **1996**, *37*, 5511.
54. P. von Matt, A. De Mesmaeker, U. Pieles, W. Zürcher, K.-H. Altmann, *Tetrahedon Lett* **1999**, *40*, 2899.
55. T. P. Prakash, A. M. Kawasaki, A. S. Fraser, G. Vasquez, M. Manoharan, *J. Org. Chem.* **2002**, *67*, 357.
56. T. P. Prakash, M. Manoharan, A. M. Kawasaki, E. A. Lesnik, S. R. Owens, G. Vasquez, *Organic Lett.* **2000**, *2*, 3995.
57. E. S. Krider, J. E. Miller, T. J. Meade, *Bioconjugate Chem.* **2002**, *13*, 155.
58. G. Wang, W. E. Seifert, *Tetrahedon Lett.* **1996**, *36*, 6515.
59. J. L. Sessler, B. Wang, A. Harriman, *J. Am. Chem. Soc.* **1993**, *115*, 10418.
60. J. L. Sessler, B. Wang, A. Harriman, *J. Am. Chem. Soc.* **1995**, *117*, 704.
61. A. Berman, E. S. Izraeli, H. Levanon, B. Wang, J. L. Sessler, *J. Am. Chem. Soc.* **1995**, *117*, 8252.
62. N. Solladié, M. Gross, *Tetrahedon Lett.* **1999**, *40*, 3359.
63. N. Solladié, C. Sooambar, H. Herschbach, J.-M. Strub, E. Leize, A. Van Dorsselaer, A. M. Talarico, B. Ventura, L. Flamigni, *New J. Chem.* **2005**, *29*, 1504.
64. M. Endo, T. Shiroyama, M. Fujitsuka, T. Majima, *J. Org. Chem.* **2005**, *70*, 7468.
65. K. Nakatani, C. Dohno, I. Saito, *J. Org. Chem.* **1999**, *64*, 6901.
66. C. J. Yu, H. Yowanto, Y. Wan, T. J. Meade, Y. Chong, M. Strong, L. H. Donilon, J. F. Kayyem, M. Gozin, G. F. Blackburn, *J. Am. Chem. Soc.* **2000**, *122*, 6767.

67. D. J. Hurley, Y. Tor, *J. Am. Chem. Soc.* **1998**, *120*, 2194.
68. P. Maillard, J.-L. Guerquin-Kern, C. Huel, M. Momenteau, *J. Org. Chem.* **1993**, *58*, 2774.
69. K. S. Akerfeldt, R. M. Kim, D. Camac, J. T. Groves, J. D. Lear, W. F. DeGrado, *J. Am. Chem. Soc.* **1992**, *114*, 9656.
70. I. Bouamaied, E. Stulz, *Synlett* **2004**, 1579.
71. M. Balaz, A. E. Holmes, M. Benedetti, P. C. Rodriguez, N. Berova, K. Nakanishi, G. Proni, *J. Am. Chem. Soc.* **2005**, *127*, 4172.
72. M. Cornia, S. Binacchi, T. Del Soldato, F. Zanardi, G. Casiraghi, *J. Org. Chem.* **1995**, *60*, 4964.
73. V. Kral, J. L. Sessler, H. Furuta, *J. Am. Chem. Soc.* **1992**, *114*, 8704.
74. X. Jiang, R. K. Pandey, K. M. Smith, *Tetrahedon Lett.* **1995**, *36*, 365.
75. L. G. Marzili, D. L. Banville, G. Zon, W. D. Wilson, *J. Am. Chem. Soc.* **1986**, *108*, 4188.
76. I. Dubey, G. Prativel, B. Meunier, *J. Chem. Soc., Perkin Trans.* **2000**, 3088.
77. N. N. Dioubankova, A. D. Malakhov, Z. O. Shenkarev, V. A. Korshun, *Tetrahedron* **2004**, *60*, 4617.
78. W. H. Prusoff, W. L. Holmes, A. D. Welch, *Cancer Res.* **1953**, *13*, 221.
79. R. M. K. Dale, D. C. Ward, D. C. Livingston, E. Martin, *Nucleic Acid Res.* **1975**, *2*, 915.
80. D. Lipkin, F. B. Howard, D. Nowotny, M. Sano, *J. Biol. Chem.* **1963**, *238*, 2249.
81. M. J. Robins, P. J. Barr, J. Giziewicz, *Can. J. Chem.* **1982**, *60*, 554.
82. C. McGuigan, R. N. Pathirana, R. Snoeck, G. Andrei, E. De Clercq, J. Balzarini, *J. Med. Chem.* **2004**, *47*, 1847.
83. W.-W. Sy, *Synthetic Commun.* **1990**, *20*, 3391.
84. S. Matysiak, H.-P. Fitznar, R. Schnell, W. Pfleiderer, *Helv. Chim. Acta* **1998**, *81*, 1545.
85. K. K. Ogilvie, S. L. Beaucage, A. L. Schifman, N. Y. Theriault, K. L. Sadana, *Can. J. Chem.* **1978**, *56*, 2768.
86. M. J. Robins, V. Samano, M. D. Johnson, *J. Org. Chem.* **1990**, *55*, 410.
87. P. Rothemund, *J. Am. Chem. Soc.* **1935**, *57*, 2010.
88. A. D. Alder, F. R. Longo, J. D. Finarelli, J. Goldmacher, J. Assour, L. Korsakoff, *J. Org. Chem.* **1967**, *32*, 476.
89. J. S. Lindsey, I. C. Schreiman, H. C. Hsu, P. C. Kearney, A. M. Marguerettaz, *J. Org. Chem.* **1987**, *52*, 827.
90. J. S. Lindsey, H. C. Hsu, I. C. Schreiman, *Tetrahedron Lett.* **1986**, *27*, 4969.
91. R. W. Wagner, D. S. Lawrence, J. S. Lindsey, *Tetrahedron Lett.* **1987**, *28*, 3069.
92. J. S. Lindsey, R. W. Wagner, *J. Org. Chem.* **1989**, *54*, 828.
93. J. S. Lindsey, S. Prathapan, T. E. Johnson, R. W. Wagner, *Tetrahedron* **1994**, *50*, 8941.
94. P. D. Rao, S. Dhanaleshimi, B. J. Littler, J. S. Lindsey, *J. Org. Chem.* **2000**, *65*, 7323.
95. G. R. Geier, J. S. Lindsey, *Tetrahedron* **2004**, *60*, 11435.
96. K. Tomizaki, A. B. Lysenko, M. Taniguchi, J. S. Lindsey, *Tetrahedron* **2004**, *60*, 2011.
97. R. W. Wagner, T. E. Johnson, J. S. Lindsey, *J. Am. Chem. Soc.* **1996**, *118*, 11166.
98. J.-S. Hsiao, B. P. Krueger, R. W. Wagner, T. E. Johnson, J. K. Delaney, D. C. Mauzarell, G. R. Fleming, J. S. Lindsey, D. F. Bocian, R. J. Donohoe, *J. Am. Chem. Soc.* **1996**, *118*, 11181.
99. N. Nishino, R. W. Wagner, J. S. Lindsey, *J. Org. Chem.* **1996**, *61*, 7534.
100. H. L. Anderson, J. K. M. Sanders, *J. Chem. Soc., Perkin Trans. 1* **1995**, 2223.
101. J. J. Piet, P. N. Taylor, H. L. Anderson, A. Osuka, J. M. Warman, *J. Am. Chem. Soc.* **2000**, *122*, 1749.

102. J. Geuze, C. Ruinard, J. Soeterbroek, P. E. Verkade, B. M. Wepster, *Recl. Trav. Chim. Pays-Bas* **1956**, *75*, 301.
103. M. S. Newman, L. F. Lee, *J. Org. Chem.* **1972**, *37*, 4468.
104. S. J. Angyal, *Org. React.* **1954**, *8*, 197.
105. J. March, *Advanced Organic Chemistry*, John Wiley & Sons, 4th Ed. 1992.
106. Y. L. Chow, Y. M. Naguib, *Rev. Chem. Intermed.* **1984**, *5*, 325.
107. P. Siemsen, R. C. Livingston, F. Diederich, *Angew. Chem. Int. Ed.* **2000**, *39*, 2632.
108. F. Diederich, P. J. Stang, *Metal-catalysed Cross-coupling Reactions*, Wiley-VCH 1997.
109. C. Cai, A. Vasella, *Helv. Chim. Acta* **1995**, *78*, 2053.
110. A. Elangovan, Y.-H. Wang, T.-I. Ho, *Organic Lett.* **2003**, *5*, 1841.
111. N. E. Leadbeater, B. J. Tominack, *Tetrahedron Lett.* **2003**, *44*, 8653.
112. Y. Liang, Y.-X. Xie, J.-H. Li, *J. Org. Chem.* **2006**, *71*, 379.
113. D. A. Alonso, C. Nájera, M. C. Pacheco, *Tetrahedron Lett.* **2002**, *43*, 9365.
114. Y. Nishihara, K. Ikegashira, K. Hirabayashi, J. Ando, A. Mori, T. Hiyama, *J. Org. Chem.* **2000**, *65*, 1780.
115. Q. Liu, D. J. Burton, *Tetrahedron Lett.* **1997**, *38*, 4371.
116. C. Glaser, *Ber. Dtsch. Chem. Ges.* **1869**, *2*, 422.
117. C. Glaser, *Ann. Chem. Pharm.* **1870**, *154*, 137.
118. S. G. DiMagno, V. S.-Y. Lin, M. J. Therien, *J. Org. Chem.* **1993**, *58*, 5983.
119. C. J. Medforth in *The Porphyrin Handbook*, K. M. Kadish, K. M. Smith, R. Guilard; Academic Press: San Diego 2000, Vol. 5, pp 3-80.
120. H. Iwamoto, K. Hori, Y. Fukazawa, *Tetrahedron Lett.* **2005**, *46*, 731.
121. E. Steiner, P. W. Fowler, *Chem. Phys. Chem.* **2002**, 114.
122. Y. Okuno, T. Kamikado, S. Yokoyama, S. Mashiko, *J. Mol. Struct. (Theochem)* **2003**, *631*, 13.
123. M. Sirish, V. A. Chertkov, H.-J. Schneider, *Chem. Eur. J.* **2002**, *8*, 1181.
124. J. R. Platt, *J. Opt. Soc. Amer.* **1953**, *43*, 252.
125. M. Gouterman, *J. Mol. Spectrosc.* **1961**, *6*, 138.
126. M. Gouterman, G. H. Wagnière, *J. Mol. Spectrosc.* **1963**, *11*, 108.
127. I. T. Oliver, W. A. Rawlinson, *Biochem. J.* **1955**, *61*, 641.
128. A. Antipas, J. W. Buchler, M. Gouterman, P. D. Smith, *J. Am. Chem. Soc.* **1978**, *100*, 3015.
129. H. L. Anderson, *Chem. Commun.* **1999**, 2323.
130. Y. Yamaguchi, *J. Chem. Phys.* **2004**, *120*, 7963.
131. L. Agrofoglio, I. Gillaizeau, Y. Saito, *Chem. Rev.* **2003**, *103*, 1875.
132. S. Eppacher, N. Solladié, A. Vasella, *Helv. Chim. Acta* **2004**, *87*, 2926.
133. M. J. Robins, P. J. Barr, *J. Org. Chem.* **1983**, *48*, 1854.
134. F. W. Hobbs, *J. Org. Chem.* **1989**, *54*, 3420.
135. H. Hasimoto, M. G. Nelson, C. Switzer, *J. Am. Chem. Soc.* **1993**, *115*, 7128.
136. C. McGuigan, C. J. Yarnold, G. J. Jones, S. Velázquez, H. Barucki, A. Brancale, G. Andrei, R. Snoeck, J. Balzarini, *J. Med. Chem.* **1999**, *42*, 4479.
137. S. I. Khan, M. W. Grinstaff, *J. Org. Chem.* **1999**, *64*, 1077.
138. T. Benneche, P. Strande, K. Undheim, *Synthesis* **1983**, 762.
139. E. J. Corey, M. G. Bock, *Tetrahedron Lett.* **1975**, 3269.
140. L. Bunch, P.-O. Norrby, K. Frydenvang, P. Krogsgaard-Larsen, U. Madsen, *Organic Lett.* **2001**, *3*, 433.
141. P. Sieber, *Helv. Chim. Acta* **1977**, *60*, 2711.
142. S. Kawahara, T. Wada, M. Sekine, *Tetrahedron Lett.* **1996**, *37*, 509.
143. H. Sajiki, T. Ikawa, K. Hattori, K. Hirota, *Chem. Commun.* **2003**, 654.

144. D. B. Brayan, R. F. Hall, K. G. Holden, W. F. Huffman, J. G. Gleason, *J. Am. Chem. Soc.* **1977**, *99*, 2353.
145. A. E. Weber, M. G. Steiner, P. A. Krieter, A. E. Colletti, J. R. Tata, T. A. Halgren, R. G. Ball, J. J. Doyle, T. W. Schorn, R. A. Stearns, R. R. Miler, P. K. S. Siegl, W. J. Greenlee, A. A. Patchett, *J. Med. Chem.* **1992**, *35*, 3755.
146. M. E. Jung, M. A. Lyster, *J. Org. Chem.* **1977**, *42*, 3761.
147. J. P. Marsh, L. Goodman, *J. Org. Chem.* **1965**, *30*, 2491.
148. G. W. Anderson, F. M. Callahan, *J. Am. Chem. Soc.* **1960**, *82*, 3359.
149. A. Bouzide, G. Sauvé, *Tetrahedron Lett.* **1999**, *40*, 2883.
150. Y. Wu, D. C. Limburg, D. E. Wilkinson, M. J. Vaal, G. S. Hamilton, *Tetrahedron Lett.* **2000**, *41*, 2847.
151. J. S. Yadav, V. S. Reddy, K. S. Rao, K. Harikishan, *Synlett* **2002**, 826.
152. H. G. Khorana, *Chem. Rev.* **1953**, *53*, 145.
153. D. F. DeTar, R. Silverstein, *J. Am. Chem. Soc.* **1966**, *88*, 1013.
154. D. F. DeTar, R. Silverstein, *J. Am. Chem. Soc.* **1966**, *88*, 1020.
155. M. Smith, J. G. Moffatt, *J. Am. Chem. Soc.* **1958**, *80*, 6204.
156. E. F. V. Scriven, *Chem. Soc. Rev.* **1983**, *12*, 129.
157. W. König, R. Geiger, *Chem. Ber.* **1970**, *103*, 788.
158. W. König, R. Geiger, *Chem. Ber.* **1970**, *103*, 2024.
159. W. König, R. Geiger, *Chem. Ber.* **1970**, *103*, 2034.
160. M. D. Ward, *Chem. Soc. Rev.* **1997**, *26*, 365.
161. C. A. Hunter, J. K. M. Sanders, A. J. Stone, *Chem. Phys.* **1989**, *133*, 395.
162. M. Kasha, *Radiat. Res.* **1963**, *20*, 55.
163. M. Kasha, H. R. Rawls, M. A. El-Bayoumi, *Pure Appl. Chem.* **1965**, *11*, 371.
164. T. Förster, *Ann. Phys.* **1948**, *2*, 55.
165. T. Förster, *Discuss. Faraday Soc.* **1959**, 27, 7.
166. L. Stryer, R. P. Haugland, *Proc. Natl. Acad. Sci. U. S. A.* **1967**, *58*, 719.
167. D. L. Dexter, *J. Chem. Phys.* **1953**, *21*, 836.
168. J.-M. Lehn, *Angew. Chem. Int. Ed. Engl.* **1988**, *27*, 89.
169. J.-M. Lehn, *Science* **2002**, *295*, 2400.
170. A. Satake, Y. Kobuke, *Tetrahedron* **2005**, *61*, 13.
171. M. Choi, T. Yamazaki, I. Yamazaki, T. Aida, *Angew. Chem., Int. Ed.* **2004**, *43*, 150.
172. K. Tomizaki, L. Yu, L. Wei, D. F. Bocian, J. S. Lindsey, *J. Org. Chem.* **2003**, *68*, 8199.
173. I.-W. Hwang, T. Kamada, T. K. Ahn, D. M. Ko, T. Nakamura, A. Tsuda, A. Osuka, D. Kim, *J. Am. Chem. Soc.* **2004**, *126*, 16187.
174. C. C. Mak, N. Bampos, S. L. Darling, M. Montalti, L. Prodi, J. K. M. Sanders, *J. Org. Chem.* **2001**, *66*, 476.
175. R. A. Haycock, A. Yartsev, U. Michelsen, V. Sundström, C. A. Hunter, *Angew. Chem. Int. Ed.* **2000**, *39*, 3616.
176. J. Bretar, J.-P. Gieselbrecht, M. Gross, N. Solladié, *Chem. Commun.* **2001**, 733.
177. R. Rein, M. Gross, N. Solladié, *Chem. Commun.* **2004**, 1992.
178. L. Flamigni, A. M. Talarico, B. Ventura, R. Rein, N. Solladié, *Chem. Eur. J.* **2006**, *12*, 701.
179. C. Ikeda, Y. Tanaka, T. Fujihara, Y. Ishii, T. Ushiyama, K. Yamamoto, N. Yoshioka, H. Inoue, *Inorg. Chem.* **2001**, *40*, 3395.
180. C. Ikeda, A. Satake, Y. Kobuke, *Org. Lett.* **2003**, *5*, 26, 4935.
181. K. Kameyama, A. Satake, Y. Kobuke, *Tetrahedon Lett.* **2004**, *45*, 7617.
182. M. Schmittel, R. S. K. Kishore, *Org. Lett.* **2004**, *6*, 12, 1923.
183. T. S. Balaban, R. Goddard, M. Linke-Schaetzel, J.-M. Lehn, *J. Am. Chem. Soc.* **2003**, *125*, 4233.

184. E. Iengo, E. Zangrando, E. Alessio, *Eur. J. Inorg. Chem.* **2003**, 2371.
185. E. Iengo, E. Zangrando, E. Alessio, J.-C. Chambron, V. Hitz, L. Flamigni, J.-P. Sauvage, *Chem. Eur. J.* **2003**, *9*, 5879.
186. K. Sugou, K. Sasaki, K. Kitajima, T. Iwaki, Y. Kuroda, *J. Am. Chem. Soc.* **2002**, *124*, 1182.
187. J. Wojaczyński, L. Latos-Grażyński, *Coord. Chem. Rev.* **2000**, *204*, 113.
188. B. J. Holliday, C. A. Mirkin, *Angew. Chem. Int. Ed.* **2001**, *40*, 2022.
189. A. Robertson, S. Shinkai, *Coord. Chem. Rev.* **2000**, *205*, 157.
190. H. E. Toma, K. Araki, *Coord. Chem. Rev.* **2000**, *196*, 307.
191. S. Leininger, B. Oleynuk, P. J. Stang, *Chem. Rev.* **2000**, *100*, 853.
192. A. Vidal-Ferran, N. Bampos, J. K. M. Sanders, *Inorg. Chem.* **1997**, *36*, 6117.
193. P. N. Taylor, H. L. Anderson, *J. Am. Chem. Soc.* **1999**, *121*, 11538.
194. G. S. Wilson, H. L. Anderson, *Chem. Commun.* **1999**, 1539.
195. U. Michelsen, C. A. Hunter, *Angew. Chem. Int. Ed.* **2000**, *39*, 764.
196. M. Gardner, A. J. Guerin, C. A. Hunter, U. Michelsen, C. Rotger, *New. J. Chem.* **1999**, 309.
197. E. B. Fleischer, A. M. Shachter, *Inorg. Chem.* **1991**, *30*, 3763.
198. R. V. Slone, J. H. Hupp, *Inorg. Chem.* **1997**, *36*, 5422.
199. C. M. Drain, F. Nifiatis, A. Vasenko, J. D. Batteas, *Angew. Chem. Int. Ed.* **1998**, *37*, 2344.
200. T. N. Milic, N. Chi, D. G. Yablon, G. W. Flynn, J. D. Batteas, C. M. Drain, *Angew. Chem. Int. Ed.* **2002**, *41*, 2117.
201. J. N. H. Reek, A. P. H. J. Schenning, A. W. Bosman, E. W. Meijer, M. J. Crossley, *Chem. Commun.* **1998,** 11.
202. L. Baldini, P. Ballester, A. Casnati, R. M. Gomila, C. A. Hunter, F. Sansone, R. Ungaro, *J. Am. Chem. Soc.* **2003**, *125*, 14181.
203. SPECFIT, Global Least Squares fitting by Factor Analysis and Marquart Minimization.
204. H. Gampp, M. Maeder, C. J. Meyer, A. D. Zuberbühler, *Talanta* **1986**, *33*, 943.
205. H. Gampp, M. Maeder, C. J. Meyer, A. D. Zuberbühler, *Talanta* **1985**, *32*, 95.
206. K. Hirose, *J. Inclusion Phenom. Macrocyclic Chem.* **2001**, *39*, 193.
207. P. Ballester, A. Costa, A. M. Castilla, P. M. Deyà, A. Frontera, R. M. Gomila, C. A. Hunter, *Chem. Eur. J.* **2005**, *11*, 2196.
208. C. A. Hunter, M. N. Meah, J. K. M. Sanders, *J. Am. Chem. Soc.* **1990**, *112*, 5773.
209. H. L. Anderson, C. A. Hunter, M. N. Meah, J. K. M. Sanders, *J. Am. Chem. Soc.* **1990**, *112*, 5780.
210. H.-J. Kim, N. Bampos, J. K. M. Sanders, *J. Am. Chem. Soc.* **1999**, *121*, 8120.
211. C. A. Hunter, R. Tregonning, *Tetrahedron* **2002**, *58*, 691.
212. C. C. Mak, D. Pomeranc, M. Montelti, L. Prodi, J. K. M. Sanders, *Chem. Commun.* **1999**, 1083.
213. G. S. Wilson, H. L. Anderson, *Chem. Commun.* **1999**, 1539.
214. L. Baldini, P. Ballester, A. Casnati, R. M. Gomila, C. A. Hunter, F. Sansone, R. Ungaro, *J. Am. Chem. Soc.* **2003**, *125*, 14181.
215. R. R. Sinden, *DNA Structure and Function*, Academic Press, Inc., New York, **1994**.
216. J. D. Watson, F. H. Crick, *Nature* **1953**, *171*, 737.
217. Y. Kyogoku, R. C. Lord, A. Rich, *Proc. Nat. Acad. Sci. U.S.A.* **1967**, *57*, 250.
218. Y. Kyogoku, R. C. Lord, A. Rich, *Biochim. Biophys. Acta* **1969**, *179*, 10.
219. T. J. Murray, S. C. Zimmerman, *J. Am. Chem. Soc.* **1992**, *114*, 4010.
220. J. Pranata, S. G. Wierschke, W. L. Jorgensen, *J. Am. Chem. Soc.* **1991**, *113*, 2810.

221. S. C. Zimmerman, P. S. Corbin, *Struct. Bond.* **2000**, *96*, 63.
222. A. D. Hamilton, D. Little, *J. Chem. Soc., Chem. Commun.* **1990**, 297.
223. T. K. Park, J. Schroeder, J. Rebek, Jr., *J. Am. Chem. Soc.* **1991**, *113*, 5125.
224. L. J. Prins, D. N. Reinhoudt, P. Timmerman, *Angew. Chem. Int. Ed.* **2001**, *40*, 2382.
225. M. M. Conn, J. Rebek, Jr., *Chem. Rev.* **1997**, *97*, 1647.
226. M. J. Krische, J.-M. Lehn, *Struct. Bond.* **2000**, *96*, 3.
227. R. E. Melendez, A. J. Carr, B. R. Linton, A. D. Hamilton, *Struct. Bond.* **2000**, *96*, 31.
228. G. M. Witesides, J. P. Mathias, C. T. Seto, *Science* **1991**, *254*, 1312.
229. R. P. Sijbesma, E. W. Meijer, *Chem. Commun.* **2003**, *1*, 5.
230. A. D. Hamilton, N. Pant, *J. Chem. Soc., Chem. Commun.* **1988**, 765.
231. S.-K. Chang, A. D. Hamilton, *J. Am. Chem. Soc.* **1988**, *110*, 1318.
232. S. C. Zimmerman, W. Wu, Z. Zeng, *J. Am. Chem. Soc.* **1991**, *113*, 196.
233. J. L. Sessler, B. Wang, A. Harriman, *J. Am. Chem. Soc.* **1995**, *117*, 704.
234. F. H. Beijer, R. P. Sijbesma, J. A. J. M. Vekemans, E. W. Meijer, H. Kooijman, A. L. Spek, *J. Org. Chem.* **1996**, *61*, 6371.
235. I. Willner, J. Rosengaus, S. Biali, *Tetrahedon Lett.* **1992**, *33*, 3805.
236. J. A. Zerkowski, J. C. MacDonald, C. T. Seto, D. A. Wierda, G. M. Whitesides, *J. Am. Chem. Soc.* **1994**, *116*, 2382.
237. M. B. Steffensen, E. E. Simanek, *Organic Lett.* **2003**, *5*, 2359.
238. D. W. P. M. Löwik, C. R. Lowe, *Eur. J. Org. Chem.* **2001**, 2825.
239. T. Carofiglio, A. Varotto, U. Tonellato, *J. Org. Chem.* **2004**, *69*, 8121.
240. Y. Ni, R. R. Puthenkovilakom, Q. Huo, *Langmuir* **2004**, *20*, 2765.
241. S. Kotsovolou, A. Chiou, R. Verger, G. Kokotos, *J. Org. Chem.* **2001**, *66*, 962.
242. H. Hayashi, K. Nakanishi, C. Brandon, J. Marmur, *J. Am. Chem. Soc.* **1973**, *95*, 8749.
243. P. J. Kocienski, G. Cernigliaro, G. Felstein, *J. Org. Chem.* **1977**, *42*, 353.
244. E. Kaiser, J. P. Tam, T. M. Kubiak, R. B. Merrifield, *Tetrahedron Lett.* **1988**, *29*, 303.
245. W. L. Jorgensen, J. Pranata, *J. Am. Chem. Soc.* **1990**, *112*, 2008.
246. T. J. Murray, S. C. Zimmerman, S. V. Kolotuchin, *Tetrahedron* **1995**, *51*, 635.
247. E. E. Fenlon, T. J. Murray, M. H. Baloga, S. C. Zimmerman, *J. Org. Chem.* **1993**, *58*, 6625.
248. S. C. Zimmerman, T. J. Murray, *Tetrahedron Lett.* **1994**, *35*, 4077.
249. J. Sartorius, H.-J. Schneider, *Chem. Eur. J.* **1996**, *2*, 1446.
250. K. Hirose, *J. Inclusion Phenom. Macrocyclic Chem.* **2001**, *39*, 193.
251. L. Fielding, *Tetrahedron* **2000**, *56*, 6151.

TITLE OF THE DISERTATION:

Oligonucleotides with Pendant Porphyrins: towards Self-Assembled Multi-Porphyrinic Nano-Materials.

SUMMARY OF THE DISERTATION:

The light-harvesting antennae in the photosynthetic system consist of a large number of pigments, which are responsible for absorption of photons. The extraordinary efficiency of the excited state migration among the pigments is ascribed to their parallel orientation and favoured spacing within the light-harvesting complexes. This arrangement, controlled by weak interactions between pigments and polypeptides, assumes three ring-shaped light-harvesting antennae.

Aiming to organize porphyrins in accordance with the natural system, we have chosen oligonucleotidic backbone for the elaboration of multi-porphyrinic nanosystems. In this respect, the synthesis of oligonucleotides functionalized with porphyrins was realized. The preparation of these systems was based on oligomerization at O-3' and O-5' positions of the 2'-deoxyuridine derivative functionalized with a porphyrin. Architecture of our system has been designed on the basis of rigid and flexible linkers. The porphyrins were appended to C-5 position of the uracile by a rigid linker and the uridines were mutually linked by a flexible linker, with the goal to work out parallel orientation of porphyrins *via* anticipated conformation of the oligonucleotidic chain. In this context, we have synthesized the mono-, di-, tetra- and octa-deoxynucleosides with pendant porphyrins.

An appropriate arrangement of free-base and zinc(II) porphyrins within the oligonucleotidic molecular wire allowed us to highlight an energy transfer. The contribution of the zinc(II)-porphyrin to the emission of the free-base pophyrins was evidenced.

The range of oligonucleotides have been metallated with zinc(II) targeting to examine effectiveness of the oligomerization degree of these molecular architectures on their ability to complex a bidentate base such as DABCO. We have observed that the coordination of DABCO is favoured as one goes toward higher degree of oligomerization due to imposed conformational pre-organization within the oligonucleotidic backbone.

At last, we were interested in self-assembly by means of hydrogen bonding, which could be established between the uracil nucleobase and a complementary synton such as triazine functionalized with porphyrins. The quantitative studies of stability of those supramolecular architectures have evidenced an influence of secondary intermolecular π-π interactions between the porphyrins within the supramolecular complex.

KEY WORDS:

Porphyrins, Uridines, Oligonucleotides, Hydrogen bond, Self-assembly, Supramolecular complexes, Energy transfer, Fluorescence.